Evolution of Erosional Unconformities in the Cenozoic Succession of the Cayman Islands

by

Ting Liang

A thesis submitted in partial fulfillment of the requirements for the degree of

Doctor of Philosophy

Department of Earth and Atmospheric Sciences
University of Alberta

ABSTRACT

The carbonate succession on Grand Cayman and Cayman Brac, located close to each other in the Caribbean Sea, includes the Bluff Group that is formed of the unconformity-bounded Brac Formation (early Oligocene), Cayman Formation (middle Miocene), and Pedro Castle Formation (early Pliocene), which is overlain by the Ironshore Formation (Pleistocene). The erosional unconformities that now separate these formations developed during the sea-level lowstands.

The karst relief of at least 62 m on the upper surface of the Cayman Formation on Grand Cayman provides the minimum estimate for the Messinian drop of sea level in Caribbean. The rugged interior landscape and peripheral rims on this surface reflect the interplay between the rate of runoff and rainfall. Compared to Grand Cayman, the upper surface of the Cayman Formation on the uplifted central core of Cayman Brac is tilted with up to 120 m of the Cayman Formation lost to erosion, more pronounced peripheral rims, and lower karst relief. Nevertheless, exposures of this formation on the two islands are characterized by phytokarst, sinkholes, photolineaments, and solution-widened joints. Such comparisons indicate that uplift played an important role in the development of this erosional unconformity.

Sinkholes developed in the Cayman Formation on Grand Cayman and Cayman Brac are open, filled with water, or filled with lithified deposits that include rootcrete, and breccias that are formed of dolostone, white limestone and black limestone lithoclasts that are held in white (oncoids or skeletal), yellow, and orange limestone matrices. The rare earth elements (REE) and isotopes of these sinkhole-filling deposits are different from those derived from the bedrock carbonates. Interpretation of these data indicates that the (1) rootcrete, oncoids, and the red and orange limestones are terrestrial in origin, whereas the other sinkhole-filling deposits are of marine origin, (2) red and orange limestones probably formed under more arid condition than the other sinkhole-filling deposits, (3) formation of the black limestone lithoclasts, oncoids, and rootcrete was probably related to biogenic factors, and (4) REE can be used to determine provenance. The sinkhole-filling deposits offer a record of the processes that took place while the erosional unconformities were developing.

PREFACE

This thesis is an original work completed by Ting Liang, with the assistance of Dr. Brian Jones. The overall theme of the thesis was initially outlined by Dr. Jones and then developed through discussions between the two of us. Chapters two and four of this thesis were published as the following two papers:

Liang, T., Jones, B., 2014. Deciphering the impact of sea-level changes and tectonic movement on erosional sequence boundaries in carbonate successions: A case study from Tertiary strata on Grand Cayman and Cayman Brac, British West Indies. Sedimentary Geology 305, 17-34.

This data for this paper came from Digital Elevation Data that came from the Department of Lands and Survey of the Cayman Islands government. Much of the stratigraphy data came from a database that Dr. Jones had assembled over the last 30 years. For this paper, I undertook the data analysis and produced the initial drafts of the manuscript, which were then extensively edited by Dr. Jones.

Liang, T. and Jones, B., 2015. Petrographic and geochemical features of sinkhole-filling deposits associated with an erosional unconformity on Grand Cayman. Sedimentary Geology 315, 64-82.

This paper was based on samples that had been collected by Dr. Jones and by myself. I obtained the analyses and then wrote the initial version of the manuscript. Dr. Jones assisted provided valuable feedback on the interpretation of the results and extensively edited the manuscript.

Chapter three has been submitted as:

Liang, T., Jones, B., 2015. Ongoing, long-term evolution of an unconformity that originated as a karstic surface in the Late Miocene: A case study from the Cayman Islands, British West Indies. Sedimentary Geology.

The digital elevation data used in this paper came from Department of Lands and Survey of the Cayman Islands government. I did the data analyses and write the initial drafts of the manuscript. Dr. Brian Jones provided additional data and contributed through extensive discussions of the concepts and extensive editing of the manuscript.

All papers reflect the fact that both authors were actively involved in their development and writing.

ACKNOWLEDGEMENT

I would not have been able to complete my PhD without the support of many people throughout my thesis research.

First and foremost, I am greatly indebted to my supervisor Dr. Brian Jones for taking me to work on this project. Three-year research work under the guidance of Dr. Jones has taught me many valuable lessons including the importance of thinking out of the box, the significance of proper editing, and most importantly, the necessity to put my own work globally. Many thanks to Dr. Jones for his advice, constuctive criticism, encouragement, patience and countless hours of editing the thesis. Without his help, my dissertation would never have taken flight.

I would also like to thank Dr. Karlis Muehlenbachs for generously providing his laboratory for the stable isotope analysis; Mr. Mark Labbe and Mr. Martin Von Dollen for preparing the thin sections; Mrs. Diane Caird for running the XRD samples; Mr. Guangcheng Chen for running the ICP-MS analyses; Mr. George Braybrook for taking the SEM photomicrographs used in this study; and Mr. Valery Companiytsev, who provided technical support for ArcGIS 10.

I am grateful to the Natural Sciences and Engineering Research Council of Canada, which funded this research (Grant A6090 to Jones); Department of Lands and Survey of the Cayman Islands government, which provided the data from which the digital elevation models for Grand Cayman and Cayman Brac were derived; Mr. Hendrik van Genderen (Water Authority of Cayman Islands), who helped in collection of some of the samples. I am also grateful to the Chinese Scholarship Council for providing financial support during my study in University of Alberta.

It has been a pleasure to work with the members of the Carbonate Research Group: Hongwen Zhao, Josh Thomas, Alexandra Der, Megan Black, Rong Li, Min Ren and Erjun Zheng. It was enjoyable to share the lab with them.

Finally, thanks go to my parents for their love, patience, constant support, and encouragement throughout my thesis research.

TABLE OF CONTENTS

LIST OF TABLES

LIST OF FIGURES

CHAPTER 1: INTRODUCTION

1. Introduction

Carbonate rocks are deposited during sea-level highstands, whereas subaerial erosion that produces erosional unconformity takes place during sea-level lowstands. Erosional unconformities are important in stratigraphy and sedimentology because they (1) form sequence boundaries that separate carbonate successions (Esteban and Klappa, 1983; James and Choquette, 1990; Clari et al., 1995; Hillgärtner, 1998; Sattler et al., 2005), (2) may indicate surfaces have experienced meteoric diagenetic alteration or dolomitization (e.g., Esteban and Klappa, 1983; James and Choquette, 1988; Tucker, 1990; Wright and Smart, 1994; Saller et al., 1994, 1999; Whitaker et al., 1999; Budd et al., 2002; Miller et al., 2012; Zhao and Jones, 2012a), (3) give rise to the development of calcretes and paleosols (e.g., Alonso-Zarza and Wright, 2010), and (4) may lead to the development of surface and subsurface karst (e.g., Frisia and Borsato, 2010).

During recent decades, carbonate geologists have devoted a lot of effort to investigate the factors that control the diagenetic regimes that develop in association with an erosional unconformity (Goldstein, 1988; Dickson and Saller, 1995; Rankey, 1997; Budd et al., 1995, 2002; Saller et al., 1999; Smith and Read, 1999; Weidlich, 2010; Miller et al., 2012). These factors include duration of the exposure, fluctuation of sea level, tectonics, paleogeography, paleoclimate, aquifer configuration, and/or properties (i.e., lithology, porosity and permeability) of the bedrock. Theoretically, the diagenetic products should record the paleo-geological conditions that were active when an erosional unconformity was developing. Such an approach, however, can be greatly hindered by the overprinting of fabrics that may result from repeated periods of exposure.

As with meteoric diagenesis, karst landforms and the void-filling deposits deposits associated with an erosional unconformity are also controlled by many different factors. Understanding the factors that control the development of karst landforms and the void-filling deposits could help to (1) improve stratigraphic analysis of the carbonate strata, (2) develop criteria by which paleokarst could be recognized in ancient strata, and (3) reconstruct the geological conditions that existed during a period when denudation dominated. Nevertheless, the landforms that can develop on an erosional unconformity have rarely been studied. This is because (1) karst landforms, especially those with minor relief are buried and therefore hard to decipher, (2) the positive karst forms, such as tower karst and cone karst, may have been damaged and destroyed as sea level rose (Purdy and Waltham, 1999), and (3) the karst landforms are easily destroyed when inundated by fluvial systems and silicate sediments (Ford, 1988).

The karst landforms and void-filling deposits associated with erosional unconformities on the Cayman Islands are good candidates for assessing the processes that were active during sea-level lowstands because (1) Grand Cayman and Cayman Brac are geographically isolated by deep oceanic water, with little to no influences of silicate sediments and fluvial systems, (2) the unconformities are geologicallyjc young and developed during sea level lowstands, (3) modern and buried unconformities exist in the same geographic areas, (4) comparison of Grand Cayman and Cayman Brac, which have different tectonic histories, allows separation of the influences of uplift as opposed to sea level changes (Horsfield, 1975; Stoddart, 1980; Jones and Hunter, 1990; Vézina et al., 1999; Coyne et al., 2007), and (5) the formation of karst landforms is ongoing today. By focusing on erosional unconformities in the Cenozoic carbonate succession on Grand Cayman and Cayman Brac, this study is designed to (1) systematically decipher and compare the 3-D topography of each unconformity, and examine how eustasy and uplift influenced the overall stratigraphic architecture, (2) compare the karst landforms on Grand Cayman and Cayman Brac and evaluate the factors that control their formation, and (3) reveal the petrography and geochemical attributes of sinkhole-filling deposits, which may provide insights into the processes that occurred as an erosional unconformity was developing. Collectively, this study examines the geological information that is recorded by the erosional unconformity itself. Potentially, this has widespread application to other carbonate successions by providing a better understanding of (1) the geometry of carbonate strata that are bounded by erosional unconformities, (2) the development of karst features below an ancient erosional unconformity, and (3) environmental signals that can be preserved by the deposits that fill sinkholes.

2. Study area and methods

2.1. Study area

Lying close to Cuba and Jamaica, the Cayman Islands comprise Grand Cayman, Little Cayman, and Cayman Brac (Fig. 1-1). Each of these islands is a pinnacle on the Cayman Ridge, which lies parallel to the Oriente Transform Fault that separates the North America Plate from the Caribbean Plate (Perfit and Heezen, 1978; Fig. 1-1). Southwest of Grand Cayman there is the Mid-Cayman Rise, which is an active spreading center. At the north end of the Mid-Cayman Rise is the Oriente Transform Fault, which extends westward, whereas at the south end is the Swan Islands Transform Fault, which extends westward (MacDonald and Holcombe, 1978; Fig. 1-1). The Oriente Transform Fault forms the northern margin of the Cayman Trench (MacDonald and Holcombe, 1978), which is a pull-apart basin (up to 7686 m deep) located on the north margin of the Caribbean Plate (Fig. 1-1).

The Mid-Cayman Rise has probably been active since the Late Eocene (Perfit, 1977; Mattson, 1984; Rosencrantz and Sclater, 1986; Bruke, 1988; Pindell et al., 1988; Ross and Scotese, 1988; Pindell, 1991; Iturralde-Vinent, 1994; Leroy et al., 2000; Pindell and Kennan, 2009). From the Late Eocene to Oligocene, movement on the Oriente Transform Fault led to the detachment of the Cayman Islands from their parent arc and transported them to the present location (Iturralde-Vinent, 1994; Calais and Mercier de Lépinay, 1995). Since the early Middle Miocene, localized extensional features began to form (Iturralde-Vinent and Macphee, 1999; Iturralde-Vinent, 2006). This movement probably generated faults, at ~90° to the Oriente Transform Fault that divided the Cayman Ridge into a series of fault blocks. Although not known with certainty, it appears that each of the Cayman Islands is located on a separate fault blocks. Thereafter, the transpression triggered by the transcurrent (west-east) motion along the north flank of the Cayman Trench caused uplift (Rojas-Agramonte et al., 2005; Pindell and Kennan, 2009). Cayman Brac, for example, was uplifted between the Late Pliocene and ~125

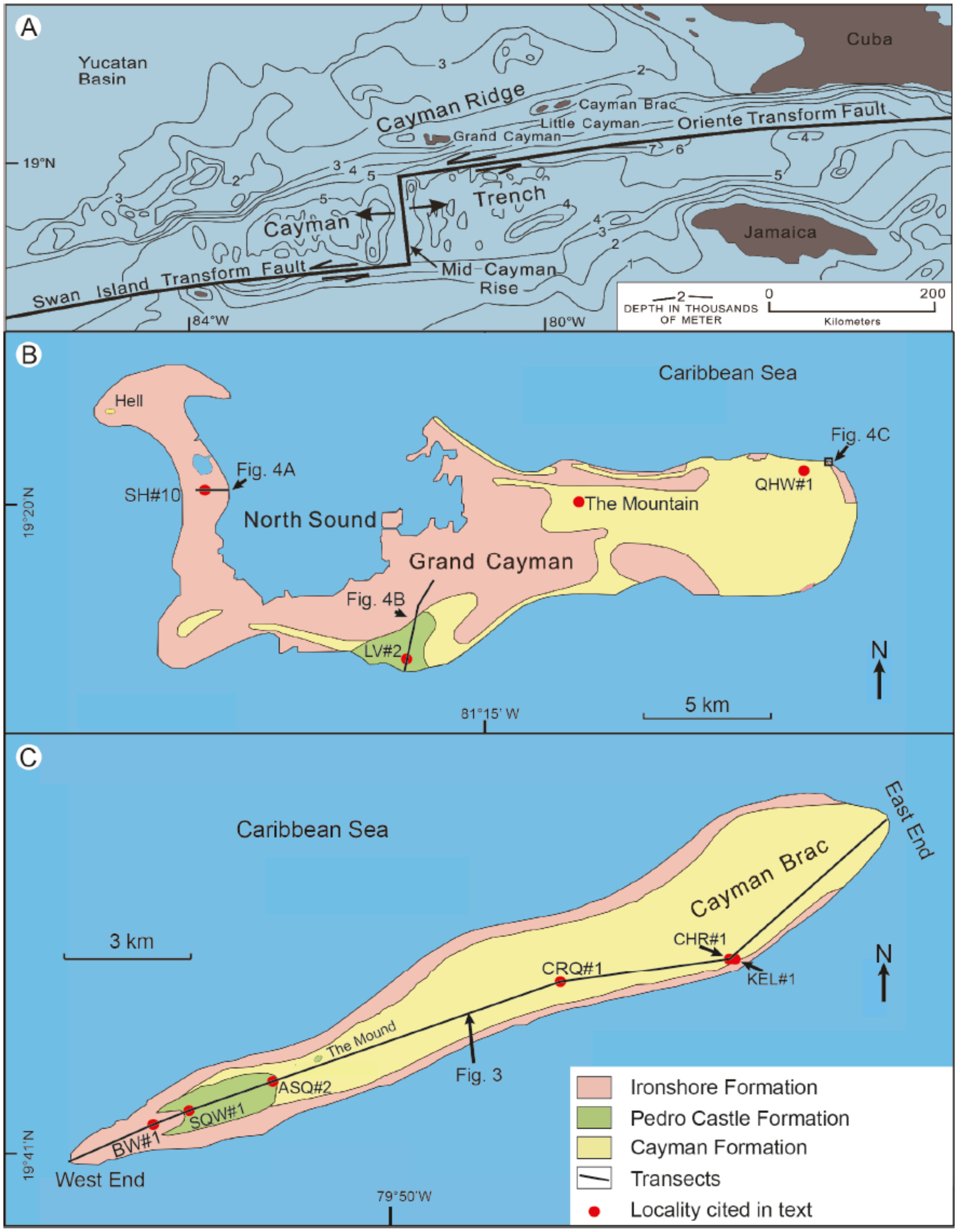

Fig. 1-1. (A) Locations of Grand Cayman and Cayman Brac relative to the Mid-Cayman Rise, the Cayman Trench, and the Oriente Transform Fault (Modified from Jones, 1994, and based on maps from Perfit and Heezen, 1978, and MacDonald and Holcombe, 1978). (B) Surface geology on Grand Cayman (modified from Jones, 1994). The wells and black lines indicate locations of transects in Figure 1-4. (C) Surface geology on Cayman Brac (modified from Jones, 1994). The wells indicate location of transect in Figure 1-3.

ka (Zhao and Jones, 2012a, 2013). In contrast, Grand Cayman, which is ~150 km away from Cayman Brac, appears to have experienced little, if any, tectonic movements since the Oligocene (Horsfield, 1975; Stoddart, 1980; Jones and Hunter, 1990; Vézina et al., 1999; Coyne et al., 2007).

Each of the Cayman Islands is a carbonate build-up isolated by deep oceanic water, with no surface streams. Eustatic sea-level changes and/or tectonic movements are responsible for the stratigraphic architectures of these islands. The highstands in the early Oligocene, middle Miocene and early Pliocene, for example, led to the deposition of the sediments that now form the Brac Formation, the Cayman Formation and the Pedro Castle Formation (Fig. 1-2), respectively (Jones, 1994; Jones, et al., 1994a 1994b). Conversely, sea level lowstands during the late Oligocene-early Miocene, the late Miocene, and the late Pliocene gave rise to the subaerial erosion, which produced the erosional unconformities that now define the boundaries between the different formations. The unconformity between the Brac Formation and the Cayman Formation, for example, initially formed during the lowstand during the late Oligocene to early Miocene, whereas the unconformity at the top of the Cayman Formation formed during the late Miocene. Subaerial erosion, which occurred from the late Pliocene onwards, gave rise to the unconformity that forms the upper surface of the Pedro Castle Formation. On most of the eastern half of Grand Cayman and much of the uplifted core of Cayman Brac, this phase of subaerial erosion completely removed the Pedro Castle Formation, and led to further modification of the upper surface of the Cayman Formation.

2.2. Methods

Subsurface unconformities on Grand Cayman and Cayman Brac were located by data obtained from wells, whereas the exposed unconformities were deciphered by analysis of outcrops and digital elevation models (DEMs). On Grand Cayman and Cayman Brac, outcrops are limited to the coastal areas, quarries, and construction sites, which have been cleared of dense tropical vegetation and thereby made accessible. Over the last 30 years, core and/or chip samples have been collected from the 112 wells drilled by Dr. Brian Jones' group and other organizations

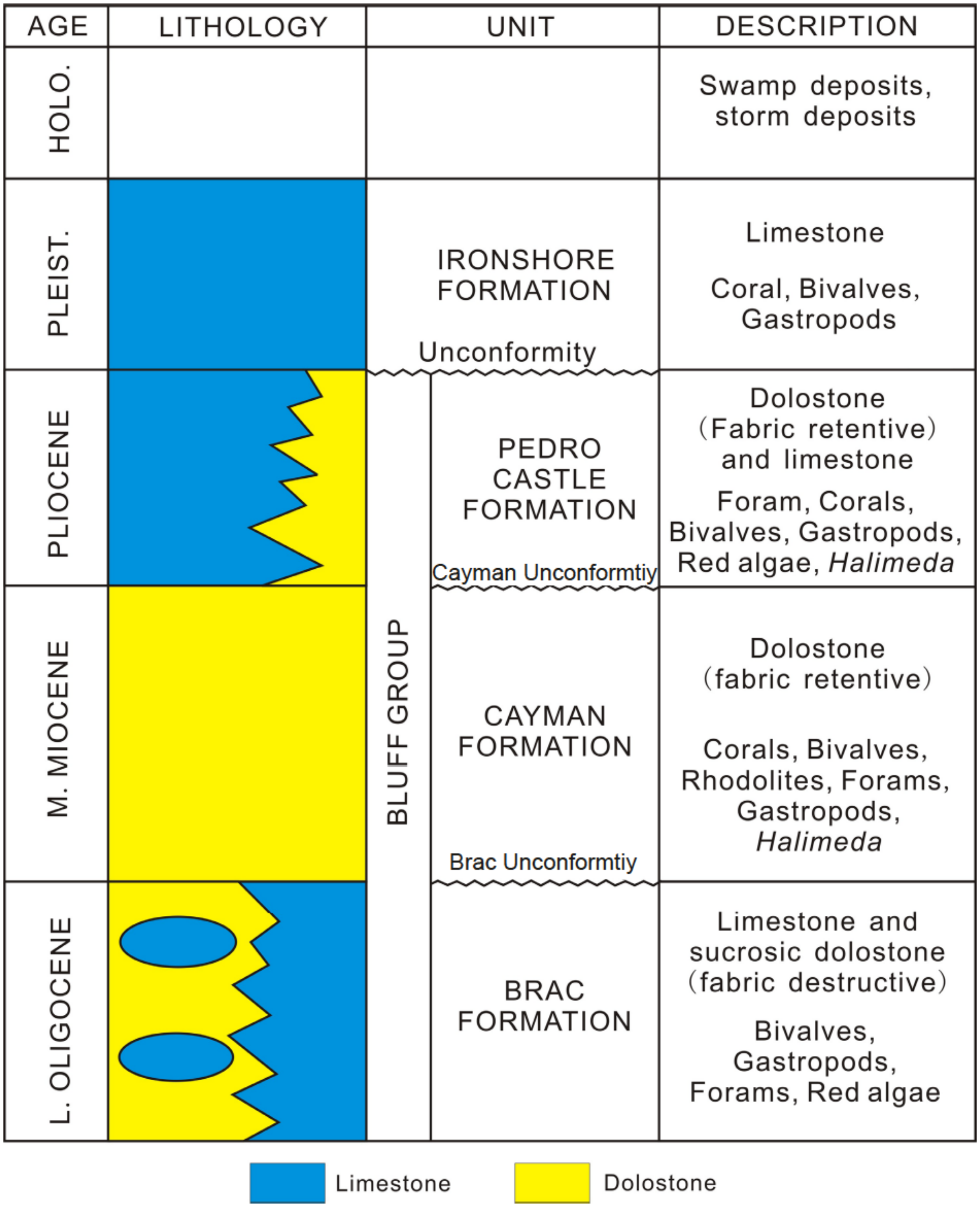

Fig. 1-2. Stratigraphic succession of the Cayman Islands (modified from Jones, 1994) showing lithology and dominant biota of each unit.

(e.g., Water Authority, Cayman Islands). On Grand Cayman, drilling has produced cored wells (54 wells), mixed cores and well cuttings (8 wells), and well cuttings (35 wells). On Cayman Brac, in contrast, the drilling is represented only by well cuttings that were collected from 15 wells. Most of the drilling on Cayman Brac was done around the periphery of the uplifted core, because the interior is largely inaccessible and water needed for drilling is absent. By using kriging method, the 3-dimentional topography of each undersurface unconformity could be interpolated from the data obtained from these scattered wells and outcrops. This procedure is automatically done by Surfer 10 software.

Elevations of the exposed unconformities on Grand Cayman and Cayman Brac came from the digital elevation models (DEMs) that were constructed from data provided by the Lands and Survey Department, Government of the Cayman Islands. DEMs, with a grid resolution of 3 m × 3 m, were used to model the appearance of the bare ground surface by using the last returns of laser scanning. As such, this new technology allows the examinations of the topography of all the exposures, including both of accessible and inaccessible areas, on Grand Cayman and Cayman Brac.

The study of sinkhole-filling deposits relies on outcrops, thin sections, X-ray diffraction (XRD), and geochemical analyses. Analysis of the sinkhole-filling deposits was limited largely to the southeastern corner of Grand Cayman, because that area (1) is easy to access, (2) has been cleared of vegetation, and (3) includes vertical sections through the sinkhole fills. The hand samples collected from the sinkholes were then analyzed petrographically and geochemically. The petrography of sinkhole-filling deposits was established from large thin sections (7.5 × 5 cm), which were made from large hand samples. Scanning electron microscopy (SEM) was used to examine the micro-fabrics of fractured hand samples, whereas the elemental content of selected spots were established by Energy-dispersive X-ray (EDX) analysis. Powdered samples (75-150 μm), made from different components of the samples, were analyzed for their mineralogy, isotopes, and rare earth elements (REE). The mineralogy of the powdered samples was quantitatively determined by X-ray diffraction analysis (XRD), which was done on a Rigaku

Geigerflex 2173 XRD system using Co Kα radiation. The powdered samples were also analyzed for carbon and oxygen stable isotopes and elements, by the standard phosphoric acid dissolution method following McCrea (1950). Element (Ca, Fe, Mn, Al, REE) concentrations were determined by inductively coupled plasma mass spectrometer (ICP-MS). Details of the technical parameters for each method are presented in the appropriate chapters.

3. Previous research

3.1. Stratigraphy and unconformities

The Tertiary carbonate succession on the Cayman Islands was originally named the "Bluff Limestones" by Matley (1926). Based on Lepidocyclina found in the buff colored, massive and hard limestones in sheer cliffs along the northeast coast of Cayman Brac, a Middle Oligocene age was assigned to the "Bluff Limestone" (Matley, 1926). The Pleistocene limestones that overlie the Bluff Limestones were named the Ironshore Formation (Matley, 1926). Subsequent investigations revealed there is extensive dolomite in Bluff Limestone (Jones et al., 1984; Pleydell, 1987; Jones and Hunter, 1989). Thus, the term "Bluff Limestone" was modified to "Bluff Formation" in order to remove the lithological connotation (Jones and Hunter, 1989). Jones and Hunter (1989) identified an unconformity in the Bluff Formation, which was used to divide the formation into the Cayman Member and the overlying Pedro Castle Member. Later these two members were elevated to formational status (Jones et al., 1994a). Subsequently, the Brac Formation, which contains Lepidocyclina-rich limestone and dolostone, was identified in the cliff faces on the eastern end of Cayman Brac (Jones et al., 1994b). Thus, the stratigraphy was amended so that the Bluff Formation becomes the "Bluff Group", which encompassed the Brac Formation, the Cayman Formation and the Pedro Castle Formation (Jones et al., 1994a, 1994b). Based on fossils and Sr isotope data, the Brac Formation, the Cayman Formation and the Pedro Castle Formation were formed in early Oligocene, middle Miocene and Pliocene, respectively (Jones et al., 1994a, 1994b).

For the ease of communication, the unconformities in the Bluff Group were initially named according to the formation that it caps (Jones and Hunter, 1994b). Thus, the Brac Unconformity denoted the upper surface of the Brac Formation, whereas the Cayman Unconformity defined the upper surface of the Cayman Formation. The Pedro Castle Unconformity is the upper surface of the Pedro Castle Formation. In each case, the unconformity may be overlain by a younger formation and/or exposed to the atmosphere.

3.2. Identification of unconformities

The unconformities in the Bluff Group are identified based on the contrast in lithology, hardness, diagenesis, and fossils between the successions above and below the unconformity being considered. The unconformity between the Brac Formation and the Cayman Formation, for example, was identified in outcrops and wells on the eastern half of Cayman Brac (Jones, 1994; Jones and Hunter, 1994a; Jones et al., 1994a; Uzelman, 2009; Zhao and Jones, 2012b), because (1) the Brac Formation is formed of limestones intermixed with fabric-destructive, coarsely crystalline and sucrosic dolostones, whereas the Cayman Formation is formed of finely crystalline, fabric-retentive dolostones (Jones and Hunter, 1994a; Jones et al., 1994a; Uzelman, 2009; Zhao and Jones, 2012b), (2) the biota in the upper part of the Brac Formation is characterized by numerous large Lepidocyclina, which are not found in the Cayman Formation (Jones, 1994; Jones and Hunter, 1994a; Jones, et al., 1994a), (3) the upper surface of the Brac Formation forms the flat roof of caves (Jones et al., 1994a; Uzelman, 2009; Zhao and Jones, 2012b), (4) there is evidence of an old spring at the boundary between the Cayman Formation and the Brac Formation, and (5) borings that penetrate the upper surface of the Brac Formation (Jones and Hunter, 1994a; Jones et al., 1994a; Uzelman, 2009).

The unconformity between the Cayman Formation and the Pedro Castle Formation has been identified in outcrops and cores on the western half of Grand Cayman and the west end of Cayman Brac (Jones and Hunter, 1989, 1994b; Jones, 1994; Jones et al., 1994a, 1994b; Wignall, 1995). The criteria used to distinguish this karst surface include (1) the fabric-retentive, finely crystalline dolostones in the Cayman Formation contrasts with the intercalated limestones and dolostones in the Pedro Castle Formation (Jones, 1994; Jones and Hunter, 1994b; Jones et al., 1994a, 1994b; Arts, 2000), (2) dolostones in the Cayman Formation are generally harder than the dolostones and limestones in the Pedro Castle Formation (Jones and Hunter, 1989, 1994b; Jones, 1994; Jones et al., 1994a; Wignall, 1995; Art, 2000; MacNeil, 2001), (3) fossils in the Cayman Formation that are different from those in the Pedro Castle Formation, as the Cayman Formation has more colonial corals and fewer free-living coral (Jones and Hunter, 1989; Jones, 1994, Jones et al., 1994a, 1994b), (4) limpid dolomite and caymanite are common in cavities in the dolostones of the Cayman Formation but rare in the limestones and dolostones of the Pedro Castle Formation (Jones and Hunter, 1989, 1994a, 1994b; Jones, 1992a, 1994; Jones et al., 1994a, 1994b), (5) borings are common on unconformity (Jones and Hunter 1989, 1994b; Jones, 1992b; Jones et al., 1994a, 1994b; Wignall, 1995), and (6) large caves, which are abundant in the Cayman Formation are rare in the Pedro Castle Formation (Jones and Hunter, 1989; Jones, 1992b, 1994a).

The unconformity between the Pedro Castle Formation and the Ironshore Formation is widely recognized in the wells that have been drilled on the western part of Grand Cayman and the west end of Cayman Brac. Its identification is based on the following facts: (1) the Pedro Castle Formation is formed of well-lithified limestones and/or dolostones that contrast sharply with the soft and friable limestones in the overlying Ironshore Formation (Jones, 1994; Jones et al., 1994b; Wignall, 1995; Vézina, 1997; Coyne, 2003; Etherington, 2004), and (2) well-preserved fossils are common in the Ironshore Formation but rare in the Pedro Castle Formation (Cerridwen, 1989; Hunter and Jones, 1990; Jones, 1990, 1994; Jones and Hunter, 1990, 1994a; Cerridwen and Jones, 1991; Jones et al., 1994a, 1994b).

3.3. Karst landforms on erosional unconformities

The topography of the unconformity between the Brac Formation and Cayman Formation is difficult to define accurately because of the paucity of wells and outcrops that include this unconformity. Nevertheless, data from the outcrop along the cliff face on the eastern end of Cayman Brac and wells KEL#1 and CRQ #1 indicate that the Brac Unconformity probably dips westward at ~0.5° (Fig. 1-3) (Jones, 1994; Jones and Hunter, 1994a; Jones et al., 1994a;

Uzelman, 2009). The highest point of the Brac Unconformity at the East End is 33 m above sea level (asl), whereas the lowest point yet found on the western end of the island is 16 m below sea level (bsl), in well BW#1. Evidence from outcrop and various wells also indicates that there is a relief of at least 25 m on this unconformity (Jones, 1994). The topography of this unconformity on Grand Cayman, however, is poorly known because (1) it is not found in any outcrops, (2) it is generally too deep to be included in most of the wells that have been drilled, (3) it has never been found in any of the cored wells.

The upper surface of the Cayman Formation is characterized by peripheral rims along the coasts that enclose an atoll-shape depression (Fig. 1-4), with it base being more than 30 m bsl under North Sound (Jones and Hunter, 1994b). Over much of the western half of Grand Cayman,

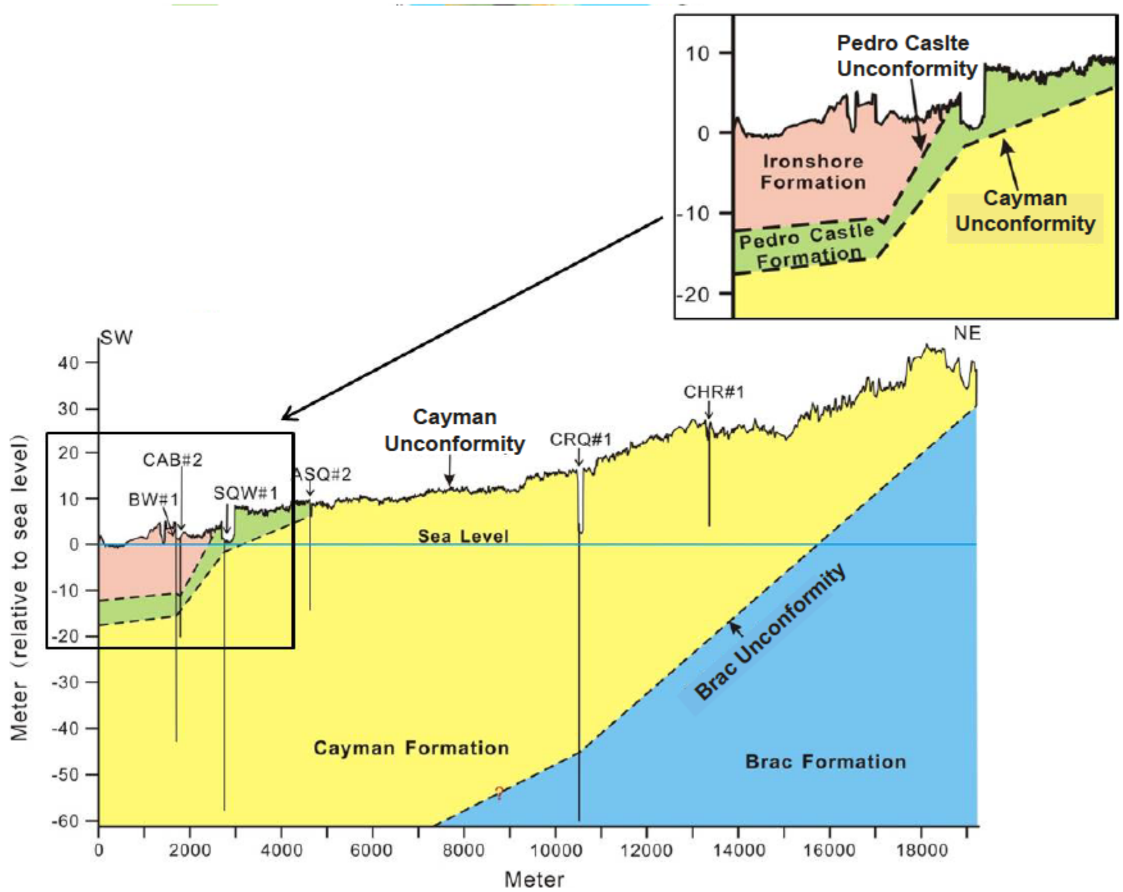

Fig. 1-3. Stratigraphic relationships between the Brac Formation, Cayman Formation, Pedro Castle Formation, and Ironshore Formation along the East-West Transect on the uplifted core of Cayman Brac (modified from Jones, 2005). See Figure 1-1C for precise locations of wells.

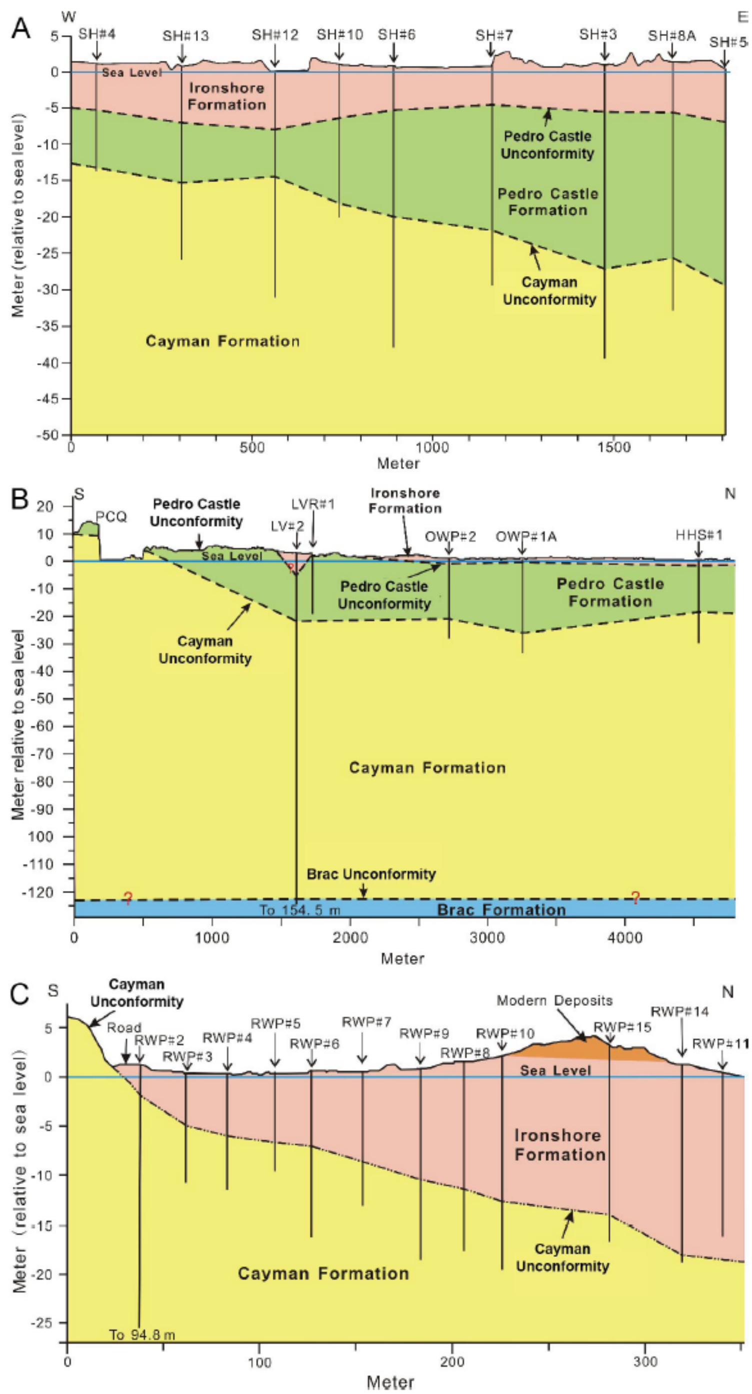

Fig. 1-4. Stratigraphic relationships between the Cayman Formation, Pedro Castle Formation and Ironshore Formation on Grand Cayman. (A) Safe Haven Transect on the western half of Grand Cayman (modified from Jones and Hunter, 1994b). See Figure 1-1B for precise locations of wells. (B) Lower Valley Transect on Grand Cayman (modified from Jones and Hunter, 1994b). See Figure 1-1B for precise locations of wells. (C) Along the Roger's Wreck Point Transect on the northeastern corner of Grand Cayman (modified from Vézina, 1997). See Figure 1-1B for precise locations of wells.

the Cayman Formation is generally below sea level and overlain by the Pedro Castle Formation, whereas over the eastern half of the island, the formation is typically above sea level and exposed to the atmosphere (Jones and Hunter, 1994b). A relief of at least 60 m for the upper surface of the Cayman Formation is obtained by comparing the peak of "The Mountain" (22 m asl) and the base of a paleo-sinkhole drilled by well QHW#1 (Jones and Hunter, 1994b).

Sinkholes, solution-widened joints, and phytokarst characterize most exposures of the Cayman Formation on the eastern part of Grand Cayman (Jones and Smith, 1988; Squair, 1988; Jones, 1989, 1992b). Numerous sinkholes, up to 10 m deep and with a diameter up to 30 m, are found on Grand Cayman (Doran, 1954; Folk et al., 1973; Jones and Smith, 1988; Jones, 1989, 1992b). Many of these sinkholes are lined with laminar rootcrete (Jones, 1992b; Alonso-Zarza and Jones, 2007). Joints, which have been solution-widened, are open, water-filled, or filled with various types of precipitates and/or sediments. Typically, the orientations of the joints are similar to the faults that define the fault blocks, indicating tectonic control (Rigby and Roberts, 1976). Nevertheless, fieldwork, satellite images, and stratigraphic maps have not revealed any evidence of tectonic displacement or folding of the strata on Grand Cayman (Der, 2012). The weathered surface of the Cayman Formation has suffered extensive phytokarst development, which is responsible for its black, honeycomb appearance (Folk et al., 1973; Jones and Smith, 1988; Jones, 1989). Pinnacles and pits are common. Pinnacles are characterized by concavities that are separated from each other by razor-sharp edges, whereas pits are irregular in shape and have straight sides (Squair, 1988).

On the uplifted core of Cayman Brac, the upper surface of the Cayman Formation is a tilted karst surface, with most of it exposed to the atmosphere (Jones et al., 1994b; Jones, 2005). A relief of 62 m is obtained if the exposed Cayman Formation on East End (46 m asl) is compared with the position of the lower boundary found in well BW#1 (16 m bsl). However, the heavy tropical vegetation found on Cayman Brac hinders a detailed assessment of the karst features. Nevertheless, large-scale positive karst features, such as tower karst, which characterize many tropical karst landscapes, are not found on Grand Cayman and Cayman Brac.

3.4. Sinkhole (joints)-filling deposits

Karst features, such as sinkholes and joints, are common sites for deposition of sediments and precipitation of various minerals, which may contain geological information that cannot be obtained from other sources (Smart et al., 1988; Jones, 1992b; Miller et al., 2012). On Grand Cayman, many of the sinkholes contain a wide array of sinkhole-filling deposits, including rootcrete, terra rossa, and breccias formed of limestone and dolostone lithoclasts held in limestone matrices (Jones and Smith, 1988; Jones, 1989, 1992b; Alonso-Zarza and Jones, 2007). The lack of dolomitization or dolomite development in the breccias indicates these fills post date the last phase of dolomitization (Jones and Smith, 1988; Jones, 1992b). In addition, the petrographic features in those sinkhole-filling deposits show that they were different in terms of provenances and ages (Jones and Smith, 1988; Jones, 1992b).

4. Objectives

Various studies have focused attention on different aspects of the unconformities found on Grand Cayman and Cayman Brac. On Grand Cayman, for example, the Cayman Unconformity has been studied, with emphasis being placed on its topography (Jones and Hunter, 1994b), karst features (Jones and Smith, 1988; Squair, 1988), and cavity-filling deposits (Jones, 1992b). On Cayman Brac, in contrast, the unconformities have received little attention because of limited data (Jones, 1994; Jones and Hunter, 1994a). Over the last ten years, numerous wells have been drilled on Cayman Brac and the eastern half of Grand Cayman. Data from these wells make it possible to define the attitude of the buried unconformities on Grand Cayman and Cayman Brac. Furthermore, the production of DEMs and deciphering of the karst landscapes in inaccessible areas provides additional information on the nature of these unconformities and exposed surfaces. Although sinkhole-filling deposits on these two islands are widespread (Jones and Smith, 1988; Jones, 1992b), their petrographic and geochemical properties have never been examined.

The main objectives of this thesis, which is focused on the unconformities within the Tertiary succession found on Grand Cayman and Cayman Brac, are as follows:

- Delineation of the factors that controlled development of the topography on the erosional unconformities on Grand Cayman and Cayman Brac, with a focus on the role exerted by uplift versus eustatic sea-level changes. Given that the topography of the unconformities dictates the thickness of a carbonate formation, these factors are important in stratigraphic architecture.

- Deciphering and comparing the karst forms developed on the exposed dolostones of the Cayman Formation on Grand Cayman and Cayman Brac. In doing so, the factors controlling the development of various karst forms, especially uplift versus eustatic sea-level changes, can be deciphered.
- Assessment of the possibility that petrographic and geochemical attributes (i.e., isotopes and rare earth elements) in sinkhole-filling deposits can be used to reveal a marine or non-marine provenance. In so doing, the paleo-environment that existed during a period when the erosional unconformities developed can be reconstructed.

This thesis is presented in a paper-based format. The second and the forth chapters have been published in a peer-reviewed journal.

Chapter Two: This chapter improves the criteria that are used to identify the unconformities in the carbonate sequences of the Cayman Islands. By using these criteria, the positions of the unconformities can be located in wells and outcrops. These scattered data, together with the topographic data on the exposure strata obtained from DEMs, generated interpolated surfaces that show the topographic features associated with the unconformities. These topographic features are explained in terms of the changes in sea level, tectonic movement, and/or coastal erosion. Most importantly, by comparison of unconformities between Grand Cayman and Cayman Brac, this paper examine the roles that tectonic uplift and changes in sea level play in the topographic development of weathering surfaces.

Published as: Liang, T. and Jones, B., 2014. Deciphering the impact of sea-level changes and tectonic movement on erosional sequence boundaries in carbonate successions: A case study from Tertiary strata on Grand Cayman and Cayman Brac, British West Indies. Sedimentary Geology 305, 17-34.

Chapter Three: This chapter uses DEMs, together with field observation, to examine various karst forms developed on the exposed Cayman Formation on Grand Cayman and Cayman Brac. In so doing, the factors that control the development of karst landforms are examined. In particular, comparison of karst landforms between the two islands allows the evaluation of the effects of tectonic movements as opposed to eustatic sea-level changes. The results demonstrate that the landforms on these two islands reflect the interplay between the drop of sea level, climate, tectonic movements, and phytokarst development.

In submission as: Liang, T. and Jones, B., 2015. Ongoing, long-term evolution of an unconformity that originated as a karstic surface in the Late Miocene: A case study from the Cayman Islands, British West Indies. Sedimentary Geology.

Chapter Four: This chapter focuses on various sinkhole-filling deposits associated with the exposed surface of the Cayman Formation on Grand Cayman and Cayman Brac, and documents their petrographic features, stable isotope, and trace elements (i.e., Al, Fe, Mn, Y, and REE). In so doing, the processes that take place during a period when an erosional unconformity is developing are unraveled. Most importantly, this study shows that REE signatures in carbonate deposits can be used to "fingerprint" deposits and determine if they have a marine or non-marine provenance.

Published as: Liang, T. and Jones, B., 2015. Petrographic and geochemical features of sinkhole-filling deposits associated with an erosional unconformity on Grand Cayman. Sedimentary Geology 315, 64-82.

Chapter Five: This chapter summarizes the all of the conclusions that have been reached from the study.

References

Alonso-Zarza, A.M., Jones, B., 2007. Root calcrete formation on Quaternary karstic surfaces of Grand Cayman. Geologica Acta 5, 77-88.

Alonso-Zarza, A.M., Wright, V.P., 2010. Calcretes. In: Alonso-Zarza, A.M., Tanner, L.H. (Eds.), Developments in Sedimentology. Elsevier, Oxford, pp. 225-267.

Arts, A.E., 2000. Sedimentology and stratigraphy of the Pedro Castle Formation, SW Grand Cayman, British West Indies. Unpublished M.Sc. Thesis, University of Alberta, Canada, 107 pp.

Budd, D.A., Saller, A.H., Harris, P.M. (Eds), 1995. Unconformities and porosity in carbonate strata. American Association of Petroleum Geologists Memoir 63, 313 pp.

Budd, D.A., Gaswirth, S.B., Oliver, W.L., 2002. Quantification of macroscopic sub-aerial exposure features in carbonate rocks. Journal of Sedimentary Research 72, 917-928.

Burke, K., 1988. Tectonic evolution of the Caribbean. Annual Review of Earth and Planetary Sciences 16, 201-231.

Calais, E., Mercier de Lépinay, B., 1995. Strike-slip tectonic processes in the northern Caribbean between Cuba and Hispaniola (Windward Passage). Marine Geophysical Researches 17, 63-95.

Cerridwen, S.A., 1989. Paleoecology of Pleistocenemollusca fromthe Ironshore Formation, Grand Cayman, B.W.I. Unpublished M.Sc. Thesis, University of Alberta, Canada, 271 pp.

Cerridwen, S.A., Jones, B., 1991. Distribution of bivalves and gastropods in the Pleistocene Ironshore Formation, Grand Cayman, British West Indies. Caribbean Journal of Science 27, 97-116.

Choquette, P.W., James, N.P., 1988. Introduction. In: James, N.P., Choquette, P.W. (Eds.), Paleokarst. Springer-Verlag, Berlin, Germany, pp. 1-21.

Clari, P.A., Dela Pierre, F., Martire, L., 1995. Discontinuities in carbonate successions; identification, interpretation and classification of some Italian examples. Sedimentary Geology 100, 97-121.

Coyne, M.K., 2003. Transgressive-regressive cycles in the Ironshore Formation, Grand Cayman, British West Indies. Unpublished M.Sc. Thesis, University of Alberta, Canada, 98 pp.

Coyne, M.K., Jones, B., Ford, D., 2007. Highstands during Marine Isotope Stage 5: evidence from the Ironshore Formation of Grand Cayman, British West Indies. Quaternary Science Reviews 26, 536-559.

Der, A.J., 2012. Deposition and sea level fluctuations during Miocene Times, Grand Cayman, British West Indies Indies. Unpublished M.Sc. Thesis, University of Alberta, Canada, 101 pp.

Dickson, J., Saller, A.H., 1995. Identification of subaerial exposure surfaces and porosity preservation in Pennsylvanian and lower Permian shelf limestones, eastern Central Basin Platform, Texas. In: Budd, D.A., Saller, A.H., Harris, P.M. (Eds.), Unconformities in carbonate strata-their recognition and the significance of associated porosity. American Association of Petroleum Geologists Memoir 57, pp. 239-257.

Doran, E., 1954. Landforms of Grand Cayman, British West Indies. Texas Journal of Science 6, 360-377.

Esteban, M., Klappa, C.F., 1983. Subaerial exposure environment. In: Scholle, P.A., Bebout, D.G., Moore, C.H. (Eds.), Carbonate Depositional Environments. American Association of Petroleum Geologists, Memoir 33. American Association of Petroleum Geologists, Tulsa, United States, pp. 1-54.

Etherington, D., 2004. Sedimentology and depositional architecture of the Cayman (Miocene) and Pedro Castle (Pliocene) Formations on Western Grand Cayman, British West Indies. Unpublished M.Sc. Thesis, University of Alberta, Canada, 122 pp.

Folk, R.L., Roberts, H.H., Moore, C.H., 1973. Black phytokarst from Hell, Cayman Islands, British West Indies. Geological Society of America Bulletin 84, 2351-2360.

Ford, D., Williams, P.W., 2007. Karst Hydrogeology and Geomorphology. Wiley, United Kingdom, 562 pp.

Frisia, S., Borsato, A., 2010. Karst. In: Alonso-Zarza, A.M., Tanner, L.H. (Eds.), Carbonates in Continental Settings: Facies, Environments and Processes. Developments in Sedimentology.

Elsevier, Oxford, pp. 269-318.

Goldstein, R.H., 1988, Cement stratigraphy of Pennsylvanian Holder Formation, Sacramento Mountains, New Mexico. American Association of Petroleum Geologists Bulletin 72, 425-438.

Hillgärtner, H., 1998. Discontinuity surfaces on a shallow-marine carbonate platform (Berriasian, Valanginian, France and Switzerland). Journal of Sedimentary Research 68, 1093-1108.

Horsfield, W.T., 1975. Quaternary vertical movements in the Greater Antilles. Geological Society of America Bulletin 86, 933-938.

Hunter, I.G., Jones, B., 1990. Sedimentology of the late Pleistocene Ironshore Formation on Grand Cayman. In: Larue, D.K., Draper, G. (Eds.), Transactions of the 12th Caribbean Geological Conference. 12th Caribbean Geological Conference, Virgin Islands, United States, pp. 104-114.

Iturralde-Vinent, M.A., 1994. Cuban Geology: A New Plate-Tectonic Synthesis. Journal of Petroleum Geology 17, 39-70.

Iturralde-Vinent, M.A., 2006. Meso-Cenozoic Caribbean paleogeography: implications for the historical biogeography of the region. International Geology Review 48, 791-827.

Iturralde-Vinent, M.A., Macphee, R.D.E., 1999. Paleogeography of the Caribbean region: implications for Cenozoic biogeography. Bulletin of the American Museum of Natural History 238, 1-95.

James, N.P., Choquette, P.W., 1988. Palaeokarst. Springer Verlag, Berlin, 416 pp.

Jones, B., 1989. The role of micro-organisms in phytokarst development on dolostones and limestones, Grand Cayman, British West Indies. Canadian Journal of Earth Sciences 26, 2204-2213.

Jones, B., 1990. Tunicate spicules and their syntaxial overgrowths: examples from the Pleistocene Ironshore Formation, Grand Cayman, British West Indies. Canadian Journal of Earth Sciences 27, 525-532.

Jones, B., 1992a. Caymanite, a cavity-filling deposit in the Oligocene-Miocene Bluff Formation of the Cayman Islands. Canadian Journal of Earth Sciences 29, 720-736.

Jones, B., 1992b. Void-filling deposits in karst terrains of isolated oceanic islands: a case study from Tertiary carbonates of the Cayman Islands. Sedimentology 39, 857-876.

Jones, B., 1994. Geology of the Cayman Islands. In: Brunt, M.A., Davies, J.E. (Eds.), The Cayman Islands: Natural History and Biogeography. Kluwer, Dordrecht, The Netherlands, pp. 13-49.

Jones, B., 2005. Dolomite crystal architecture: genetic implications for the origin of the Tertiary dolostones of the Cayman Islands. Journal of Sedimentary Research 75, 177-189.

Jones, B., Hunter, I.G., 1989. The Oligocene-Miocene Bluff Formation on Grand Cayman. Caribbean Journal of Science 25, 71-85.

Jones, B., Hunter, I.G., 1990. Pleistocene paleogeography and sea levels on the Cayman Islands, British West Indies. Coral Reefs 9, 81-91.

Jones, B., Hunter, I.G., 1994a. Evolution of an isolated carbonate bank during Oligocene, Miocene and Pliocene Times, Cayman Brac, British West Indies. Facies 30, 25-50.

Jones, B., Hunter, I.G., 1994b. Messinian (Late Miocene) karst on Grand Cayman, British Indies: an example of an erosional sequence boundary. Journal of Sedimentary Research 64, 531-541.

Jones, B., Hunter, I.G., Kyser, T.K., 1994a. Revised stratigraphic nomenclature for Teriary strata of the Cayman Islands, British West Indies. Caribbean Journal of Science 30, 53-68.

Jones, B., Hunter, I.G., Kyser, T.K., 1994b. Stratigraphy of the Bluff Foramtion (Miocene-Pliocene) and the newly defined Brac Formation (Oligocene), Cayman Brac, British West Indies. Caribbean Journal of Science 30, 30-51.

Jones, B., Lockhart, E., Squair, C., 1984. Phreatic and vadose cements in the Tertiary Bluff Formation of Grand Cayman Island, British West Indies. Bulletin of Canadian Petroleum Geology 32, 382-397.

Jones, B., Luth, R.W., 2003. Temporal evolution of Tertiary dolostones on Grand Cayman as determined by $^{87}Sr/^{86}Sr$. Journal of Sedimentary Research 73, 187-205.

Jones, B., Smith, D.S., 1988. Open and filled karst features on the Cayman Islands: implications for the recognition of paleokarst. Canadian Journal of Earth Sciences 25, 1277-1291.

Leroy, S., Mauffret, A., Patriat, P., Mercier de Lépinay, B., 2000. An alternative interpretation of the Cayman Trough evolution from a reidentification of magnetic anomalies. Geophysics Journal International 141, 539-557.

MacDonald, K.C., Holcombe, T.L., 1978. Inversion of magnetic anomalies and sea-floor spreading in the Cayman Trough. Earth and Planetary Science Letters 40, 407-414.

MacNeil, A., 2001. Sedimentology, diagenesis, and dolomitization of the Pedro Castle Formation on the Cayman Brac, British West Indies. Unpublished M.Sc. Thesis, University of Alberta, Canada, 128 pp.

Matley, C.A., 1926. The geology of the Cayman Islands (British West Indies) and their relation to the Bartlett Trough. Quarterly Journal of the Geological Society of London 82, 352-387.

Mattson, P.H., 1984. Caribbean Structural Breaks And Plate Movements. Geological Society of America 162, 131-152.

McCrea, J.M., 1950. On the isotopic chemistry of carbonates and a paleotemperature scale. The Journal of Chemical Physics 18, 849-857.

Miller, C.R., James, N.P., Bone, Y., 2012. Prolonged carbonate diagenesis under an evolving late Cenozoic climate: Nullarbor Plain, southern Australia. Sedimentary Geology 261-262, 33-49.

Perfit, M.R., 1977. Petrology and geochemistry of mafic rocks from the Cayman Trench evidence for spreading. Geology 5, 105-110.

Perfit, M.R., Heezen, B.C., 1978. The geology and evolution of the Cayman Trench. Geological Society of America Bulletin 89, 1155-1174.

Pindell, J.L., 1991. Geologica rationale for hydrocarbon exploration in the Caribbean and adjacent regions. Journal of Petroleum Geology 14, 237-257.

Pindell, J.L., Cande, S.C., Pitman, W.C., Rowley, D, Dewey, J, LaBrecque, J, Haxby, W, 1988. A plate-kinematic framework for models of Caribbean evolution. Tetonophysics 155, 121-138.

Pindell, J.L., Kennan, L., 2009. Tectonic evolution of the Gulf of Mexico, Caribbean and northern South America in the mantle reference frame: an update. Geological Society of

London Special Publications 328, 1-55.

Pleydell, S.M., 1987. Aspects of diagenesis and ichnology in the Oligocene-Miocene Bluff Formation of Grand Cayman Island, British West Indies. Unpublished Master Thesis, University of Alberta, 209 pp.

Purdy, E.G., Waltham, D., 1999. Reservoir implication of modern karst topography. American Association of Petroleum Geologists Bulletin 83, 1774-1794.

Rankey, E.C., 1997, Relations between relative changes in sea level and climate shifts: Pennsylvanian-Permian mixed carbonate–siliciclastic strata, western United States. Geological Society of America Bulletin 109, 1089-1100.

Rigby, J.K., Roberts, H.H., 1976. Geology, reefs and marine communities of Grand Cayman, British West Indies. In: Roberts, J.K., Roberts, H.H. (Eds.), Grand Cayman: geology, sediments, and marine communities. Brigham Young University, Geology Studies, Special Publication 4, pp. 1-95.

Rojas-Agramonte, Y., Neubauer, F., Handler, R., Garcia-Delgado, D.E., Friedl, G., Delgado-Damas, R., 2005. Variation of palaeostress patterns along the Oriente transform wrench corridor, Cuba: significance for Neogene–Quaternary tectonics of the Caribbean realm. Tectonophysics 396, 161-180.

Rosencrantz, E., Sclater, J.G., 1986. Depth and age in the Cayman Trough. Earth and Planetary Science Letters 79, 133-144.

Ross, M.I., Scotese, C.R., 1988. A hierarchical tectonic model of the gulf of Mexico and Caribbean region. Tectonophysics 155, 139-168.

Saller, A.H., Budd, D.A., Harris, P.M., 1994. Unconformities and porosity development in carbonate strata: Ideas from a Hedberg Conference. American Association of Petroleum Geologists Bulletin 78, 857-872.

Saller, A.H., Dickson, J.A.D., Matsuda, F., 1999. Evolution and distribution of porosity associated with sub-aerial exposure in upper Palaeozoic platform limestones, West Texas. American Association of Petroleum Geologists Bulletin 83, 1835-1844.

Sattler, U., Immenhauser, A., Hillgaertner, H., Esteban,M., 2005. Characterization, lateral variability and lateral extent of discontinuity surfaces on a carbonate platform (Barremian to lower Aptian, Oman). Sedimentology 52, 339-361.

Smart, P.L., Palmer, R.J., Whitaker, F., Wright, V.P., 1988. Neptunian dikes and fissure fills: an overview and account of some modern examples. In: James, N.P., Choquette, P.W. (Eds.), Paleokarst. Springer-Verlag, New York, pp. 149-163.

Smith, L.B., JR., Read, J.F., 1999, Application of high-resolution sequence stratigraphy to tidally influenced upper Mississippian carbonates, Illinois Basin. In: Harris, P.M., Saller, A.H., and Simo, J.A. (Eds.), Advances in Carbonate Sequence Stratigraphy: Applications to Reservoirs, Outcrops and Models. Society for Sedimentary Geology-Special Publication 63, pp. 107-126.

Squair, C.A., 1988. Surface karst on Grand Cayman Island, British West Indies. Unpublished M.Sc. Thesis, University of Alberta, Canada, 107 pp.

Stoddart, D.R., 1980. Geology and geomorphology of Little Cayman. Atoll Research Bulletin 241, 11-16.

Tucker, M., 1990. Diagenetic processes, products and environments. In: Tucker, M.E., Wright, V.P., Dickson, J.A.D. (Eds.), Carbonate Sedimentology. Blackwell Scientific Publications, Oxford, pp. 314-364.

Uzelman, B.C., 2009. Sedimentology, diagenesis, and dolomitization of the Brac Formation (Lower Oligocene), Cayman Brac, British West Indies. Unpublished M.Sc. Thesis, University of Alberta, Canada, 120 pp.

Vézina J.V., 1997. Stratigraphy and sedimentology of the Pleistocene Ironshore Formation at Rogers Wreck Point, Grand Cayman: a 400 Ka Record of Sea-level Highstands. Unpublished M.Sc. Thesis, University of Alberta, Canada, 131 pp.

Vézina, J.V., Jones, B., Ford, D.C., 1999. Sea-level highstands over the last 500,000 years: evidence from the Ironshore Formation on Grand Cayman, British West Indies. Journal of Sedimentary Research 69, 317-327.

Weidlich, O., 2010. Meteoric diagenesis in carbonates below karst unconformities: heterogeneity and control factors. In: Van Buchem, F.S.P., Gerdes, K.D., Esteban, M. (Eds.), Mesozoic and Cenozoic Carbonate Systems of the Mediterranean and the Middle East: Stratigraphic and Diagenetic Reference Models. Geological Society of London, Special Publications 329, pp. 291-315.

Whitaker, F., Smart, P., Hague, Y., Waltham, D., Bosence, D., 1999. Structure and function of a coupled two-dimensional diagenetic and sedimentological model of carbonate platform evolution. Society for Sedimentary Geology- Special Publication 62, 337-355.

Wignall, B.D., 1995. Sedimentology and diagenesis of the Cayman (Miocene) and Pedro Castle (Pliocene) Formations at Safe Haven, Grand Cayman, British West Indies. Unpublished M.Sc. Thesis, University of Alberta, Canada, 110 pp.

Wright, V.P., Smart, P.L., 1994. Paleokarst (dissolution diagenesis): Its Occurrence and hydrocarbon exploration significance. In: Wolf, K.H., Chilingarian, G.V. (Eds.), Developments in Sedimentology 51- Diagenesis IV. Elsevier Science, Amsterdam, pp. 477-517.

Zhao, H.W., Jones, B., 2012a. Origin of "Island Dolostones": a case study from the Cayman Formation (Miocene), Cayman Brac, British West Indies. Sedimentary Geology 243-244, 191-206.

Zhao, H.W., Jones, B., 2012b. Genesis of fabric-destructive dolostones: a case study of the Brac Formation (Oligocene), Cayman Brac, British West Indies. Sedimentary Geology 267-268, 36-54.

Zhao, H.W., Jones, B., 2013. Distribution and interpretation of rare earth elements and yttrium in Cenozoic dolostones and limestones on Cayman Brac, British West Indies. Sedimentary Geology 284-285, 26-38.

CHAPTER 2: DECIPHERING THE IMPACT OF SEA-LEVEL CHANGES AND TECTONIC MOVEMENT ON EROSIONAL SEQUENCE BOUNDARIES IN CARBONATE SUCCESSIONS: A CASE STUDY FROM TERTIARY STRATA ON GRAND CAYMAN AND CAYMAN BRAC, BRITISH WEST INDIES [1]

1. Introduction

The stratigraphic architecture of carbonate successions on isolated oceanic islands reflects the balance between deposition that takes place during sea-level highstands and erosion that takes place during sea-level lowstands (Choquette and James, 1988; Esteban, 1991; Mylroie and Carew, 1995). Thus, the three-dimensional geometry of a formation on such islands is controlled, to a large extent, by the topographies of the bounding unconformities. This is especially true if the relief on those unconformities is high when compared to the thickness of the formation. Although a variety of factors, such as the duration of exposure, climate, bedrock type, paleohydrology, paleotopography, and vegetation, may affect the development of an unconformity (Wright, 1982, 1996; Esteban and Klappa, 1983; Wright and Smart, 1994; Saller et al., 1994, 1999; Budd et al., 2002; Weidlich, 2010), it has long been recognized that eustatic changes in sea level and tectonic movements are the key factors in their development (Choquette and James, 1988). Identifying the impact of eustasy as opposed to tectonism on unconformity development is, however, commonly problematic because both processes can produce exactly the same effects (Choquette and James, 1988; Budd et al., 1995; Dickinson et al., 2002).

Grand Cayman and Cayman Brac, British West Indies, are ideal for examining this issue. Within 150 km of each other (Fig. 2-1), these isolated islands have experienced the same eustatic changes, climate, and depositional conditions from the Oligocene to present. Grand Cayman and Cayman Brac are, however, located on different fault blocks that have different tectonic histories (Horsfield, 1975; Stoddart, 1980; Jones and Hunter, 1990; Vézina et al., 1999;

1 This chapter was published as: Liang, T., Jones, B., 2014. Deciphering the impact of sea-level changes and tectonic movement on erosional sequence boundaries in carbonate successions: A case study from Tertiary strata on Grand Cayman and Cayman Brac, British West Indies. Sedimentary Geology 305, 17-34.

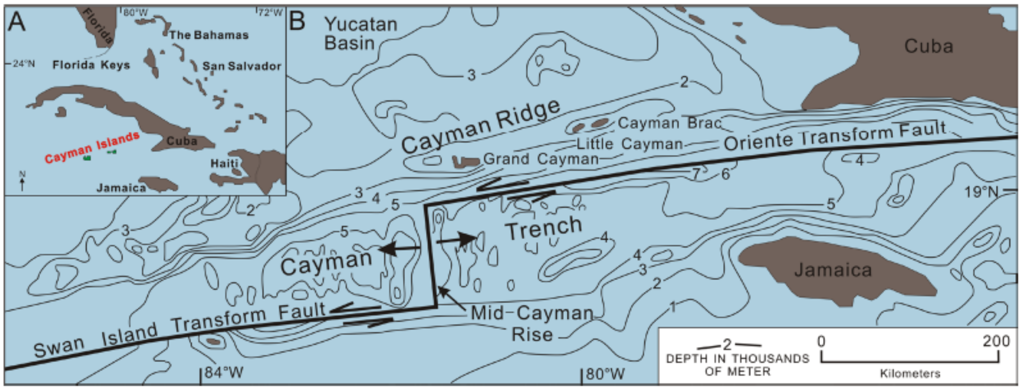

Fig. 2-1. (A) Location of Cayman Islands; (B) Locations of Grand Cayman and Cayman Brac relative to the Mid-Cayman Rise, the Cayman Trench, and the Oriente Transform Fault (Modified from Jones, 1994, and based on maps from Perfit and Heezen, 1978, and MacDonald and Holcombe, 1978).

Coyne et al., 2007). Grand Cayman, with flat-lying strata, is a low-lying island that appears to have experienced little, if any, tectonic movement. In contrast, Cayman Brac, which rises up to 46 m above sea level (asl) at its east end, with the strata dipping gently to the southwest, has been tectonically tilted. By comparing the stratigraphic architectures of these two islands, the impact of tectonics can be separated from the impacts of eustasy on the development of the unconformities found in in the Oligocene to Pleistocene successions. Thus, this paper (1) delineates the topography of each unconformity on Grand Cayman and Cayman Brac, (2) compares the topographic features of each unconformity on each island, (3) illustrates the stratigraphic architectures dictated primarily by eustatic sea-level changes, and (4) identifies the influences of local tectonic activity on subaerially-formed unconformities.

2. Methods

The present-day topographies of Grand Cayman and Cayman Brac are illustrated by using digital elevation models (DEMs) developed from data provided by the Lands and Survey Department, Government of the Cayman Islands. The DEM, with a grid resolution of 3 m, used the Universal Transverse Mercator (UTM) projection system and the North American Datum of 1927. The elevation information, including the heights and profile graphs, were obtained through spatial analyst tools provided in ArcGIS 10 software.

Over the last 30 years, 97 wells on Grand Cayman and 15 wells on Cayman Brac have been drilled and sampled. On Grand Cayman, these wells yielded cores (54 wells), a mixture of cores and well cuttings (8 wells), or well cuttings (35 wells) with each sample being collected over an interval of 0.8 m. On Cayman Brac, well cuttings (15 wells) collected over 0.8 m intervals are the only samples available. Collectively, these samples, accompanied with outcrops, allow analysis of the sequences and delineation of the unconformities between different formations. The spatial architectures of these unconformities were interpolated from the scattered wells and outcrops by using the kriging method, according to a spherical semi-variogram model. This procedure was done by the 3D Surface extension of Surfer 10 software.

3. Geologic setting

Grand Cayman and Cayman Brac are located on the Cayman Ridge (Jones, 1994; Vézina et al., 1999), which parallels the Oriente Transform Fault that separates the Caribbean Plate from the North American Plate (Perfit and Heezen, 1978; Fig. 2-1). The Oriente Transform Fault extends eastward from the north end of the Mid-Cayman Rise, which is an active spreading center, whereas the Swan Island Transform Fault extends westward from the south end of the Mid-Cayman Rise (MacDonald and Holcombe, 1978). The Cayman Trench (Fig. 2-1B), with its northern margin defined by the Oriente Transform Fault, is a pull-apart basin, with the depths up to 7686 m.

Between the Late Eocene and Oligocene, the Oriente Transform Fault detached Grand Cayman and Cayman Brac from their parent arc and transported them to their present locations (Iturralde-Vinent, 1994; Calais and Mercier de Lépinay, 1995). Since the early Middle Miocene, localized extensional features began to form (Iturralde-Vinent and Macphee, 1999; Iturralde-Vinent, 2006), resulting in Cayman Brac being on a different fault block than Grand Cayman (Matley, 1926; Horsfield, 1975; Stoddart, 1980; Vézina et al., 1999). After the Late Miocene (7.25 Ma using the time scale of Gradstein et al., 2012, their Fig. 1.2), Cayman Brac experienced tectonic tilting until about 125 ka. In contrast, Grand Cayman appears to have remained tectonically stable (Jones and Hunter, 1990; Vézina et al., 1999; Zhao and Jones, 2012a, 2013).

Matley (1926) originally assigned the Tertiary strata of the Cayman Islands to the Bluff Limestone. Jones et al. (1994a, 1994b) subsequently renamed the succession as the Bluff Group with the constituent formations being the unconformity bounded Brac Formation (Lower Oligocene), Cayman Formation (Middle Miocene), and Pedro Castle Formation (Pliocene). The Ironshore Formation (Pleistocene) unconformably overlies the Bluff Group (Fig. 2-2). The Brac Formation, exposed only on Cayman Brac, is formed of limestones that are locally replaced by coarsely crystalline, fabric-destructive dolomite (Jones and Hunter, 1994a; Uzelman, 2009; Zhao and Jones, 2012b). The bioclastic wackestones to grainstones included numerous large Lepidocyclina along with fewer small foraminifera, red algae, echinoid plates, gastropods, and bivalves but only scattered corals (*Porites*). Jones and Hunter (1994a) suggested that these facies developed in low to moderate energy conditions on a shallow carbonate bank. The Cayman Formation is formed largely of finely crystalline, fabric retentive dolostones (Jones, 1994). On the east central part of Grand Cayman, however, limestones and dolomitic limestones dominate the succession. The mudstones to grainstones in this formation includes numerous hemispherical and branching corals, bivalves, gastropods, red algae, foraminifera, Halimeda, and rhodoliths (Jones, 1994; Jones and Hunter, 1994a; Wignall, 1995; Der, 2012). The Pedro Castle Formation is formed of limestones and finely crystalline, fabric-retentive dolostones and includes facies like those in the Cayman Formation (Jones, 1994; Jones and Hunter, 1994a; Wignall, 1995; Arts, 2000; MacNeil, 2001). The sediments that now form the Cayman Formation and Pedro Castle Formation accumulated in low to moderate energy conditions on a bank in water that was 0 to 30 m deep (Jones and Hunter, 1994a). Although corals are common in both formations, no reefs have been found. The Ironshore Formation is formed of limestones that contain numerous, well-preserved corals, bivalves, and gastropods and formed in shallow water conditions (Jones, 1994; Coyne, 2003; Vézina, 1997; Vézina et al., 1999). Reefs are present in the Ironshore Formation. Dolomitization of the Bluff Group, which involved two and possibly three phases of dolomitization that took place during the Late Miocene, Late Pliocene, and possibly the early Pleistocene, was mediated by normal seawater-like fluids under near surface conditions (Jones

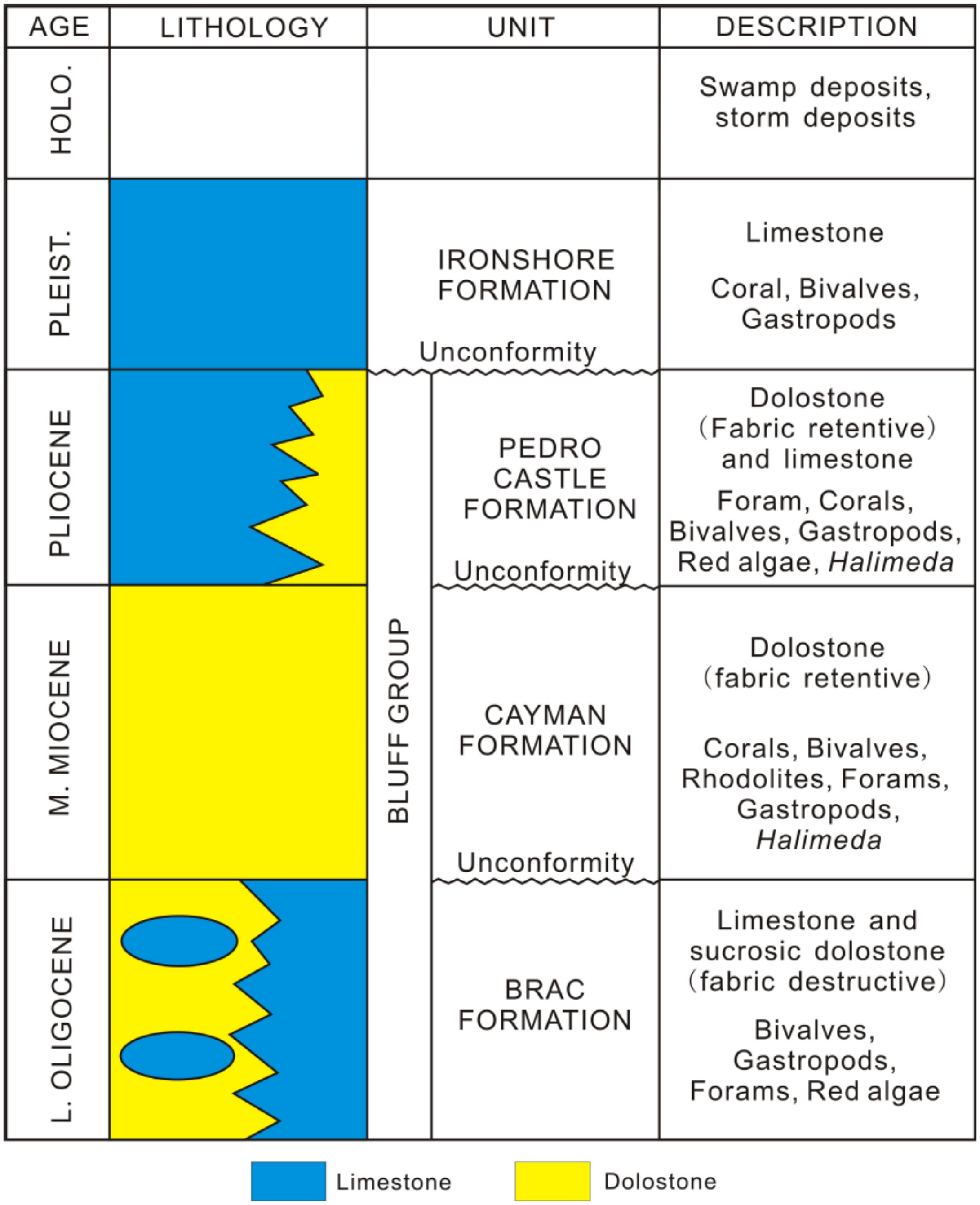

Fig. 2-2. Stratigraphic succession of the Cayman Islands (modified from Jones, 1994) showing lithology and dominant biota of each unit.

and Luth, 2003; MacNeil and Jones, 2003; Zhao and Jones, 2012a, 2012b).

4. Unconformities

The lack of an accepted convention for the labeling and/or naming unconformities hinders the discussion of successions, like that on the Cayman Islands, that includes numerous unconformities. Conceptually, unconformities in the Tertiary succession of the Cayman Islands can be named according to various protocols as follows, each of which has its own advantages and disadvantages.

1) Named according to the formation that they cap. The Cayman Unconformity was originally named because it delineated the upper boundary of the Cayman Formation and separated it from the overlying Pedro Castle Formation (Jones and Hunter, 1994b). This approach, however, masks situations where the unconformity has experienced multiple phases of erosion. On many parts of the Cayman Islands, for example, the Cayman Formation is overlain by limestones of the Ironshore Formation or is exposed at the surface where it is being actively weathered today.

2) Named according to their time of formation. Although this approach is perhaps the most informative from a time perspective, it is difficult to use in practice because it relies on accurate knowledge of the age of each formation and the evolution of the succession. On the Cayman Islands, this issue is compounded by the difficulty in precisely dating the formations and that the unconformities are time transgressive.

3) Named according to the formations below and above the unconformity. This is the easiest approach because it reflects the formations found below and above an unconformity at a particular locality. This approach also provides inferences regarding the minimum length of time represented by the unconformity at a particular locality.

Herein, an unconformity at a particular locality is named according to option 3. For example, the Brac-Cayman Unconformity (B-C Unconformity) separates the Brac Formation from the overlying Cayman Formation, whereas the Cayman-Pedro Castle Unconformity (C-P Unconformity) is the boundary between the Cayman Formation and the Pedro Castle Formation. Similarly, the Pedro Castle-Ironshore Unconformity (P-I Unconformity) is the unconformity separating the Pedro Castle Formation from the overlying Ironshore Formation. In contrast, the Cayman-Ironshore Unconformity (C-I Unconformity) would apply if the Ironshore Formation lies on top of the Cayman Formation. On Grand Cayman and Cayman Brac, the Cenozoic formations are commonly exposed at the surface and are therefore being actively weathered today and hence represent an unconformity that is still developing. These boundaries are designated by the name of the exposed formation and the letter W (for weathering) – for example, the C-W Unconformity indicates that the Cayman Formation is exposed at the surface.

5. Topographies of Grand Cayman and Cayman Brac

5.1. Grand Cayman

Today, most of Grand Cayman is less than 3 m asl with no surface rivers or streams (Fig. 2-3). North Sound on the western part of the island is a large lagoon that is surrounded by low-

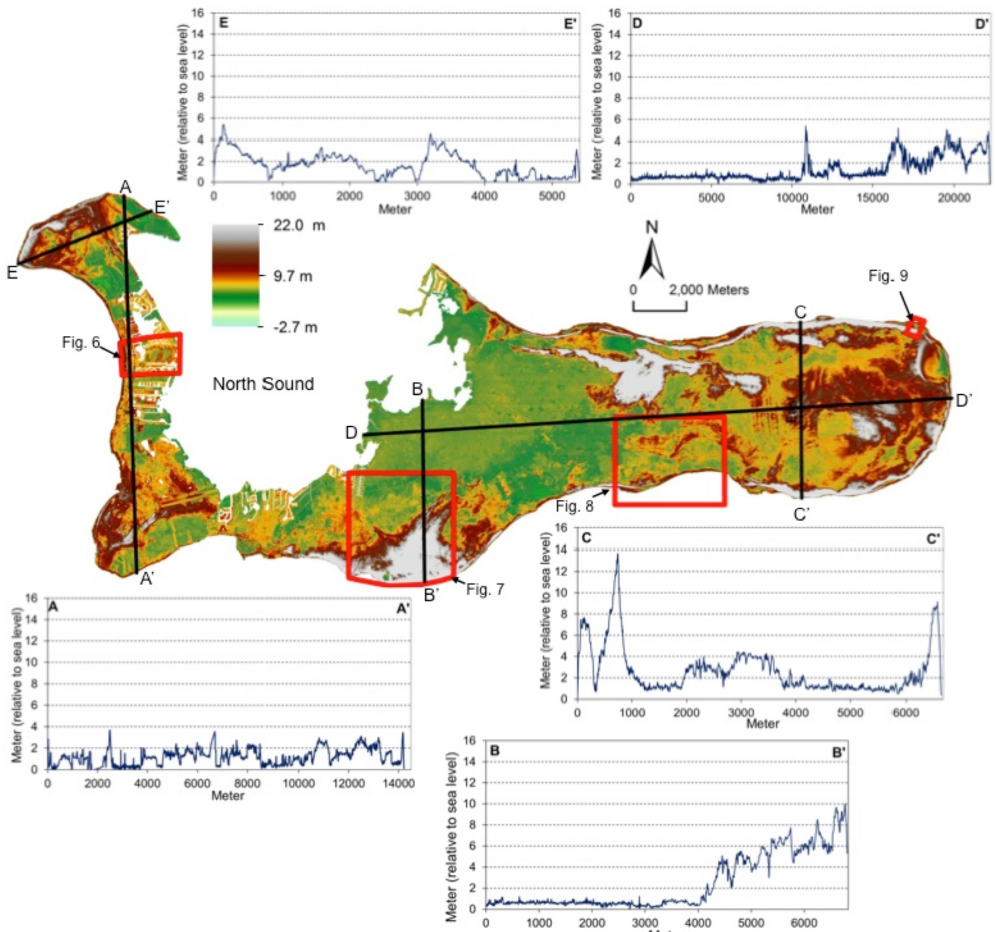

Fig. 2-3. Topography of Grand Cayman based on digital elevation modeling. The topographic transects (A-A', B-B', C-C', D-D' and E-E') show changes in elevation through Grand Cayman. Red squares label the locations of Figures 2-6, 2-7, 2-8, 2-9 on Grand Cayman.

lying land (0-1.2 m asl) and mangrove swamps. The highest land is found on the Mountain that rises up to 22 m asl, and the area around Pedro Castle where the land is up to 16.7 m asl (Fig. 2-3). A peripheral ridge (Jones and Hunter, 1994b), which rises up to 13.5 m asl, is the most dominant topographic feature on the eastern part of the island (Fig. 2-3). The interior regions over the eastern part of the island, which are lower than the peripheral ridge, are no more than 4.5 m asl (Fig. 2-3).

5.2. Cayman Brac

Cayman Brac is characterized by a central elevated core that is up to 46 m asl, which is surrounded by a narrow, low-lying platform that is typically 1-2 m asl (Fig. 2-4). There are no surface rivers or streams on this island. The surface of the core gradually rises from sea level

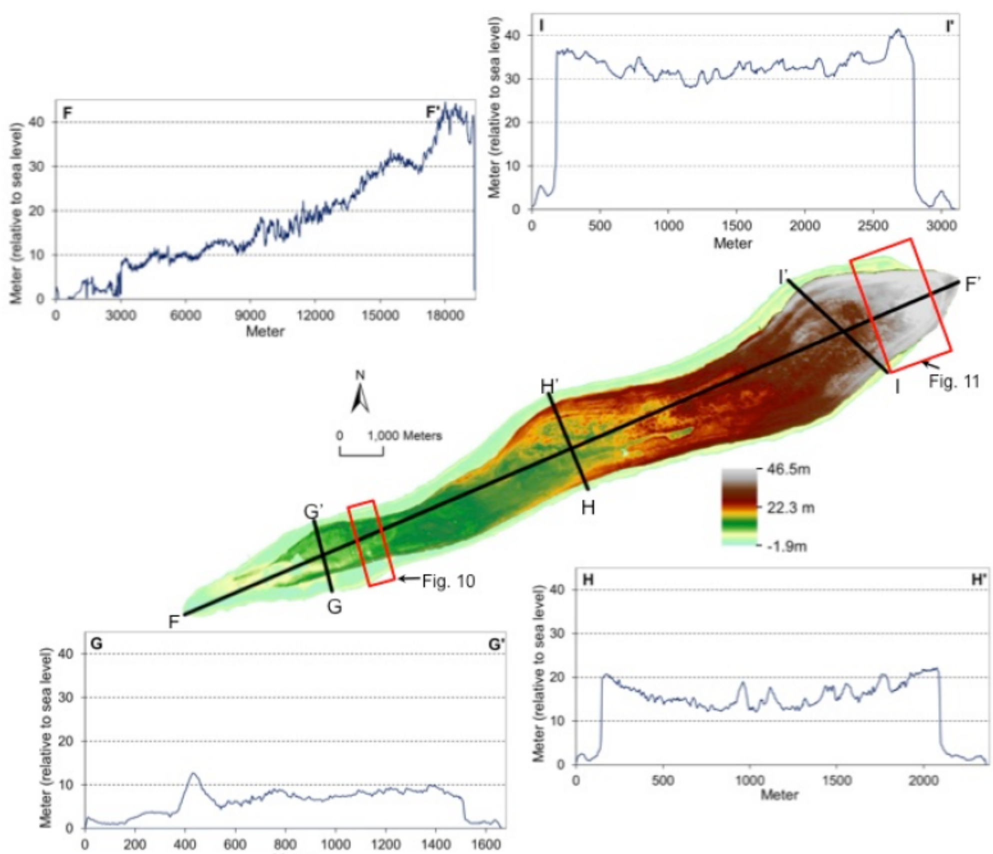

Fig. 2-4. Topography of Cayman Brac based on Digital Elevation Modeling. The topographic transects (F-F', G-G', H-H', and I-I') show changes in elevation through Cayman Brac. Red squares label the locations of Figures 2-10, 2-11 on Cayman Brac.

at its western end to 46 m asl at its eastern end (Fig. 2-4), which is characterized by vertical to overhanging cliffs. Along the NW-SE axis of the core, the interior surface is 5 to 15 m lower than the peripheral edges of the core.

6. Surface geology of Grand Cayman and Cayman Brac

6.1. Grand Cayman

On Grand Cayman, there are surface exposures of the Cayman Formation, the Pedro Castle Formation, and the Ironshore Formation. Evident on the much of the eastern half of Grand Cayman, the elevated ridge in the southwest corner, and at Hell (Fig. 2-5A), the exposed Cayman Formation is characterized by rugged surface topography, with abundant pits, pinnacles, holes and phytokarst (Matley, 1926; Folk et al., 1973; Jones, 1989, 1994). In contrast, the exposed Pedro Castle Formation with its subdued topography, is largely confined to the area around Pedro Castle (Jones, 1994; Arts, 2000), whereas the exposed Ironshore Formation is restricted to the low-lying areas around North Sound and along the eastern coast of Grand Cayman.

6.2. Cayman Brac

On Cayman Brac, the uplifted core of the island is formed of limestones and dolostones of the Bluff Group. Although the Brac Formation is exposed in the lower parts of the cliff faces at the east end of the island, the upper surface of the Brac Formation is not exposed to modern weathering. The Cayman Formation is exposed over most of the island, whereas the exposed Pedro Castle Formation is restricted to the west end of the island and the Mound (Fig. 2-5B). The Ironshore Formation is exposed on the low-lying platform that fringes the uplifted core (Fig. 2-5B).

7. Unconformities in the Tertiary-Pleistocene succession

7.1. Criteria for Distinguishing Each Unconformity

The Brac Formation, the Cayman Formation, the Pedro Castle Formation, and the Ironshore Formation are separated from each other by unconformities. The recognition of

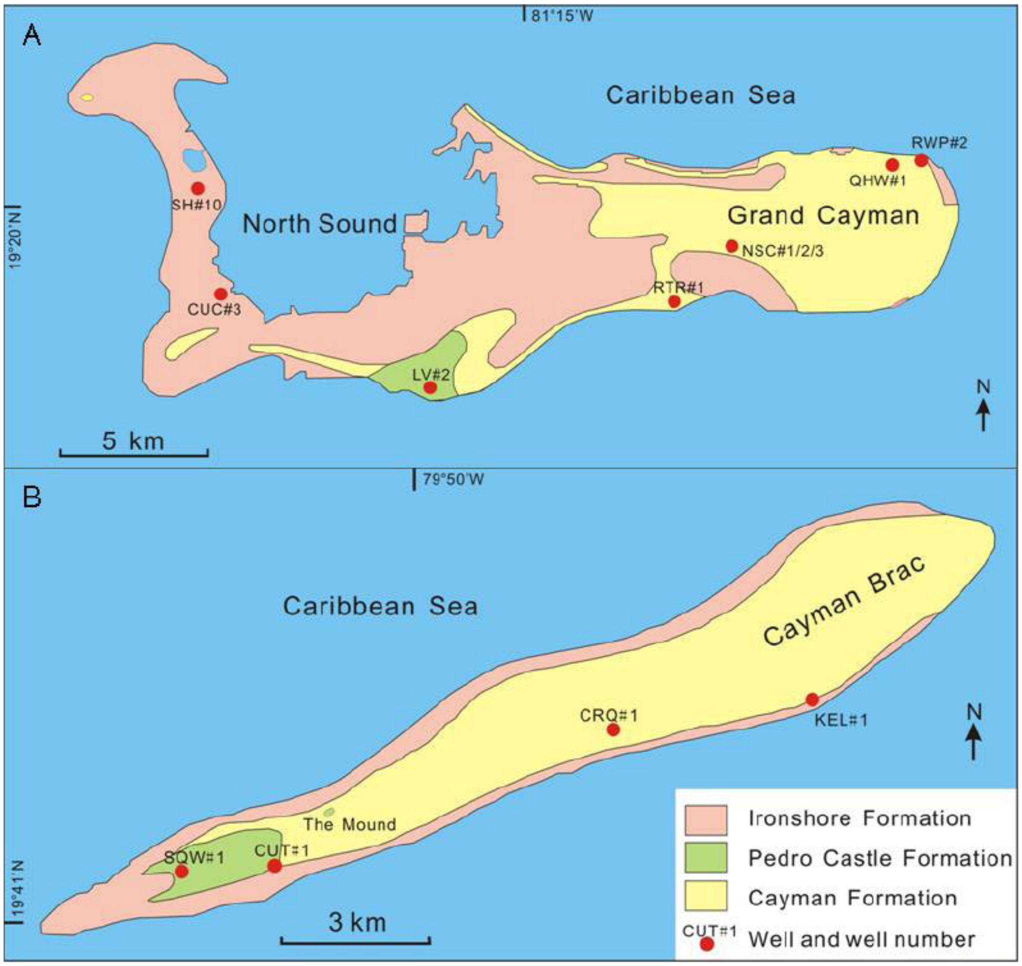

Fig. 2-5. Surface geology on (A) Grand Cayman, and (B) Cayman Brac (modified from Jones, 1994).

each unconformity is based on comparison of features in the formations below and above each unconformity.

7.1.1. Brac-Cayman (B-C) Unconformity

This unconformity developed on top of the Brac Formation during the Late Oligocene (Chattian) and Early Miocene and represents a period of about 15 million years (Jones and Hunter, 1994a; Jones et al., 1994a; Uzelman, 2009). Evident in the cliff faces on the east end of Cayman Brac (Jones, 1994; Jones and Hunter, 1994a; Jones et al., 1994a; Uzelman, 2009; Zhao and Jones, 2012b), this unconformity is defined by the following criteria.

1) The Brac Formation is formed of limestones and coarsely crystalline, fabric-destructive

and sucrosic dolostones whereas the overlying Cayman Formation is formed of finely crystalline, fabric-retentive dolostones (Jones and Hunter, 1994a; Jones et al., 1994a; Uzelman, 2009; Zhao and Jones, 2012b).

2) Limestones and dolostones in the upper part of the Brac Formation contain numerous large Lepidocyclina, but only scattered corals and bivalves. In contrast, dolostones in the overlying Cayman Formation contain a biota dominated by corals, bivalves, and gastropods (Jones, 1994; Jones and Hunter, 1994a; Jones et al., 1994a).

3) The permeability contrast between the Brac Formation and Cayman Formation is highlighted by (a) evidence of an old spring that used to emanate from the B-C Unconformity (Uzelman, 2009; Zhao and Jones, 2012b), and (b) caves, including Great Cave, in the upper part of the Brac Formation with flat roofs that coincide with the B-C Unconformity (Jones et al., 1994a; Uzelman, 2009; Zhao and Jones, 2012b).

4) At some localities borings have their apertures at the B-C unconformity (Jones and Hunter, 1994a; Jones et al., 1994a; Uzelman, 2009).

Application of these criteria on Grand Cayman is difficult because the Brac Formation and the B-C Unconformity are not exposed. This problem is exacerbated because (1) this unconformity has not yet been found in any core, and (2) Lepidocyclina has not yet been found in any sample from Grand Cayman. Thus, identification of the B-C Unconformity on Grand Cayman must rely on significant changes in lithology, textures, and/or age of the strata as indicated by their $^{87}Sr/^{86}Sr$ ratios. In this study, the B-C Unconformity on Grand Cayman is located according to the following criteria.

1) Lithological change is a difficult criterion to apply because the Cayman Formation on Grand Cayman is now known to be formed of limestones and dolostones (Der, 2012), whereas on Cayman Brac it is formed entirely of dolostones. Nevertheless, a sudden downhole lithological change from dolostones to limestones, evident in most of the deep wells (> 100 m), is taken as a possible indicator of the B-C Unconformity.

2) Dolostones in the Brac Formation are characterized by fabric-destructive textures,

whereas those in the Cayman Formation exhibit fabric-retentive fabrics (Jones and Hunter, 1994a; Jones et al., 1994a; Uzelman, 2009; Zhao and Jones, 2012a, 2012b).

3) Dating of these strata generally relies on $^{87}Sr/^{86}Sr$ ratios because the fossils are typically not age-diagnostic. On Cayman Brac, the limestones and dolostones from the Brac Formation are characterized by average $^{87}Sr/^{86}Sr$ ratios of 0.70808-0.708189 and 0.708939-0.70900, respectively (Jones et al., 1994a; Jones and Luth, 2003). Similar values have been obtained on Grand Cayman. The dolostones from the Brac Formation in LV#2, for example, yielded $^{87}Sr/^{86}Sr$ ratios of 0.70895 (Jones and Luth, 2003), which are significantly lower than the ratio in the basal beds of the Cayman Formation (0.70907-0.70911) (Jones and Luth, 2003). Thus, the B-C Unconformity can be established by the contrasts in the $^{87}Sr/^{86}Sr$ ratios. Caution must be used, however, because it now appears that the strata immediate below and above the B-C Unconformity in some areas were dolomitized by the same phase of dolomitization that occurred during the Late Miocene (Jones and Luth, 2003; Uzelman, 2009; Zhao and Jones, 2012b).

7.1.2. The Cayman-Pedro Castle (C-P) Unconformity

This unconformity, which separates the Cayman Formation from the overlying Pedro Castle Formation, formed during the Messinian and represents a period of 1.5 million years (Jones and Hunter, 1994b). Evident on the western half of Grand Cayman and the western end of Cayman Brac, recognition of the C-P Unconformity depends on the following criteria.

1) The Cayman Formation is formed largely of fabric-retentive, finely crystalline dolostones, whereas the Pedro Castle Formation is formed of intercalated limestone and dolostones (Jones, 1994; Jones and Hunter, 1994b; Jones et al., 1994a, 1994b; Arts, 2000). This criterion, however, must be used with caution because (a) in some areas, the basal part of the Pedro Castle Formation is formed of dolostones that are similar to those in the underlying Cayman Formation (Jones and Hunter, 1989, 1994a; Jones, 1994; Jones et al., 1994a, 1994b), and (b) the Cayman Formation found in the interior of the east end of Grand Cayman is formed of limestone and dolomitic limestone (Der, 2012).

2) Dolostones in the Cayman Formation are generally massive and hard, whereas the

dolostones and limestones in the basal part of the overlying Pedro Castle Formation are typically poorly cemented and relatively soft (Jones and Hunter, 1989, 1994b; Jones, 1994; Jones et al., 1994a; Wignall, 1995; Arts, 2000; MacNeil, 2001). This change is evident during drilling. The percent of core recovery and the average drilling time, for example, increase dramatically when the drilling crosses the C-P Unconformity (Jones, 1994; Jones and Hunter, 1994b; Jones et al., 1994b; Wignall, 1995; Etherington, 2004).

3) Although the fossils in the Cayman Formation and the Pedro Castle Formation are generally similar (Jones, 1994; Jones et al., 1994a, 1994b), minor differences in their coral faunas can help in the delineation of the unconformity. The Cayman Formation commonly contains colonial corals but few free-living corals, whereas the Pedro Castle Formation commonly contains numerous large free-living corals but few colonial corals (Jones and Hunter, 1989; Jones, 1994; Jones et al., 1994a, 1994b).

4) Cavities in the uppermost part of the Cayman Formation typically contain isopachous limpid dolomite and calcite cements (Jones and Hunter, 1989, 1994a, 1994b; Jones et al., 1994a, 1994b). In contrast, cavities in the Pedro Castle Formation rarely contain limpid dolomite (Jones and Hunter, 1989, 1994a, 1994b; Jones et al., 1994a, 1994b).

5) Cavities in the Cayman Formation commonly contain various internal sediments, including caymanite and coarse skeletal dolostones (Jones and Hunter, 1989; Jones, 1992a, 1994). In contrast, internal sediments are rare in the cavities in the Pedro Castle Formation (Jones and Hunter, 1989; Jones, 1992a, 1994).

6) In some outcrops, like those in the Pedro Castle area, the C-P Unconformity is well exposed with an irregular surface (Jones and Hunter, 1994b). The apertures of sponge, bivalve and worm borings are common on the unconformity (Jones and Hunter, 1989, 1994b; Jones, 1992b; Jones et al., 1994a, 1994b; Wignall, 1995).

7) On Grand Cayman and Cayman Brac, large caves and sinkholes are developed in the Cayman Formation below the C-P Unconformity, whereas they are rare in the Pedro Castle Formation (Jones and Hunter, 1989, 1994a; Jones, 1992b).

7.1.3. Pedro Castle-Ironshore (P-I) Unconformity

The unconformity between the Pedro Castle Formation and the overlying Ironshore Formation probably developed during the Middle and Late Pliocene (Wignall, 1995). Although common in the subsurface on the western half of Grand Cayman and the western end of Cayman Brac, the P-I Unconformity has never been found in exposed surface outcrops (Jones, 1994). Recognition of this unconformity in the subsurface is generally based on the following criteria.

1) The Pedro Castle Formation is formed of hard, well-lithified dolostones and limestones, whereas the overlying Ironshore Formation is formed of soft, friable limestones (Jones, 1994; Jones et al., 1994b; Wignall, 1995; Vézina, 1997; Coyne, 2003; Etherington, 2004).

2) Fossils in the Pedro Castle Formation have been extensively leached and/or replaced by dolomite (Jones, 1994; Jones and Hunter, 1994a; Jones et al., 1994a, 1994b), whereas fossils in the Ironshore Formation are very well preserved (Cerridwen, 1989; Hunter and Jones, 1990; Jones, 1990, 1994; Jones and Hunter, 1990; Cerridwen and Jones, 1991).

7.1.4. Brac-Ironshore (B-I) Unconformity and Cayman-Ironshore (C-I) Unconformity

In some areas, the Ironshore Formation rests directly on the Brac Formation or the Cayman Formation. On the east end of Cayman Brac, for example, the Ironshore Formation found on the coastal platform sits on top of the Brac Formation. This situation arose because pre-Pleistocene coastal marine erosion in that area removed the Cayman Formation and the upper part of the Brac Formation. In the coastal areas in the middle and the western parts of Cayman Brac and the east end of Grand Cayman, the Ironshore Formation rests directly on the Cayman Formation. In those areas, marine erosion during and/or after Pliocene led to the removal of the Pedro Castle Formation and the upper part of the Cayman Formation. In these situations, the B-I and C-I unconformities are easily identified because of the contrast between the poorly lithified limestones of the Ironshore Formation and the hard, well-lithified rocks of the Cayman Formation and the Brac Formation.

7.2. Topographic Complexity of Each Unconformity

The total relief on any of the unconformities in the successions on the Cayman Islands (Figs. 2-6, 2-7, 2-8, 2-9, 2-10, 2-11, 2-12) is the difference between the maximum and minimum elevations that includes various combinations of "karst relief", "marine erosion relief", and/or "tectonic relief". Herein, "karst relief" is the maximum difference in elevation produced by erosion as a result of subaerial exposure and karstification, whereas "marine erosion relief"

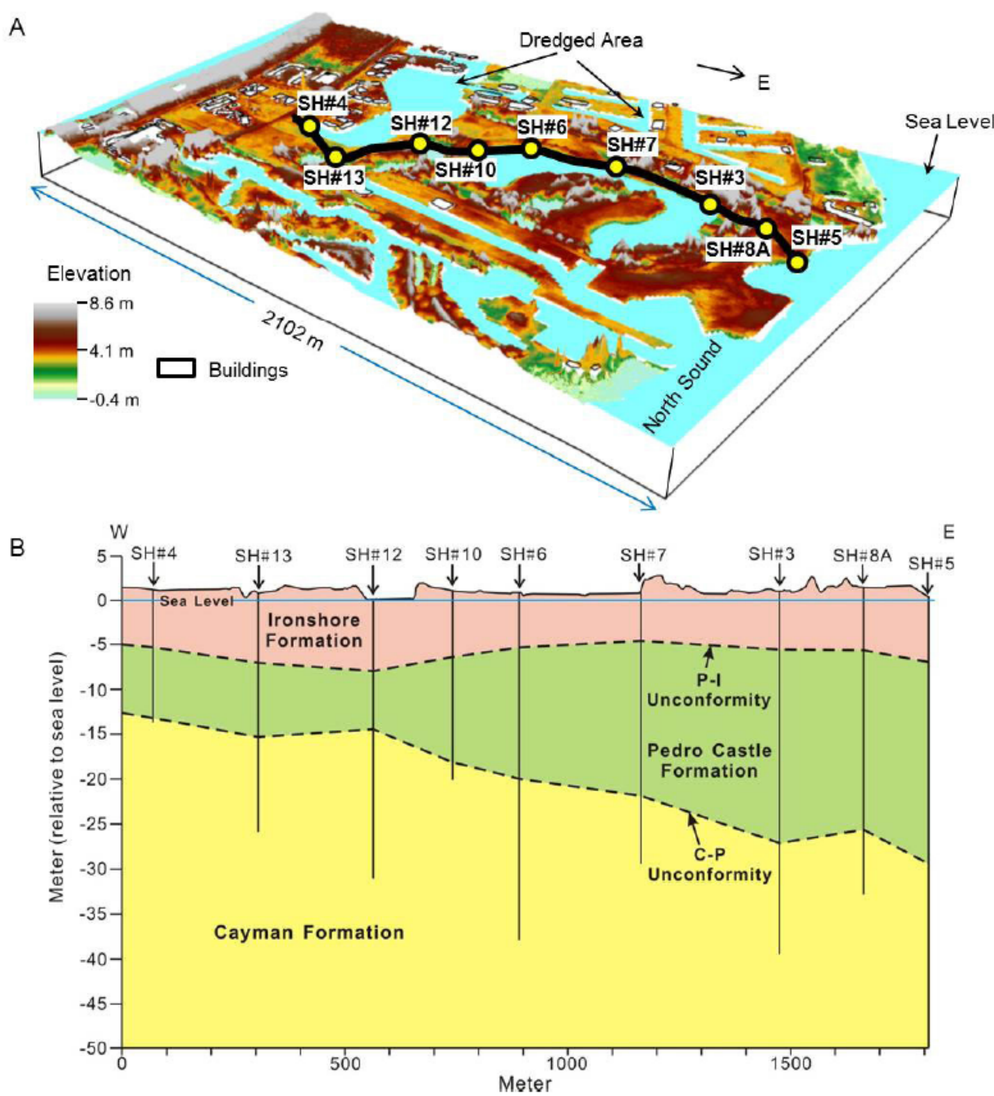

Fig. 2-6. Stratigraphic relationships between the Cayman Formation, Pedro Castle Formation and Ironshore Formation along the Safe Haven Transect on Grand Cayman. (A) Surface map of Safe Haven area showing locations of wells and the Safe Haven Transect; (B) Cross section along the Safe Haven Transect (modified from Jones and Hunter, 1994b).

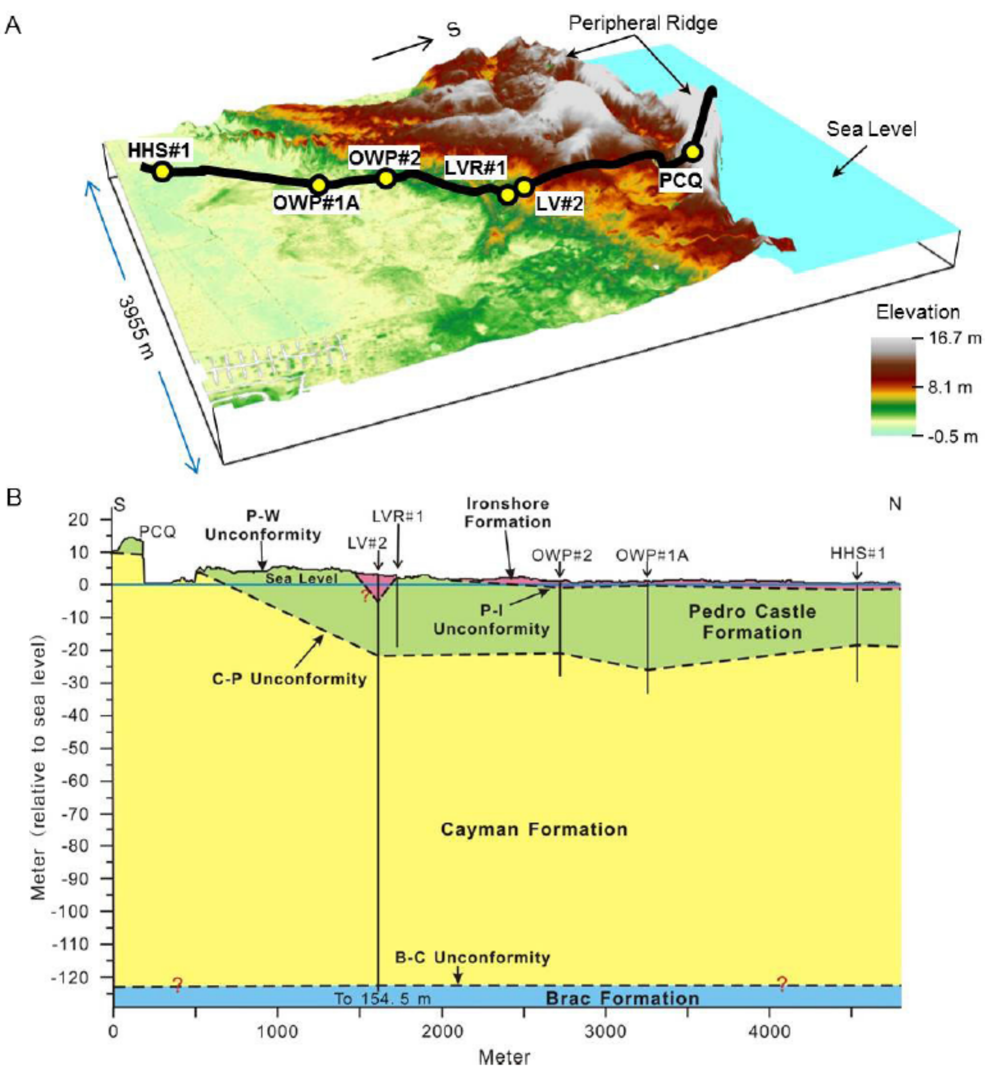

Fig. 2-7. Stratigraphic relationships between the Brac Formation, Cayman Formation, Pedro Castle Formation and Ironshore Formation along the Lower Valley Transect on Grand Cayman. (A) Surface map of Lower Valley area showing locations of wells and the Lower Valley Transect; (B) Cross section along the Lower Valley Transect (modified from Jones and Hunter, 1994b).

refers to the relief produced by coastal erosion. "Tectonic relief" is the maximum difference in elevation produced by tectonic displacement.

7.2.1. B-C Unconformity

On Grand Cayman, only eight wells penetrated the Brac Formation. NSC#1/2/3 on the east end of Grand Cayman (Fig. 2-8), for example, encounters the B-C Unconformity at ~140 m below sea level (bsl), whereas in LV#2 near Pedro Castle it is ~122 m (bsl) (Fig. 2-7). Wells

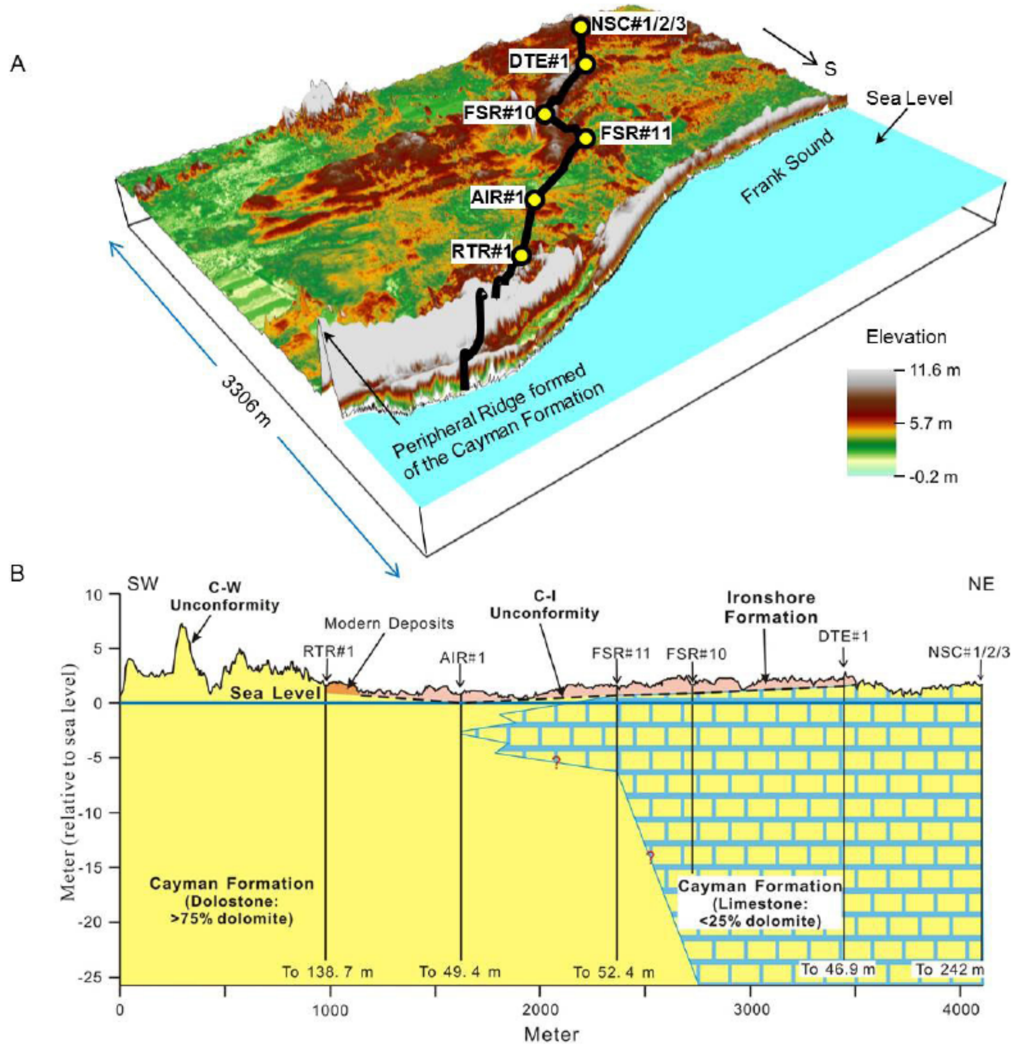

Fig. 2-8. Stratigraphic relationships between the Cayman Formation and Ironshore Formation along the South Central Coast Transect on Grand Cayman. (A) Surface map of south central coast showing locations of wells and the South Central Coast Transect; (B) Cross section along the South Central Coast Transect.

(CUC#1-4, GTH#1 and SHT#4) on the west part of Grand Cayman generally penetrate this unconformity at 100-115 m bsl. Data from these wells indicate that the karst relief on this unconformity is at least 40 m (Fig. 2-13).

On Cayman Brac, the B-C Unconformity dips to the west at ~0.5° (Jones, 1994; Jones and Hunter, 1994a; Jones et al., 1994a; Uzelman, 2009), with the highest point at the east end of the island at 33 m asl (Fig. 2-12). Given that the Brac Formation had still not been located in well

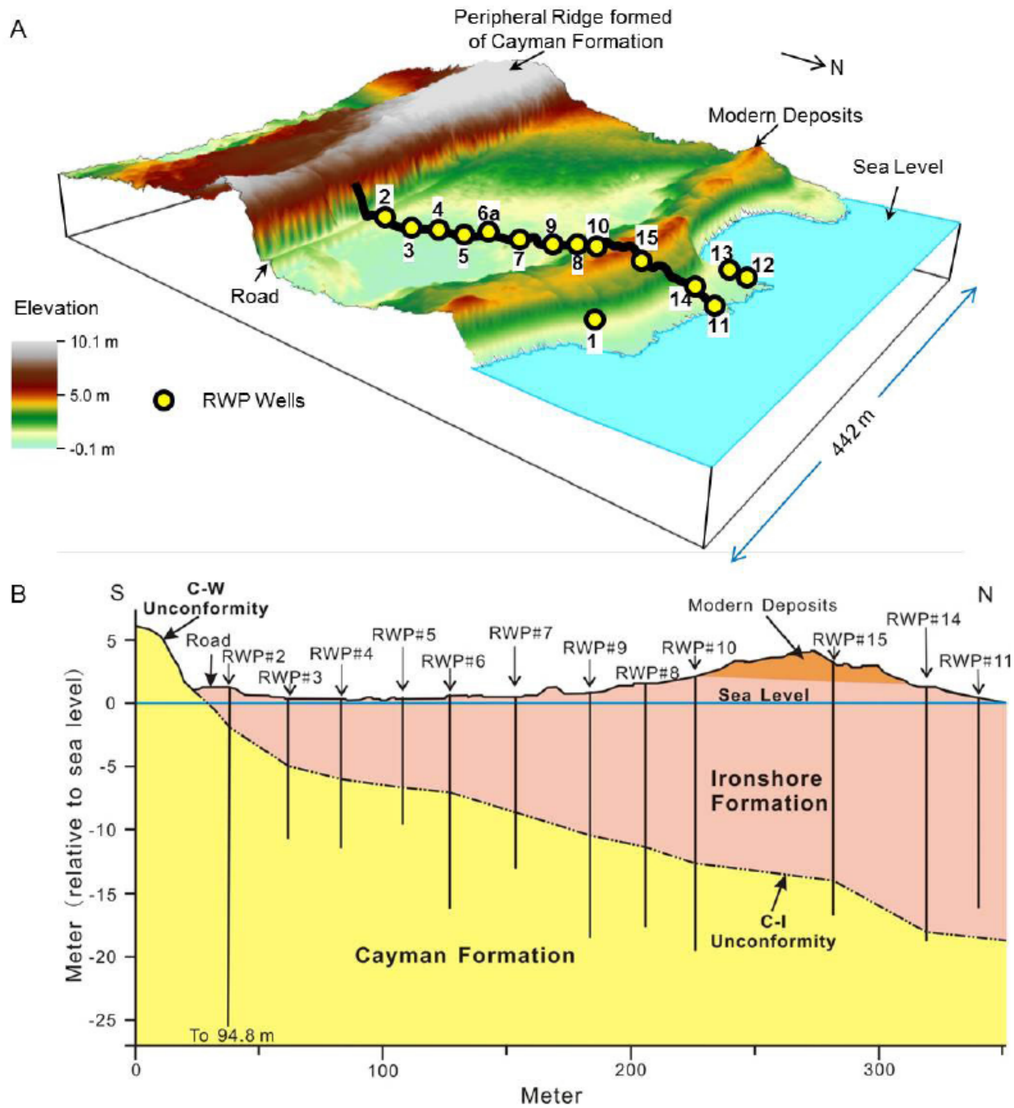

Fig. 2-9. Stratigraphic relationships between the Cayman Formation and Ironshore Formation along the Roger's Wreck Point Transect on Grand Cayman. (A) Surface map of Roger's Wreck Point showing locations of wells and the Roger's Wreck Point Transect; (B) Cross section along the Roger's Wreck Point Transect (modified from Vézina, 1997).

SQW#1 when it was terminated at 50 m bsl (Fig. 2-12), the total relief of the B-C Unconformity must be > 83 m (Fig. 2-13). Karst relief on this unconformity, evident only on the east end of Cayman Brac, is at least 25 m.

7.2.2. C-P Unconformity

Karst relief of this unconformity on Grand Cayman is at least 62 m (Jones and Hunter,

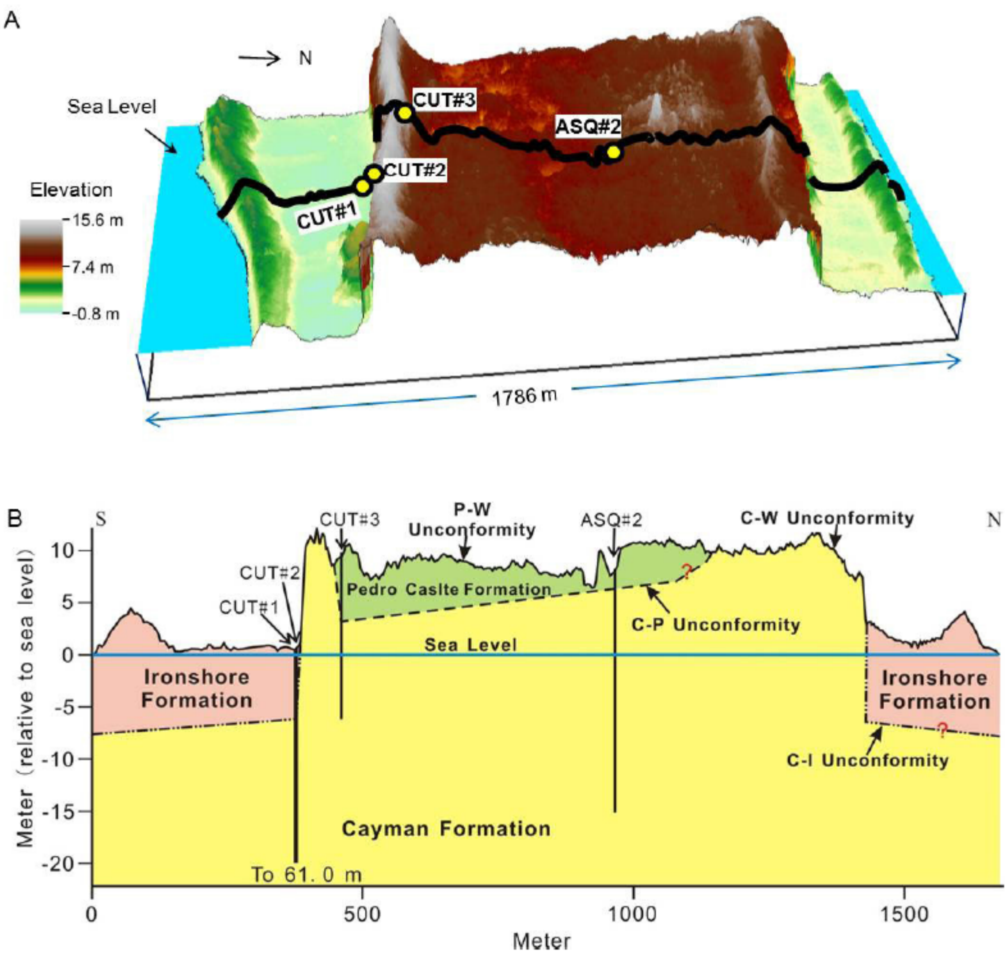

Fig. 2-10. Stratigraphic relationships between the Cayman Formation, Pedro Castle Formation and Ironshore Formation along the West End Transect on Cayman Brac. (A) Surface map of the west end of Cayman Brac showing locations of wells and the West End Transect; (B) Cross section along the West End Transect.

1994b), determined from the comparison between the sinkhole QHW#2 (40 m bsl) and the C-W Unconformity exposed at The Mountain, which rises to 22 m asl (Fig. 2-13). On the western half of Grand Cayman, this unconformity is 10 to 30 m bsl with a slope of 0.6-1.4° towards North Sound (Figs. 2-6, 2-7, 2-14). In contrast, the Pedro Castle Formation on the eastern half of Grand Cayman is missing and the Cayman Formation is either exposed at the surface or overlain by the Ironshore Formation (Figs. 2-8, 2-14). In the interior of the eastern part of the island, the upper surface of the Cayman Formation is 0 to 4.5 m asl and therefore higher than on the western part of the island (Figs. 2-8, 2-14). Along the coasts, however, the peripheral rims, formed of the

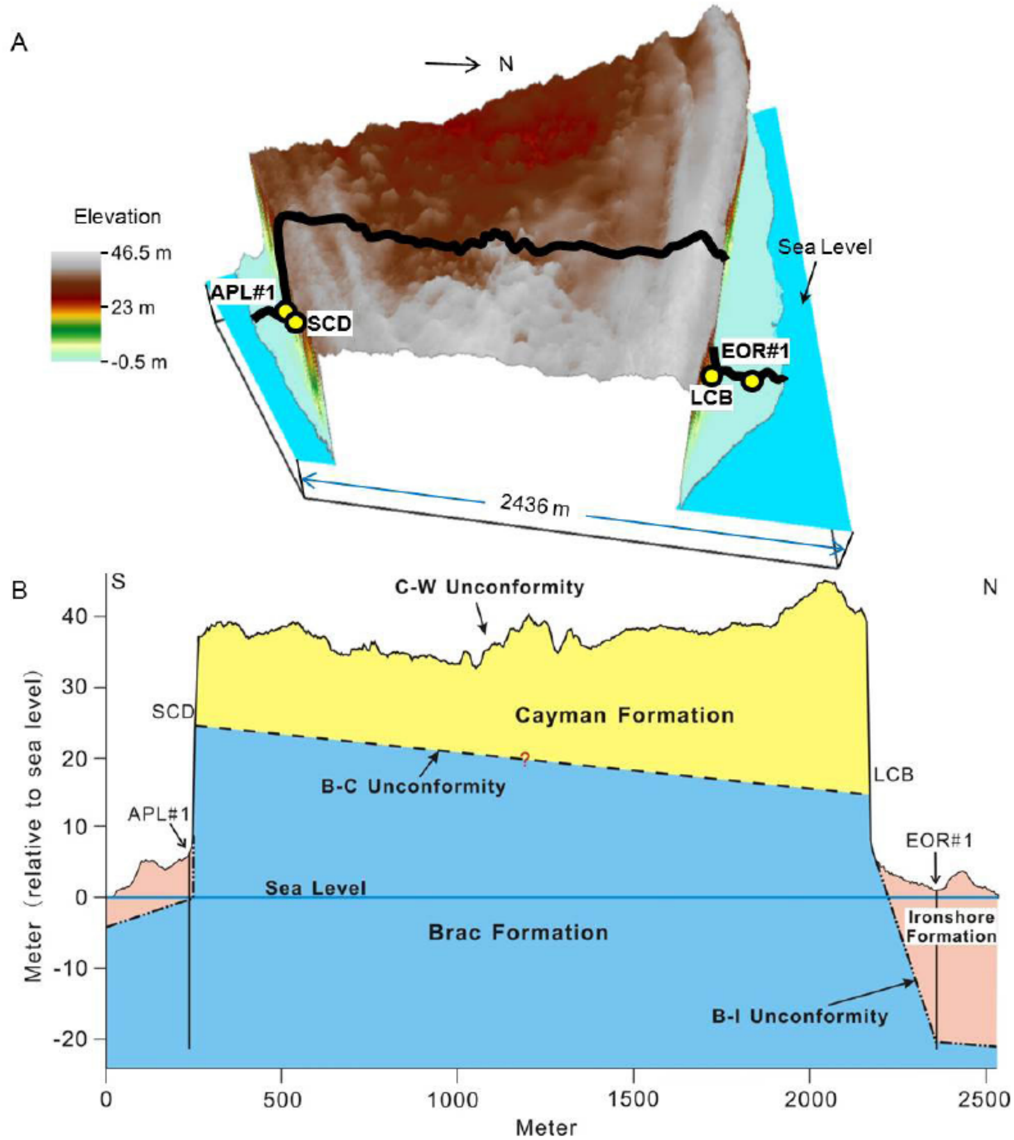

Fig. 2-11. Stratigraphic relationships between the Cayman Formation, Pedro Castle Formation, and Ironshore Formation along the East End Transect on Cayman Brac. (A) Surface map of the east end of Cayman Brac showing locations of wells and the East End Transect; (B) Cross section along the East End Transect (modified from Uzelman, 2009).

Cayman Formation, rise up to 13.5 m asl (Figs. 2-3, 2-8, 2-9).

On Cayman Brac, the total relief on the C-P Unconformity is at least 62 m, determined from the comparison between the C-W Unconformity on the east end (33-46 m asl) and the C-P Unconformity in well BW#1 (~16 m bls) (Figs. 2-12, 2-13). The C-W Unconformity exposed on most of the uplifted core, dips westward, with the development of peripheral rims (Figs. 2-4,

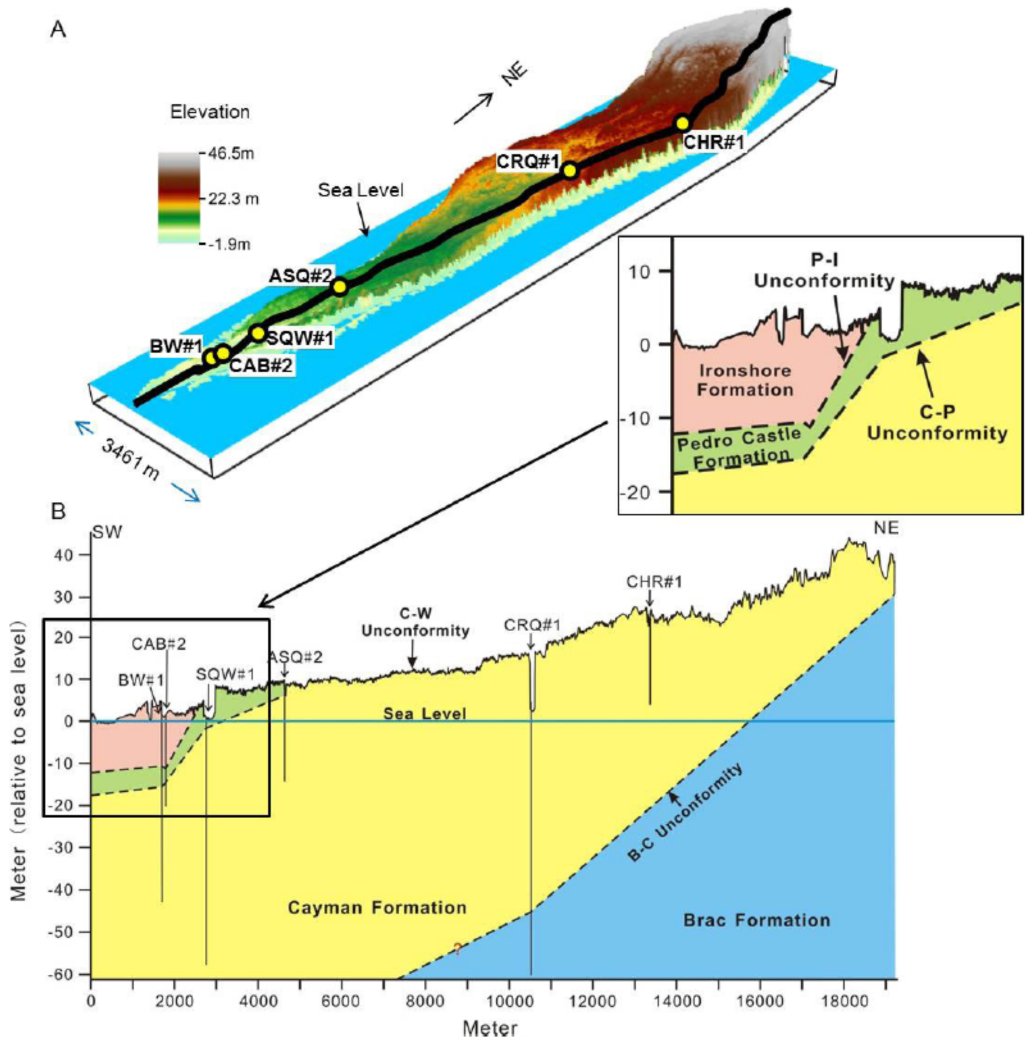

Fig. 2-12. Stratigraphic relationships between the Brac Formation, Cayman Formation, Pedro Castle Formation, and Ironshore Formation along the East-West Transect on Cayman Brac. (A) Surface map of the uplifted core on Cayman Brac showing locations of wells and the East-West Transect; (B) Cross section along the East-West Transect (modified from Jones, 2005).

2-12, 2-15). On the west end, the Cayman Formation is overlain by the Pedro Castle Formation, with the C-P Unconformity gradually deepening westward (Figs. 2-12, 2-15). Karst relief of the C-P Unconformity is difficult to determine because multiple phases of subaerial erosion have modified that unconformity.

7.2.3. P-I Unconformity

On Grand Cayman, the P-I Unconformity on the western part of the island is a subdued

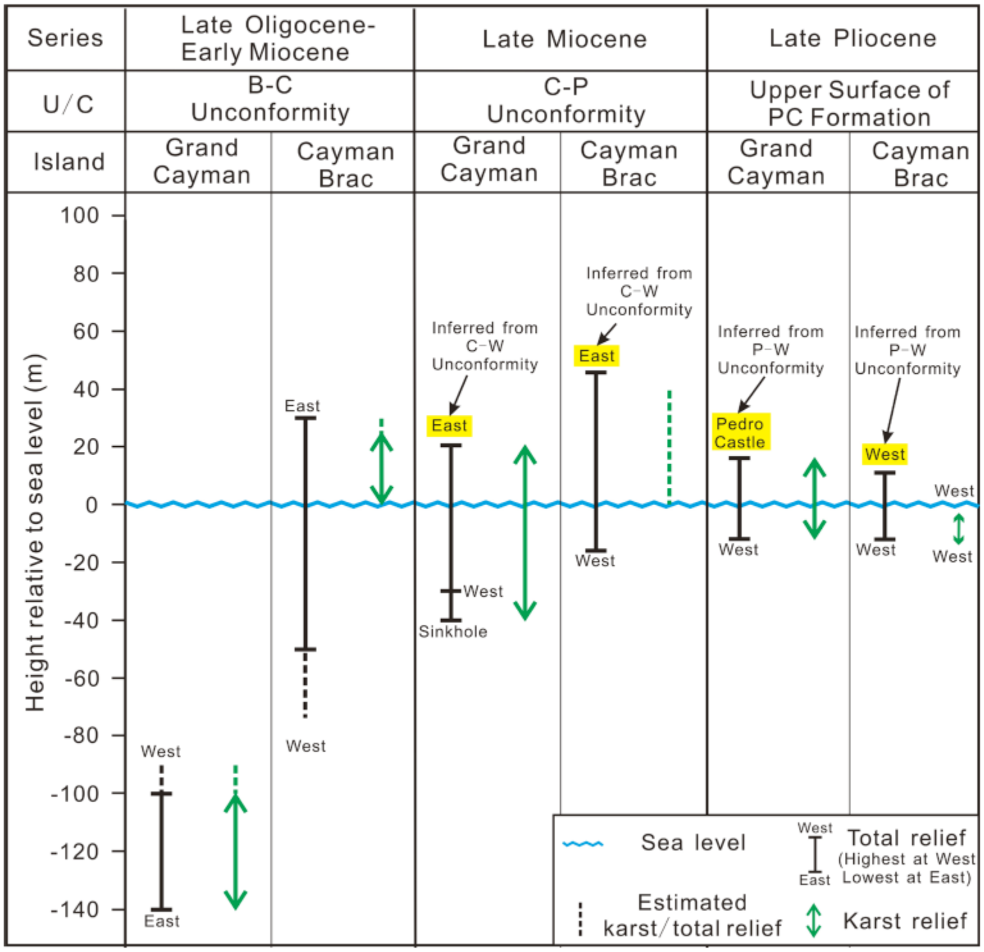

Fig. 2-13. Schematic diagram showing the total relief (black lines) and karst relief (green lines) on the B-C Unconformity, C-P Unconformity and upper surface of the Pedro Castle (PC) Formation on Grand Cayman and Cayman Brac.

surface (Figs. 2-6, 2-7, 2-14). A karst relief of 29 m on the top surface of the Pedro Castle Formation comes from the comparison between the P-W Unconformity exposed in the Pedro Castle area (17 m asl) and the P-I Unconformity in well CUC#3 (12 m bsl) (Fig. 2-13).

On Cayman Brac, the P-W Unconformity, which is up to 9.1 m asl, is replaced by the P-I Unconformity that dips westward to ~12 m bsl in well CAB#2 (Figs. 2-10, 2-12). This comparison indicates that the total relief on the top of the Pedro Castle Formation is at least 20 m (Fig. 2-13). Data from wells CAB#2 and CAB#3, on the west end of the island, indicate that the karst relief on this unconformity is > 7 m (Fig. 2-13).

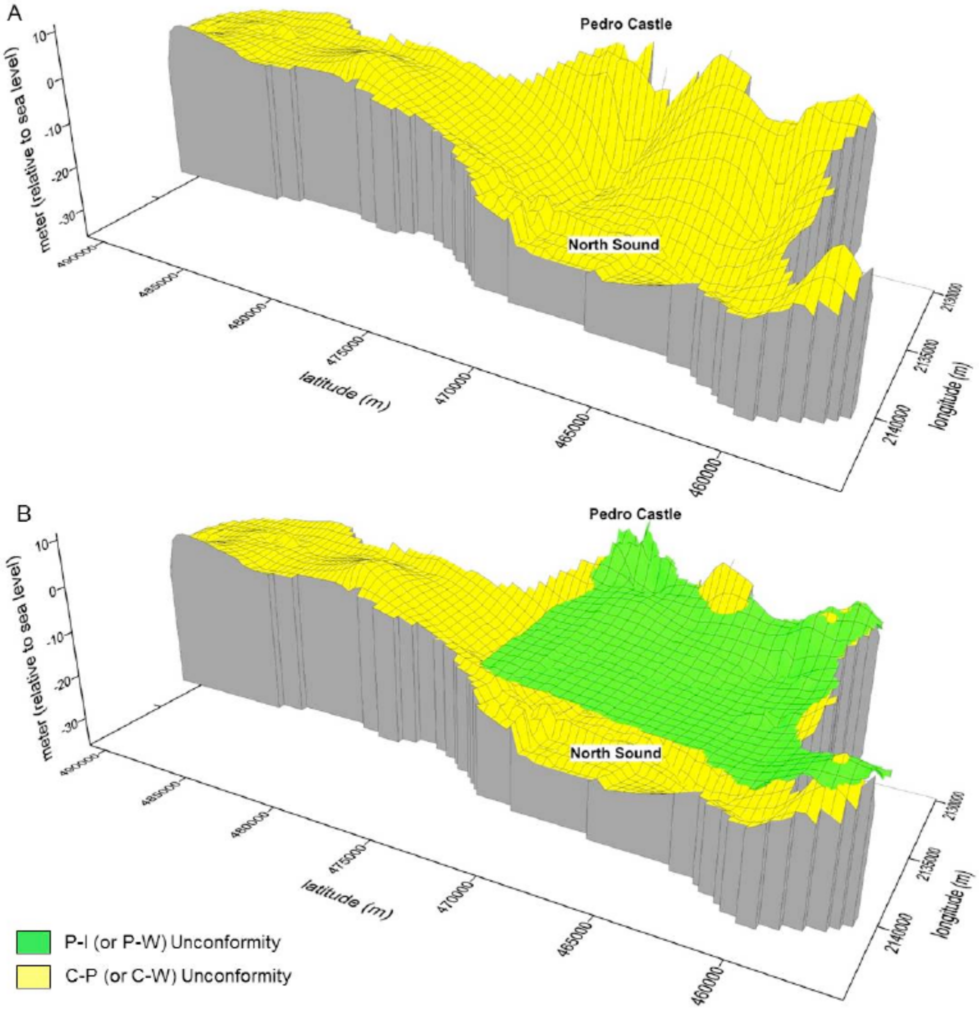

Fig. 2-14. Sketch diagram showing the topography on the C-P (or C-W) Unconformity and P-I (or P-W) Unconformity on Grand Cayman. The view is from a north direction. (A) Conceptual model showing the topography on the C-P (or C-W) Unconformity; (B) Conceptual model showing the topography on the P-I (or P-W) Unconformity.

7.2.4. B-I Unconformity and C-I Unconformity

On the northeast corner of Grand Cayman, the Ironshore Formation rests on top of a ~350 m wide shore platform that was cut into the Cayman Formation by marine erosion (Fig. 2-9). There, the C-I Unconformity deepens seaward from ~1 m asl to ~18 m bsl, with a slope of ~3.5° (Fig. 2-9). Thus, the marine erosion relief on the C-I Unconformity is at least 17 m.

On the east end of Cayman Brac the B-I Unconformity is 0.9 m bsl to 21 m bsl (Fig.

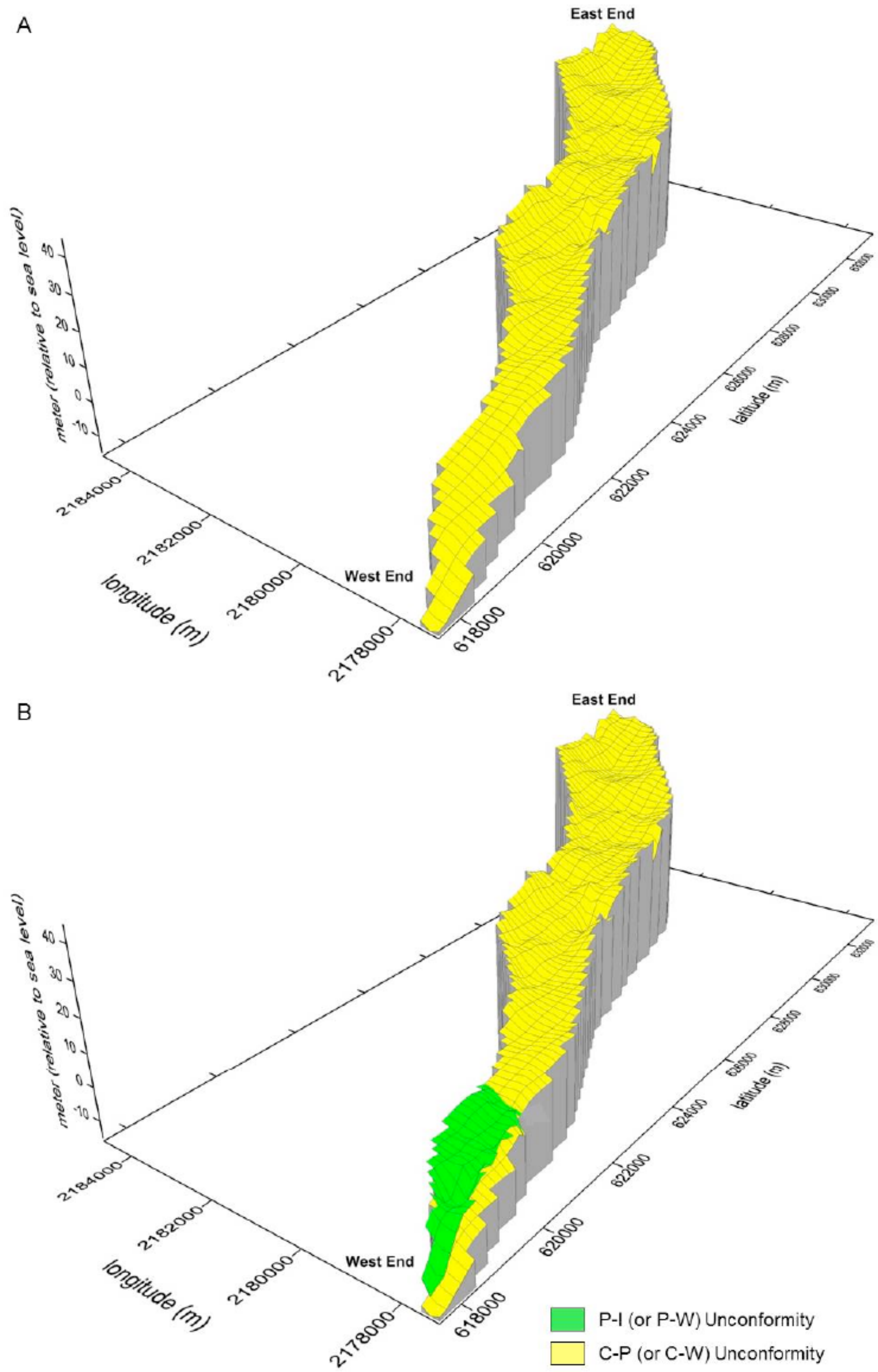

Fig. 2-15. Sketch diagram showing the topography on the C-P (or C-W) Unconformity and P-I (or P-W) Unconformity on the uplifted core of Cayman Brac. The view is from West End to East End. (A) Conceptual model showing the topography on the C-P (or C-W) Unconformity; (B) Conceptual model showing the topography on the P-I (or P-W) Unconformity.

2-11). The marine relief on this unconformity is at least 20 m. Towards the west, the B-I Unconformity is replaced by the C-I Unconformity (Fig. 2-10). The top surface of the Cayman Formation forms a 300 to 400 m wide shore platform at ~6 bsl, with the varying little on the C-I Unconformity (Fig. 2-10).

8. Coastal erosion

On carbonate islands, coastal erosion can take place while the exposed parts of the island in the interior of the island are undergoing karst development. Coastal erosion commonly leads to the development of wave-cut shore platforms (e.g., Stephenson, 2000; Trenhaile, 2000) with a cliff on its landward side (Bradley and Griggs, 1976; Lajoie, 1986; Anderson et al., 1999; Speed and Cheng, 2004; Passaro et al., 2011) that develops from the combined effects of wave activity, subaerial weathering, and biological activity (Stephenson, 2000). Evidence for erosion includes (1) a beveled platform, with a seaward slope of 2-4° (Blanchon and Jones, 1995; Speed and Cheng, 2004; Passaro et al., 2011; Bowles and Cowgill, 2012), (2) truncation of underlying strata so that no positive karst features (e.g., tower karst, pinnacles) remain (Blanchon and Jones, 1995; Anderson et al., 1999; Speed and Cheng, 2004), (3) an unconformity that separates older carbonate strata from the overlying strata (Speed and Cheng, 2004), (4) a carbonate succession that abuts against a cliff face formed of older carbonates (Speed and Cheng, 2004), (5) a wave-cut notch on the cliff face (Jones and Hunter, 1990; Blanchon and Jones, 1995; Johnson, 2001; Blanchon et al., 2002), (6) the arbitrary truncation of carbonate facies by the cliff face (Speed and Cheng, 2004), and (7) the progradation of the platform cover through time, with a receding cliff (Anderson et al., 1999; Vézina et al., 1999; Speed and Cheng, 2004). Constraining the time of shore platform formation is difficult and usually relies on the constructional features that developed during the next sea-level highstand (e.g., Blanchon and Jones, 1995; Anderson et al., 1999; Speed and Cheng, 2004).

On Grand Cayman and Cayman Brac there is evidence for shore platforms that were cut into the Cayman Formation and Brac Formation. At Rogers Wreck Point, for example, a cliff with a wave-cut notch at 6 m asl marks the landward limit of a shore platform that was cut into the Cayman Formation. That platform now lies beneath limestones of the Ironshore Formation, which thickens over a distance of 350 m, from ~1 m at the foot of the cliff face to at least 21 m at the coast (Fig. 2-9). Although the same shore platform is evident on Cayman Brac, there are some subtle but important stratigraphic differences associated with it. On the east end of the island, the platform was cut into the Brac Formation and the limestones of the Ironshore Formation were deposited on top of it (Fig. 2-11). In the central and western parts of the island, however, the platform was cut into the Cayman Formation and the Ironshore Formation therefore rests on that formation (Fig. 2-10). These contrasts in stratigraphy indicate that Cayman Brac must have been uplifted and tilted before the shore platform developed (Zhao and Jones, 2012a, 2013). The correspondence between the shore platforms around Grand Cayman and Cayman Brac indicates that they developed after the Late Pliocene (~3.6 Ma) but before deposition of the Ironshore Formation began about 400 ka. Similar platforms, also cut into Pliocene limestones, have been identified around Cave Hill on Barbados (Speed and Cheng, 2004) and on southern Cuba (Rojas-Agramonte et al., 2005).

9. Discussion

Grand Cayman and Cayman Brac are two small islands isolated by their positions in the Caribbean Sea distant from any other land masses, but subject to tectonic activity because of their proximity to the Cayman Spreading Centre and the Oriente Transform Fault (Fig. 2-1). Given that this has been the case for at least the last 35 million years, the evolution of the carbonate successions found on these islands must reflect eustatic changes in sea level and local tectonic activity. The challenge is to interpret the unconformities found in these successions so that the effects of eustatic sea level changes can be isolated from the tectonic effects.

Available evidence indicates that the islands near the Oriente Transform Fault were not uplifted until the Middle Miocene when faults perpendicular to the Oriente Transform Fault started to form (Iturralde-Vinent and Macphee, 1999; Iturralde-Vinent, 2003, 2006; Rojas-Agramonte et al., 2005, 2006; Mann et al., 2007). After that, the tectonic history of Grand Cayman and Cayman Brac was different. There is no evidence of faulting, structural offset, or folding of Oligocene to Pliocene strata on Grand Cayman. Similarly, there is no clear evidence of tectonic tilting on Grand Cayman because (1) the peripheral ridges formed of the Cayman Formation have a similar elevation on the north, east, and south coasts of the island (Fig. 2-3), (2) strata in the Cayman Formation appear to be horizontal, and (3) variations in the elevation of the C-W Unconformity are inconsistent with tilting of the strata. In contrast, there is clear evidence of tilting on Cayman Brac with (1) the B-C Unconformity being up to 33 m asl on the east end of the island but > 50 m bsl on the middle part of the island, (2) the C-W Unconformity being up to 46 m asl on the east end of the island but close to sea level on the west end of the island, and (3) evidence of westward dipping strata in the Cayman Formation (Fig. 2-12).

It is possible that Grand Cayman may have experienced vertical tectonic movements with little or no associated tilting. Recognition of such tectonic movement is difficult because the sedimentologic and stratigraphic results would be similar to those resulting from eustatic sea level changes. The fact that the unconformities found in the succession on Grand Cayman can be matched with known global lowstands, however, argues against this notion (Jones, 1994; Jones and Hunter, 1994b). Furthermore, regional evidence indicates that Grand Cayman was not displaced by the Late Miocene-Pliocene transpression between the Caribbean Plate and the North American Plate that was responsible for the tilting and sinistral/dextral displacement of other islands along the tectonic corridor associated with the Oriente Transform Fault (Iturralde-Vinent, 1998; Rojas-Agramonte et al., 2005; Mann et al., 2007).

It seems probable that Cayman Brac began to tilt to the west in the Late Pliocene (~3.6 Ma) (Zhao and Jones, 2012a, 2013). That uplift on Cayman Brac ceased no later than 125 ka is shown by a wave-cut notch at 6 m asl that formed when sea level was 6 m higher than today (Jones and Hunter, 1990; Vézina et al, 1999). On Grand Cayman and Cayman Brac, shore platforms cut into the Tertiary limestones and dolostones after the Late Pliocene (~3.6 Ma) were subsequently covered by Pleistocene limestones (Figs. 2-9, 2-10, 2-11). Such relationships indicate that the islands have probably been tectonically stable since deposition of the Ironshore Formation began no later than 400 ka.

Available evidence indicates that the B-C Unconformity on these two islands developed during the lowstand that followed a eustatic drop in sea level of 30 to 75 m that took place in the Late Oligocene-Early Miocene (Pekar and Miller, 1996; Kominz et al., 1998; Miller et al. 1998, 2005; Van Sickel et al., 2004). The B-C Unconformity, with a karst relief of at least 40 m on Grand Cayman, is a manifestation of that drop of sea level. Although the total relief on the B-C Unconformity on Cayman Brac is difficult to ascertain with certainty, it must be more than 83 m (Fig. 2-12). Today, the B-C Unconformity on Grand Cayman is 100-140 m bsl, whereas it is up to 33 m asl on the east end of Cayman Brac. Thus, the difference of elevations between the B-C Unconformity on Grand Cayman and the east end of Cayman Brac is 133-173 m. Given that uplift took place between 3.6 Ma to 0.4 Ma, the rate of uplift on the east end of Cayman Brac was 0.04 to 0.05 mm/year. This rate is much slower than that for other Caribbean Islands. Plio-Pleistocene terraces in the Rio Maya Formation on south Cuba, uplifted up to 200 m asl, rose at 4 mm/year on the central and western parts and 12-15 mm/year on the eastern part of Cuba (Iturralde-Vinent, 2003; Rojas-Agramonte et al., 2005), respectively. The mean uplift rate on Barbados between the Middle Eocene and 500 ka was 0.12-0.22 mm/year (Jones, 2009), and increased to 0.44 to 0.53 mm/year over the last 500 ka (Speed and Cheng, 2004; Radtke and Schellmann, 2006). It seems, therefore, that uplift on Cayman Brac was not as rapid as for other Caribbean islands, or that the duration of uplift on Cayman Brac has been overestimated.

The B-C Unconformity at the west end of Cayman Brac is probably ~120 m bls, which is similar to the depths where it is found on Grand Cayman (Fig. 2-13). Similarly, the C-P Unconformity and the P-I Unconformity on Grand Cayman are at similar elevations to those on the west end of Cayman Brac (Fig. 2-13). This suggests that the axis of rotation for the uplift of Cayman Brac was close to the west end of the island.

The drop in sea level during the Messinian (terminal Miocene), estimated to be from 30 to 180 m (Pigram et al., 1992; Aharon et al., 1993; Zhang and Scott, 1996; Hodell et al., 2001; Blanc-Valleron et al., 2002; Rouchy and Caruso, 2006), took place between 0.6 and 0.8 Ma (Hodell et al., 2001; Rouchy and Caruso, 2006; Jiménez-Moreno et al., 2013). This lowstand led to the development of the C-P Unconformity that has a karst relief of at least 62 m on Grand Cayman (Fig. 2-13). This must be regarded as a minimum estimate because much of the upper part of the Cayman Formation has been lost by subaerial erosion that is still ongoing today. On Grand Cayman, the Cayman Formation is at least 144 m thick. On Cayman Brac, the Cayman Formation is 15-20 m thick on the east end of the island and ~ 62 m thick on the middle part of the island (Fig. 2-12). Assuming that the Cayman Formation on the two islands were originally of similar thicknesses, this means that at least 120 m of the formation has been removed from the east end of the island and at least 80 m on the central part of the island. The wedge-shaped form of the Cayman Formation on Cayman Brac, with tapering to the east, is due to the proportional relationship that exists because uplift increases the volume of the bedrock above base level, and commonly induces faults and fractures, which serve as avenues of solution (Purdy and Waltham, 1999).

Peripheral rims along the margin of a platform or around an isolated oceanic island may be a product of karst development associated with subaerial exposure of the platform (e.g., Purdy, 1974; Purdy and Winterer, 2001) or reef development (Schlager, 2003; Schlager and Warrlich, 2009a, 2009b; Schlager and Purkis, 2013). The unconformity that caps the Cayman Formation on Grand Cayman and Cayman Brac has an atoll-like topography with peripheral rims that surround a central depression. With ample evidence of dissolution features but no evidence of reefs in the peripheral rim on Grand Cayman, Jones and Hunter (1994b) argued it was best explained by Purdy's (1974) model, which emphasized the inherited karstic origin for this type of topography. Supported by laboratory experiments, Purdy (1974) proposed the "oversupply", "balanced" and "undersupply" models for explaining the topographic features that develop on flat or inclined limestone surfaces once they are exposed to the atmosphere. The models are based on the balance between the amount of rainfall and the rate at which the water flows off the edges of the limestone surfaces. With the "oversupply model", which functions when rainfall exceeds the rate of runoff, dissolution rates on the interior and edges are similar, because there is a continuous solution film over the entire surface. This produces a subdued surface with no peripheral rims or solution depressions in the central part. In the "undersupply" and "balanced" models, rainfall is less than the rate of runoff. In the "balanced model", rainfall maintains a solution meniscus over the interior part of the carbonate surface, but runoff is reduced. As a consequence, a solution depression with a smooth floor develops in the interior of the island while leaving a peripheral rim around the margins. With the "undersupply model", rainfall is too low to maintain a continuous solution film over the surface and an uneven pattern of dissolution evolves. On Grand Cayman, the C-P Unconformity is characterized by an atoll-shape depression that is surrounded by peripheral rims on the north, west and south margins (Jones and Hunter, 1994b). This topography is consistent with a situation that may be transitional between the "balanced" and "undersupply" models of Purdy (1974).

On the eastern part of Grand Cayman, post-Miocene erosion removed the Pedro Castle Formation so that the Cayman Formation is now widely exposed. Today, the C-W Unconformity is above present sea level, with peripheral rims along the south, east, and north coasts (Figs. 2-3, 2-14). Although modified by post-Miocene weathering and/or marine erosion, those rims are inherited from the peripheral rim that developed during the Messinian lowstand. This suggestion is supported by the fact that the rims are formed of the Cayman Formation with no trace of the Pedro Castle Formation, and the distance between the landward limit of the peripheral rims and coastline is relative constant at ~400 m (Fig. 2-3).

Purdy (1974) suggested that the peripheral rim developed in the "balanced" and "undersupply" models would be intensified if the surface of a limestone block is inclined because this promotes runoff in one direction and thereby prevents dissolution on the upslope edges of the uplifted block. Comparison of the C-W Unconformity on Cayman Brac and Grand Cayman supports this suggestion. On Cayman Brac, the difference in elevations between the peripheral rims and the central depression is up to 15 m on the east end (Fig. 2-4), whereas on Grand Cayman is no more than 9 m (Fig. 2-3). Moreover, the peripheral rim of the C-W Unconformity on Cayman Brac is more pronounced on the eastern upslope margin than on the western downslope margin (Figs. 2-4, 2-10, 2-11, 2-15). On Grand Cayman, such differences in the elevation of the peripheral rim are not apparent.

Sediments that now form the Pedro Castle Formation were probably deposited during the Middle Pliocene highstand, which was up to 22 m asl (Dowsett and Cronin, 1990; Miller et al., 2005, 2011, 2012; Dwyer and Chandler, 2009; Sosdian and Rosenthal, 2009). It seems probable, therefore, that the Pedro Castle Formation once covered much of Grand Cayman and Cayman Brac (Zhao and Jones, 2012a, 2013). Evidence for this suggestion includes the (1) P-W Unconformity at Pedro Castle on Grand Cayman that is up to 16 m asl, (2) Pedro Castle Formation being preserved in sinkholes on the eastern part of Grand Cayman, and (3) Pedro Castle Formation being found on the Mound on Cayman Brac. The drop in sea level to 90 m bsl that occurred in the Late Pliocene (Miller et al., 2012) probably coincided with the tectonic tilting of Cayman Brac to the west (Zhao and Jones, 2012b, 2013). Subaerial erosion that started during this lowstand led to the removal of the Pedro Castle Formation from most of Cayman Brac and from the eastern half of Grand Cayman, and development of the P-I Unconformity and the P-W Unconformity.

Unconformities in the Oligocene to Pleistocene succession on the Cayman Islands developed in response to karst processes and coastal erosion that operated during sea-level lowstands. With little tectonic movement on Grand Cayman, such unconformities are characterized by rugged topographies, which partly reflect the associated lowstand positions. In contrast, due to the uplift of Cayman Brac between the Late Pliocene and ~400 ka, the Oligocene to Pliocene carbonate succession was tilted to the west. As a result karst processes and coastal erosion on the uplifted zone, enhanced by fractures and faults, led to the removal of much of the Pedro Castle Formation and the upper part of the Cayman Formation.

10. Conclusions

The exposed carbonate succession on Grand Cayman and Cayman Brac is formed of the Brac Formation (Lower Oligocene), Cayman Formation (Middle Miocene), Pedro Castle Formation (Middle Pliocene), and Ironshore Formation (Pleistocene). The deposition of each formation was terminated by the drop in sea level, which produced an unconformity by karst processes and/or by marine coastal erosion.

Although close to each other, Grand Cayman and Cayman Brac have experienced different tectonic histories since the Late Pliocene, and consequently exhibit different stratigraphic architectures.

1) Grand Cayman has experienced little tectonic movement since the Late Oligocene, whereas Cayman Brac was uplifted between the Late Pliocene (~3.6 Ma) and ~400 ka. The uplift on the east end of Cayman Brac is up to 133-173 m, with an uplift rate between 0.04 and 0.05 mm/year. The west end of Cayman Brac is close to the rotation axis of the uplift, with little displacement.

2) With little, if any, tectonic movement, unconformities on Grand Cayman are characterized by rugged topographies. The Cayman-Pedro Castle Unconformity, for example, shows a dish-shape depression surrounded by peripheral rims. The karst relief on those unconformities reflects the magnitude of sea-level fall.

3) Uplift on Cayman Brac tilted Tertiary strata and enhanced the surface karst processes. The Pedro Castle Formation has been removed from most of Cayman Brac since the Late Pliocene, whereas the removal of the Cayman Formation is geographically variable due to the uplift. On the east end of Cayman Brac, 120 m of the Cayman Formation was removed, whereas on the middle of this island about 80 m was lost to subaerial erosion.

4) The Cayman-Pedro Castle Unconformity indicates a transitional stage between the "balanced" and "undersupply" models of Purdy (1974). The peripheral rims on the exposed Cayman Formation on Grand Cayman and Cayman Brac are the remnant of the peripheral rims that developed during the Messinian lowstand. Compared to those on Grand Cayman, the peripheral rims on Cayman Brac are more pronounced due to uplift.

5) Coastal erosion after the Late Pliocene (~3.6 Ma) but before ~400 ka cut into the Cayman Formation and the Brac Formation and consequently erased the ancestral topography in the coastal areas. Overlain by the Ironshore Formation, the Cayman-Ironshore Unconformity and the Brac-Ironshore Unconformity were developed in the coastal areas.

References

Aharon, P., Goldstein, L.S., Wheeler, C.W., Jacobson, G., 1993. Sea-level events in the South Pacific linked with Messinian salinity crisis. Geology 21, 771-775.

Anderson, R.S., Densmore, A.L., Ellis, M.A., 1999. The generation and degradation of marine terraces. Basin Research 11, 7-19.

Arts, A.E., 2000. Sedimentology and stratigraphy of the Pedro Castle Formation, SW Grand Cayman, British West Indies. Unpublished M.Sc. Thesis, University of Alberta, Canada, 107 pp.

Blanchon, P., Jones, B., 1995. Marine-planation terraces on the shelf around Grand Cayman: a result of stepped Holocene sea-level rise. Journal of Coastal Research 11, 1-33.

Blanchon, P., Jones, B., Ford, D.C., 2002. Discovery of a submerged relic reef and shoreline off Grand Cayman: further support for an early Holocene jump in sea level. Sedimentary Geology 147, 253-270.

Blanc-Valleron, M.M., Pierre, C., Caulet, J.P., Caruso, A., Rouchy, J.M., Cespuglio, G., Sprovieri, R., Pestrea, S., Di Stefano, E., 2002. Sedimentary, stable isotope and micropaleontological records of paleoceanographic change in the Messinian Tripoli Formation (Sicily, Italy). Palaeogeography, Palaeoclimatology, Palaeoecology 185, 255-286.

Bowles, C.J., Cowgill, E., 2012. Discovering marine terraces using airborne LiDAR along the Mendocino-Sonoma coast, northern California. Geosphere 8, 386-402.

Bradley, W.C., Griggs, G.B., 1976. Form, genesis, and deformation of central California wave-cut platforms. Geological Society of America Bulletin 87, 433-449.

Budd, D.A., Gaswirth, S.B., Oliver, W.L., 2002. Quantification of macroscopic sub-aerial exposure features in carbonate rocks. Journal of Sedimentary Research 72, 917-928.

Budd, D.A., Saller, A.H., Harris, P.M., 1995. Foreword. In: Budd, D.A., Saller, A.H., Harris, P.M. (Eds.), Unconformities and Porosity in Carbonate Strata: American Association of Petroleum Geologists, Memoir 63. American Association of Petroleum Geologists, Tulsa, United States, pp. vii-xii.

Calais, E., Mercier de Lépinay, B., 1995. Strike-slip tectonic processes in the northern Caribbean between Cuba and Hispaniola (Windward Passage). Marine Geophysical Researches 17, 63-95.

Cerridwen, S.A., 1989. Paleoecology of Pleistocene mollusca from the Ironshore Formation, Grand Cayman, B.W.I. Unpublished M.Sc. Thesis, University of Alberta, Canada, 271 pp.

Cerridwen, S.A., Jones, B., 1991. Distribution of bivalves and gastropods in the Pleistocene Ironshore Formation, Grand Cayman, British West Indies. Caribbean Journal of Science 27, 97-116.

Choquette, P.W., James, N.P., 1988. Introduction. In: James, N.P., Choquette, P.W. (Eds.), Paleokarst. Springer-Verlag, Berlin, Germany, pp. 1-21.

Coyne, M.K., 2003. Transgressive-regressive cycles in the Ironshore Formation, Grand Cayman, British West Indies. Unpublished M.Sc. Thesis, University of Alberta, Canada, 98 pp.

Coyne, M.K., Jones, B., Ford, D., 2007. Highstands during Marine Isotope Stage 5: evidence from the Ironshore Formation of Grand Cayman, British West Indies. Quaternary Science Reviews 26, 536-559.

Der, A.J., 2012. Deposition and sea level fluctuations during Miocene Times, Grand Cayman, British West Indies Indies. Unpublished M.Sc. Thesis, University of Alberta, Canada, 101 pp.

Dickinson, J.A., Wallace, M.W., Holdgate, G.R., Gallagher, S.J., Thomas, L., 2002. Origin and timing of Miocene-Pliocene unconformity in Southeast Australia. Journal of Sedimentary Research 72, 288-303.

Dowsett, H.J., Cronin, T.M., 1990. High eustatic sea level during the middle Pliocene: evidence from the Southeastern U.S. Atlantic Coastal Plain. Geology 18, 435-438.

Dwyer, G.S., Chandler, M.A., 2009. Mid-Pliocene sea level and continental ice volume based on coupled benthic Mg/Ca Palaeotemperatures and oxygen isotopes. Philosophical Transactions of the Royal Society A–Mathematical Physical and Engineering Sciences 367, 157-168.

Esteban, M., 1991. Paleokarst: case histories. In: Esteban, M., Smart, P.L., Wright, V.P. (Eds.), Paleokarsts and Paleokarstic Reservoirs. Occasional Publication Series 2. University of

Reading, Postgraduate Research Institute for Sedimentology, United Kingdom, pp. 121-146.

Esteban, M., Klappa, C.F., 1983. Subaerial exposure environment. In: Scholle, P.A., Bebout, D.G., Moore, C.H. (Eds.), Carbonate Depositional Environments. American Association of Petroleum Geologists, Memoir 33. American Association of Petroleum Geologists, Tulsa, United States, pp. 1-54.

Etherington, D., 2004. Sedimentology and depositional architecture of the Cayman (Miocene) and Pedro Castle (Pliocene) Formations on Western Grand Cayman, British West Indies. Unpublished M.Sc. Thesis, University of Alberta, Canada, 122 pp.

Folk, R.L., Roberts, H.H., Moore, C.H., 1973. Black phytokarst from Hell, Cayman Islands, British West Indies. Geological Society of America Bulletin 84, 2351-2360.

Gradstein, F.M., Ogg, G., Schmitz, M., 2012. The Geologic Time Scale, 2012. Elsevier, 1176 pp.

Hodell, D.A., Curtis, J.H., Sierro, F.J., Raymo, M.E., 2001. Correlation of late Miocene to early Pliocene sequences between the Mediterranean and North Atlantic. Paleoceanography 16, 164-178.

Horsfield, W.T., 1975. Quaternary vertical movements in the Greater Antilles. Geological Society of America Bulletin 86, 933-938.

Hunter, I.G., Jones, B., 1990. Sedimentology of the late Pleistocene Ironshore Formation on Grand Cayman. In: Larue, D.K., Draper, G. (Eds.), Transactions of the 12th Caribbean Geological Conference. 12th Caribbean Geological Conference, Virgin Islands, United States, pp. 104-114.

Iturralde-Vinent, M.A., 1994. Cuban geology: A new plate-tectonic synthesis. Journal of Petroleum Geology 17, 39-70.

Iturralde-Vinent, M.A., 1998. Synopsis de la constitución geológica de Cuba. In: Melgarejo, J.C., Proenza, J.A. (Eds.), Geologíay Metalogénia de Cuba: Una Introducción. Acta Geológica Hispánica 33, 9-56.

Iturralde-Vinent, M.A., 2003. Ensayo sobre la paleogeografía del Cuaternario de Cuba. V Congreso de Geología y Minería 24-28, 54-74.

Iturralde-Vinent, M.A., 2006. Meso-Cenozoic Caribbean paleogeography: implications for the historical biogeography of the region. International Geology Review 48, 791-827.

Iturralde-Vinent, M.A., Macphee, R.D.E., 1999. Paleogeography of the Caribbean region: implications for Cenozoic biogeography. Bulletin of the American Museum of Natural History 238, 1-95.

Jiménez-Moreno, G., Pérez-Asensio, J.N., Larrasoaña, J.C., Aguirre, J., Civis, J., Rivas-Carballo, M.R., Valle-Hernández, M.F., González-Delgado, J.A., 2013. Vegetation, sea-level and climate changes during the Messinian salinity crisis. Geological Society of America Bulletin 125, 432-444.

Johnson, R.G., 2001. Last interglacial sea stands on Barbados and an anomalous deglaciation timed by differential uplift. Journal of Geophysical Research 106, 11543-11551.

Jones, B., 1989. The role of micro-organisms in phytokarst development on dolostones and limestones, Grand Cayman, British West Indies. Canadian Journal of Earth Sciences 26, 2204-2213.

Jones, B., 1990. Tunicate spicules and their syntaxial overgrowths: examples from the Pleistocene Ironshore Formation, Grand Cayman, British West Indies. Canadian Journal of Earth Sciences 27, 525-532.

Jones, B., 1992a. Caymanite, a cavity-filling deposit in the Oligocene-Miocene Bluff Formation of the Cayman Islands. Canadian Journal of Earth Sciences 29, 720-736.

Jones, B., 1992b. Void-filling deposits in karst terrains of isolated oceanic islands: a case study from Tertiary carbonates of the Cayman Islands. Sedimentology 39, 857-876.

Jones, B., 1994. Geology of the Cayman Islands. In: Brunt, M.A., Davies, J.E. (Eds.), The Cayman Islands: Natural History and Biogeography. Kluwer, Dordrecht, The Netherlands, pp. 13-49.

Jones, B., 2005. Dolomite crystal architecture: genetic implications for the origin of the Tertiary dolostones of the Cayman Islands. Journal of Sedimentary Research 75, 177-189.

Jones, B., Hunter, I.G., 1989. The Oligocene-Miocene Bluff Formation on Grand Cayman.

Caribbean Journal of Science 25, 71-85.

Jones, B., Hunter, I.G., 1990. Pleistocene paleogeography and sea levels on the Cayman Islands, British West Indies. Coral Reefs 9, 81-91.

Jones, B., Hunter, I.G., 1994a. Evolution of an isolated carbonate bank during Oligocene, Miocene and Pliocene Times, Cayman Brac, British West Indies. Facies 30, 25-50.

Jones, B., Hunter, I.G., 1994b. Messinian (Late Miocene) karst on Grand Cayman, British Indies: an example of an erosional sequence boundary. Journal of Sedimentary Research 64, 531-541.

Jones, B., Hunter, I.G., Kyser, T.K., 1994a. Revised stratigraphic nomenclature for Tertiary strata of the Cayman Islands, British West Indies. Caribbean Journal of Science 30, 53-68.

Jones, B., Hunter, I.G., Kyser, T.K., 1994b. Stratigraphy of the Bluff Formation (Miocene-Pliocene) and the newly defined Brac Formation (Oligocene), Cayman Brac, British West Indies. Caribbean Journal of Science 30, 30-51.

Jones, B., Luth, R.W., 2003. Temporal evolution of Tertiary dolostones on Grand Cayman as determined by $^{87}Sr/^{86}Sr$. Journal of Sedimentary Research 73, 187-205.

Jones, R.W., 2009. Stratigraphy, palaeoenvironmental interpretation and uplift history of Barbados based on foraminiferal and other palaeontological evidence. Journal of Micropalaeotology 28, 37-44.

Kominz, M.A., Miller, K.G., Browning, J.V., 1998. Long-term and short-term global Cenozoic sea-level estimates. Geology 26, 311-314.

Lajoie, K.R., 1986. Coastal tectonics. In: Wallace, R.E. (Ed.), Active Tectonics. National Academy Press, Washington, DC, United States, pp. 95-124.

MacDonald, K.C., Holcombe, T.L., 1978. Inversion of magnetic anomalies and sea-floor spreading in the Cayman Trough. Earth and Planetary Science Letters 40, 407-414.

MacNeil, A., 2001. Sedimentology, diagenesis, and dolomitization of the Pedro Castle Formation on the Cayman Brac, British West Indies. Unpublished M.Sc. Thesis, University of Alberta, Canada, 128 pp.

MacNeil, A., Jones, B., 2003. Dolomitization of the Pedro Castle Formation (Pliocene), Cayman

Brac, British West Indies. Sedimentary Geology 162, 219-238.

Mann, P., Demets, C., Wiggins-Grandison, M., 2007. Toward a better understanding of the Late Neogene strike-slip restraining bend in Jamaica: geodetic, geological, and seismic constraints. In: Cunningham, W.D., Mann, P. (Eds.), Tectonics of Strike-Slip Restraining and Releasing Bends. Geological Society of London, Special Publications 290, pp. 239-253.

Matley, C.A., 1926. The geology of the Cayman Islands (British West Indies) and their relation to the Bartlett Trough. Quarterly Journal of the Geological Society of London 82, 352-387.

Miller, K.G., Kominz, M.A., Browning, J.V., Wright, J.D., Mountain, G.S., Katz, M.E., Sugarman, P.J., Cramer, B.S., Christie-Blick, N., Pekar, S.F., 2005. The Phanerozoic record of global sea-level change. Science 310, 1293-1298.

Miller, K.G., Mountain, G.S., Browning, J.V., Kominz, M., Sugarman, P.J., Christie-Blick, N., Katz, M.E., Wright, J.D., 1998. Cenozoic global sea level, sequences, and the New Jersey Transect: results from coastal plain and continental slope drilling. Reviews of Geophysics 36, 569-601.

Miller, K.G., Mountain, G.S., Wright, J.D., Browning, J.V., 2011. A 180-million-year record of sea level and ice volume variations from continental margin and deep-sea isotopic records. Oceanography 24, 40-53.

Miller, K.G., Wright, J.D., Browning, J.V., Kulpecz, A., Kominz, M., Naish, T.R., Cramer, B.S., Rosenthal, Y., Peltier, W.R., Sosdian, S., 2012. High tide of the warm Pliocene: implications of global sea level for Antarctic deglaciation. Geology 40, 407-410.

Mylroie, J.E., Carew, J.L., 1995. Karst development on carbonate islands. In: Budd, D.A., Saller, A.H., Harris, P.A. (Eds.), Unconformities in Carbonate Strata-Their Recognition and the Significance of Associated Porosity. American Association of Petroleum Geologists Memoir 63. American Association of Petroleum Geologists, Tulsa, United States, pp. 55-76.

Passaro, S., Ferranti, L., De Alteriis, G., 2011. The use of high-resolution elevation histograms for mapping submerged terraces: tests from the eastern Tyrrhenian Sea and the eastern Atlantic Ocean. Quaternary International 232, 238-249.

Pekar, S., Miller, K.G., 1996. New Jersey Oligocene “Icehouse” sequences (ODP Leg 150X) correlated with global $\delta^{18}O$ and Exxon eustatic records. Geology 24, 567-570.

Perfit, M.R., Heezen, B.C., 1978. The geology and evolution of the Cayman Trench. Geological Society of America Bulletin 89, 1155-1174.

Pigram, C.J., Davies, P.J., Feary, D.A., Symonds, P.A., 1992. Absolute magnitude of the second-order middle to late Miocene sea level fall, Marion Platform, Northeast Australia. Geology 20, 858-862.

Purdy, E.G., 1974. Reef configurations: cause and effect. In: Laporte, L.F. (Ed.), Reefs in Time and Space. Society of Economic Paleontologists and Mineralogists Special Publication 18, pp. 9-76.

Purdy, E.G., Waltham, D., 1999. Reservoir implication of modern karst topography. American Association of Petroleum Geologists Bulletin 83, 1774-1794.

Purdy, E.G., Winterer, E.L., 2001. Origin of atoll lagoons. Geological Society of America Bulletin 113, 837-854.

Radtke, U., Schellmann, G., 2006. Uplift history along the Clermont Nose Traverse on the West Coast of Barbados during the last 500,000 years- implications for paleo-sea level reconstructions. Journal of Coastal Research 22, 350-356.

Rojas-Agramonte, Y., Neubauer, F., Bojar, A.V., Heil, E., Handler, R., Garcia Delgado, D.E., 2006. Geology, age and tectonic evolution of the Sierra Maestra Mountains, southeastern Cuba. Geologica Acta 4, 123-150.

Rojas-Agramonte, Y., Neubauer, F., Handler, R, Garcia-Delgado, D.E., Friedl, G., Delgado-Damas, R., 2005. Variation of palaeostress patterns along the Oriente transform wrench corridor, Cuba: significance for Neogene-Quaternary tectonics of the Caribbean realm. Tectonophysics 396, 161-180.

Rouchy, J.M., Caruso, A., 2006. The Messinian salinity crisis in the Mediterranean basin: A reassessment of the data and an integrated scenario. Sedimentary Geology 188-189, 35-67.

Saller, A.H., Budd, D.A., Harris, P.M., 1994. Unconformities and porosity development in carbonate strata: ideas from a Hedberg Conference. American Association of Petroleum Geologists Bulletin 78, 857-872.

Saller, A.H., Dickson, J.A.D., Matsuda, F., 1999. Evolution and distribution of porosity associated with sub-aerial exposure in upper Palaeozoic platform limestones, West Texas. American Association of Petroleum Geologists Bulletin 83, 1835-1844.

Schlager, W., 2003. Benthic carbonate factories of the Phanerozoic. International Journal of Earth Science 92, 445-464.

Schlager, W., Purkis, S.J., 2013. Bucket structure in carbonate accumulations of the Maldive, Chagos and Laccadive archipelagos. International Journal of Earth Science 102, 2225-2238.

Schlager, W., Warrlich, G., 2009a. Record of sea-level fall in tropical carbonates. Basin Research 21, 209-224.

Schlager, W., Warrlich, G., 2009b. Falling-stage systems tract in tropical carbonate rocks. In Swart, P.K., Eberli, G.P., McKenzie, J.A. (Eds.), Perspectives in Carbonate Geology: A Tribute to the Career of Robert Nathan Ginsburg. International Association of Sedimentologists, Special Publication 41, 305-325.

Sosdian, S., Rosenthal, Y., 2009. Deep-sea temperature and ice volume changes across the Pliocene-Pleistocene climate transitions. Science 325, 306-310.

Speed, R.C., Cheng, H., 2004. Evolution of marine terraces and sea level in the last interglacial, Cave Hill, Barbados. Geological Society of America Bulletin 116, 219-232.

Stephenson, W.J., 2000. Shore platforms: a neglected coastal feature? Progress in Physical Geography 24, 311-327.

Stoddart, D.R., 1980. Geology and geomorphology of Little Cayman. Atoll Research Bulletin 241, 11-16.

Trenhaile, A.S., 2000. Modeling the development of wave-cut shore platforms. Marine Geology 166, 163-178.

Uzelman, B.C., 2009. Sedimentology, diagenesis, and dolomitization of the Brac Formation (Lower Oligocene), Cayman Brac, British West Indies. Unpublished M.Sc. Thesis, University of Alberta, Canada, 120 pp.

Van Sickel, W.A., Kominz, M.A., Miller, K.G., Browning, J.V., 2004. Late Cretaceous and Cenozoic sea-level estimates: backstripping analysis of borehole data, onshore New Jersey. Basin Research 16, 451-465.

Vézina J.V., 1997. Stratigraphy and sedimentology of the Pleistocene Ironshore Formation at Rogers Wreck Point, Grand Cayman: a 400 Ka Record of Sea-level Highstands. Unpublished M.Sc. Thesis, University of Alberta, Canada, 131 pp.

Vézina, J.V., Jones, B., Ford, D.C., 1999. Sea-level highstands over the last 500,000 years: evidence from the Ironshore Formation on Grand Cayman, British West Indies. Journal of Sedimentary Research 69, 317-327.

Weidlich, O., 2010. Meteoric diagenesis in carbonates below karst unconformities: heterogeneity and control factors. In: Van Buchem, F.S.P., Gerdes, K.D., Esteban, M. (Eds.), Mesozoic and Cenozoic Carbonate Systems of the Mediterranean and the Middle East: Stratigraphic and Diagenetic Reference Models. Geological Society of London, Special Publications 329, pp. 291-315.

Wignall, B.D., 1995. Sedimentology and diagenesis of the Cayman (Miocene) and Pedro Castle (Pliocene) Formations at Safe Haven, Grand Cayman, British West Indies. Unpublished M.Sc. Thesis, University of Alberta, Canada, 110 pp.

Wright, V.P., 1982. The recognition and interpretation of paleokarsts: two examples from the Lower Carboniferous of South Wales. Journal of Sedimentary Petrology 5, 83-94.

Wright, V.P., 1996. Use of paleosols in sequence stratigraphy of peritidal carbonates. In: Hesselbo, S.P., Parkinson, D.N. (Eds.), Sequence Stratigraphy in British Geology. Geological Society of London, Special Publication 103, pp. 63-74.

Wright, V.P., Smart, P.L., 1994. Paleokarst (dissolution diagenesis): its occurrence and Hydrocarbon Exploration Significance. Developments in Sedimentology 51, 477-517.

Zhang, J., Scott, D.B., 1996. Messinian deep-water turbidites and glacioeustatic sea-level changes in the North Atlantic: linkage to the Mediterranean salinity crisis. Paleoceanography

11, 277-297.

Zhao, H.W., Jones, B., 2012a. Origin of “Island Dolostones”: a case study from the Cayman Formation (Miocene), Cayman Brac, British West Indies. Sedimentary Geology 243-244, 191-206.

Zhao, H.W., Jones, B., 2012b. Genesis of fabric-destructive dolostones: a case study of the Brac Formation (Oligocene), Cayman Brac, British West Indies. Sedimentary Geology 267-268, 36-54.

Zhao, H.W., Jones, B., 2013. Distribution and interpretation of rare earth elements and yttrium in Cenozoic dolostones and limestones on Cayman Brac, British West Indies. Sedimentary Geology 284-285, 26-38.

CHAPTER 3: ONGOING, LONG-TERM EVOLUTION OF AN UNCONFORMITY THAT ORIGINATED AS A KARSTIC SURFACE IN THE LATE MIOCENE: A CASE STUDY FROM THE CAYMAN ISLANDS, BRITISH WEST INDIES[1]

1. Introduction

The evolution of carbonate successions on isolated oceanic islands is fundamentally controlled by changes in sea level and tectonic activity (cf. Schlanger and Premoli Silva, 1986; Lincoln and Schlanger, 1987; Jones and Hunter, 1994b; Liang and Jones, 2014). Weathering that takes place while the islands are subaerially exposed commonly leads to loss of strata and significant surface and subsurface modification of the exposed carbonates (Bathurst, 1975; Esteban and Klappa, 1983; James and Choquette, 1990; Flügel, 2004; Frisia and Borsato, 2010). Karst surfaces, which commonly develop under the influence of hot, humid climates, are particularly important because they (1) form the antecedent topography that may influence the early stages of sedimentation during the ensuing highstand (e.g., Purdy, 1974; Purdy and Winterer, 2001; Liang and Jones, 2014), (2) will become the unconformities (i.e., sequence boundaries) that separate successive depositional packages (Esteban and Klappa, 1983; James and Choquette, 1990; Tucker, 1990; Wright, 1994; Clari et al., 1995; Hillgärtner, 1998; Sattler et al., 2005; Alonso-Zarza and Tanner, 2006; Brasier, 2011), and (3) will delineate horizons with which meteoric diagenesis and/or dolomitization may be genetically related (Esteban and Klappa, 1983; James and Choquette, 1988; Tucker, 1990; Wright and Smart, 1994; Saller et al., 1994, 1999; Whitaker et al., 1999; Budd et al., 2002; Frisia and Borsato, 2010; Miller et al., 2012; Zhao and Jones, 2012). The karst topography that develops on erosional surfaces like these is controlled by the complex interplay between numerous variables, including eustatic changes in sea level, tectonics, climate, hydrogeology, lithology, vegetation, porosity and permeability of the bedrock (White, 1984, 1988; Ford and Williams, 2007). The impact of factors such as sea-level

1 This chapter has been submitted to *Sedimentary Geology* as: Liang, T. and Jones, B., Ongoing, long-term evolution of an unconformity that originated as a karstic surface in the Late Miocene: A case study from the Cayman Islands, British West Indies.

change and tectonic movement are commonly difficult to decipher because they may produce the same end-result.

This study focuses on the unconformity that defines the upper boundary of the Cayman Formation (Miocene) that is found on Grand Cayman and Cayman Brac (Figs. 3-1, 3-2). This unconformity, named the Cayman Unconformity by Jones and Hunter (1994b), first developed during the Messinian when sea level was 30-180 m below present day sea level (Berggren and Haq, 1976; Adams et al., 1977; Vail et al., 1977; Cita and Ryan, 1978; Loutit and Keigwin, 1982; Hodell and Kennett, 1986; Pigram et al., 1992; Aharon et al., 1993; Zhang and Scott, 1996). Since then, this unconformity has experienced a complex developmental history. Today, parts of the original unconformity are still covered by younger sediments whereas other parts are exposed to the atmosphere and being actively weathered. Where exposed on the eastern part of Grand Cayman and the uplifted core of Cayman Brac, the surface is characterized by extensive phytokarst, pinnacles, sinkholes, and solution-widened joints (Doran, 1945; Folk et al., 1973; Jones and Smith, 1988; Squair, 1988; Jones, 1989, 1992a, 1992b). Although these islands have undergone different tectonic histories over the last 3.6 myrs (Zhao and Jones, 2012, 2013; Liang and Jones, 2014), they are both free of surface streams and siliciclastic sediments.

This study focuses on the multistage evolution of the Cayman Unconformity by examining its geological evolution and the factors that have controlled its continued development in areas where it is now exposed on Grand Cayman and Cayman Brac. Comparison between the two islands allows an assessment of the influences that tectonic uplift as opposed to eustatic sea level changes have had on the development of this unconformity. By doing so, this study demonstrates the complex developmental history that is responsible for the development of unconformities in carbonate successions on isolated oceanic islands.

2. Methods

The karst forms exposed on the upper surface of the Cayman Formation were delineated by various techniques, including digital elevation models (DEMs), air photo interpretation, and field observations. The DEMs used herein were imaged by the last returns from laser scanning,

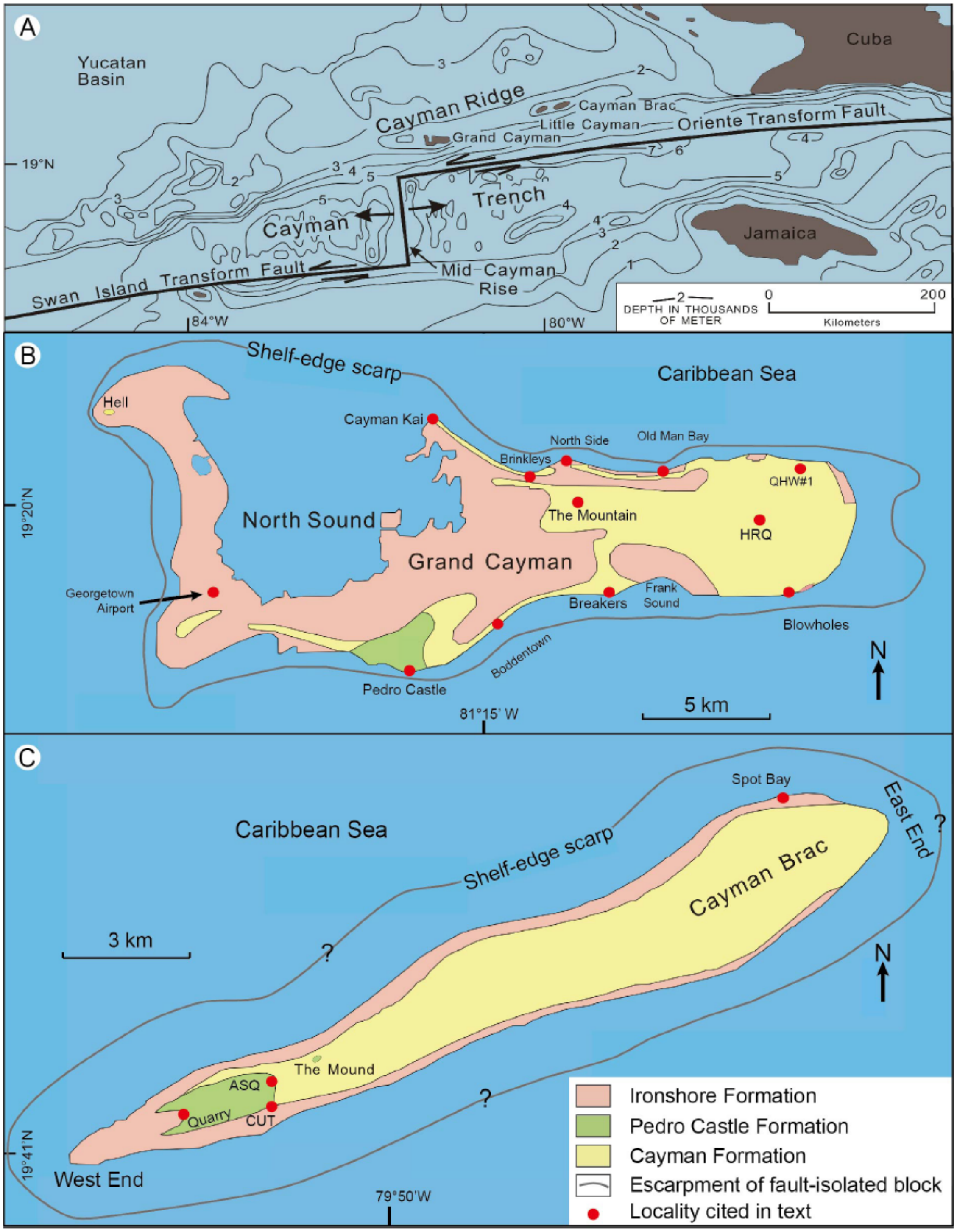

Fig. 3-1. (A) Location of Cayman Islands relative to the Mid-Cayman Rise, the Cayman Trench, and the Oriente Transform Fault (modified from Jones, 1994, and based on maps from Perfit and Heezen, 1978, MacDonald and Holcombe, 1978). (B) Surface geology on Grand Cayman (modified from Jones, 1994). The gray line delineates the shelf-edge scarp of Grand Cayman (modified from Blanchon and Jones, 1995). (C) Surface geology on Cayman Brac (modified from Jones, 1994).

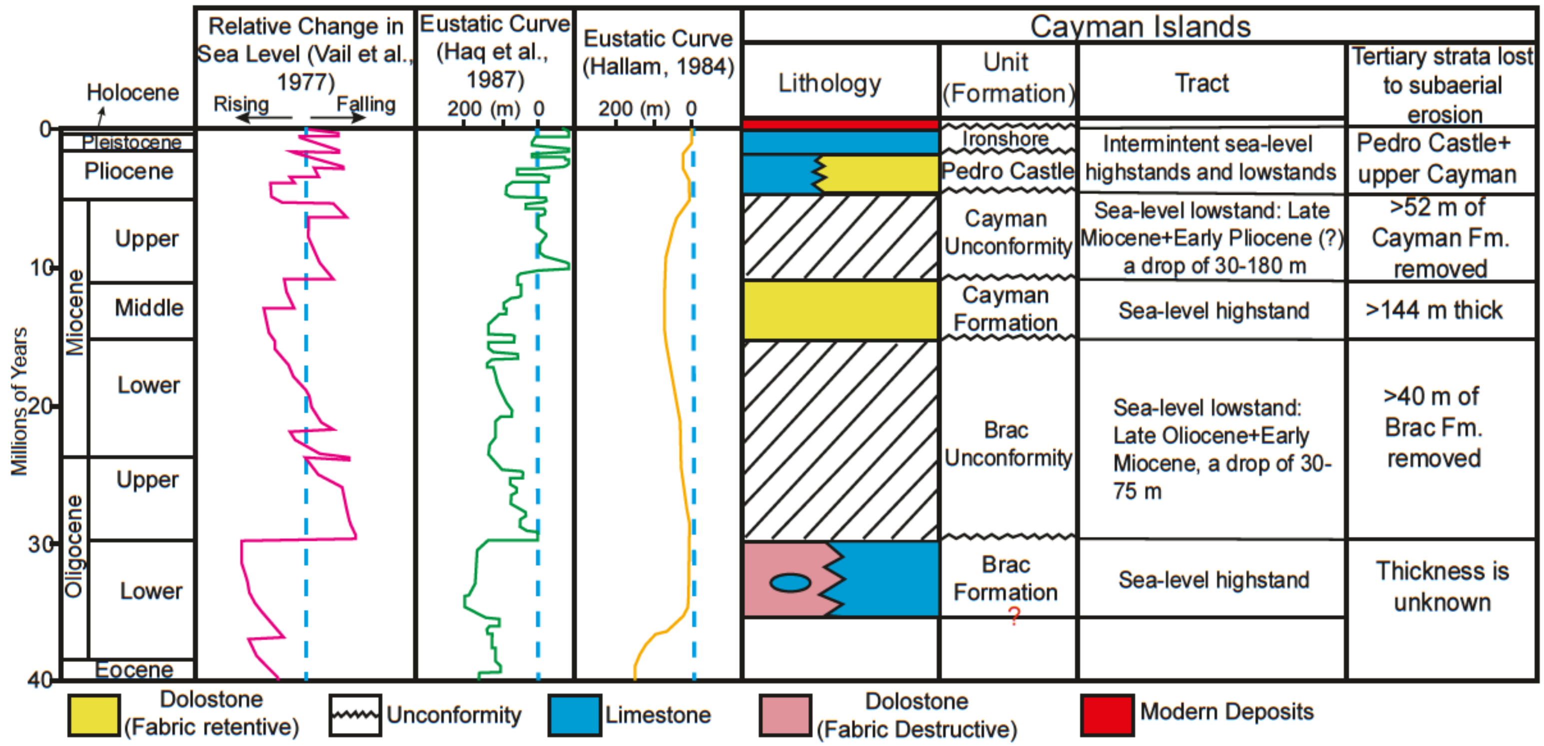

Fig. 3-2. Stratigraphic succession of the Cayman Islands (modified from Jones, 1994, 2005; Jones and Hunter, 1994a, 1994b; Jones et al., 1994a) showing lithology, dominant biota of each unit. Each unit is shown relative to the global sea level curves as given by Vail et al. (1977), Hallam (1984), and Haq et al. (1987).

which represent the appearance of the bare ground surface. Developed from data provided by the Lands and Survey Department, Government of the Cayman Islands, the high-resolution DEMs, with grid size of 3 m × 3 m, were analyzed using ArcGIS 10 software. This allows production of three-dimensional (3D) geometrical views of area that are otherwise inaccessible.

The “Hillshade” tool in ArcGIS 10 can create a shaded relief model of a surface by considering the illumination and shadows. As such, topographic highs, lows, open sinkholes, and photolineaments on the exposed Cayman Formation were highlighted by overlying the original DEMs onto the Hillshade map.

Open sinkholes, which may contain water, were defined by comparison between depression-free DEMs and the original DEMs. The depression-free DEMs were generated automatically by the “Fill” tool in ArcGIS 10. Open sinkholes were identified by their sub-rounded to elliptical shape, their location on the exposed Cayman Formation, and that they are clearly not man-made. Given that the DEMs have a horizontal resolution of 3 m, sinkholes, solution-widened joints, and phytokarst features smaller than 3 m × 3 m could not be identified from the DEMs. Assessment of the small-scale features was restricted to examination of outcrops located along the coast because much of the interior of Grand Cayman and Cayman Brac is covered with dense tropical vegetation and is therefore largely inaccessible.

3. Terminology

Folk et al. (1973), based on exposures of the Cayman Formation at Hell on Grand Cayman, coined the term “phytokarst” as “a landform produced by rock solution in which boring plant filaments are the main agent of destruction”. Phytokarst has a honeycomb appearance with unoriented concavities (Folk et al., 1973; Jones, 1989), and surfaces that are covered by organic coatings that include fungi, sporangia, spores, mucilage, algae, and bacteria (Jones, 1989). Due to the organic-rich coatings, weathered phytokarst surfaces are grey to black and contrast sharply with the white dolostones of the Cayman Formation (Folk et al., 1973; Jones, 1989).

A sinkhole (= doline) is a closed depression, which originates through dissolution, collapse, and/or subsidence (Gams, 1994, 2003; Sauro, 2003; Ford and Williams, 2007). Sinkholes are typically circular to subcircular in plan form and can be up to ~1 km in diameter and depths to several hundred metres (Sauro, 2003; Ford and Williams, 2007). Herein, the term sinkhole also includes "pit caves" as defined by Pace et al. (1993), Mylroie and Carew (1995), and Harris et al. (1995). Given that sinkholes may occur individually or in densely packed groups, the intensity (i.e., random, clustered, or regular) is used to define the distribution of sinkholes (Ford and Williams, 2007).

Joints are pull-apart breaks in consolidated rocks, with no displacement in any direction (Monroe, 1970; Ford and Williams, 2007). Commonly created by pressure release during erosion (Ford and Williams, 2007), they are prone to solution widening (e.g., Jones and Smith, 1988; Ford and Williams, 2007).

Photolineaments are narrow linear trends detectable on air photographs or satellite images (Ford and Williams, 2007) that typically reflect the presence of closely spaced high-angle faults or fractures with little or no displacement (Ford and Williams, 2007; Sabins, 2007).

4. Geologic setting

The Cayman Islands, which are located on the Cayman Ridge, include Grand Cayman, Cayman Brac, and Little Cayman (Jones, 1994; Fig. 3-1). To the south of these islands lies the Oriente Transform Fault, which separates the Caribbean Plate from the North American Plate (Perfit and Heezen, 1978; Fig 3-1A). The Oriente Transform Fault extends eastward from the north end of the Mid-Cayman Rise, which is an active spreading center that is located to the southwest of Grand Cayman. The Swan Island Transform Fault extends westward from the south end of Mid-Cayman Rise (MacDonald and Holcombe, 1978). The Oriente Transform Fault defines the northern margin of the Cayman Trench (Fig. 3-1A), which is up to 7686 m deep.

Between the late Eocene and Oligocene, the Oriente Transform Fault detached the Cayman Islands from their parent arc and transported them to their present locations (Iturralde-Vinent, 1994; Calais and Mercier de Lépinay, 1995). Since the early Middle Miocene, localized extensional features began to form (Iturralde-Vinent and Macphee, 1999; Iturralde-Vinent, 2006), resulting in each of the Cayman Islands being located on a different fault-isolated block (Matley, 1926; Horsfield, 1975; Stoddart, 1980; Vézina et al., 1999; Liang and Jones, 2014). The faults that define the margins of the Grand Cayman block and the Cayman Brac block gave rise to the shelf edge scarps (= escarpment), which extend downward into the oceanic basins (Rigby and Roberts, 1976). On the eastern part of the Grand Cayman block, the north and south escarpments are generally orientated west to east and parallel to the shoreline whereas the eastern margin is oriented north to south (Fig. 3-1B). Although the precise positions of the escarpments that define the Cayman Brac block have not yet been accurately resolved, air photos analyses indicate that they are probably parallel to the shorelines (Fig. 3-1C).

After the Late Miocene (7.25 Ma using the time scale of Gradstein et al., 2012, their Fig. 1.2), Cayman Brac experienced tectonic tilting until about 400 ka, whereas Grand Cayman appears to have remained tectonically stable (Jones and Hunter, 1990; Vézina et al., 1999; Zhao and Jones, 2012, 2013; Liang and Jones, 2014). Thus, Cayman Brac is characterized by an uplifted core that is flanked by low-lying, peripheral platform.

Matley (1926) originally assigned the exposed Neogene strata of the Cayman Islands to the Bluff Limestone, which was subsequently renamed as the Bluff Group (Jones et al., 1994a, 1994b). Unconformably overlain by the Pleistocene Ironshore Formation, the Bluff Group includes the Brac Formation, Cayman Formation, and Pedro Castle Formation, which were deposited during sea-level highstands that occurred in the early Oligocene, Middle Miocene, and Pliocene, respectively (Jones et al., 1994a, 1994b; Fig. 3-2). Each formation is bounded by unconformities that developed during sea-level lowstands. Development of the Cayman Unconformity started during the last 1.5 million years of the Miocene (Jones and Hunter, 1994b; Der, 2012; Liang and Jones, 2014) when the sea level was low during the Messinian salinity crisis. On Grand Cayman and Cayman Brac, much of this weathered surface was subsequently overlain by the Pedro Castle Formation, which resulted from sedimentation during the early Pliocene (Jones, 1994; Jones and Hunter, 1994a; Jones et al., 1994a, 1994b; Zhao and Jones, 2012, 2013; Liang and Jones, 2014). Subaerial erosion that took place during subsequent lowstands resulted in the Pedro Castle Formation being removed from the eastern half of Grand

Cayman and most of Cayman Brac and renewed exposure of the underlying Cayman Formation. Today, therefore, the Cayman Unconformity represents a composite weathering surface that has evolved through multiple stages of development.

5. The Cayman Unconformity

Differences in the topography of the Cayman Unconformity on Grand Cayman and Cayman Brac reflect the different tectonic histories of the two islands. The Cayman Unconformity on Grand Cayman, with a relief of 52 m, is characterized by (1) a deep depression (30 m below sea level) that is located under the modern day North Sound (Fig. 3-3), and (2) peripheral rims that are evident along the south, east, and north coasts on the eastern part of the island (Jones and Hunter, 1994b, their Fig. 12; Liang and Jones, 2014, their Fig. 14A; Fig. 3-3). Based on present-day surface exposures, Grand Cayman can be divided into the western and eastern parts with the boundary being defined by the eastern boundary of the Ironshore Formation, which stretches from Cayman Kai along the eastern side of The Mountain and then to Breakers (Fig. 3-1B). Over most of the western half of the island, the Cayman Unconformity is buried beneath the Pedro Castle Formation and/or the Ironshore Formation apart from isolated outcrops like that at Hell.

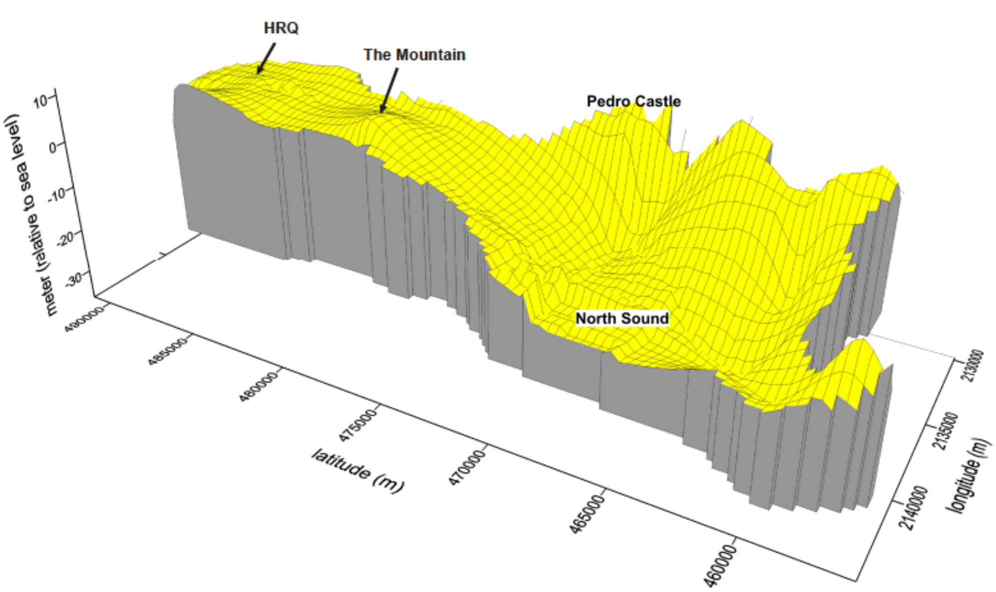

Fig. 3-3. Topography on upper surface of the Cayman Formation on Grand Cayman (from Liang and Jones, 2014, their Fig. 14). Surface is interpolated by Surfer 10 software from digital elevation data, outcrops and well data.

As such, it is typically located below present-day sea level. On the eastern half of the island, the widely exposed Cayman Unconformity has a relief of up to 23 m (Fig. 3-4).

Uplift of the east end of Cayman Brac means that the Cayman Unconformity now dips westward at an angle of ~0.5° (Jones, 1994; Jones and Hunter, 1994a; Jones et al., 1994b; Uzelman, 2009; Zhao and Jones, 2012, 2013; Liang and Jones, 2014; Fig. 3-5). This unconformity surface, with a maximum relief of 62 m, is either covered by the Pedro Castle Formation (west end of island only) or exposed. The exposed Cayman Unconformity, evident over much of the uplifted core, rises up to 46 m above sea level (asl) at the east end of the island. Peripheral rims are readily apparent on this weathered surface (Figs. 3-5, 3-6). Peripheral rims

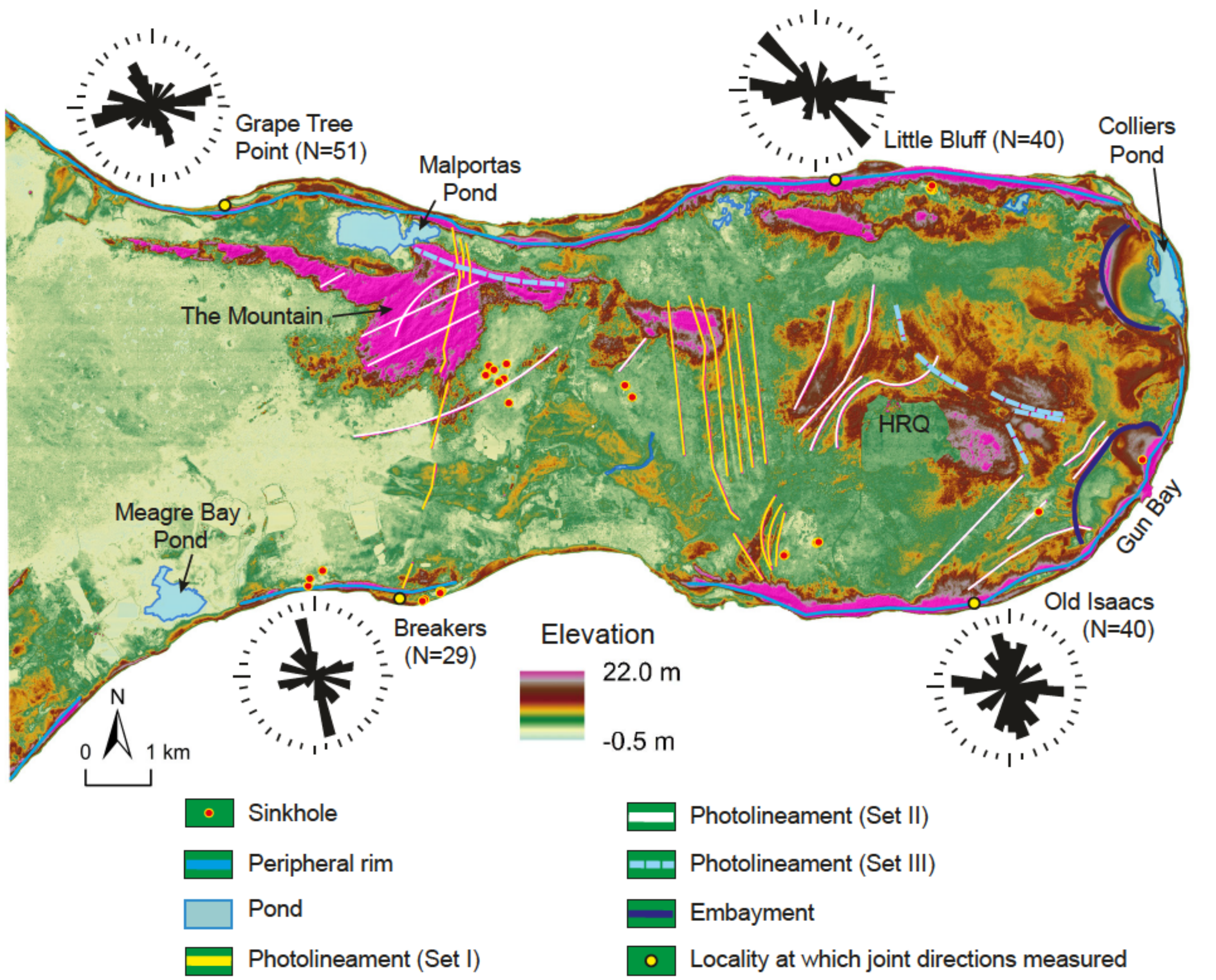

Fig. 3-4. Karst landforms and topography on the eastern half of Grand Cayman based on digital elevation models. The rose diagrams for joint orientations on Grand Cayman are from Rigby and Roberts (1976, their Fig. 30).

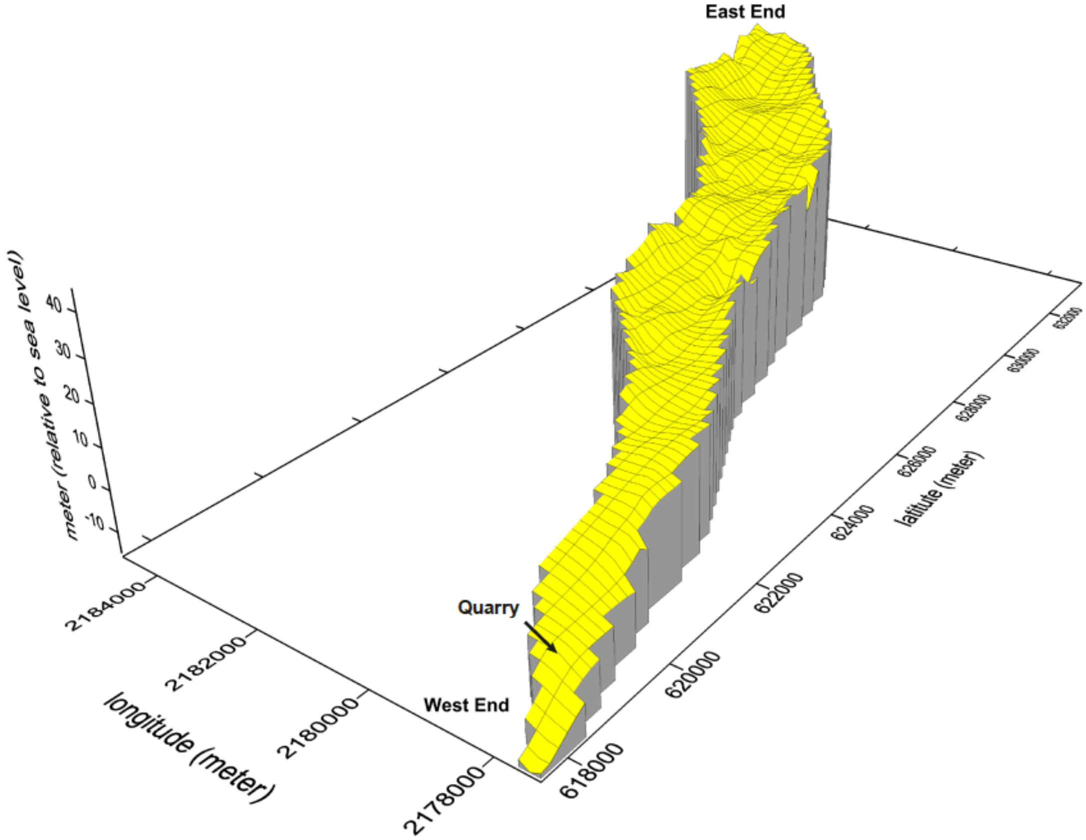

Fig. 3-5. Topography on upper surface of the Cayman Formation on the uplifted core of Cayman Brac (from Liang and Jones, 2014, their Fig. 15). Surface is interpolated by Surfer 10 software from digital elevation data, outcrops and drilling wells.

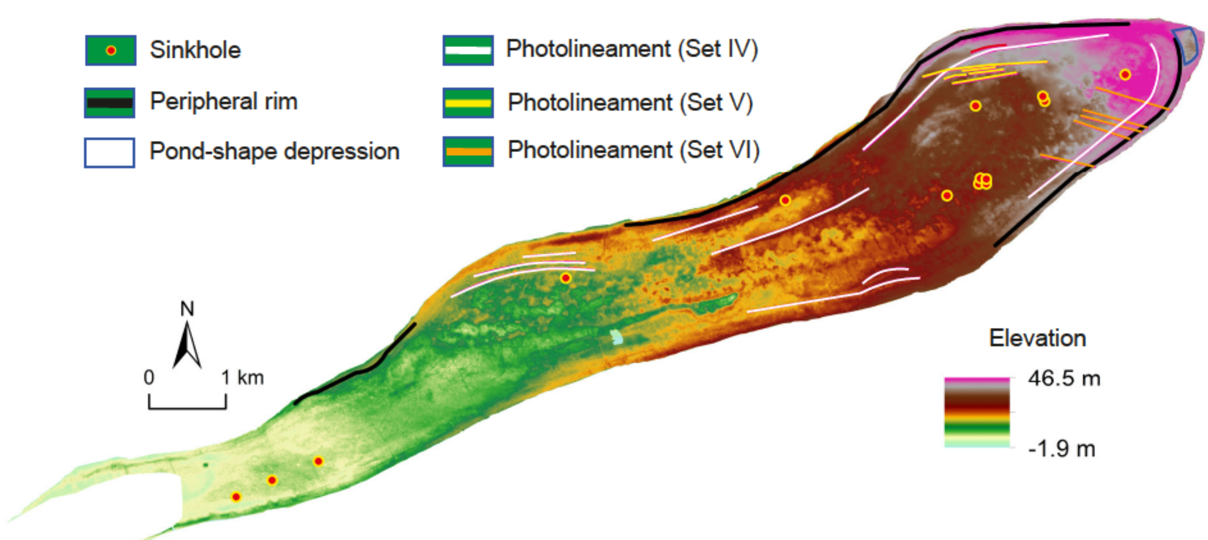

Fig. 3-6. Karst landforms and topography on exposed Cayman Unconformity exposed on the uplifted core of Cayman Brac. Based on digital elevation models.

on the eastern upslope margin are more pronounced than those on the western down slope margin (Figs. 3-5, 3-6).

6. Cayman Unconformity buried by younger strata

On Grand Cayman and Cayman Brac, exposures that show the Cayman Unconformity overlain by younger strata are rare. In a quarry near Pedro Castle, the Cayman Unconformity, which dips at <1° to the northwest, is evident as a well-defined surface that is highlighted by the contrast in colour between the Cayman Formation and the overlying Pedro Castle Formation (Fig. 3-7A). The unconformity is generally smooth with no evidence of small-scale surface karst features. Penetrating into the dolostones from the unconformity are numerous sponge borings (Fig. 3-7B) and rare bivalve (Lithophaga) borings. In a small quarry located about 1 km southwest of the western end of the Georgetown airport runway, the Cayman Unconformity forms the quarry floor and is overlain by limestones of the Ironshore Formation (Fig. 3-7C). Although a relief of about 2 m is evident on the unconformity, the surface is generally smooth and devoid of small-scale karst features.

On Cayman Brac, the best exposures of the Cayman Unconformity are in a quarry that is located on the west end of the island (Fig. 3-7D). As in the Pedro Castle Quarry, the Cayman Unconformity is highlighted by the contrast in the colors of the dolostones that form the Cayman Formation and the Pedro Castle Formation (Fig. 3-7E). There, the unconformity is characterized by small-scale variations in relief (Fig. 3-7E) and in some areas, sponge borings. No small-scale karst features are evident on the unconformity.

7. Cayman Unconformity exposed to atmosphere

Exposed surfaces of the Cayman Formation on Grand Cayman and Cayman Brac are characterized by (1) various topographic features including peripheral rims, topographic highs and lows, (2) karst features that include sinkholes and honeycombed rock pinnacles, and (3) solution-widened joints and photolineaments (Matley, 1926; Doran, 1954; Folk et al., 1973; Rigby and Roberts, 1976; Stoddart, 1980; Jones et al., 1984; Smith, 1987; Jones and Smith,

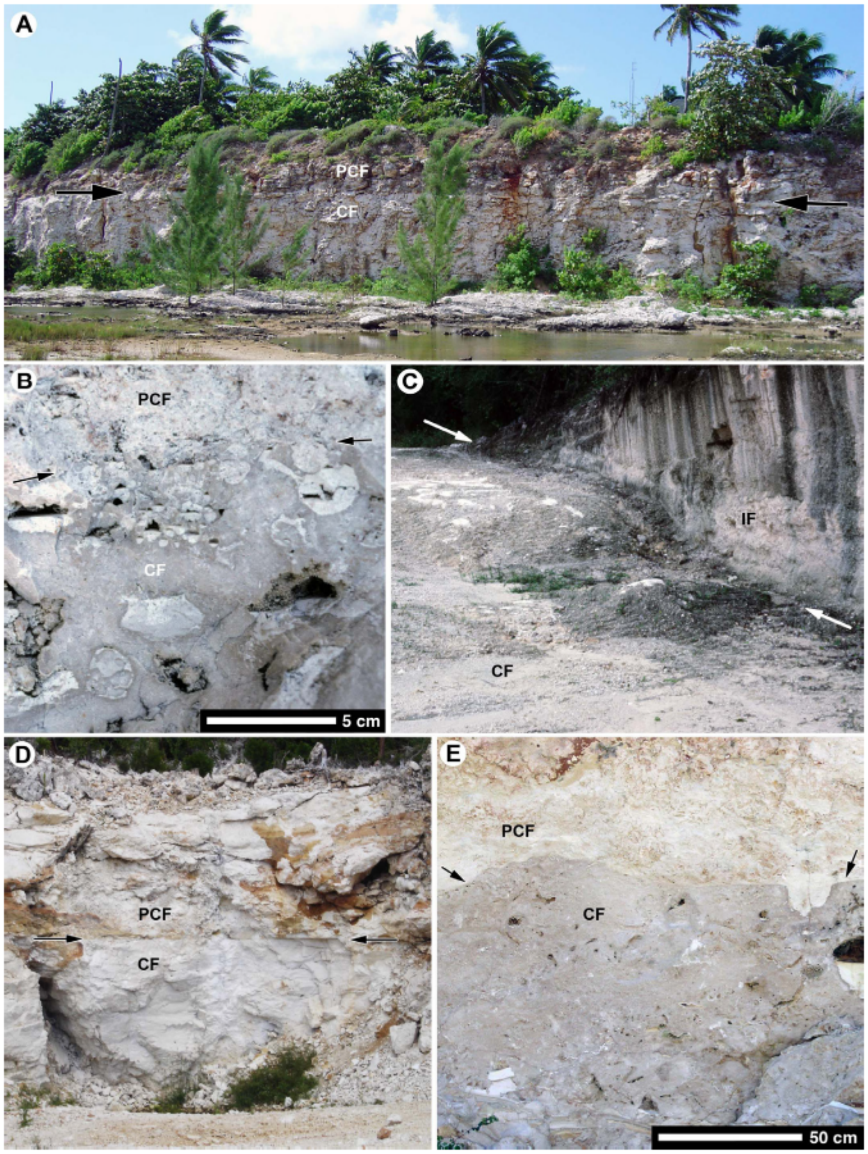

Fig. 3-7. Features of the Cayman Unconformity in outcrops where the Cayman Formation (CF) is overlain by the Pedro Castle Formation (PCF) or Ironshore Formation (IF). (A) South wall of Pedro Castle Quarry (Grand Cayman) showing the Cayman Unconformity (arrows) between the Cayman Formation and the Pedro Castle Formation. Quarry wall is about 10 m high, with the unconformity being about 8 m above sea level. (B) Close-up showing sponge borings extending down from Cayman Unconformity (arrows) and small cavities partly filled with internal sediments. Pedro Castle Quarry. (C) Limestones of the Ironshore Formation resting on top of irregular upper surface of the Cayman Formation (= Cayman Unconformity). Quarry southwest of west end of runway at Georgetown Airport. (D) General view of Cayman Unconformity (arrows) between the Cayman Formation and Pedro Castle Formation in quarry located at west end of Cayman Brac. Quarry wall is about 5 m high. (E) Minor relief on the Cayman Unconformity. Quarry at west end of Cayman Brac.

1988; Squair, 1988; Jones, 1989, 1992b, 1994; Jones and Hunter, 1994b; Liang and Jones, 2014).

7.1. Topographic features

7.1.1. Grand Cayman

Peripheral rims on the Cayman Unconformity, which rise 8-14 m asl, are developed in the coastal areas of the eastern part of Grand Cayman (Figs. 3-4, 3-8). The landward limit of the peripheral rims, which are formed of dolostones that belong to the Cayman Formation and the coastline, is constant (Jones and Hunter, 1994b; Liang and Jones, 2014).

Exposures in the interior of the island are characterized by a rugged surface, with much (up to 70 %) of it being less than 3 m asl. Topographic highs, which are > 3 m asl, are developed locally (Fig. 3-4), such as "The Mountain" (up to 22 m), the area around High Rock Quarry (HRQ,

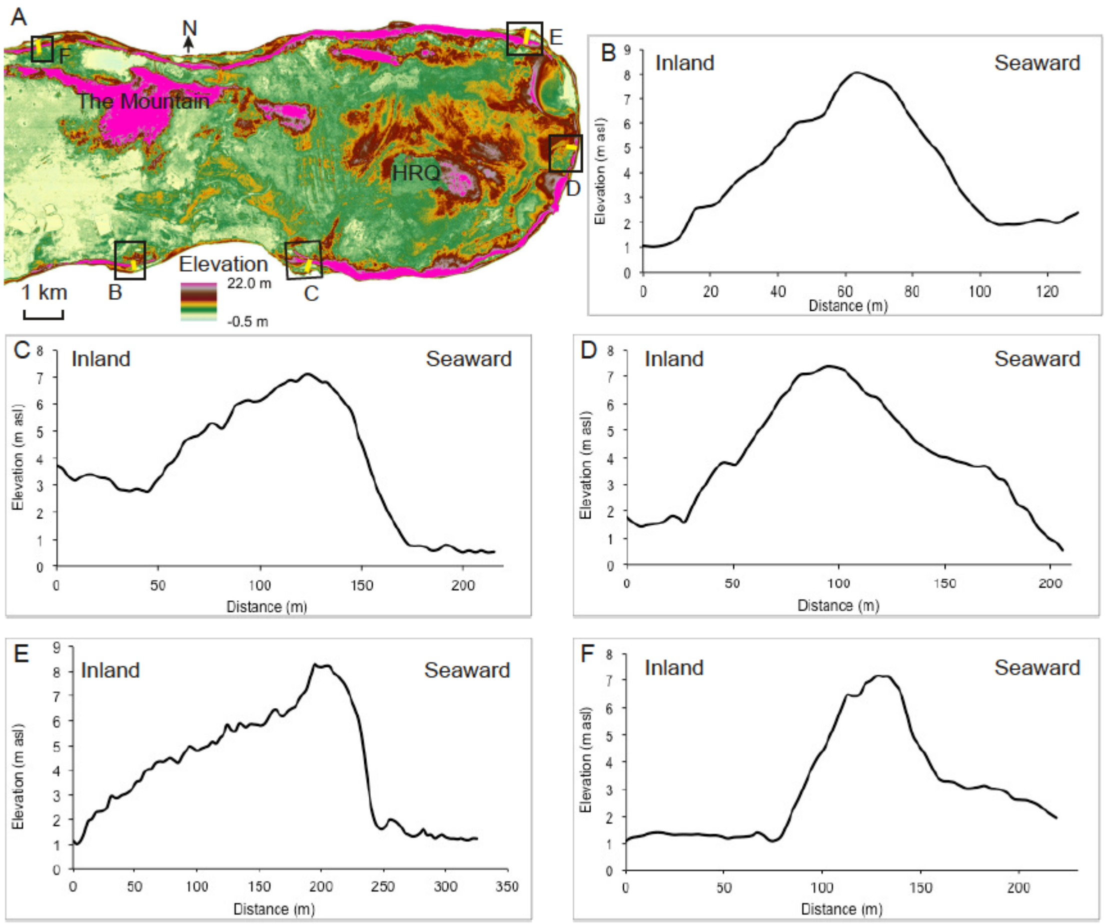

Fig. 3-8. Topographic transects (B, C, D, E and F) across peripheral rims in the coastal areas on the eastern half of Grand Cayman.

up to 9.3 m), and an inaccessible area between "The Mountain" and HRQ (up to 9.4 m).

In some of the coastal regions, there are large, brackish water ponds that are 0.4 to 1.2 m deep (Doran, 1954), and floored close to sea level (Fig. 3-9). These shallow ponds, including Meagre Bay Pond, Colliers Pond, and Malportas Pond, are irregular in shape (Fig. 3-4). Meagre Bay Pond, located on the south shore close to Boddentown, ~ 1 km wide and 1 km long, is located behind a high beach barrier (Fig. 3-9B). This pond desiccates completely during periods of prolonged dry weather (Rigby and Roberts, 1976). Colliers Pond, located in the northeast part of the island, is 0.5 km wide and 1.5 km long, and located behind a beach sand barrier (Fig. 3-9C). During dry weather, the shallowest areas of Colliers Pond commonly desiccate (Rigby and Roberts, 1976). Malportas Pond, 2 km long and 0.7 km wide lies between a ridge formed of the Cayman Formation that stretches from North Side and Old Man Bay (up to 9.0 m asl), and "The Mountain" (Fig. 3-9D). The shallowest areas commonly desiccate during dry weather (Rigby and Roberts, 1976).

Embayment-shaped depressions, up to 1.8 km in diameter, are evident in the Guy Bay and Colliers areas, which are located on the east coast (Fig. 3-4). The bottom of these depressions are

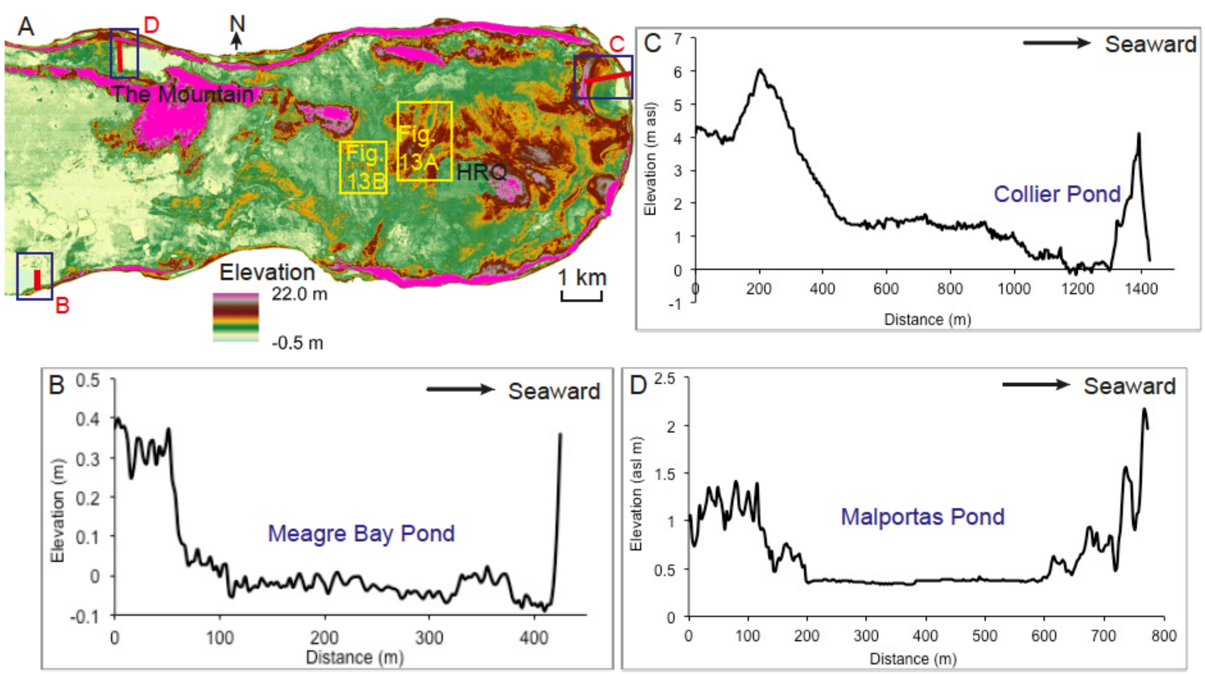

Fig. 3-9. Topographic transects showing changes in elevation through ponds (B, C, and D) on the eastern half of Grand Cayman. Yellow squares indicate locations of Figure 3-13A and 3-13B.

flat, with elevations being 1-2 m asl (Figs. 3-4, 3-9C). Their landward margins are topographic highs formed of the Cayman Formation, whereas their seaward margin varies. At Colliers, the embayment is separated from the offshore shelf by Colliers Pond, which act as a buffer zone between them. In contrast, the depression at Gun Bay is separated from offshore shelf by a peripheral rim.

7.1.2. Cayman Brac

On the uplifted core, peripheral rims that are up to 15 m higher than the surrounding land, are more pronounced than those on Grand Cayman (Figs. 3-6, 3-10). On the interior of the island, the elevation of the exposed Cayman Unconformity decreases gradually from the east end to the west end (Figs. 3-5, 3-6). Exposures on the upslope are more rugged and have steeper slopes than those in the downslope area (Figs. 3-5, 3-6, 3-10). DEMs reveal an elliptical

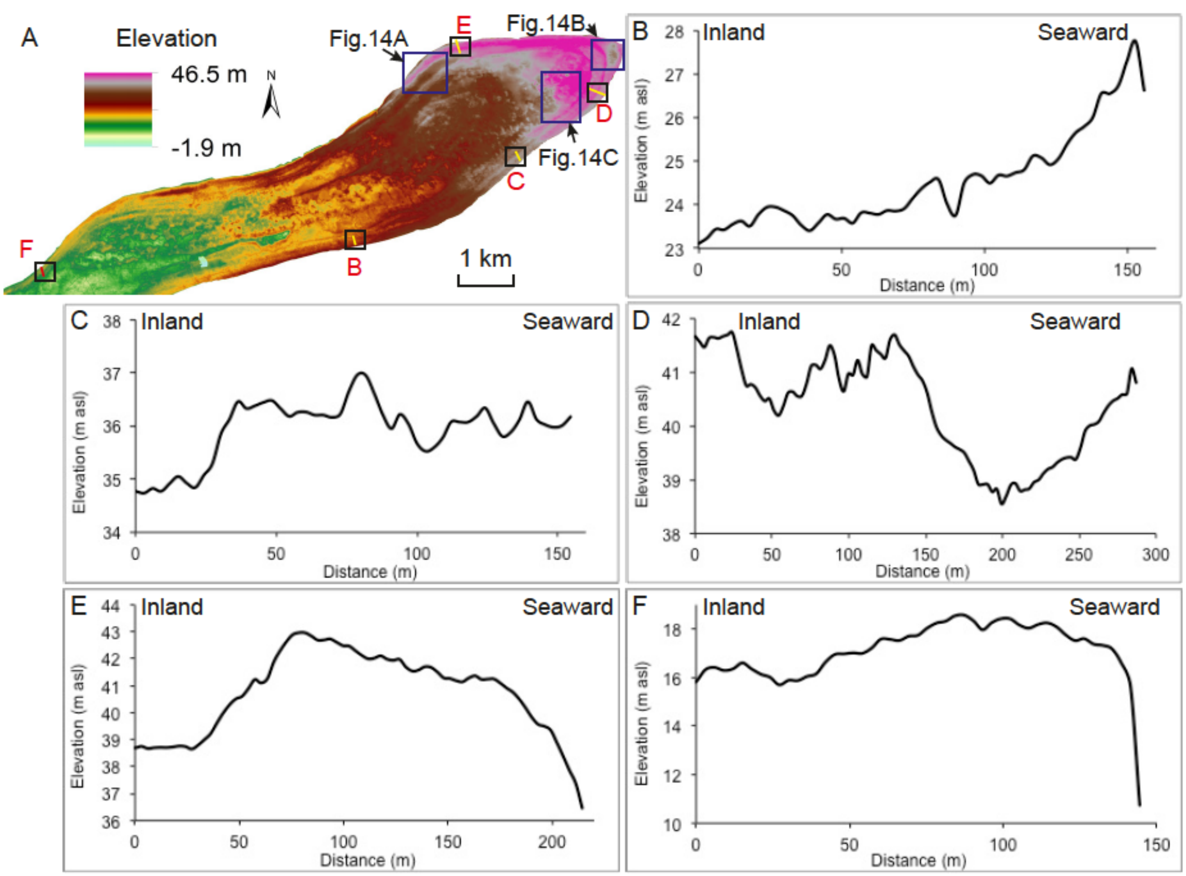

Fig. 3-10. Topographic transects (B, C, D, E and F) showing changes in elevations of peripheral rims along the coastal areas on Cayman Brac. Blue squares indicate locations of Figure 3-14A, 3-14B and 3-14C.

depression near East End that is about 300 m long and 200 m wide (Fig. 3-6). This bowl-shaped depression, with a relief up to 8 m is developed behind the vertical cliff that defines the edge of the bluff in this area. It is morphologically similar to ponds and the embayments found on Grand Cayman, suggesting that it may have originated in a similar manner prior to uplift of the island.

7.2. Karst features

On Grand Cayman and Cayman Brac, the exposed Cayman Formation is characterized by numerous sinkholes that are up to 10 m deep and 30 m in diameter (Doran, 1954; Folk et al., 1973; Jones and Smith, 1988; Jones, 1989, 1992b; Liang and Jones, 2015). These sinkholes may be open, filled with water, or filled with a variety of deposits, including rootcrete and various types of breccias that includes limestone and dolostone lithoclasts held in white limestone matrices, or red or orange limestone matrices (Doran, 1954; Jones and Smith, 1988; Jones, 1992b; Liang and Jones, 2015). The dolostones between the sinkholes has been weathered into honeycombed, sharp and jagged ridges and honeycombed, conical- or rectangular-shaped (up to 5 m high) pinnacles (Folk et al., 1973; Jones and Smith, 1988; Jones, 1989). The surfaces of the ridges and pinnacles and the walls of the sinkholes are dark grey to black in color due to the extensive phytokarst development (Matley, 1926; Doran, 1954; Folk et al., 1973; Stoddart, 1980; Jones and Smith, 1988; Squair, 1988; Jones, 1989; Fig. 3-11).

7.2.1. Grand Cayman

Forty large sinkholes, up to 20 m in diameter and up to 0.7 m deep, have been recognized on the DEMs that cover the inaccessible areas of the island (Fig. 3-4). Given that the sinkholes may be filled or partly filled by various deposits, the depths obtained from DEMs have to be treated as minimum estimates. Small sinkholes (< 3 m in diameter) cannot be recognized on DEMs because of resolution limits, and detailed mapping is impossible because the dense tropical vegetation and rugged surface produced by phytokarst mean that much of the island is inaccessible. On Grand Cayman, sinkholes identifiable on the DEMs are typically close to the photolineaments, especially in the area near “The Mountain” where photolineaments of Set I and

Fig. 3-11. Features commonly found on surface exposures of the Cayman Formation. (A) View of phytokarst at Hell, Grand Cayman showing jagged pinnacles around sinkholes and solution-widened joints that are filled with water and sediment. Pinnacles in foreground are up 1.5 m high. (B) Phytokarst developed in interior of Cayman Brac. (C) Sinkhole that is about 1 m in diameter and at least 20 m deep developed in dolostones of the Cayman Formation, interior of Cayman Brac. (D) Solution-widened joint in dolostones of Cayman Formation, quarry at west end of Cayman Brac. Note that the width of this joint at water level is about 2 m.

Set II intersect (Fig. 3-4).

7.2.2. Cayman Brac

Fourteen large sinkholes, 6 to 25 m in diameter and up to 10 m deep, have been detected on the DEMs that show the surface topography of the exposed Cayman Formation on Cayman Brac (Fig. 3-6). Most of the sinkholes identified from the DEMs are located on the eastern upslope areas of the interior part of the island (Fig. 3-6). The distribution, as revealed by the DEMs, is biased because none of the small, deep sinkholes, with the diameter up to 1 m and the depth up to 20 m, can be detected on the DEMs.

7.3. Joints and photolineaments

7.3.1. Grand Cayman

On Grand Cayman, three major joint sets that trend NNW-SSE, ENE-WSW, W-E are commonly apparent in areas where the Cayman Formation is well exposed (Rigby and Roberts, 1976; Jones, 1992b; Fig. 3-4). Near Grape Tree Point, for example, two major sets trending at NNW-SSE and ENE-WSW are apparent (Fig. 3-4). In contrast, at Little Bluff, Breaker and Old Issacs, the W-E and NNW-SSE sets dominate (Fig. 3-4). Vertical or westward dipping (~25°) solution-widened joints, up to 4 m wide (Fig. 3-12), in the Old Isaacs area, are open or filled with various deposits (Jones, 1992b). There is no correlation between the orientation of the joints and their width (Jones, 1992b). The vertical joints are commonly filled with flowstone and various types of breccia that are characterized by white dolostone lithoclasts held in white, red and orange limestone matrices, and dolostone matrices, whereas the westward dipping joints are commonly filled by caymanite (Jones and Smith, 1988; Jones, 1992b).

On Grand Cayman, three sets of photolineaments, comprising Set I that trends N-S, Set II that trends ENE-WSW, and Set III that trends NNW-SSE, are evident in the Cayman Formation that is exposed in the areas around "The Mountain" and HRQ (Fig. 3-4). Around the Mountain, the N-S and ENE-WSW sets are more common than the NNW-SSE set (Fig. 3-4). Photolineaments in the areas around HRQ show similar trends to those in "The Mountain",

Fig. 3-12. Solution-widened joint (~ 1 m wide) in dolostones of the Cayman Formation, Old Isaacs on Grand Cayman. The NNW-SSE joint is filled largely with dolostones lithoclasts that came from the Cayman Formation.

including the ENE-WSW set and the NNW-SSE set (Fig. 3-4). Photolineaments in the area between "The Mountain" and HRQ are dominated by the N-S set (Fig. 3-4).

In areas close to HRQ, transects across the photolineaments (sets I and II), derived from the DEMs, show that they are formed of ridges that are separated by valleys, with a local relief up to 2 m (Fig. 3-13). Each of the ridges appears symmetric, with gentle slopes (up to 5°) that merge with the valleys that are 20-100 m wide (Fig. 3-13). Although photolineaments are detectable on DEMs (Fig. 3-13), they are impossible to detect on surface outcrops in the field because of the dense tropical vegetation that grows in those areas.

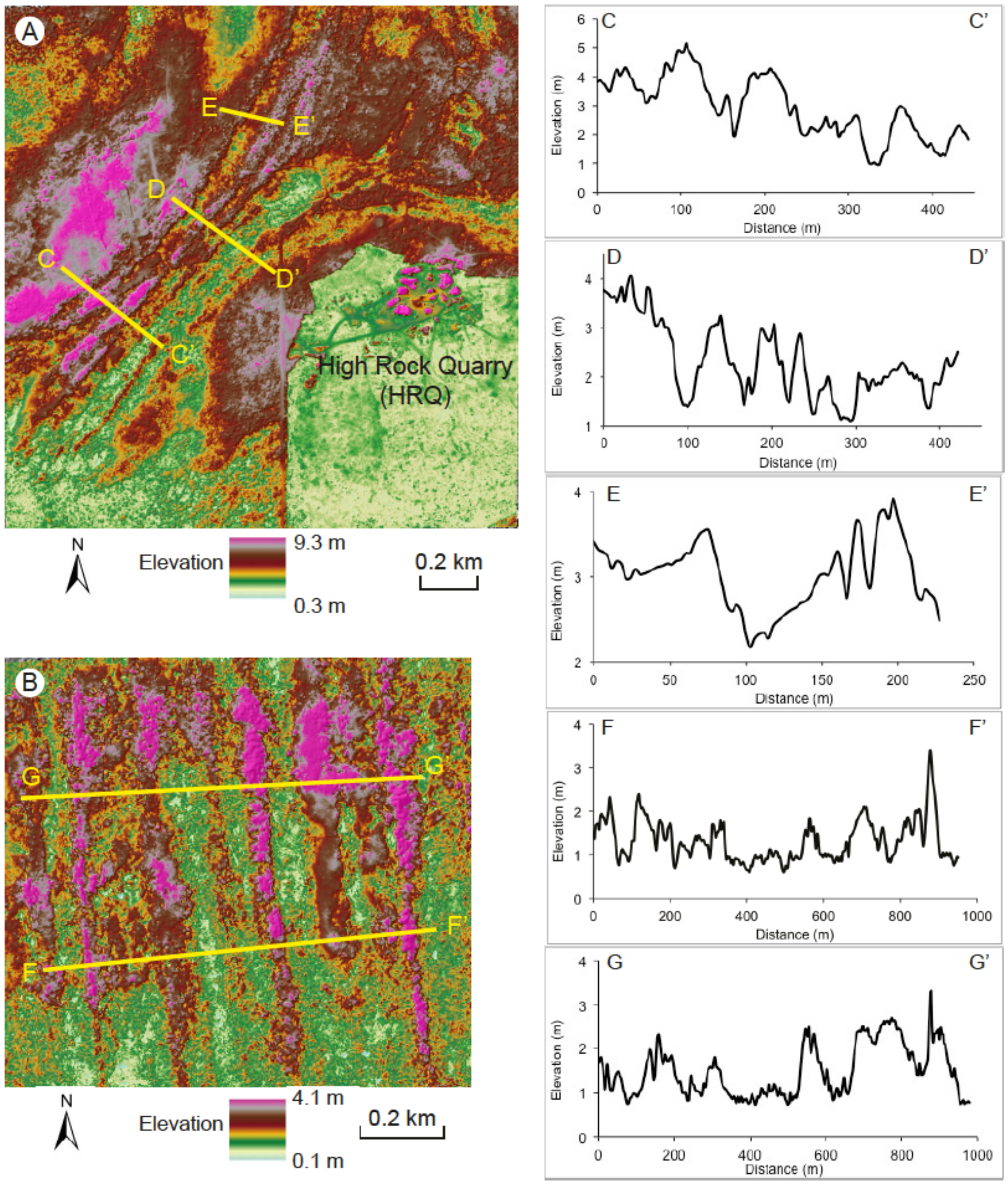

Fig. 3-13. Topographic transects (C-C', D-D', E-E', F-F', and G-G') showing topography of photolineaments on Grand Cayman. See Figure 3-9 for precise location.

The orientations of the photolineaments are similar to those of the joints. The NNW-SSE trending joints and NNW-SSE photolineaments (Set III) are parallel the northeastern or eastern margin of the Grand Cayman block. The ENE-WSW trending joints present at Grape Tree Point, is comparable with the lineaments trending at ENE-WSW (Set II), which are parallel to the NE trending faults that define the southeastern margin of Grand Cayman block of Grand Cayman (Fig.

3-4). The E-W joints are consistent with the E-W faults that define the south and north margins of Grand Cayman block (Fig. 3-4). The N-S photolineaments, in contrast, appear to be parallel to the eastern edge of the Grand Cayman block.

7.3.2. Cayman Brac

On Cayman Brac, DEMs show that photolineaments are limited to the periphery of the uplifted core and dominated by three sets trending at ENE-WSW (Set IV in Fig. 3-6), E-W (Set V in Fig. 3-6), and WNW-ESE (Set VI in Fig. 3-6). Sets V and VI are only evident on the eastern half of the uplifted core.

Although the photolineaments in Set IV on Cayman Brac have a similar orientation to those in Set II on Grand Cayman, the orientations of the other photolineament sets on Cayman Brac and Grand Cayman differ. Transects across Set IV photolineaments shows that each photolineament is a ridge, which is separated from its neighbours by valleys that are up to 150 m wide (Figs. 3-6, 3-14D, 3-14F, 3-14H). Each of the ridges appears to be symmetric, with a gentle slope of 2-3° on each side (Figs. 3-14D, 3-14F, 14H). The relief of the photolineaments is variable, with the highest relief of up to 5 m being in the northeastern area (Figs. 3-6, 3-14D, 3-14F, 3-14H). Set V (E-W) photolineaments, with a relief up to 1.5 m, is only evident on the northeastern margin of the uplifted core (Figs. 3-6, 3-14E). A transect across this areas shows that each photolineament is a ridge, with a relief up to 1.5 m, which is separated from its neighbours by valleys that are up to 12 m wide (Figs. 3-6, 3-14E). The ridges are symmetrical with slopes up to 3.5°. Set VI (WNW-ESE) photolineaments, evident only on the southeastern corner of the uplifted core, are less obvious on the DEMs than the other two sets of photolineaments. Their relief (Set VI) between the ridges and surrounding valleys is typically lower than 1 m (Fig. 3-14G). On each side of the ridges, the slopes are < 2° (Fig. 3-14G). Valleys between these ridges are up to 15 m wide.

In general, the photolineaments are parallel to the faults that define the boundaries of the Cayman Brac fault block. The ENE-WSW (Set IV) photolineaments are parallel to the north and south margins of the Cayman Brac fault block (Figs. 3-1, 3-6). Set V, trending approximately E-W,

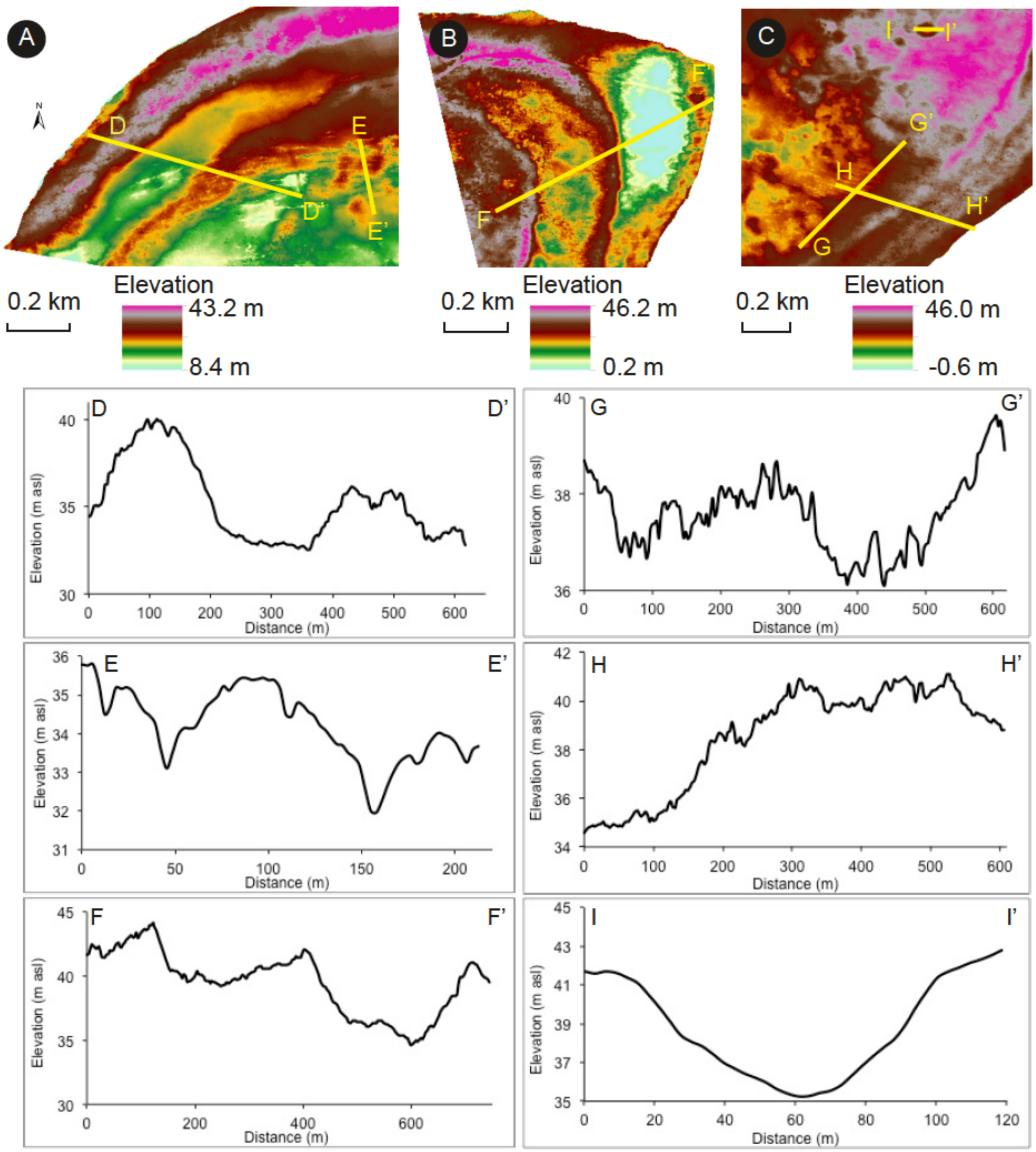

Fig. 3-14. Topographic transects (D-D', E-E', F-F', G-G', H-H', and I-I') showing topography of the photolineaments on Cayman Brac. See Figure 3-10 for precise location. Note that the peripheral rims on the upslope margin are more pronounced than those on Grand Cayman.

is parallel to the escarpment between Spot Bay and East End, whereas the WNW-ESE trending set (Set VI) appears to parallel to the northeastern most limit of the Cayman Brac fault block (Figs.

3-1, 3-6).

8. Modifications of the exposed Cayman Unconformity

8.1. Topographic features

Based on laboratory experiments, Purdy (1974) suggested that the development of surface features on an exposed carbonate block depends on the balance between the rate of rainfall and the rate of the fluid flow off that block. In the "oversupply model", in which the former exceeds the later, a solution film will continuously cover the entire surface and a subdued surface will be produced. In the " balanced model", in which rainfall is slightly less than runoff, a solution meniscus will form over the interior part of the block. This leads to the formation of a continuous peripheral rim that surrounds a central solution depression that is characterized by a smooth floor. The "undersupply model", when the rate of rainfall is much lower than that of runoff, leads to a discontinuous solution film over the block and the formation of discontinuous peripheral rims and a rugged surface on the interior. According to these models, the peripheral rims that developed on the exposed surface of the Cayman Formation during the late Miocene probably formed when the rate of rainfall was less than that of the runoff (Jones and Hunter, 1994b; Liang and Jones, 2014).

Uplift of Cayman Brac led to greater modification of the surface exposures of the Cayman Formation than on Grand Cayman. Based on his experiments, Purdy (1974) suggested that the peripheral rims on the surface of an inclined carbonate block would be intensified because surface runoff would be promoted in one direction and thereby lessen dissolution on the upslope edge of the block. This is applicable to Cayman Brac where the peripheral rim is more pronounced on the eastern upslope margin than on the western downslope margin. In addition, this unidirectional runoff also led to accentuation of the karst relief on the eastern upslope edge on Cayman Brac.

Embayment-shaped depressions found on the east coasts of Grand Cayman and Cayman Brac (Fig. 3-4) probably formed by wave activity. Their location on the eastern ends of the islands is consistent with the fact that those coasts experience the greatest fetch of any coast on the islands (Blanchon and Jones, 1995).

There are no surface streams or rivers on the Cayman Islands. Squair (1988) attributed the absence of surface rivers on Grand Cayman to (1) low relief, (2) small area (175 km^2), and/or (3) the high porosity and permeability of the bedrock. Observations indicate that the high porosity and permeability of the host carbonate is the most plausible explanation for the lack of surface water on Grand Cayman and Cayman Brac because any rain that falls on Grand Cayman and Cayman Brac quickly drains into the bedrock via joints, sinkholes and any other cracks that exist in the rock (Squair, 1988; Ng et al., 1992).

8.2. Sinkholes

On Grand Cayman, DEMs show that large sinkholes (> 3 m in diameter) are commonly located close to the photolineaments. Such an association is expected given that sinkholes are commonly found in association with joints and fault systems that provide avenues for water movement and commonly focus dissolution in specific areas (White and White, 1995; Denizman and Randazzo, 2000; Faivre and Reiffsteck, 2002; Waltham, 2002; Denizman, 2003; Florea, 2005; Gao et al., 2005; Basso et al., 2013).

Small sinkholes are common in all areas where the Cayman Formation is exposed and do not appear to be intimately linked to joints, photolineaments, or any other feature. This probably reflects the fact that development of the small sinkholes may be due to many different processes, including soil development, biological activity, and local contrasts in porosity and permeability of the bedrock (Pace et al., 1993; Harris et al., 1995; Mylroie and Carew, 1995; Ford and Williams, 2007).

8.3. Joints and photolineaments

In many areas, like that on the southeast coast of Grand Cayman, joint development seems to have been an ongoing process. The presence of joints that are filled entirely with caymanite, which is a laminated, multicolored dolostone, indicates that the joints were formed and filled prior to dolomitization (Jones and Smith, 1988; Jones, 1992b, his Fig. 5). In contrast, other joints that are filled by flowstone must have formed after the last phase of dolomitization. The open joints may have been formed more recently. Given the suggestion that joints on Grand Cayman are largely dictated by a regional tectonic control (Rigby and Roberts, 1976), the different timing of joints suggests the regional tectonic stresses along the margin of the Grand Cayman block are probably active periodically. This suggestion is feasible, given the fact that the Cayman Islands are located in a tectonic active zone.

On Grand Cayman, the orientations of the photolineaments are generally similar to the joint directions that have been measured from outcrops (Rigby and Roberts, 1976; Ng et al., 1992). This suggests that the photolineaments may be surface expressions of subsurface joints and/or faults that reflect a tectonic control (Ng et al., 1992). Determining if these photolineaments represent joints or faults, however, is impossible because they cannot be located in the field due to the dense, tropical vegetation that covers these areas. Regardless of their origin, the photolineaments probably represent subsurface features that are important elements of porosity and permeability and provide pathways for fluid movement (Ng, 1990; Ng et al., 1992). Indeed, Ng et al. (1992, their Fig. 11) suggested that the joints system might define the boundaries of the freshwater lens found on the eastern part of the island.

On Cayman Brac, the photolineaments have different orientations from those on Cayman Brac, probably because the tectonic stresses on that island were different from those on Grand Cayman (Ng et al., 1992). This is consistent with the conclusion that these two islands are located on different fault blocks (Matley, 1926; Horsfield, 1975; Stoddart, 1980; Vézina et al., 1999). Furthermore, the photolineaments on Cayman Brac are most prominent on the eastern part of the island, suggesting that tectonic stresses on the eastern part of the Cayman Brac block were probably higher than those that affected the western part of the island. This suggestion is consistent with the fact that uplift was highest on the east end of Cayman Brac (Liang and Jones, 2014). On the uplifted core, identifiable photolineaments are limited to the periphery of the uplifted core. It is possible, however, that photolineaments in the interior of the uplifted core have been disguised by the development of other karst forms.

9. Discussion

The 30 to 180 m sea-level fall associated with the Messinian lowstand (Berggren and Haq, 1976; Adams et al., 1977; Vail et al., 1977; Cita and Ryan, 1978; Loutit and Keigwin, 1982; Hodell and Kennett, 1986; Pigram et al., 1992; Aharon et al., 1993; Zhang and Scott, 1996) led to the development of the Cayman Unconformity (Jones and Hunter, 1994b). On Grand Cayman, the lowest point (~ 40 m bsl) yet found on this surface is in a paleo-sinkhole on the northeast corner of the island (Jones and Hunter, 1994b). On the western half of Grand Cayman and the west end of Cayman Brac, the Cayman Unconformity is covered by the Pedro Castle Formation and/or Ironshore Formation (Fig. 3-7). This buried unconformity provides a snapshot of the karst elements that existed prior to the sedimentation that took place following the Messinian lowstand. The most dominant topographic feature is an atoll-shape depression, below North Sound, that has its base more than 30 bsl (Jones and Hunter, 1994b, their Fig. 12; Wignall, 1995, his Fig. 8; Liang and Jones, 2014, their Fig. 14; Fig. 3-3). On the western half of Grand Cayman, the peripheral rims that are found discontinuously along the southern, western and northern margins of the depression are now buried below younger strata. Available data show that the buried Cayman Unconformity typically dips from peripheral rims into the atoll-shaped depression with a slope of 0.6-1.4° (Jones and Hunter, 1994b; Wignall, 1995; Liang and Jones, 2014). The buried Cayman Unconformity is generally a smooth surface with minor topographic variations that is locally characterized by bivalve and sponge borings (Jones, 1992b; Wignall, 1995; Fig. 3-7B). The presence of these borings implies that the bedrock must have been hard and lithified before the Pliocene transgression. Some large sinkholes that are associated with the buried Cayman Unconformity (Jones, 1992b) are filled with various combinations of caymanite, limestone, and dolomitized wakestones, packstones, and grainstones (Jones and Smith, 1988; Jones, 1992b). The erosive processes associated with the transgression that followed the Messinian lowstand probably destroyed any small-scale surface karst features that once existed on the Cayman Unconformity (Wignall, 1995).

Today, the Cayman Formation that is exposed over most of the eastern half of Grand Cayman and much of the uplifted core on Cayman Brac is characterized by a highly weathered surface that typically has a desiccated, fretted, black, and honeycombed appearance (Fig. 3-11). The thickness of strata lost to erosion and the development of karst landforms on the upper surface of the Cayman Formation (Figs. 3-15, 3-16) reflect the interplay between eustatic sea level, tectonic movement, and the climatic conditions that existed during the lowstands.

The net loss of strata from the eastern part of Grand Cayman and the central part of Cayman Brac was the product of at least two phases of weathering, including: (1) Phase A that took place during the Messinian before deposition of the sediments that now form the Pedro Castle Formation, and (2) Phase B that followed the highstand that led to deposition of the sediments that now form the Pedro Castle Formation. Erosion on the eastern part of Grand Cayman and on the core of Cayman Brac during phase B removed virtually all of the Pedro Castle Formation and the upper part of the Cayman Formation. The influence of climate on the development of karst landforms has been documented by many studies (e.g., Lehmann, 1936, 1954; Lehmann et al., 1956; Corbel, 1957; Tricart and Cailleux, 1972; Büdel, 1982) with rainfall commonly being deemed the key factor (e.g., Choquette and James, 1988; Smart and Whitaker, 1991; Wright, 1991; Saller et al., 1994; Ford and Williams). The topography of the Cayman Unconformity on Grand Cayman, for example, is lower on the western half than that on the eastern half of the island. This contrast in elevations is consistent with the fact that today, the highest rainfall is on the western part of Grand Cayman (Jones and Hunter, 1994b).

On Grand Cayman, a relief of at least 52 m developed on the surface of the Cayman Formation during the Messinian lowstand. Given that the Messinian lowstand lasted for ~1.5 million years (Kastens, 1992; Hodell et al., 2001; Rouchy and Caruso, 2006; Jiménez-Moreno et al., 2013), this translates into a denudation rate of 0.03-0.04 mm/year on the western part of the island. Today, on the eastern part of the island, there is a maximum relief of 23 m on the exposed surface of the Cayman Formation, which is topographically higher than the Cayman Unconformity on the western part of the island. Although the cumulative length of time

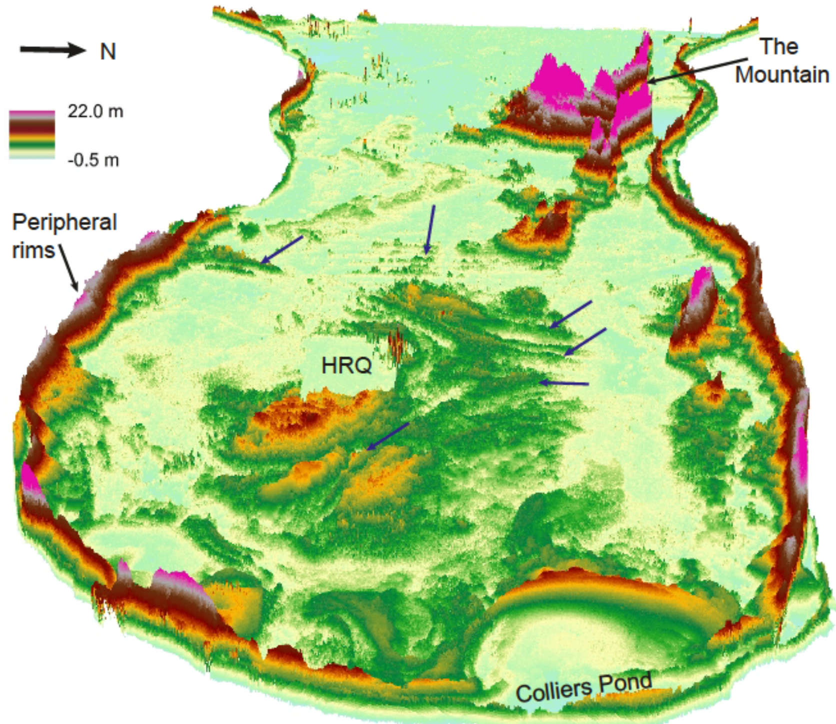

Fig. 3-15. Oblique view of the exposed Cayman Unconformity on the eastern half of Grand Cayman that is still evolving today. Note development of photolineaments (red arrows) in the area between The Mountain and HRQ. Vertical exaggeration is 5, in order to illustrate the karst landforms.

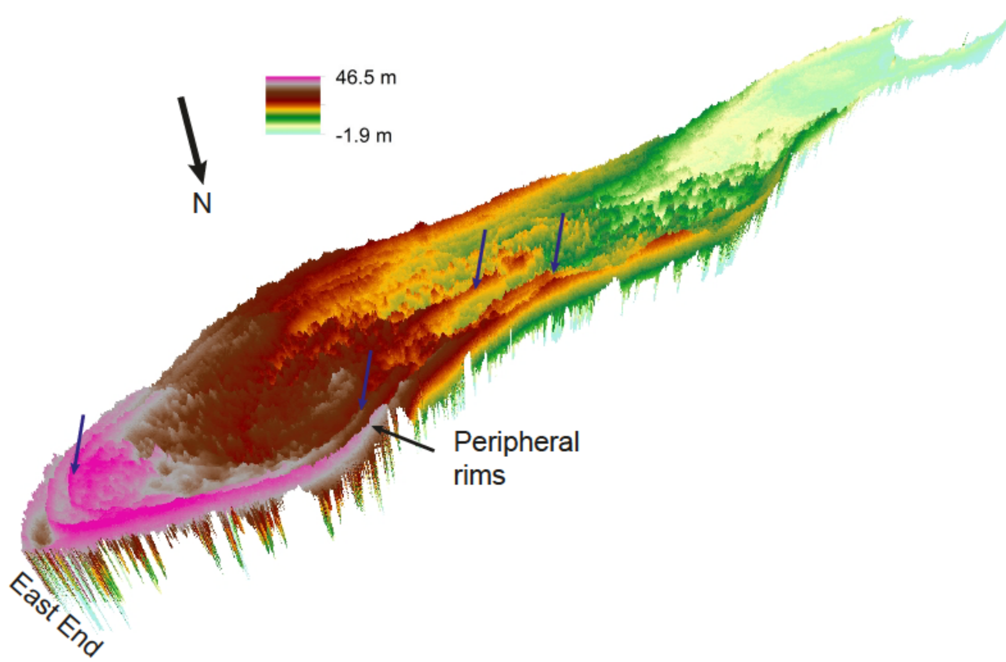

Fig. 3-16. Oblique view of the exposed, Cayman Unconformity on the uplifted core of Cayman Brac. Blue arrows indicate photolineaments. Vertical exaggeration is 5, in order to illustrate the karst landforms.

represented by erosion phases A and B is difficult to determine because of the oscillating sea levels that characterized the period that followed deposition of the Pedro Castle Formation, it is estimated to be a maximum of ~ 4.7 myrs, which is the length of the Messinian lowstand plus the time between the end of deposition of the Pedro Castle Formation (3.6 Ma) and the onset of deposition of the sediments that now form the Ironshore Formation (~400 ka). Given the relief of the Cayman Unconformity on the eastern part of this island is up to 23 m and the fact that the Pedro Castle Formation, which is at least 45 m thick (Jones, 1994; Jones et al., 1994b; Der, 2012; Liang and Jones, 2014), has been removed, the total thickness of lost strata is at least 68 m. This means that denudation rate on the Cayman Formation on the eastern half of Grand Cayman is between 0.01 and 0.02 mm/year. Irrespective of the actual rate, it is readily apparent that the denudation rate over the eastern part of the island was low, especially when compared to the rate of erosion that affected the western part of the island during the Messinian.

The rate of subaerial erosion on a carbonate block can be enhanced by tectonic uplift because this increases the volume of the bedrock that is exposed above base level and commonly induces faults and fractures that serves as pathways by which aggressive solutions can penetrate the rock (Purdy and Waltham, 1999). This pattern is evident on Cayman Brac, where the eastern end of the island was tectonically uplifted at an average rate of 0.04-0.05 mm/year, starting about 3.6 myrs ago (Zhao and Jones, 2012, 2013; Liang and Jones, 2014). Phase B weathering began with the onset of uplift and available evidence indicates that the core of this island has remained above sea level since that time. On the Cayman Islands, the Cayman Formation is up to 165 m thick and the Pedro Castle Formation is at least 45 m thick (Jones, 1994; Jones et al., 1994b; Der, 2012; Liang and Jones, 2014). On Cayman Brac, the Pedro Castle Formation has been stripped from most of the island, now being found only on the west end of the island where it is no more than 6 m thick. The thickness of the Cayman Formation increases from 20 m on the east end of the island to at least 100 m in the western part of the island (Jones, 1994; Jones et al., 1994b). Given that uplift was coincident with Phase B, oscillating sea levels characterizing the period that followed deposition of the Pedro Castle Formation did not affect the uplifted core of Cayman

Brac. Therefore, as much as 190 m of strata (145 m of Cayman Formation and 45 m of Pedro Castle Formation) may have been lost from the east end of Cayman Brac due to erosion that took place during weathering phases A and B over an estimated period of 5.1 million years. This translates into an average denudation rate of 0.03-0.04 mm/year. Determining the denudation rate during weathering Phase A as opposed to Phase B, however, is impossible because the amount of erosion that took place on the Cayman Formation during the Messinian lowstand cannot be determined for that part of the island.

On Grand Cayman and Cayman Brac, the buried Cayman Unconformity is found only on the western part of the islands, whereas the exposed Cayman Unconformity is found on the eastern and central parts of each island. This situation can be attributed to the following factors.

- The weathering rate during Phase A (Messinian lowstand) was probably higher on the western parts of each island, possibly due to higher rainfall in those areas. This produced topographic lows that were subsequently filled-in during the next highstand and therefore became the sites where the maximum thicknesses of Pedro Castle Formation now exist. As a result, the strata of this formation were not completely removed during the subsequent phases of subaerial erosion.
- Weathering during Phase B (late Pliocene onwards) appears to have had the greatest impact on the strata of the Cayman Formation and Pedro Castle Formation that were exposed on the eastern parts of these islands. For Cayman Brac, this can probably be attributed to the uplift that preferentially elevated the eastern end of the island. It is difficult, however, to assess the reason for this on Grand Cayman because there is no evidence pointing to the preferential uplift of the eastern end of that island.

Karst landforms can vary from locality to locality in accord with local climates, tectonic movement, and the nature of the substrates being weathered. In the Caribbean region, for example, Jamaica and Cuba have karst landscapes that are characterized by cockpit karst, cone karst, and tower karst (e.g., Pulina and Fagundo, 1992; Donovan, 2002), which are the norm in humid tropics (Lehmann, 1936; Lehmann, 1954; Corbel, 1957). In contrast, Grand Cayman and Cayman Brac lack these large-scale, positive karst landforms. Purdy and Waltham (1999) argued that the development of large-scale, positive karst landforms was favoured by the uplift of strata with well-developed joint and fault systems that provide pathways for fluid penetration. This has, for example, lead to the development of large-scale karst landforms in many areas of the world (e.g., Sweeting, 1958; Williams, 1972; Brook and Ford, 1978; Waltham et al., 1983; Drogue and Bidaux, 1992; Purdy and Waltham, 1999; Ford and Williams, 2007), including the Guilin tower karst in China (Drogue et al., 1988; Drogue and Bidaux, 1992; Sweeting, 1995; Purdy and Waltham, 1999) and Jamaican cockpit and conical hills (Sweeting, 1958; Purdy and Waltham, 1999). Although Grand Cayman and Cayman Brac are located on individual fault blocks, there is no evidence of faults that cut through the islands. The joint systems that are present in the Cayman Formation tend to be localized and irregularly distributed. Thus, the lack of large-scale karst features in the Cayman Formation can probably be attributed to the lack of faults and the poorly developed joint systems.

The development of an erosional unconformity in carbonate successions on isolated oceanic islands, such as Grand Cayman and Cayman Brac, is dictated by numerous variables, including eustatic sea-level changes, climatic conditions and tectonic movement. Uplift, in particular, may influence the development of the karst landforms by increasing the magnitude of base-level lowering, and controlling the runoff direction (Williams, 1972; Purdy and Waltham, 1999). Although the impact of uplift as opposed to eustatic sea-level changes on the development of erosional unconformity is commonly difficult to establish, the contrasts between the Cayman Unconformity on Grand Cayman and Cayman Brac shows that uplift plays an important role. In general, uplift leads to accentuation of the topographic features and increased rates of erosion.

10. Conclusions

The upper surface of the Cayman Formation is an erosional unconformity that has developed through numerous phases of weathering between the late Miocene and the present day. Detailed comparison of the Cayman Unconformity on Grand Cayman and Cayman Brac has led to the following important conclusions, which are also applicable to processes that have affected carbonate successions on isolated islands throughout the world.

- The karst topography on an erosional unconformity is commonly characterized by (1) various topographic features including peripheral rims, atoll-shape depressions and topographic highs, (2) karst features, such as sinkholes and pinnacles, and (3) solution-widened joints and photolineaments.
- Development of karst topography on an erosional unconformity on isolated carbonate islands reflects the interplay between eustatic sea-level changes, climate, and tectonic movements.
- The denudation rate on relatively flat landscapes is controlled largely by rainfall patterns. During the Messinian, the denudation rate of 0.03-0.04 mm/year on the western part of Grand Cayman was much higher than that on the eastern part of this island. This difference is attributed to rainfall being a maximum on the western part of the island, as it is today.
- Tectonic uplift enhances the denudation rate on an erosional unconformity. The denudation rate on Cayman Brac over the last 5.1 million years was 0.03- 0.04 mm/year, which was more rapid than that on the eastern half of Grand Cayman where it was 0.01-0.02 mm/year.
- Photolineaments might be the surface expression of faults and/or joints, which are dictated by the region stress along the margin of fault-isolated block.

The conclusions derived from the carbonate successions on Grand Cayman and Cayman Brac are applicable to other isolated oceanic islands found throughout the world. Critically, it has shown that thick successions of strata can be lost to erosion as karst processes are focused on the exposed carbonates. The processes that control the development of unconformities in these settings commonly lead to the loss of significant thicknesses of bedrock and greatly impact the stratigraphic architecture of the successions.

References

Adams, C.G., Benson, R.H., Kidd, R.B., Ryan, W.B.F., Wright, R.C., 1977. The Messinian salinity crisis and evidence of late Miocene eustatic changes in the world ocean. Nature 269, 383-386.

Aharon, P., Goldstein, L.S., Wheeler, C.W., Jacobson, G., 1993. Sea-level events in the South Pacific linked with Messinian salinity crisis. Geology 21, 771-775.

Alonso-Zarza, A.M., Tanner, L.H., 2006. Paleoenvironmental record and applications of calcretes and palustrine carbonates. Special Paper-Geological Society of America 416, 239 pp.

Basso, A., Bruno, E., Parise, M., Pepe, M., 2013. Morphometric analysis of sinkholes in a karst coastal area of southern Apulia (Italy). Environmental Earth Sciences 70, 2545-2559.

Bathurst, R.G.C., 1975. Carbonate Sediments and Their Diagenesis 12. Elsevier Science Publishing Company, Amsterdam, 658 pp.

Berggren, W.A., Haq, B.U., 1976. The Andulusian stage (late Miocene): biostratigraphy, biochronology and paleoecology. Palaeogeography, Palaeodimatology Palaeoecology 20, 67-129.

Blanchon, P., Jones, B., 1995. Marine-planation terraces on the shelf around Grand Cayman: a result of stepped Holocene sea-level rise. Journal of Coastal Research 11, 1-33.

Brasier, A.T., 2011. Searching for travertines, calcretes and speleothems in deep time: processes, appearances, predictions and the impact of plants. Earth-Science Reviews 104, 213-239.

Brook, G.A., Ford, D.C., 1978. The origin of labyrinth and tower karst and the climatic conditions necessary for their development. Nature 275, 493-496.

Budd, D.A., Gaswirth, S.B., Oliver, W.L., 2002. Quantification of macroscopic sub-aerial exposure features in carbonate rocks. Journal of Sedimentary Research 72, 917-928.

Büdel, J., 1982. Climatic Geomorphology. Princeton University Press, New Jersey, 443 pp.

Calais, E., Mercier de Lépinay, B., 1995. Strike-slip tectonic processes in the northern Caribbean between Cuba and Hispaniola (Windward Passage). Marine Geophysical Researches 17, 63-95.

Choquette, P.W., James, N.P., 1988. Introduction. In: James, N.P., Choquette, P.W. (Eds.), Paleokarst. Springer-Verlag, Berlin, Germany, pp. 1-21.

Cita, M.B., Ryan, W.B.F., 1978. The Bou Regreg section of the Atlantic coast of Morocco: Evidence, timing and significance of a late Miocene regressive phase. Rivista Italiana di Paleontologia e Stratigraphia 84, 1051-1082.

Clari, P.A., Dela Pierre, F., Martire, L., 1995. Discontinuities in carbonate successions; identification, interpretation and classification of some Italian examples. Sedimentary Geology 100, 97-121.

Corbel, J., 1957. Les Karsts du Nord-Quest de I'Europe. Institute des Etudes Rhodaniennes, University de Lyon, Memoirs et Documents 12, 531 pp.

Denizman, C., 2003. Morphometric and spatial distribution parameters of karstic depressions, lower Suwannee River Basin, Florida. Journal Cave and Karst Studies 65, 29-35.

Denizman C., Randazzo A., 2000. Post-Miocene subtropical karst evolution, lower Suwannee River Basin, Florida. Geological Society of America Bulletin 112, 1804-1813.

Der, A.J., 2012. Deposition and sea level fluctuations during Miocene Times, Grand Cayman, British West Indies Indies. Unpublished M.Sc. Thesis, University of Alberta, Canada, 101 pp.

Donovan, S.K., 2002. A karst of thousands: Jamaica's limestone scenery. Geology Today 18, 143-151.

Doran, E., 1954. Landforms of Grand Cayman, British West Indies. Texas Journal of Science 6, 360-377.

Drogue, C., Bidaux, P., 1992. Structural and hydrogeological origin of tower karst in southern China (Lijiang plain in the Guilin region). Zeitschrift für Geomorphologie Neue Folge, Supplement-Band 36, 25-36.

Drogue, C., Moumtaz, R., Daoxian Y., 1988. Structure of karstic reservoirs according to microtectonic and fissural analysis; area of the experimental site of Yaji, Guilin, China. Proceedings of the International Association of Hydrologists 21st Congress, Karst Hydrogeology and Karst Environment Protection 21, 735–740.

Esteban, M., Klappa, C.F., 1983. Subaerial exposure environment. In: Scholle, P.A., Bebout, D.G., Moore, C.H. (Eds.), Carbonate Depositional Environments. American Association of Petroleum Geologists Memoir 33. American Association of Petroleum Geologists, Tulsa, United States, pp. 1-54.

Faivre, S., Reiffsteck, P., 2002. From doline distribution to tectonic movements: example of the Velebit mountain range, Croatia. Acta Carsologica 31, 139-154.

Florea, L., 2005. Using state-wide GIS data to identify the coincidence between sinkholes and geologic structure. Journal of Cave Karst Studies 67, 120-124.

Flügel, E., 2004. Microfacies of Carbonate Rocks: Analysis, Interpretation and Application. Springer-Verlag, Berlin, 976 pp.

Folk, R.L., Roberts, H.H., Moore, C.H., 1973. Black phytokarst from Hell, Cayman Islands, British West Indies. Geological Society of America Bulletin 84, 2351-2360.

Ford, D., Williams, P.W., 2007. Karst Hydrogeology and Geomorphology. John Wiley and Sons, Chichester, United Kingdom, 562 pp.

Frisia, S., Borsato, A., 2010. Karst. In: Alonso-Zarza, A.M., Tanner, L.H. (Eds.), Carbonates in Continental Settings: Facies, Environments and Processes: Developments in Sedimentology. Elsevier, Oxford, United Kingdom, pp. 269-318.

Gams, I., 1994. Types of contact karst. Geografia Fisica e Dinamica Quateraria 17, 37-46.

Gams, I., 2003. Kras v Sloveniji v prostoru in času. Založba ZRC, ZRC SAZU, Ljubljana, 516 pp.

Gao, Y., Alexander, E.C. Jr, Barnes, R.J., 2005. Karst database implementation in Minnesota: analysis of sinkhole distribution. Environmental Geology 47, 1083-1098.

Gradstein, F.M., Ogg, G., Schmitz, M., 2012. The Geologic Time Scale. Elsevier, Oxford, United Kingdom, 1176 pp.

Hallam, A., 1984. Pre-Quaternary sea-level changes. Annual Review of Earth and Planetary Sciences 12, 205-243.

Haq, B.U., Hardenbol, J., Vail, P.R., 1987. Chronology of fluctuating sea levels since the Triassic.

Science 235, 1156-1167.

Harris, J. G., Mylroie, J.E., Carew, J.L., 1995. Banana Holes: unique karst features of the Bahamas. Carbonates and Evaporites 10, 215-224.

Hillgärtner, H., 1998. Discontinuity surfaces on a shallow-marine carbonate platform (Berriasian, Valanginian, France and Switzerland). Journal of Sedimentary Research 68, 1093-1108.

Hodell, D.A., Curtis, J.H., Sierro, F.J., Raymo, M.E., 2001. Correlation of late Miocene to early Pliocene sequences between the Mediterranean and North Atlantic. Paleoceanography 16, 164-178.

Hodell, D.A., Kennett, J.P., 1986. Late Miocene-early Pliocene stratigraphy and paleoceanography of the South Atlantic and Southwest Pacific Ocean: a synthesis Paleoceanography 1, 285-311.

Horsfield, W.T., 1975. Quaternary vertical movements in the Greater Antilles. Geological Society of America Bulletin 86, 933-938.

Iturralde-Vinent, M.A., 1994. Cuban geology: A new plate-tectonic synthesis. Journal of Petroleum Geology 17, 39-70.

Iturralde-Vinent, M.A., 2006. Meso-Cenozoic Caribbean paleogeography: implications for the historical biogeography of the region. International Geology Review 48, 791-827.

Iturralde-Vinent, M.A., Macphee, R.D.E., 1999. Paleogeography of the Caribbean region: implications for Cenozoic biogeography. Bulletin of the American Museum of Natural History 238, 1-95.

James, N.P., Choquette, P.W., 1988. Paleokarst. Springer-Verlag, New York, 416 pp.

James, N.P., Choquette, P.W., 1990. Limestones-the meteoric diagenetic environment. In: McIlreath, I.A., Morrow, D.W. (Eds.), Diagenesis. Geological Association of Canada, Ottawa, Canada, pp. 35-74.

Jiménez-Moreno, G., Pérez-Asensio, J.N., Larrasoaña, J.C., Aguirre, J., Civis, J., Rivas-Carballo, M.R., Valle-Hernández, M.F., González-Delgado, J.A., 2013. Vegetation, sea-level and climate changes during the Messinian salinity crisis. Geological Society of America Bulletin

125, 432-444.

Jones, B., 1989. The role of micro-organisms in phytokarst development on dolostones and limestones, Grand Cayman, British West Indies. Canadian Journal of Earth Sciences 26, 2204-2213.

Jones, B., 1992a. Caymanite, a cavity-filling deposit in the Oligocene-Miocene Bluff Formation of the Cayman Islands. Canadian Journal of Earth Sciences 29, 720-736.

Jones, B., 1992b. Void-filling deposits in karst terrains of isolated oceanic islands: a case study from Tertiary carbonates of the Cayman Islands. Sedimentology 39, 857-876.

Jones, B., 1994. Geology of the Cayman Islands. In: Brunt, M.A., Davies, J.E. (Eds.), The Cayman Islands: Natural History and Biogeography. Kluwer, Dordrecht, The Netherlands, pp. 13-49.

Jones, B., 2005. Dolomite crystal architecture: genetic implications for the origin of the Tertiary dolostones of the Cayman Islands. Journal of Sedimentary Research 75, 177-189.

Jones, B., Hunter, I.G., 1990. Pleistocene paleogeography and sea levels on the Cayman Islands, British West Indies. Coral Reefs 9, 81-91.

Jones, B., Hunter, I.G., 1994a. Evolution of an isolated carbonate bank during Oligocene, Miocene and Pliocene times, Cayman Brac, British West Indies. Facies 30, 25-50.

Jones, B., Hunter, I.G., 1994b. Messinian (Late Miocene) karst on Grand Cayman, British Indies: an example of an erosional sequence boundary. Journal of Sedimentary Research 64, 531-541.

Jones, B., Hunter, I.G., Kyser, T.K., 1994a. Revised stratigraphic nomenclature for Teriary strata of the Cayman Islands, British West Indies. Caribbean Journal of Science 30, 53-68.

Jones, B., Hunter, I.G., Kyser, T.K., 1994b. Stratigraphy of the Bluff Formation (Miocene-Pliocene) and the newly defined Brac Formation (Oligocene), Cayman Brac, British West Indies. Caribbean Journal of Science 30, 30-51.

Jones, B., Lockhart, E., Squair, C., 1984. Phreatic and vadose cements in the Tertiary Bluff Formation of Grand Cayman Island, British West Indies. Bulletin of Canadian Petroleum Geology 32, 382-397.

Jones, B., Smith, D.S., 1988. Open and filled karst features on the Cayman Islands: implications for the recognition of paleokarst. Canadian Journal of Earth Sciences 25, 1277-1291.

Kastens, K.A., 1992. Did glacio-eustatie sea level drop trigger the Messinian salinity crisis? New evidence from Ocean Drilling Program site 654 in the Tyrrhenian Sea. Paleooceanography 7, 333-356.

Lehmann, H., 1936. Morphologische Studien auf Java. Geographische Abhandlungen 9. Stuttart, Engelhorn, Germany, 114 pp.

Lehmann, H., 1954. Der tropische Kegelkarst auf den Grossen Antillen, Part 3 of Das Karstphaenomen in den verschiedenen Klimazonen. Erdkunde 8, 130-139.

Lehmann, H.W., Krommelbein, H.K., Lotschert, W., 1956. Karstmorphologische, geologische und botanische Studien in der Sierra de los Organos auf Cuba. Erdkunde 10, 185-204.

Liang, T., Jones, B., 2014. Deciphering the impact of sea-level changes and tectonic movement on erosional sequence boundaries in carbonate successions: a case study from Tertiary strata on Grand Cayman and Cayman Brac, British West Indies. Sedimentary Geology 305, 17-34.

Liang, T. and Jones, B., 2015. Petrographic and geochemical features of sinkhole-filling deposits associated with an erosional unconformity on Grand Cayman. Sedimentary Geology 315, 64-82.

Lincoln, J.M., Schlanger, S.O., 1987. Miocene sea-level falls related to the geologic history of Midway Atoll. Geology 15, 454-457.

Loutit, T.S., Keigwin, L.D., 1982. Stable isotope evidence for latest Miocene sea-level fall in the Mediterranean region. Nature 300, 163-166.

MacDonald, K.C., Holcombe, T.L., 1978. Inversion of magnetic anomalies and sea-floor spreading in the Cayman Trough. Earth and Planetary Science Letters 40, 407-414.

Matley, C.A., 1926. The geology of the Cayman Islands (British West Indies) and their relation to the Bartlett Trough. Quarterly Journal of the Geological Society of London 82, 352-387.

Miller, C.R., James, N.P., Bone, Y., 2012. Prolonged carbonate diagenesis under an evolving late Cenozoic climate: Nullarbor Plain, southern Australia. Sedimentary Geology 261-262, 33-49.

Monroe, W.H., 1970. A Glossary of Karst Terminology. Geological Survey Water-Supply Paper 1899-K. United States Geological Survey, Washington D.C., United States, 26 pp.

Mylroie, J.E., Carew, J.L., 1995. Karst development on carbonate islands. In: Budd, D.A., Saller, A.H., Harris, P.M. (Eds.), Unconformities and Porosity in Carbonate Strata. American Association of Petroleum Geologists Memoir 63. American Association of Petroleum Geologists, Tulsa, United States, pp. 55-76.

Ng, K.C., 1990. Diagenesis of the Oligocene-Miocene Bluff Formation of the Cayman Islands; a petrographic and hydrogeochemical approach. Unpublished Ph.D Thesis, University of Alberta, Canada, 98 pp.

Ng, K.C., Jones, B, Beswick, R, 1992. Hydrogeology of Grand Cayman, British West Indies; a karstic dolostone aquifer. Journal of Hydrology 134, 273-295.

Pace, M.C., Mylroie, J.E., Carew, J.L., 1993. Petrographic analysis of vertical dissolution features on San Salvador Island, Bahamas. In: White, B. (Ed.), Proceedings of the Sixth Symposium on the Geology of the Bahamas. Bahamian Field Station, San Salvador, Bahamas, pp. 109-123.

Perfit, M.R., Heezen, B.C., 1978. The geology and evolution of the Cayman Trench. Geological Society of America Bulletin 89, 1155-1174.

Pigram, C.J., Davies, P.J., Feary, D.A., Symonds, P.A., 1992. Absolute magnitude of the second-order middle to late Miocene sea level fall, Marion Platform, Northeast Australia. Geology 20, 858-862.

Pulina, M., Fagundo, J.R., 1992. Tropical karst and chemical denudation of western Cuba. Geographia Polonica 60, 195-216.

Purdy, E.G., 1974. Reef configurations: cause and effect. In: Laporte, L.F. (Ed.), Reefs in Time and Space. Society of Economic Paleontologists and Mineralogists Special Publication 18, pp. 9-76.

Purdy, E.G., Waltham, D., 1999. Reservoir implication of modern karst topography. American Association of Petroleum Geologists Bulletin 83, 1774-1794.

Purdy, E.G., Winterer, E.L., 2001. Origin of atoll lagoons. Geological Society of America Bulletin 113, 837-854.

Rigby, J.K., Roberts, H.H., 1976. Geology, reefs and marine communities of Grand Cayman, British West Indies. In: Roberts, J.K., Roberts, H.H. (Eds.), Grand Cayman: Geology, Sediments, and Marine Communities. Brigham Young University, Geology Studies, Special Publication 4, pp. 1-95.

Rouchy, J.M., Caruso, A., 2006. The Messinian salinity crisis in the Mediterranean basin: a reassessment of the data and an integrated scenario. Sedimentary Geology 188-189, 35-67.

Sabins, F.F., 2007. Remote Sensing: Principles and Interpretation (3d ed.). Waveland Press, Long Grove, United States, 512 pp.

Saller, A.H., Budd, D.A., Harris, P.M., 1994. Unconformities and porosity development in carbonate strata: ideas from a Hedberg Conference. American Association of Petroleum Geologists Bulletin 79, 857-872.

Saller, A.H., Dickson, J.A.D., Matsuda, F., 1999. Evolution and distribution of porosity associated with sub-aerial exposure in upper Palaeozoic platform limestones, West Texas. American Association of Petroleum Geologists Bulletin 83, 1835-1844.

Sattler, U., Immenhauser, A., Hillgärtner, H., Esteban,M., 2005. Characterization, lateral variability and lateral extent of discontinuity surfaces on a carbonate platform (Barremian to lower Aptian, Oman). Sedimentology 52, 339-361.

Sauro, U., 2003. Dolines and sinkholes: aspects of evolution and problems of classification. Acta Carsologica 32, 41-52.

Schlanger, S.O., Premoli Silva, I., 1986. Oligocene sea-level falls recorded in mid-Pacific atoll and archipelagic apron settings. Geology 14, 392-395.

Smart, P.L, Whitaker, F.F., 1991. Karst processes, hydrology and porosity evolution. In: Wright, V.P., Esteban, M, Smart, P.L. (Eds.), Paleokarsts and Paleokarstic Reservoirs. University of Reading, Postgraduate Research Institute for Sedimentology, Occasional Publication Series, 2, pp. 1-55.

Smith, D.S., 1987. The genesis of speleothemic calcite deposits on Grand Cayman Island, British West Indies. Unpublished M.Sc. Thesis, University of Alberta, 171 pp.

Squair, C.A., 1988. Surface karst on Grand Cayman Island, British West Indies. Unpublished M.Sc. Thesis, University of Alberta, Canada, 107 pp.

Stoddart, D.R., 1980. Geology and geomorphology of Little Cayman. Atoll Research Bulletin 241, 11-16.

Sweeting, M.M., 1958. The karstlands of Jamaica. Geographical Journal 124, 184-199.

Sweeting, M. M., 1995. Karst in China. Springer-Verlag, Berlin, Germany, 265 pp.

Tricart, J., Cailleux, A., 1972. Introduction to Climatic Geomorphology. Longman, London, United Kingdom, 295 pp.

Tucker, M.E., 1990. Diagenetic processes, products and environments. In: Tucker, M.E., Wright, V.P., Dickson, J.A.D. (Eds.), Carbonate Sedimentology. Blackwell Science Publisher, Oxford, United Kingdom, pp. 314-364.

Uzelman, B.C., 2009. Sedimentology, diagenesis, and dolomitization of the Brac Formation (Lower Oligocene), Cayman Brac, British West Indies. Unpublished M.Sc. Thesis, University of Alberta, Canada, 120 pp.

Vail, P.R., Mitchum, R.M., Thompson, S., 1977. Seismic stratigraphy-applications to hydrocarbon exploration. American Association of Petroleum Geologists Memoir 26, 99-116.

Vézina, J.V., Jones, B., Ford, D.C., 1999. Sea-level highstands over the last 500,000 years: evidence from the Ironshore Formation on Grand Cayman, British West Indies. Journal of Sedimentary Research 69, 317-327.

Waltham, T., 2002. The engineering classification of karst with respect to the role and influence of caves. International Journal of Speleology 31, 19-35.

Waltham, A.C., Smart P.L., Friederich, H., Eavis, A.J., Atkinson, T.C., 1983. The caves of Gunung Sewu, Java. Transactions of the British Cave Research Association 10, 55-96.

Whitaker, F., Smart, P., Hague, Y., Waltham, D., Bosence, D., 1999. Structure and function of a coupled two-dimensional diagenetic and sedimentological model of carbonate platform evolution. Society for Sedimentary Geology Special Publication 62, 337-355.

White, W.B., 1984. Rate processes: chemical kinetics and karst landform development. In: LaFleur, R.G. (Ed.), Groundwater as a Geomorphic Agent. Allen and Unwin, Boston, United States, pp. 227-248.

White, W.B., 1988. Geomorphology and hydrology of carbonate terrains. Oxford University Press, London, 464 pp.

White,W.B., White, E.L., 1995. Correlation of contemporary karst landforms with paleokarst landforms: the problem of scale. Carbonates Evaporites 10,131-137.

Wignall, B.D., 1995. Sedimentology and diagenesis of the Cayman (Miocene) and Pedro Castle (Pliocene) Formations at Safe Haven, Grand Cayman, British West Indies. Unpublished M.Sc. Thesis, University of Alberta, Canada, 110 pp.

Williams, P.W., 1972. Morphometric analysis of polygonal karst in New Guinea. Geological Society of America Bulletin 83, 761-796.

Wright, V.P., 1991. Paleokarst: types, recognition, controls and association. In: Wright, V.P., Estehan, M, Smart, P.L. (Eds.), Paleokarsts and Paleokarstic Reservoirs. University of Reading, Postgraduate Research Institute for Sedimentology, Occasional Publication Series, 2, pp. 56-88.

Wright, V.P., 1994. Paleosols in shallow marine carbonate sequences. Earth-Science Reviews 35, 367-395.

Wright, V.P., Smart, P.L., 1994. Paleokarst (dissolution diagenesis): Its Occurrence and hydrocarbon exploration significance. In: Wolf, K.H., Chilingarian, G.V. (Eds.), Diagenesis IV-Developments in Sedimentology 51. Elsevier Science, Amsterdam, Netherlands, pp. 477-517.

Zhang, J., Scott, D.B., 1996. Messinian deep-water turbidites and glacioeustatic sea-level changes in the North Atlantic: linkage to the Mediterranean salinity crisis. Paleoceanography 11, 277-297.

Zhao, H.W., Jones, B., 2012. Origin of “Island Dolostones”: a case study from the Cayman

Formation (Miocene), Cayman Brac, British West Indies. Sedimentary Geology 243-244, 191-206.

Zhao, H.W., Jones, B., 2013. Distribution and interpretation of rare earth elements and yttrium in Cenozoic dolostones and limestones on Cayman Brac, British West Indies. Sedimentary Geology 284-285, 26-38.

CHAPTER 4: PETROGRAPHIC AND GEOCHEMICAL FEATURES OF SINKHOLE-FILLING DEPOSITS ASSOCIATED WITH AN EROSIONAL UNCONFORMITY ON GRAND CAYMAN [1]

1. Introduction

Erosional unconformities in carbonate successions typically represent long periods of subaerial erosion that are accompanied by loss of the rock record, vadose diagenetic and/or pedogenetic alteration, and the formation of surface and subsurface karst (Esteban and Klappa, 1983; James and Choquette, 1990; Tucker, 1990; Clari et al., 1995; Hillgärtner, 1998; Sattler et al., 2005; Alonso-Zarza and Wright, 2010). Assessing the thickness of strata lost is difficult because there is generally no physical record left. In some cases, however, this problem can be partly addressed by examining the lithoclasts and associated sediments that are found in sinkholes and caves that formed during the period of exposure. Studies like those by Daugherty et al. (1987), Smart et al. (1988), Jones (1992b), and Miller et al. (2012a), however, are scarce because there are few examples where sinkholes have been filled by carbonate rather than fluvial siliciclastic sediments (Ford, 1988).

Grand Cayman is a carbonate island that is devoid of surface fluvial systems and the lack siliciclastic sediments. On the eastern half of Grand Cayman, dolostones of the Cayman Formation (Miocene) have been exposed since the late Pliocene (~3.6 Ma), when the overlying Pedro Castle Formation was lost to subaerial erosion (Wignall, 1995; Zhao and Jones, 2013; Liang and Jones, 2014). The exposed upper surface of the Cayman Formation, which is an unconformity surface that is still developing, is characterized by numerous sinkholes. Some of these sinkholes, which are up to 30 m in diameter and 10 m deep, remain open whereas others are filled with a variety of deposits that include laminar rootcrete, breccias, loose limestone and dolostone lithoclasts, and white, red and orange limestones. Information derived from

1 This paper was published as: Liang, T. and Jones, B., 2015. Petrographic and geochemical features of sinkhole-filling deposits associated with an erosional unconformity on Grand Cayman. Sedimentary Geology 315, 64-82.

these deposits provides some insights into the processes that have been operative over the last 3.6 Ma. while this unconformity has developed. Some of these sinkhole-filling deposits have been described in terms of their spatial development and petrography (Jones and Smith, 1988; Jones, 1991, 1992a, 1992b; Alonso-Zarza and Jones, 2007). This study builds on that work by assessing the deposits through the integration of stable isotope analyses, trace element analyses, and examining the distribution of the Rare Earth Elements (REE). Using all of this information, this paper (1) compares the petrographic and geochemical features of the different types of sinkhole-filling deposits, (2) compares the geochemical signatures of the sinkhole-filling deposits with the limestones and dolostones of the bedrock found on the island, and (3) determines the provenance and sequential development of the sinkhole-filling deposits. In particular, it examines the possibility that carbonates that formed in marine or non-marine environments may be characterized by different REE signatures.

2. Terminology

Calcrete that is associated with roots has been referred as laminar calcrete (Wright et al., 1988; Alonso-Zarza, 1999), rhizogenic calcrete (Wright et al., 1995), calcified root mat (Wright et al., 1988), and rootcrete (Jones, 1992a, 1992c). Wright et al. (1995, p. 144) originally defined rhizogenic calcrete as "… calcretes which are composed largely or wholly of textures which are interpretable as due to the calcification on, in or around roots". In their definition, rhizogenic calcrete includes vertical and horizontal root mats (Wright et al., 1995, 1997). The term rootcrete was used to describe calcrete crusts that covered the surfaces of cavities that had been created by the activities associated with plant roots (Jones, 1992a).

The term "terra rossa", first used in soil science by Kubiëna (1953), has been applied to (1) red, shallow, undifferentiated soils that are associated with carbonate or calcareous material, (2) red material which is transitional between weathered carbonate and new soils, and (3) any red soil in the Mediterranean region (Stephens, 1953; Stace, 1956). In geological situations, "terra rossa" has generally been applied to any reddish, clay-rich soils that lie on limestones or dolostones (e.g., Torrent, 1995; Durn et al., 1999, 2001, 2013; Durn, 2003; Muhs and Budahn, 2009; Muhs et al., 2010), whereas reddish, Al-rich soils are generally referred to as bauxite (e.g., Ahmad and Jones, 1969; Muhs and Budahn, 2009). The chief minerals found in terra rossa are variable, but commonly include clay minerals, such as illite, kaolinites, chlorite, and various combinations of quartz, feldspar, and mica (e.g., Macleod, 1980; Garcia-Gonzalez and Recio, 1988; Moresi and Mongelli, 1988; Boero et al., 1992; Bronger and Bruhn-Lobin, 1997; Durn et al., 1999; Muhs and Budahn, 2009). Calcite and dolomite are present in some of these deposits.

Terrestrial oncoids are laminated coated grains, up to 85 mm in diameter, that develop through microbially-mediated processes in a vadose setting (Wright, 1989; Jones, 1991, 2011). The term "micrite", in this study, is applied to carbonate crystals that are less than 4 μm long (Folk, 1974; Reid and MacIntyre, 1998).

3. Geological setting

The Cayman Islands, comprising Grand Cayman, Cayman Brac and Little Cayman, are isolated oceanic islands located on the Cayman Ridge in the Caribbean Sea (Fig. 4-1). To the south of these islands lies the Oriente Transform Fault that defines the boundary between the North American Plate and the Caribbean Plate. Grand Cayman is located to the northeast of the Mid-Cayman rise, which is an active spreading center (DeMets and Wiggins-Grandison, 2007). Although located in a tectonically active area, Grand Cayman seems to have remained tectonically stable since the Miocene (Zhao and Jones, 2012, 2013; Liang and Jones, 2014).

The Tertiary carbonate succession on the Cayman Islands was originally assigned to the Bluff Limestone (Matley, 1926), which was subsequently renamed as the Bluff Group by Jones et al. (1994a, 1994b). The Bluff Group is composed of the unconformity-bounded Brac Formation (Lower Oligocene), Cayman Formation (Middle Miocene), and Pedro Castle Formation (Pliocene) (Fig. 4-2). The Ironshore Formation (Pleistocene) unconformable overlies the Bluff Group (Fig. 4-2). The Pedro Castle Formation, which used to cover all of Grand Cayman, has been largely removed from the eastern part of Grand Cayman by subaerial erosion over the last 3-4 million years. As a result, the Cayman Formation is widely exposed over much of the eastern half of Grand Cayman (Fig. 4-1). Dolomitization of the Bluff Group took place during the late Miocene

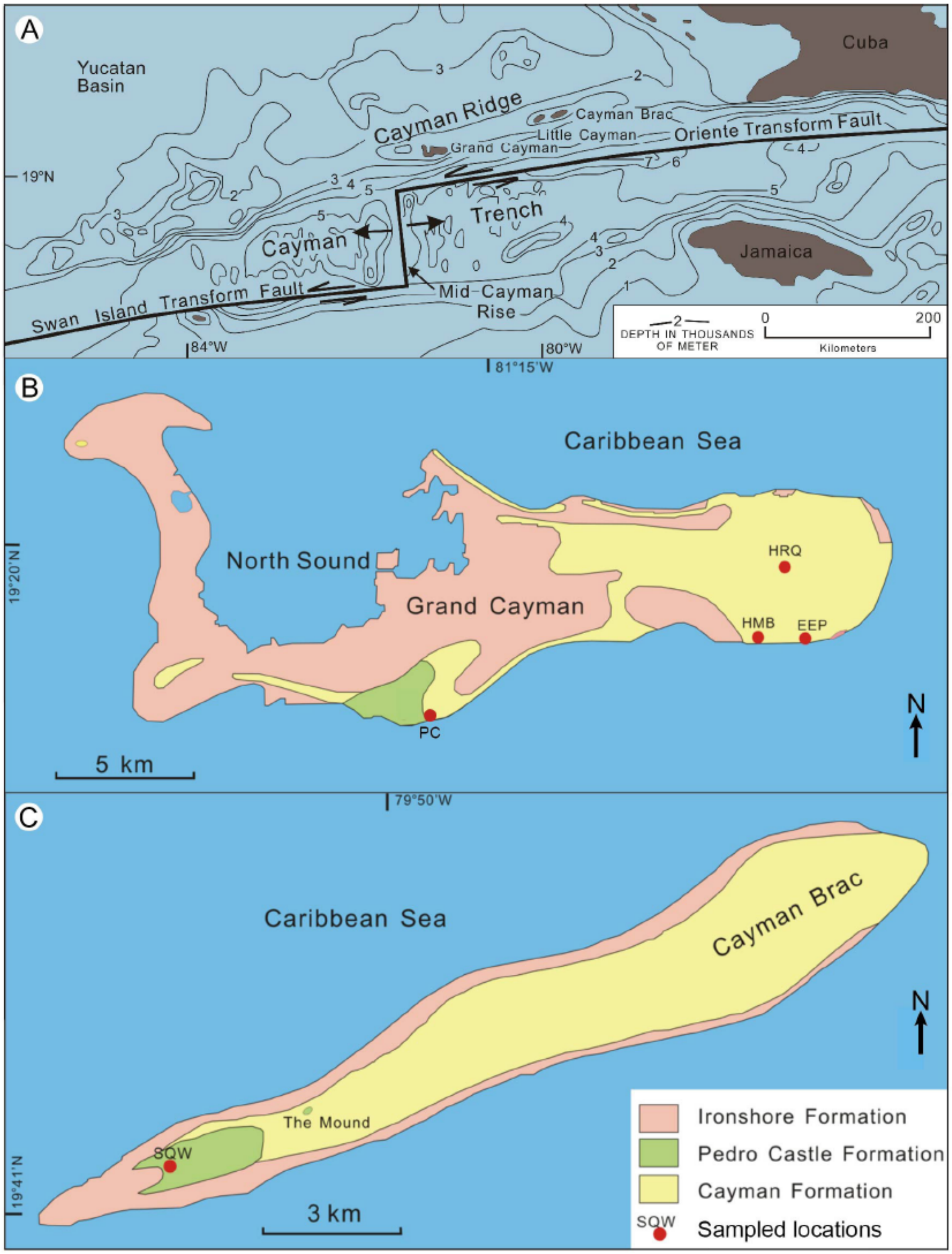

Fig. 4-1. Location and geology of Grand Cayman and Cayman Brac. (A) Location, tectonic and bathymetric setting of the Cayman Islands. Modified from Jones (1994), and based on maps from Perfit and Heezen (1978) and MacDonald and Holcombe (1978). (B) Geology map of Grand Cayman (modified from Jones, 1994) showing localities EEP (East End Pit), HRQ (High Rock Quarry), HMB (Half Moon Bay), and Pedro Castle (PC) where samples were collected. (C) Geology map of Cayman Brac (modified from Jones, 1994) showing locality SQW (Scott Quarry West).

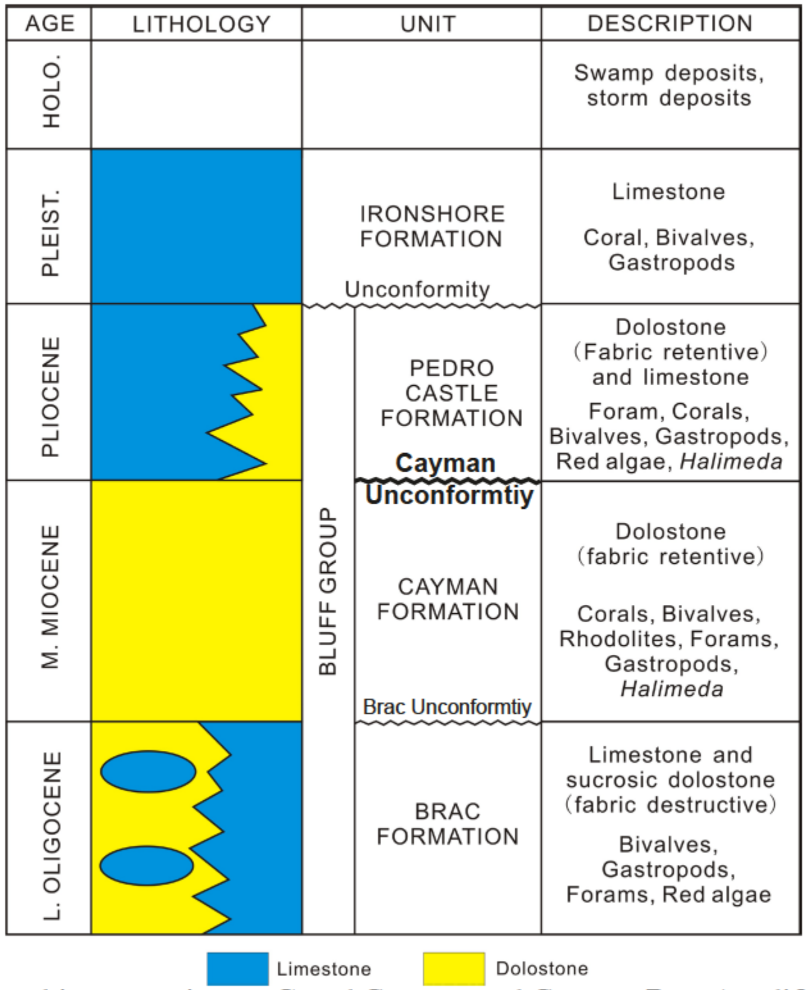

Fig. 4-2. Stratigraphic succession on Grand Cayman and Cayman Brac (modified from Jones, 1994).

and early Pliocene (Jones and Luth, 2003; MacNeil and Jones, 2003; Zhao and Jones, 2012, 2013).

The Cayman Formation is formed largely of finely crystalline, fabric retentive dolostones that contain numerous fossils, including corals, bivalves, gastropods, red algae, foraminifera, Halimeda, and rhodoliths (Jones, 1994; Jones and Hunter, 1994; Wignall, 1995; Der, 2012). The overlying Pedro Castle Formation is formed of limestones and finely crystalline, fabric-retentive dolostones with free-living corals, foraminifera, red algae, and rhodoliths, along with rare colonial corals, echinoids, and bivalves (Jones, 1994; Jones and Hunter, 1994; Wignall, 1995; Arts, 2000; MacNeil, 2001). The Ironshore Formation is formed of friable limestones that contain numerous, well-preserved corals, bivalves, and gastropods (Jones, 1994; Vézina, 1997;

Vézina et al., 1999; Coyne, 2003; Li and Jones, 2013).

4. Methodology

Sinkholes are common features of the phytokarst that characterizes much of the eastern part of Grand Cayman and the uplifted core of Cayman Brac (Fig. 4-3A, 4-3B). For this study, attention was focused largely on the southeast corner of Grand Cayman, because that area (1) has numerous open and filled sinkholes (Fig. 4-3C), (2) has been largely cleared of vegetation, (3) includes a small quarry that provides some vertical sections through the sinkholes (Fig. 4-3D), and (4) is easily accessible. Similar outcrops at other localities yielded a wide variety of different sinkhole- filling sediments (Fig. 4-3E-H). During study of the sinkholes and sinkhole-filling deposits in the field, 59 hand samples were collected for detailed study. This included five rootcrete samples that were collected from SQW on Cayman Brac (Fig. 4-1C). Thirty-three large (7.5×5 cm) thin sections were made from samples that were first impregnated with blue epoxy.

Small fracture samples (13 samples) for scanning electron microscope (SEM) analysis were carefully extracted from various samples and mounted on SEM stubs using double-sided tape and/or silver conductive glue and sputter coated with a very thin layer of gold or chrome. SEM analyses were done on a JOEL Field Emission SEM (JOEL 6301F) with an accelerating voltage of 5kV being used for imaging. The elemental composition of selected spots was determined by Energy-dispersive X-ray (EDX) analysis (Priceton Gamma-Tech X-RAY) with an accelerating voltage of 20 kV.

Powdered samples (75-150 μm) of the different components in the samples, obtained by drilling with a 2 mm diameter drill tip, were used for X-ray diffraction (XRD) analysis and geochemical analyses. Eighty-five samples were analyzed on a Rigaku Ultima IV Powder XRD system that was run at 38 kV and 38 mA using an Ultima IV X-ray generator with a Co tube. All scans were run from 5° to 90° 2θ at a speed of 2° θ/min. Using the same samples, oxygen and carbon stable isotopes were determined for 80 calcite and 21 dolomite samples. Following the method of McCrea (1950), the calcite samples were reacted with 100% phosphoric acid at 25 °C for 1-2 h, whereas the dolomite samples were reacted with 100% phosphoric acid for 2-3

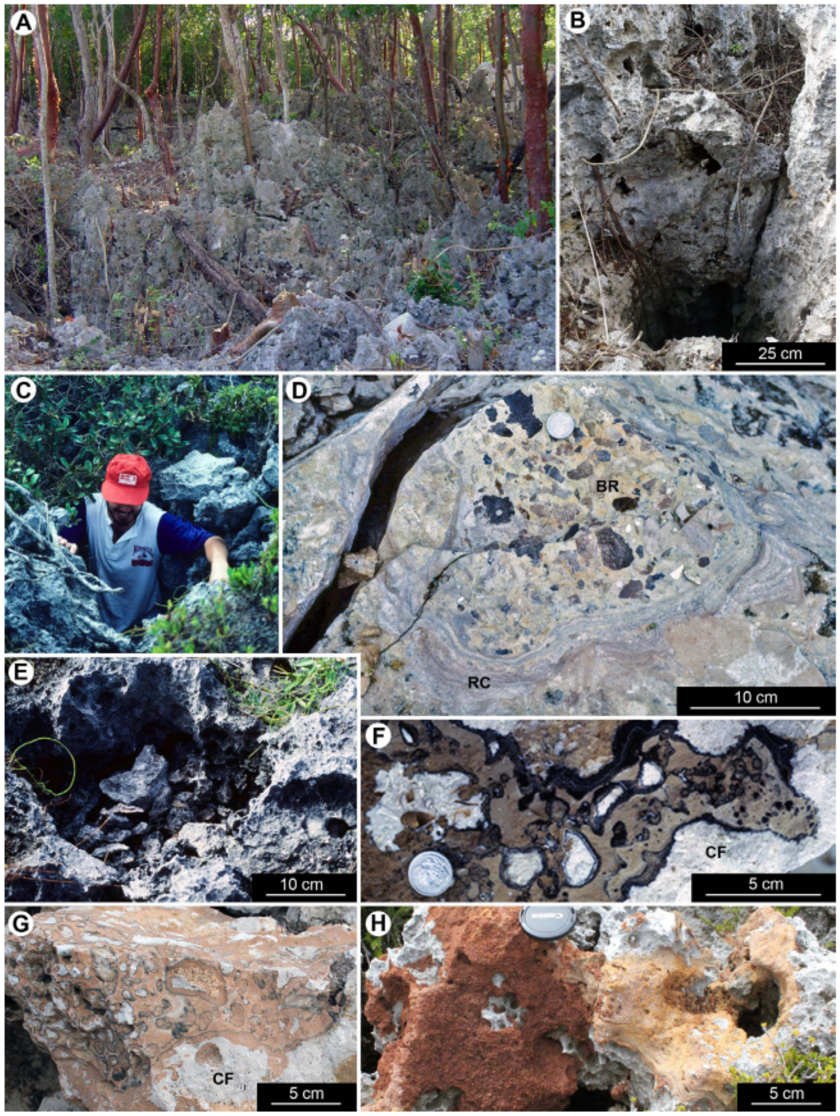

Fig. 4-3. Field photographs of sinkholes and sinkhole-filling deposits on Grand Cayman and Cayman Brac. Locality codes as for Figure 4-1. (A) General view of phytokarst surface on Cayman Formation, central part of Cayman Brac. Sinkholes are located between the pinnacles. (B) Open sinkhole in Cayman Formation on Cayman Brac that is at least 16 m deep. (C) Open sinkhole in Cayman Formation on Grand Cayman. Near EEP. (D) Cross-section through sinkhole lined with rootcrete (RC) and filled with breccia (BR). Note lithoclasts of various colors. Locality EEP. (E) Open sinkhole in Cayman Formation with loose dolostone lithoclasts (from Cayman Formation) on floor of sinkhole. Near locality EEP. (F) White dolostone lithoclasts from Cayman Formation (CF) with Mn-rich coatings filling sinkhole in Cayman Formation. Locality HRQ. (G) White dolostone lithoclasts held in red limestone matrices; note that some dolostone lithoclasts are coated by black, Mn-rich laminae. Locality HRQ. (H) Contrast between red (left) and orange limestones (right) in Pedro Castle Formation. Locality PC.

days at 25 °C at the University of Alberta's Stable Isotope Laboratory. The extracted CO_2 gas was introduced into a Finnigan-MAT 252 isotope mass spectrometer for analysis of the $\delta^{13}C$ and $\delta^{18}O$, which are reported relative to the Pee Dee Belemnite (PDB) standard normalized to NBS-18 in the per mil (‰). Analytical reproducibility was 0.05 ‰ for $\delta^{13}C$ and $\delta^{18}O$. The oxygen isotope values of the dolostones were corrected for the phosphoric acid fractionation.

Powdered samples weighing more than 0.2 g (81 samples) were analyzed for their trace elements contents (such as Mn, Fe, Al and REE) in the Radiogenic Isotope Laboratory at the University of Alberta. Those samples were first digested in 10 ml 8N HNO_3. Then, 1 ml of the solution was diluted with 8.8 ml deionized water and 0.1 ml HNO3 and 0.1 ml of an internal standard (Bi, Sc, and In). A Perkin Elmer Elan 6000 quadrupole inductively coupled plasma mass spectrometer (ICP-MS) was used to analyze the trace elements and REE in the diluted solution. The detection limits for the trace elements are from 0.01 ppm for Th to 5 ppm for P. The REE+Y distribution patterns and La/Yb-Sm/Yb parameters in these samples are illustrated by normalizing each REE+Y concentration against Post-Archean Average Shale (PAAS) (McLennan, 1989).

5. Results

5.1. Sinkholes

Numerous sinkholes are found in the Cayman Formation that is exposed on the eastern half of Grand Cayman (Matley, 1926; Doran, 1954; Jones, 1987, 1992b; Jones and Smith, 1988) and the central core of Cayman Brac (Fig. 4-3A, 4-3B). On Grand Cayman, the circular to subcircular sinkholes are 1–30 m in diameter and 1–10 m deep (Doran, 1954; Jones and Smith, 1988; Jones, 1992b) with many being water-filled. On Cayman Brac some of the open sinkholes are at least 18 m deep (Fig. 4-3B). Based on criteria developed by Cramer (1941) and Ford and Williams (2007), these sinkholes probably originated through dissolution because (1) there are no caves connecting to the bottoms of sinkholes, and (2) fracturing and rupture of the surrounding bedrock are rare.

Numerous sinkholes on Grand Cayman and Cayman Brac were subsequently filled with terra rossa and colonized by various plants, including many of the native trees. Processes association with the plant roots have modified the many of the sinkholes and mediated the formation of a wide variety of deposits. Thus, many sinkholes, like those found on the southeast corner of Grand Cayman are now partly or totally filled with rootcrete, breccia, red and orange limestones, speleothemic calcite, and modern corals and shells (Fig. 4-3). In this area, many generations of sinkholes are evident with younger ones commonly cross-cutting the older ones.

5.2. Sinkhole-filling deposits

Sinkholes developed in the white dolostones of the Cayman Formation are open (Fig. 4-3B, 4-3C) or filled with a diverse array of rootcrete, breccia, speleothem calcite, and modern corals and shells (Figs. 4-3, 4-4). There is no recognizable pattern to the distribution of the different types of sediments (Fig. 4-5).

5.2.1. Rootcrete

Rootcrete is a laminated calcareous crust, up to 8 cm thick, that follows the contour of the cavity created by roots and/or root hair (Figs. 4-4, 4-6, 4-7). XRD analysis showed that all laminae in the rootcrete, which are up to 2 mm thick, are composed largely of low-Mg calcite. These laminae are highlighted by their black and red colors, which reflect variations in trace element concentrations (Figs. 4-4, 4-6). EDX analyses on the SEM show that the black laminae typically contain Mn and Fe (Figs. 4-7A, 4-7B, 4-8A), whereas the red laminae contain Al, K, Fe, and Si (Figs. 4-7D-H, 4-8B-E). SEM analyses show that the rootcrete is formed mainly of anhedral to subhedral micrite (< 4 μm long) and euhedral microspar (5-15 μm long), along with minor amounts of Mn precipitates, Fe precipitates, chlorite, feldspar, quartz, and zeolites(?) (Fig. 4-7A-H). The micrite appears to have formed as the original groundmass, whereas the microspar formed as a cement in the small pores that once existed in the micrite. Fossils in the rootcrete include modern aragonitic gastropod and bivalve shells, which show no evidence of alteration. Borings are evident in some of the biofragments (Fig. 4-7C). Voids in the rootcrete, up to 0.2

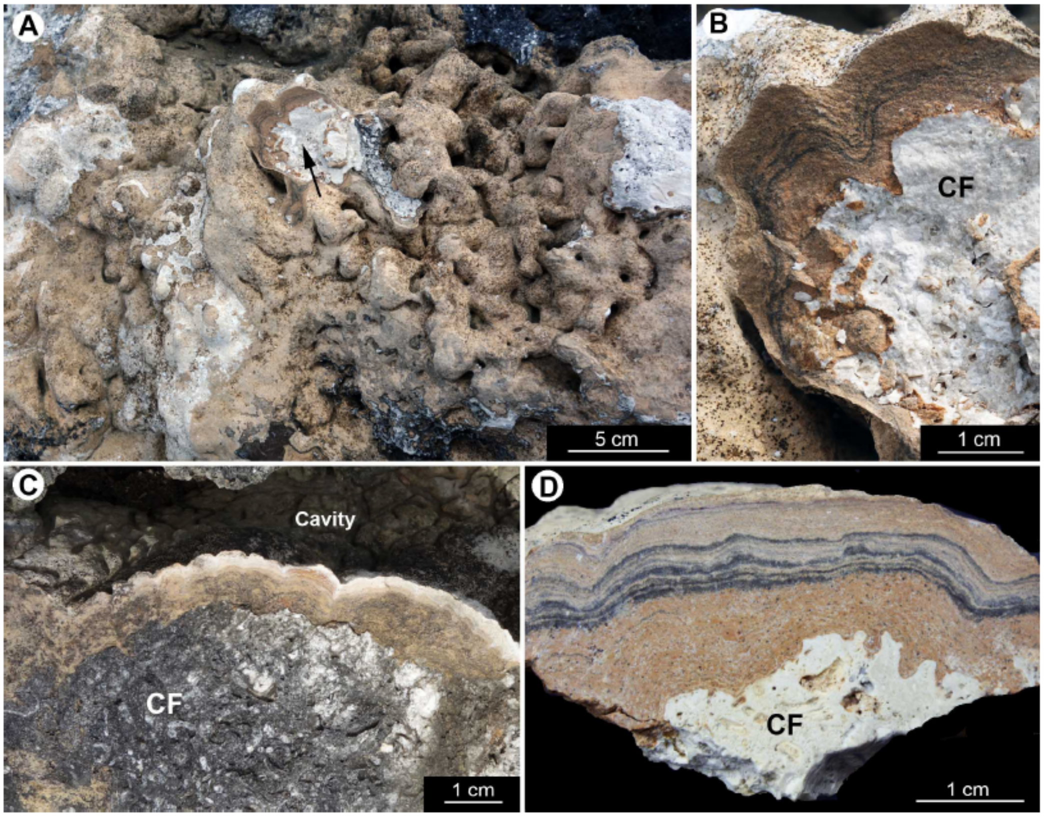

Fig. 4-4. Field photographs of rootcrete lining walls of sinkholes developed in the Cayman Formation. (A) Inner surface of rootcrete lining sinkhole. Arrow indicates location of panel B. Locality HRQ. (B) Rootcrete with Mn-rich laminae coating surface of sinkhole developed in the white dolostones of the Cayman Formation (CF). Locality HRQ. (C) Rootcrete lining wall of sinkhole developed in dolostones of the Cayman Formation (CF). Locality HRQ. (D) Cut and polished section through rootcrete developed on white dolostone of the Cayman Formation (CF). Locality HRQ.

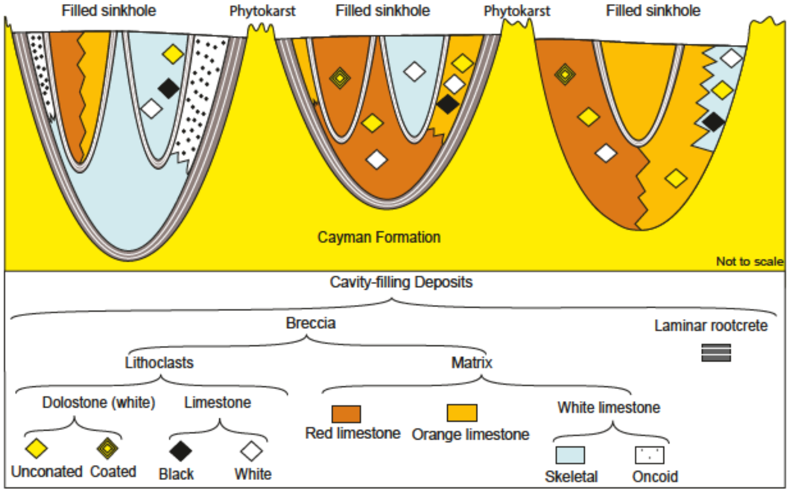

Fig. 4-5. Schematic diagram, based on the analysis of numerous sinkholes on Grand Cayman, summarizing the spatial relationships between different sinkhole-filling deposits.

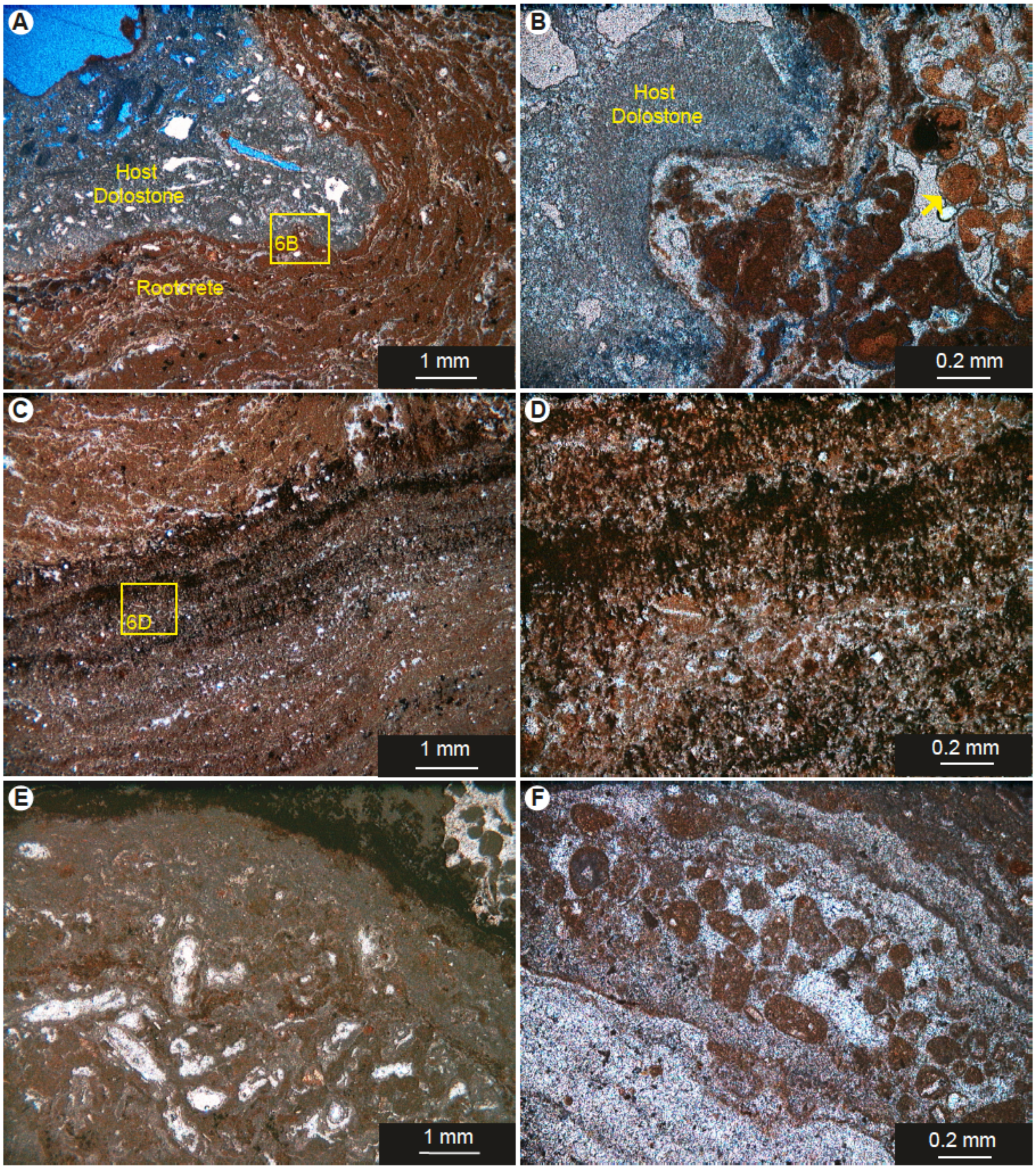

Fig. 4-6. Thin section microphotographs showing petrographic features of rootcrete. All images with plane polarized light. Locality codes as for Figure 4-1. (A) Rootcrete overlying host dolostone of the Cayman Formation. Locality HRQ. Yellow square indicates location of panel B. (B) Boundary between host dolostones and rootcrete. Note peloids in the rootcrete. Locality HRQ. (C) Contrast between laminae in rootcrete. Locality HRQ. Yellow square indicates location of panel (D). (D) Mn-rich lamina in rootcrete. Locality HRQ. (E) Alveolar septa structure. Locality EEP. (F) Peloids filling voids between septa in alveolar septa structure. Note spar calcite inside some of the peloids. Locality SQW.

mm long, are commonly lined with fiber calcite crystals that are up to 0.4 μm diameter and 15 μm long (Fig. 4-7M, 4-7N).

Alveolar-septal structures are common features of the black and red rootcrete lamina (Fig. 4-6). The arcuate micritic septa (up to 0.1 mm thick) define irregular-shaped voids that are generally < 1 mm in diameter. Beside spar calcite cement, fillings in those voids vary between different laminae. In the black laminae, for example, Mn-rich reticulate coatings, bladed crystals, or fuzzy coatings are common (Fig. 4-7A, 4-7B). The morphology of the very small Fe precipitates, which are present in some of these deposits, cannot be resolved.

In the red laminae, the voids are partly filled by spherical to vaguely laminated elliptical peloids (up to 0.4 mm in diameter) and, in some cases, feldspar, quartz, rare zeolites (?), and dolomite (Figs. 4-6B, 4-6F, 4-7D-G). Some of the vaguely laminated peloids contain spar calcite cement inside them (Fig. 4-6F). SEM and EDX analyses show that the peloids are formed of micrite and minor amounts of chlorite (Figs. 4-7H, 4-8E). Compared to the micrite that forms the alveolar septa, the peloids appear to contain more chlorite. In some samples, the chlorite forms rims composed of platelets that are arranged perpendicular to the peloid surface (Fig. 4-7H). In other samples, the chlorite is found as individual plates or fibers that are < 2 μm long (Fig. 4-7A). Euheral feldspar crystals, up to 5 μm long, subhedral quartz crystals (up to 9 μm long), and zeolites (up to 25 μm long) are present in some of the red laminae (Fig. 4-7D-G). Euhedral to subhedral dolomite crystals, up to 15 μm long, are randomly distributed in some of the rootcrete from localities HRQ and SQW (Fig. 4-7E).

All laminae in the rootcretes, irrespective of color, contain numerous calcified spores and filaments. Spherical spores, 0.9-1.3 μm in diameter, are commonly embedded in the calcite cement and/or associated with the fiber calcite. Based on their surface morphology, three types of spores, which are similar in size, are evident. Type I (Fig. 4-7J) is morphologically akin to the "ovate to spherical cocci having smooth surfaces" described by Jones (2011, his Fig. 9F). Type II (Fig. 4-7K) is similar to the "smooth spore with radiating spines" described by Jones (1991, his Fig. 9E, 2011, his Fig. 9B). Type III (Fig. 4-7L) is comparable to the "smooth spores with pores"

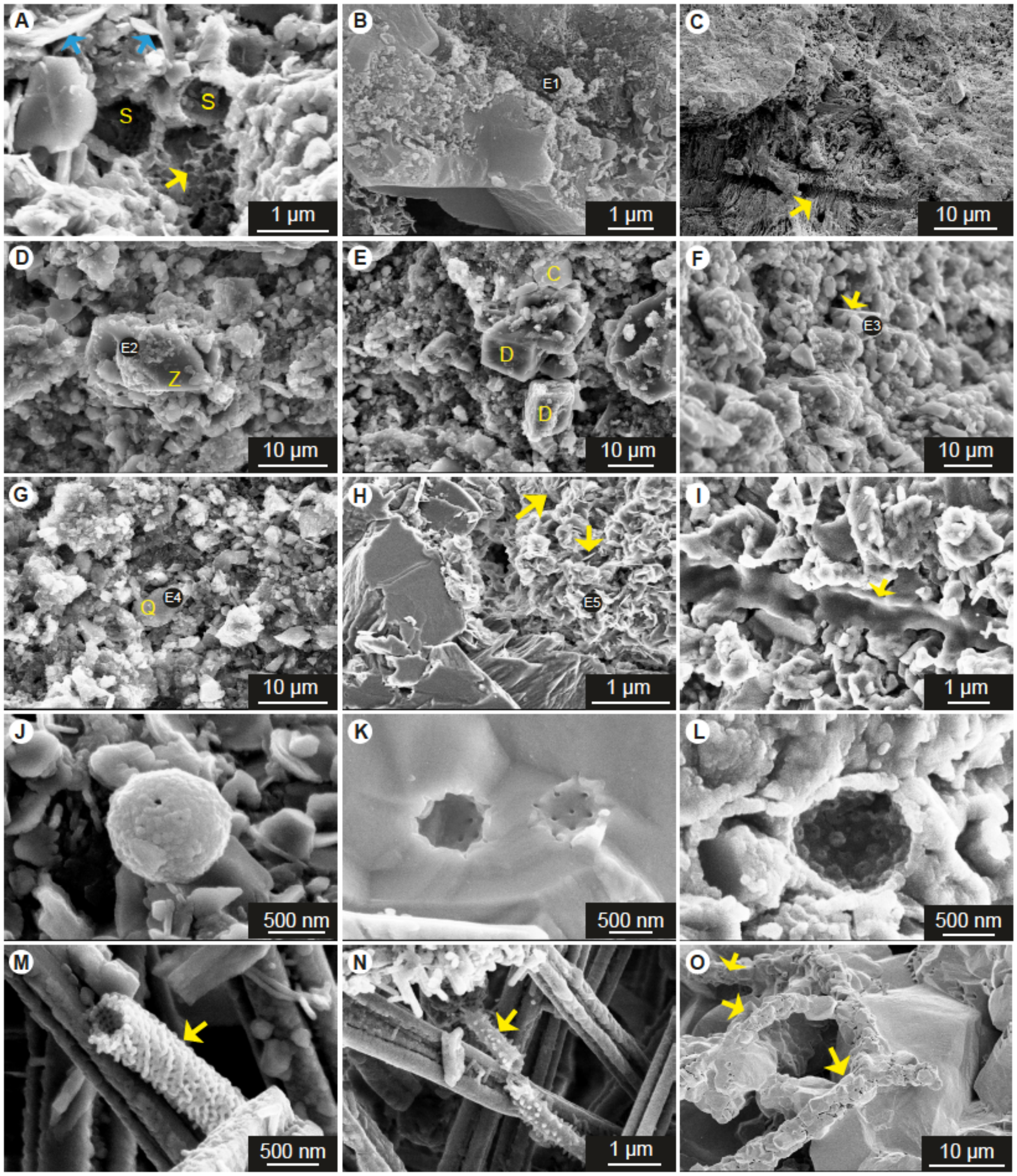

Fig. 4-7. SEM photomicrogaphs showing micro-fabrics in rootcrete. Locality codes as for Figure 4-1. Black circles labeled E1 to E5 indicate locations of EDX analyses shown in Figure 4-8. (A) Spores (S) and reticulate Mn-Fe precipitate (yellow arrow) embedded in micrite in black lamina of rootcrete. Note scattered chlorite plates (blue arrows). Locality SQW. (B) Fuzzy Mn precipitate coating on surfaces of calcite crystals. Locality EEP. (C) Boring (yellow arrow) in the biofragment derived from bivalve. Locality EEP. (D) Zeolite (Z) found in the red lamina of rootcrete. Locality HRQ. (E) Dolomite (D) rhombs associated with micrite and microspar (C) in red lamina. Locality HRQ. (F) Feldspar (yellow arrow) in red lamina. Locality HRQ. (G) Quartz (Q) in red lamina. Locality HRQ. (H) Chlorite platelets (yellow arrows) arranged perpendicular to the peloid surface, SQW. (I) Collpased filament (yellow arrow) in micrite. Locality SQW. (J) Type I spore, with smooth surface. Opening on top of

spore is probably an attachment collar. The surrounding platelets are chlorite. Locality SQW. (K) Type II, smooth spore with radiating spines. Locality SQW. (L) Type III, smooth spores with pores surrounded by low rims, SQW. (M) Type I reticulate filament (yellow arrow) with diamond-shaped openings on surface. Locality SQW. (N) Type II filament (yellow arrow) with isolated spines on surface. Locality SQW. Note fiber calcite crystals associated with the type I and type II filaments. (O) Type III, branching filaments (yellow arrows) that have been completely replaced by euhedral calcite crystals. Locality EEP.

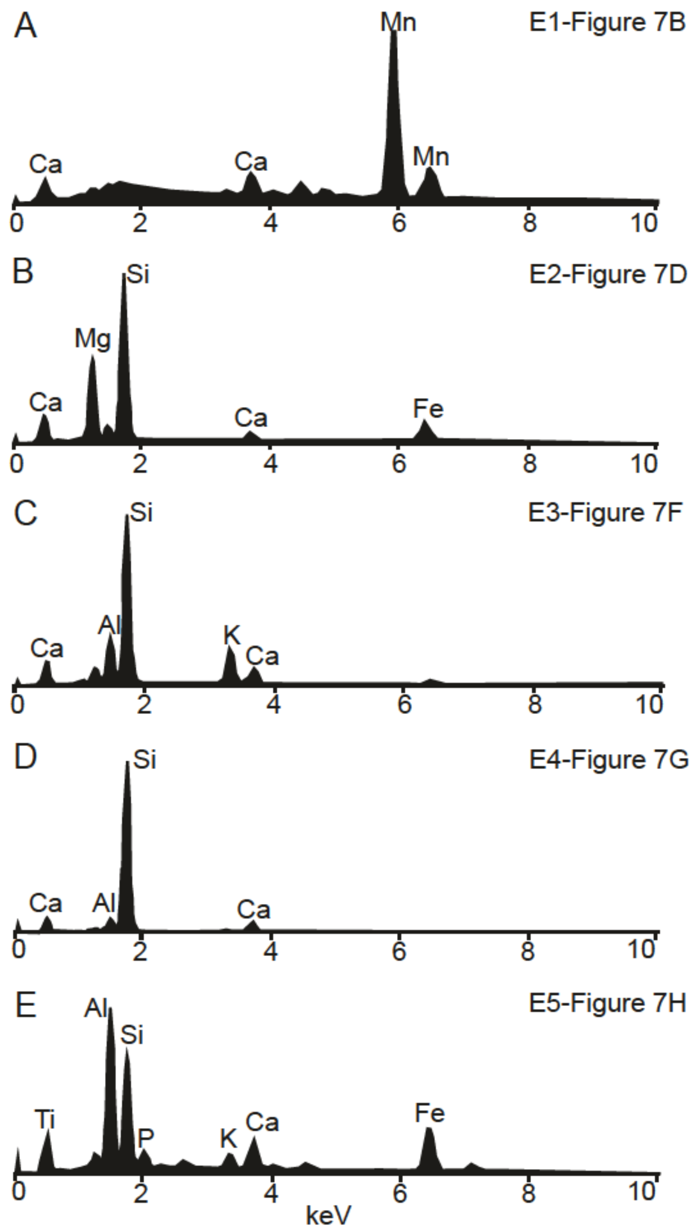

Fig. 4-8. EDX analyses for various laminae in rootcrete. See Figure 4-7 for precise locations of each analysis.

described by Jones (1991, 2011, his Fig. 9M). Many of these spores have one main opening (< 100 nm) that may be an attachment collar.

The calcified filaments, commonly found in the voids or among fiber calcite crystals, include three morphological types. Type I and Type II are non-branching filaments that are at least 15 μm long and up to 1 μm in diameter (Fig. 4-7M, 4-7N). Following the descriptions of the reticulate filaments found on the Cayman Islands (Jones, 1991, 2009, 2010b, 2011), Type I is characterized by diamond and spiral chambers (Fig. 4-7M), whereas Type II is characterized by isolated surface spines (Fig. 4-7N). Type III, up to 1 mm long and 1~2 μm in diameter, is a branching filament that has been completely replaced by euhedral calcite crystals (Fig. 4-7O).

The morphological attributes of those spores and filaments are considered to be taxa-specific because the different types are commonly intertwined with each other. Based on morphological features, the spores and filaments found in sinkholes are similar to those found in cave pearls (Jones, 2009), in notch speleothems (Jones, 2010a), cave speleothems (Jones, 2010b) and terrestrial oncoids (Jones, 2011). Those spores have been allied with actinomycetid spores (e.g., Tresner et al., 1961; Dietz and Mathews, 1969, 1971; Miyadoh et al., 1997), whereas the taxonomic affinity of filamentous microbes remains open to debate.

5.2.2. Breccia

Many of the sinkholes are filled with various types of breccia (Fig. 4-3D, 4-3F, 4-3G, 4-5). The lithoclasts are formed of dolostone or limestone. The limestone lithoclasts are further divided, based on color, into white and black/gray types. The limestone matrices are divided on the basis of color into white, red, and orange. The white limestone matrices are further divided into the skeletal and oncoid types. Different combinations of lithoclasts and matrices give rise to a diverse array of breccias.

The sub-angular to sub-rounded white dolostone lithoclasts, up to 6 cm long and 4 cm wide, (Fig. 4-3G) are formed of very finely crystalline dolomite and commonly characterized by numerous fossil mouldic cavities after corals, bivalves, foraminifera, and/or red algae (Fig. 4-9A). Some of the dolostone lithoclasts are coated with black, Mn-rich laminated crusts that are up to 1

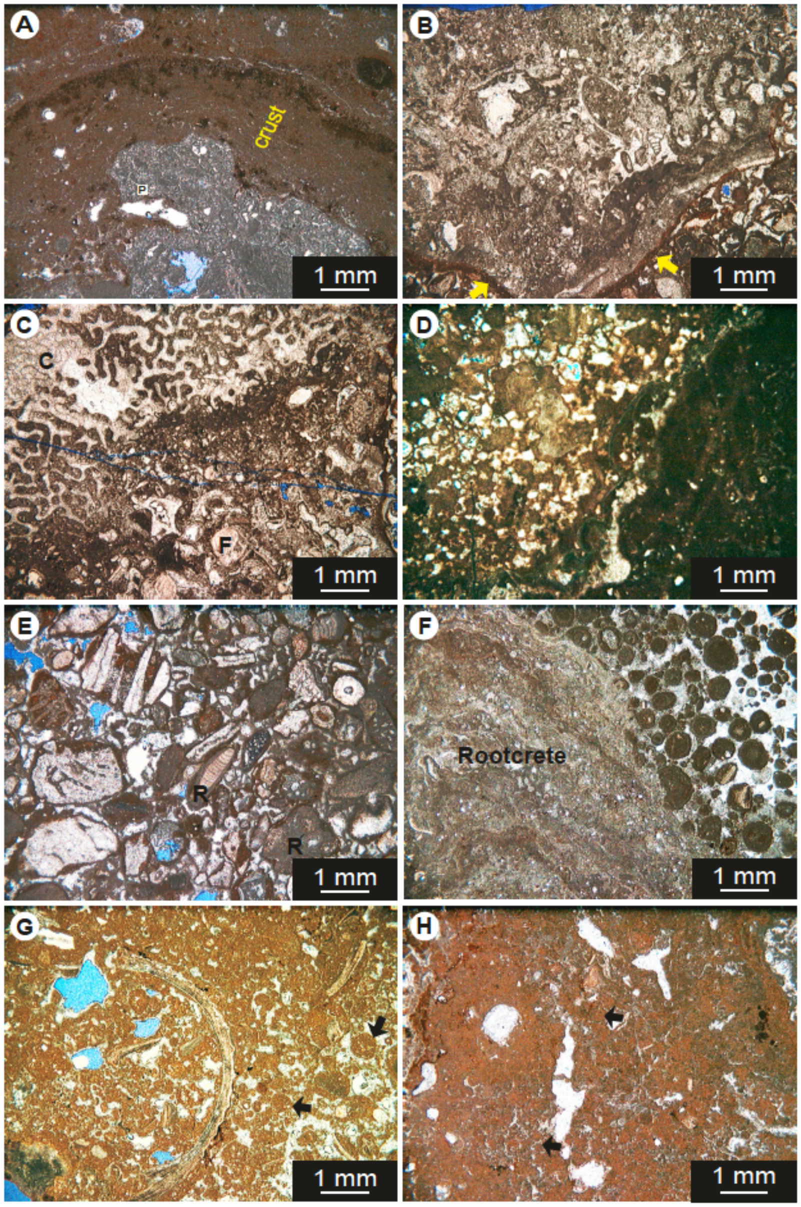

Fig. 4-9. Thin section microphotographs showing petrographic features of breccias in sinkholes. Locality codes as for Figure 4-1. (A) Coated dolostone lithoclast. Locality HRQ. (B) Skeletal white limestone lithoclasts (above yellow arrows) in the skeletal white limestone matrix (below yellow arrows). Locality EEP. (C) Micro-fabrics in skeletal black limestone lithoclast. Note corals (C) and pseudomorphically replaced foraminifera (F). Locality EEP. (D) Mudstone (right) and interclast packstone (left) in black limestone lithoclast. Locality EEP. (E) Unaltered biofragments, derived largely from red algae (R), in skeletal white limestone matrix. Locality EEP. (F) Oncoid white limestone matrix below rootcrete. Note some oncoid grains have leached biofragments as their nuclei. Locality EEP. (G) Micro-fabrics in orange limestone matrix showing peloids (black arrows), SQW. (H) Micro-fabrics in red limestone matrices showing peloids (black arrows). Locality EEP.

cm thick (Figs. 4-3F, 4-3G, 4-9A). Each lamina, up to 0.5 mm thick, mimics the morphology of the host lithoclast.

The white limestone lithoclasts include skeletal packstones to grainstones and oncoid grainstones. The skeletal packstone to grainstone lithoclasts, up to 10 cm long and 4 cm wide, include biofragments derived from corals, foraminiferas, and bivalves (Fig. 4-9B). All of these biofragments have been leached and then filled with calcite cement. The oncoid grainstone lithoclasts, 2 to 5 mm long, are formed of spherical to subspherical terrestrial oncoids (up to 0.5 mm in diameter) that are each characterized by a nucleus and a vaguely laminated cortex. SEM and EDX analyses show that the oncoids are largely formed of micrite, along with trace amount of clay minerals, Mn, and Fe. The black to dark gray limestone lithoclasts (Fig. 4-3D) are divided into skeletal packstones to grainstones and mudstone. The skeletal packstone to grainstone lithoclasts, up to 3 cm long and 2 cm wide, contain biofragments up to 1.5 cm long derived from corals, foraminifera, and bivalves that have all been leached and then cemented by calcite (Fig. 4-9C). The gray/black mudstone lithoclasts, which are up to 8 cm long and 4 cm wide, contain scattered gastropods and bivalves (Fig. 4-9D). In most breccias, these gray/black limestone lithoclasts are intermixed with the skeletal white limestone lithoclasts (Fig. 4-3D). Besides the obvious difference in color, the skeletal white lithoclasts are generally larger and more rounded than the gray/black lithoclasts.

The matrices in the breccias are formed of white, red, or orange limestone. The white limestone is divided into skeletal packstones to grainstones and oncoid grainstones. Biofragments in the skeletal white limestones were derived from red algae, foraminifera, corals, bivalves, gastropods, and echinoids (Fig. 4-9E). The biofragments, up 2 mm long and 1.5 mm wide, are typically encased by a micrite envelope (Fig. 4-9E). The red algae, foraminifera, and echinoids are commonly well preserved with many of the bivalves and gastropods still being formed of aragonite. In matrices formed of white oncoid grainstones, the spherical to subspherical terrestrial oncoids are 0.2 to 3 mm in diameter, with some having leached foraminifera or shell fragments as their nucleus (Fig. 4-9F). Based on SEM and EDX analyses, the vaguely laminated cortices are formed of micrite along with trace amount of clay minerals, Mn, and Fe. The surfaces of these oncoids are smooth or crenulated.

In previous studies (Jones and Smith, 1988; Jones, 1992b) the orange and red limestones, were called "lithified terra rossa" because they had the appearance of "soil" and were akin to the terra rossa that is found in many modern sinkholes on the island (Fig. 4-3H). XRD analysis of these rocks showed, however, that they are formed largely of calcite (> 98%) and only minor amounts of dolomite, quartz, and feldspars. No clay minerals were detected by XRD analysis. Thus, they are herein defined as limestone rather than lithified terra rossa.

The red and orange limestones are petrographically similar with both being formed largely of peloids that are held in spar calcite cement (Fig. 4-9G, 4-9H). The sub-spherical to elliptical peloids, 0.1 mm to 1.2 cm in diameter, commonly contain shell fragments derived from bivalves and/or gastropods. Foraminifera are common in the red limestones, whereas aragonitic bivalve fragments and gastropods are common in the orange limestone. Although formed largely of micrite, SEM and EDX analyses show that the peloids also contain minor amounts of clay, dolomite, quartz, and feldspars. The clay, which is probably chorite, is identified based on the bladed morphology of the crystals (< 2 μm long) that are formed of Al, Fe, and Si and trace amounts of K (Figs. 4-10, 4-11A, 4-11B). Chlorite has also been reported from bauxitic soils found on the Cayman Islands (Ahmad and Jones, 1969). SEM and EDX analyses indicate that (1) the red limestone typically contains more chlorite than the orange limestone, (2) the clay crystals in the red limestone (Fig. 4-10D) seem to be larger (up to 2 μm) than those in orange limestone (up to 1 μm) (Fig. 4-10B), (3) quartz and feldspar are more common in the red limestones than the orange limestones, and (4) the amount of Al is similar to that of Si in the orange limestones (Fig. 4-11A) but much lower than Si in the red limestones (Fig. 4-11B).

5.2.3. Speleothemic calcite

Voids (up to 1 cm wide and 3 cm long) or fractures (up to 1.5 cm wide) in the sinkhole-filling deposits are commonly lined or filled with brown speleothemic calcite. Like the flowstone covering the surface of the caves in the Cayman Formation (Smith, 1987; Jones and Smith,

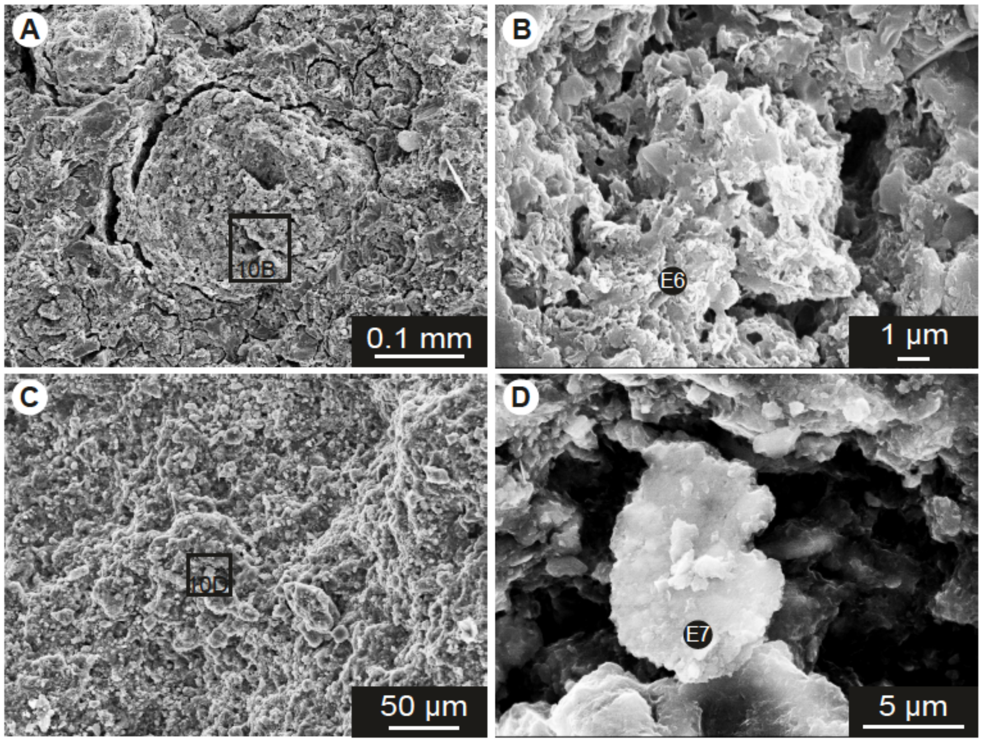

Fig. 4-10. SEM photomicrogaphs of micro-fabrics in orange and red limestones. Locality codes as for Figure 4-1. Black circles labeled E6 and E7 indicate locations of EDX analyses shown in Figure 4-11. (A) Peloid in orange limestone matrix. Locality EEP. Black square indicates location of panel (B). (B) Chlorite in orange limestone matrix. Locality EEP. (C) Chlorite in red limestone matrices. Locality HRQ. Black square indicates location of panel D. (D) A platy chlorite crystal. Locality HRQ. Note that chlorite in red limestone matrices is finer than that in red limestone matrices.

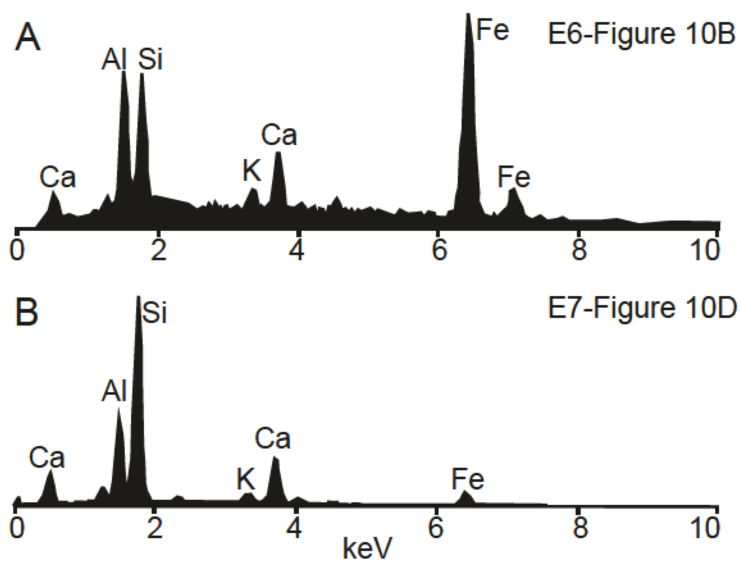

Fig. 4-11. EDX analyses for chlorite in red and orange limestones. See Figure 4-10 for precise locations of each analysis.

1988), the fibrous calcite is banded. Its precipitation conforms to the shape of the cavity. In some cases, dolostone lithoclasts are found inside the spelethemic calcite (Jones, 1987; Jones, 1992b).

5.3. Oxygen and carbon stable isotopes

The $\delta^{18}O$ and $\delta^{13}C$ values obtained from the different components of the sinkhole-filling deposits can be framed against the $\delta^{18}O$ and $\delta^{13}C$ trends that are known from the limestones of the Ironshore Formation, the calcareous crusts that formed on the unconformities in the Ironshore Formation, the dolostones from the Cayman Formation, and the limestones and dolostones from the Pedro Castle Formation (Fig. 4-12).

The negative $\delta^{18}O$ and $\delta^{13}C$ values obtained from the rootcretes, limestone lithoclasts, calcite cement in the host dolostones and dolostone lithoclasts, white limestone matrices, and speleothemic calcite follow the same $\delta^{18}O$-$\delta^{13}C$ trend, which is characterized by a wide range of $\delta^{13}C$ values and a narrow range of $\delta^{18}O$ values (Fig. 4-12). Compared to limestones from the Ironshore Formation, most samples in this group yielded more negative $\delta^{13}C$ values, ranging from -4.4 to -11.6 ‰. In contrast, the $\delta^{18}O$ values that range from -6.4 to -2.6 ‰, are compatible with those obtained from the limestones in the Ironshore Formation. The $\delta^{18}O$ and $\delta^{13}C$ in the calcite (micrite and microspar) that forms the rootcretes tend to vary between localities. Rootcretes from locality HRQ, for example, have more positive $\delta^{18}O$ (average -3.5 ‰) values than those from locality EEP (average -4.6 ‰) and locality SQW (average -5.4 ‰). The $\delta^{13}C$ values in rootcretes from HRQ (average -8.1 ‰,) are akin to those from SQW (average -9.2 ‰) but are more positive than those from EEP (average -10.5 ‰). Irrespective of location, there does not seem to be any trend in the isotope values from the base to the top of individual rootcrete crusts.

The $\delta^{18}O$ and $\delta^{13}C$ in the skeletal white limestone lithoclasts, the skeletal white limestone matrices, and the oncoid lithoclasts and matrices all fall in the ranges of -5.5 to -3.6 ‰ and -11.3 to -4.4 ‰, respectively. The two types of black limestone lithoclasts yielded similar $\delta^{18}O$ and $\delta^{13}C$ values that fall in the ranges of -5.7 to -4.5 ‰ and -11.1 to -6.5 ‰, respectively. Compatible

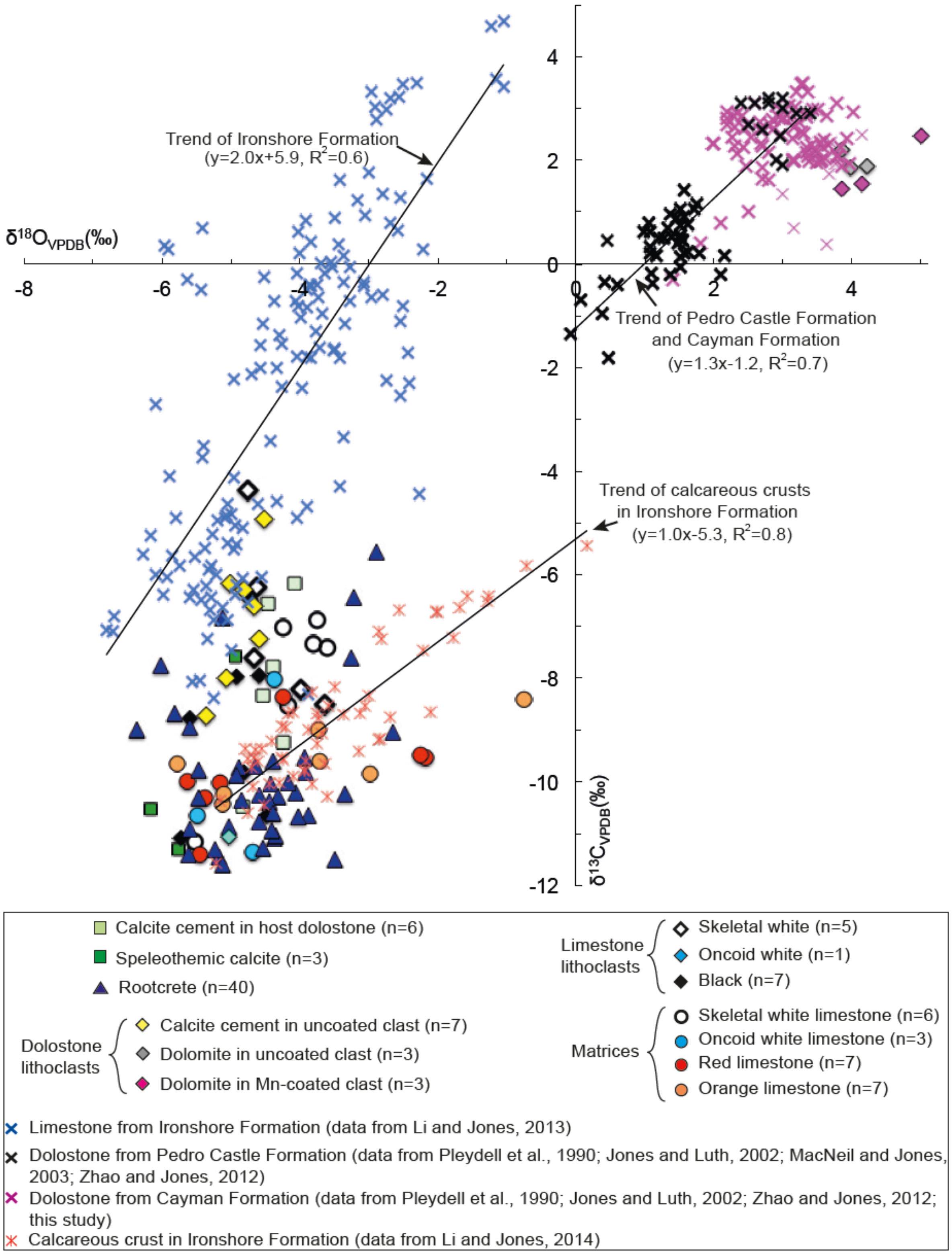

Fig. 4-12. Cross-plot of $\delta^{18}O$ versus $\delta^{13}C$ for sinkhole-filling deposits, Miocene-Pliocene limestones and dolostones.

with speleothemic calcite that lines the voids and fractures in sinkhole-filling deposits, calcite cement in the host dolostones and dolostone lithoclasts yielded $\delta^{18}O$ and variable $\delta^{13}C$ values that varied from -6.2 to -4.1 ‰ and from -11.3 to -4.9 ‰, respectively.

The negative $\delta^{18}O$ and $\delta^{13}C$ values in the red and orange limestone matrices are characterized by variable $\delta^{18}O$ and $\delta^{13}C$ that vary from -5.8 to -0.8 ‰ and -11.4 to -8.4 ‰ (Fig. 4-12), respectively. The $\delta^{18}O$ values are consistent with those obtained from the limestones of the Ironshore Formation. In contrast, the $\delta^{13}C$ values, which are much lower than those obtained from the limestones of the Ironshore Formation, are compatible with the $\delta^{13}C$ values obtained from the rootcretes.

5.4. Trace elements and REE concentration

Except for Mn and Sr, the highest concentrations of trace elements and REE are in the red and orange limestones, whereas the lowest concentrations are in the host dolostones. Compared to the host dolostone and other sinkhole-filling deposits, the rootcrete contains higher concentrations of Mn but lower concentrations of Sr. In the sinkhole-filling deposits, there is a positive correlation between the Al and REE concentrations (∑REE), between the Fe and ∑REE, and between the Mn and ∑REE (Fig. 4-13).

The red and orange limestone matrices have different concentrations of Al and Ca but similar Mn and Fe contents. The red limestone, for example, has higher Al (2533 to 4162 ppm, average 3088 ppm) than the orange limestone (1942 to 2586 ppm, average 2313 ppm). The Ca content of the red limestone (274621 to 322890 ppm, average 299246 ppm), is lower than that in the orange limestone (317138 to 349450 ppm, average 338144 ppm).

The ∑REE+Y in the lithoclasts, white limestone matrices, and speleothemic calcite found in sinkholes ranges from 0.3 to 20.0 ppm (average 8.1 ppm), whereas the ∑REE+Y of the red and orange limestone matrices varies from 21.5 to 77.6 ppm (average 46.1 ppm). The ∑REE+Y of rootcrete, in contrast, varies from 1.2 to 307.1 ppm (average 35.1 ppm).

The PAAS-nomalized REE+Y distribution patterns derived from all types of lithoclasts, white limestone matrices and speleothemic calcite are different from those derived from the

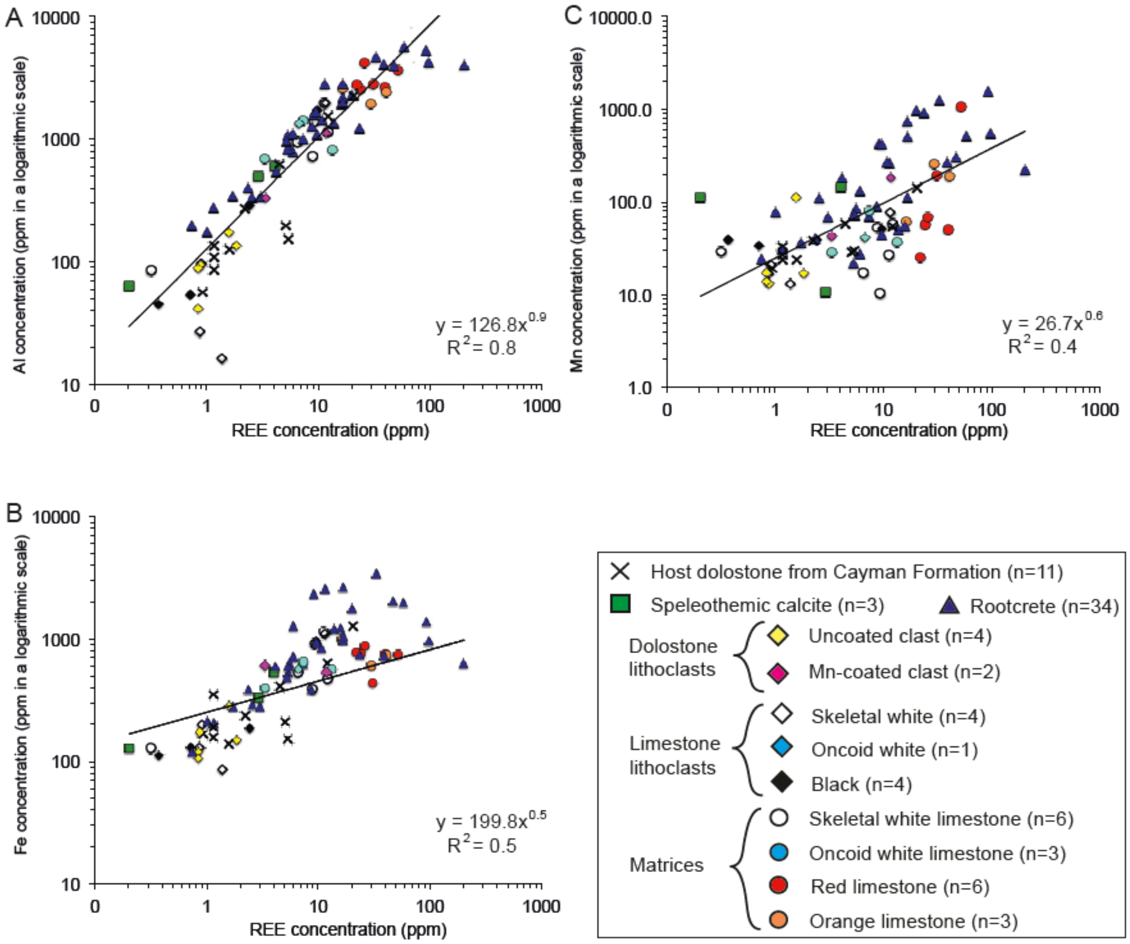

Fig. 4-13. Cross plots showing relationship between ∑REE of sinkhole-filling deposits and Al (A), Mn (B) and Fe (C).

rootcrete, and the red and orange limestones. Like the Neogene limestones and dolostones and Pleistocene limestones, all of the lithoclasts, white limestone matrices and speleothic calcite are heavy-REE (HREE) enriched (Fig. 4-14). Their La/Yb and Sm/Yb ratios vary from 0.2 to 0.7 (average 0.5) and from 0.7 to 1.0 (average 0.8), respectively (Fig. 4-15). These values are akin to those obtained from the Neogene limestones and dolostones and Pleistocene limestones, which yielded La/Yb ratios of 0.2 to 0.7 (average 0.4) and Sm/Yb ratios of 0.3 to 1.0 (average 0.7).

Rootcretes and the red and orange limestones are less enriched in HREE but relatively more enriched in light-REE (LREE) than other sinkhole-filling deposits, the Neogene limestones and dolostones, and the Pleistocene limestones (Fig. 4-14). The La/Yb (0.1 to 1.0, average 0.5) and

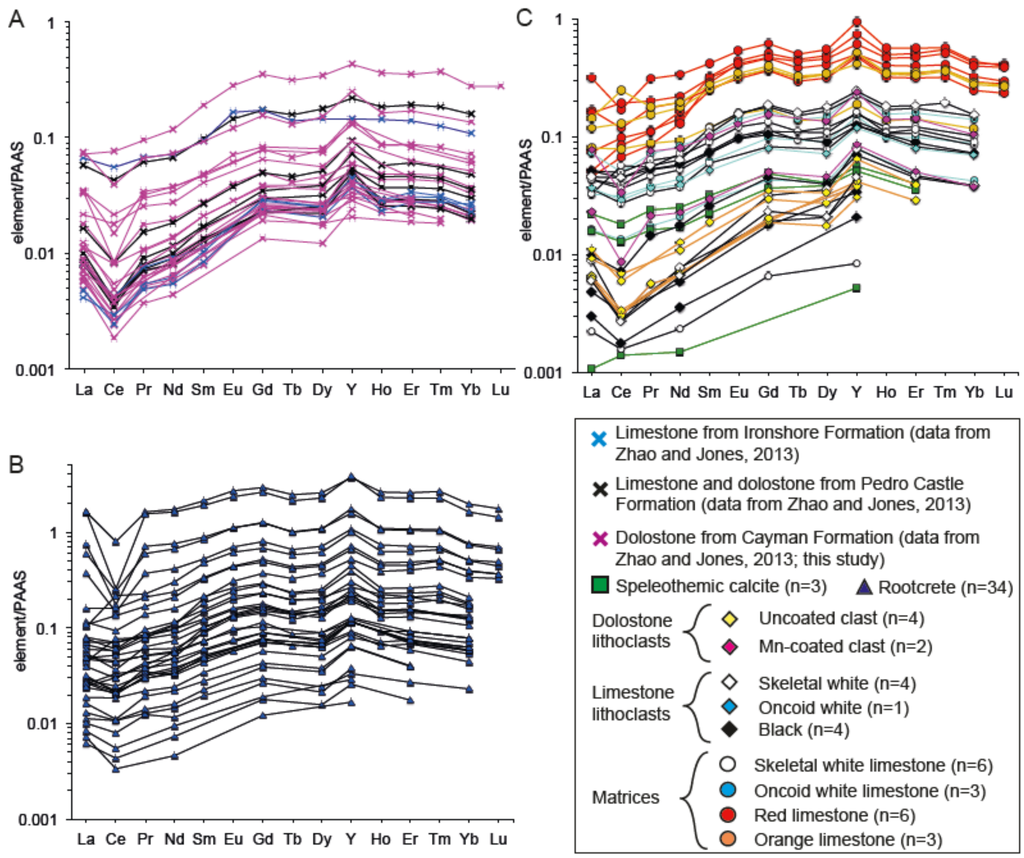

Fig. 4-14. PAAS-nomalized REE pattern of carbonates from Cenozoic succession (A) and sinkhole-filling deposits (B and C).

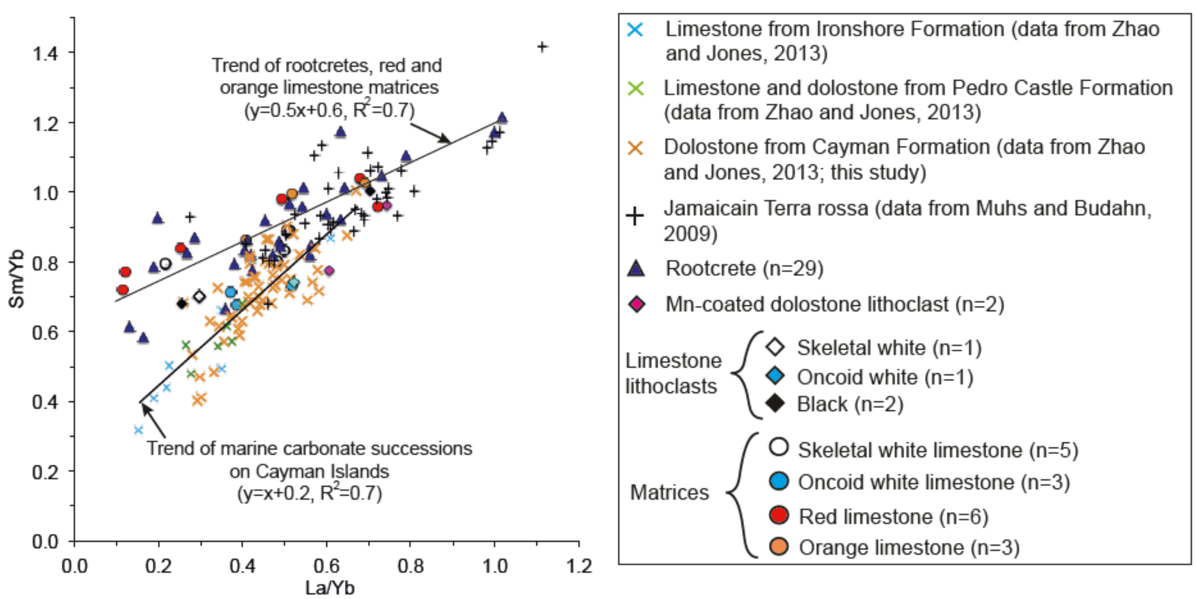

Fig. 4-15. Cross plot showing the correlation between Sm/Yb versus La/Yb in sinkhole-filling deposits, Jamaican terra rossa, and the carbonate from the Cayman Formation, Pedro Castle Formation and Ironshore Formation on Grand Cayman and Cayman Brac.

Sm/Yb (0.6 to 1.2, average 0.9) ratios obtained from the rootcrete are similar to those from the red and orange limestones (Fig. 4-15).

With respect to La/Yb and Sm/Yb ratios, the rootcretes, and the red and orange limestones follow the same trend, which is different to from the trend derived from the Neogene limestones and dolostones and Pleistocene limestones found on the Cayman Islands (Fig. 4-15). Compared to the latter group, the samples obtained from the rootcretes and the red and orange limestone matrices typically yielded higher Sm/Yb ratios but similar La/Yb. The Sm/Yb and La/Yb ratios in the rootcretes and the red and orange limestone matrices are partly overlap the range of values associated with the Jamaican terra rossa (Fig. 4-15).

6. Interpretation

6.1. Sequential development of void-filling deposits

The absolute age of the void-filling deposits is difficult to determine because they lack fossils that allow accurate dating and many of the lithologies are unlike any known from the stratigraphic succession exposed on Grand Cayman. Thus, the evolution of the sinkhole deposits can only be evaluated relative to the each other and relative to the surrounding bedrock (Table 4-1). The presence of dolostone lithoclasts derived from the Cayman Formation and/or the Pedro Castle Formation and the lack of dolomite in the rootcrete, limestone lithoclasts, and limestone matrices indicates that emplacement of these sinkhole-filling deposits postdated the last phase of dolomitization, which took place during the early Pliocene highstand (3.6-5.0 Ma), according to Zhao and Jones (2012, 2013).

Sinkholes, which are common features in areas where the Cayman Formation is exposed, can be open or filled with a variety of deposits (Fig. 4-3). The contrast between open and filled sinkholes indicates that the development of sinkholes is probably an ongoing process, with some of them now being actively filled by loose dolostone lithoclasts derived from surrounding host dolostones of the Cayman Formation (Fig. 4-3).

The formation of rootcrete and deposition of the limestone matrices were repeated many times. Rootcrete, for example, is present between the host dolostones and the sinkhole-filling deposit, or between different types of sinkhole-filling deposits (Fig. 4-5). Similarly, matrices formed of skeletal and oncoid white limestone were deposited at many different times. Some of the white limestone matrices that overlie the host dolostones, for example, were subsequently truncated by rootcrete, whereas other limestones formed after many of the rootcretes (Fig. 4-5). The poorly consolidated nature of these matrices with their well-preserved aragonitic fossils indicates that they probably formed when the limestones of the Ironshore Formation were being deposited and/or as a result of relatively modern deposition associated with storms (Table 4-1). The age of the oncoid white limestone matrices is not known and could even be forming today.

Today, loose dolostone lithoclasts found in many of the open sinkholes came from the surrounding Cayman Formation (Fig. 4-3E). Similarly, most of the white dolostone lithoclasts the lithified breccias probably came from the Cayman Formation (Table 4-1). It is possible,

Table 4-1. Sequential development of sinkhole-filling deposits associated with the exposed Cayman Formation

Component	Numbers of episodes	Provenance	Age	Evidence	Active today	Reference
Sinkhole	Multiple		Post late dolomitization		Yes	Jones and Smith, 1988 Jones, 1992b
Rootcrete	Multiple	In situ growth	Post late dolomitization	No dolomite	Probably	Jones, 1992b Alonso-Zarza and Jones, 2007
Dolostone lithoclasts	Numerous and ongoing	Cayman Formation or Pedro Castle Formation	Middle Miocene or Early Pliocene	Same lithologies as in Cayman Formation and Pedro Castle Formation	Yes	Jones, 1992b
Skeletal white and black limestone lithoclasts	Probably one	Unknown marine carbonate	Late Pliocene to Pleistocene	Lithology unlike any bedrock in area	No	Jones and Kahle, 1985 Jones, 1992b
Skeletal white matrices	At least two	Marine skeletal deposits, but not the Ironshore Formation itself	Pleistocene or modern	Well preserved fossils, poorly consolidated	Yes	Jones, 1992b
Oncoid white limestone matrices and lithoclasts	At least two	Terrestrial	Post dolomitization	Terrestrial oncoids cemented by calcite	No	Jones, 1991 Jones, 1992b Jones, 2011
Red and orange limestone matrices	At least two	In situ precipitation, mixed traces of soil	Pleistocene	Aragonitic gastropods and bivalves not leached	No	Ahmad and Jones, 1969 Jones and Smith, 1988 Jones, 1992b

however, that some could have come from the Pedro Castle Formation (Table 4-1) that once covered this part of the island.

The black and skeletal white limestone lithoclasts, which are of marine origin, cannot be related to any of bedrock succession that is exposed on the Cayman Islands today. Thus, it seems that these lithoclasts were derived from strata that have since been removed by erosion. This suggestion is feasible given that that the period between deposition of the sediments in the Pedro Castle Formation (early-middle Pliocene) and the initiation of the sedimentation for the Ironshore Formation (500-600 ka) (Jones et al., 1994b; Wignall, 1995; Vézina, 1997; Zhao and Jones, 2013; Liang and Jones, 2014) was characterized by oscillating sea levels (Dowsett and Cronin, 1990; Miller et al., 2005, 2011, 2012b; Dwyer and Chandler, 2009; Sosdian and Rosenthal, 2009). Deposition during one of the sea level highstands may have produced limestones that were removed by erosion during subsequent lowstands. Thus, the black and skeletal white limestone lithoclasts may have been derived from sequences that were 3.6 Ma to 500-600 ka old (Table 4-1).

6.2. Rootcrete

The following features indicate a biological, non-marine origin for the rootcrete.

- The presence of numerous spores and filaments (Alonso-Zarza and Jones, 2007),
- The presence of calcified root cells in some of the rootcrete (Alonso-Zarza and Jones, 2007, their Fig. 5).
- The presence of alveolar-septal structures (Fig. 4-6E), which are commonly associated with plant roots (Klappa, 1978, 1979; Wright, 1986; Wright et al., 1988; Armenteros and Daley, 1998).
- The variable size of the anhedral to subhedral micrite in rootcrete indicates that precipitation of the carbonate was probably biogenically induced (Alonso-Zarza, 1999).
- The presence of needle fiber calcite (NFC), which has been attributed to physicochemical and biological processes. The inorganic processes would have involved solutions that were supersaturated with respect to $CaCO_3$ (James, 1972; Riche et al., 1982; Jones and Peng,

2014), whereas biological processes have generally been attributed to plant root and/or fungal activity (Harrison, 1977; Calvet and Juliá, 1983; Callot et al., 1985a, 1985b; Phillips and Self, 1987).

- The voids in the alveolar-septal structures are commonly filled with peloids. The peloids may be related to roots or the activity of microorganisms that are associated with plant roots (Calvet and Juliá, 1983; Jones and Squair, 1989; Alonso-Zarza, 1999, 2003; Miller and James, 2012).
- The lack of marine fossils.
- The homogenous $\delta^{18}O$ and variable $\delta^{13}C$ of the Cayman rootcretes, which are consistent with meteoric diagenesis in the vadose zone (Meyers and Lohmann, 1985; Lohmann, 1988). The lack of positive covariance between the $\delta^{18}O$ and $\delta^{13}C$ in the rootcretes indicates that evaporation was not involved in the formation of the rootcretes.

Various features associated with the rootcretes, such as the calcified root cells and alveolar-septal structures indicate that the rootcretes probably formed around the roots when the plants were alive. After the decay of the plants, the rootcrete remains with the crust following the outline the cavity that developed while the plants were alive. The rootcrete forms an impermeable barrier that would have impeded fluid draining from the surface, including rainfall and acids produced by the plants, which is similar to the situation associated with rhizogenic calcrete horizons (Goudie, 1983; Reimann and de Caritat, 1998).

Laminar calcrete, which forms in the soil profile under biogenic control of plant roots and their associated microorganisms (Klappa, 1980; Wright et al., 1988, 1995; Alonso-Zarza, 1999), develops through in situ alteration of the host rock (e.g., James, 1972; Goudie, 1973; Arakel, 1982) and/or accretionary build-up (e.g. Wright et al., 1988, 1995; Li and Jones, 2014). For rootcrete, the in situ alteration model is discounted because the rootcrete is formed largely of calcite, whereas the host rock is formed of dolostone. As noted by Alonso-Zarza and Jones (2007), the accretion model is more feasible given that the various microorganisms contribute to the rootcrete formation by (1) binding detrital micrite onto the substrate, (2) acting as nuclei for calcite precipitation, and (3) modifying the local microenviroment so that micrite can be precipitated. Minor amounts of chlorite, feldspar, quartz, and zeolites, which were probably of detrital origin, became incorporated into the rootcrete during these accretionary processes. The incorporation of these minerals are probably responsible for the large variations in the ∑REE+Y, the correlations between ∑REE and Fe, Mn, and Al, the HREE-enriched REE+Y patterns, and the La/Yb and Sm/Yb values that are different from the Cenozoic carbonates found on the Cayman Islands (Figs. 4-13, 4-14, 4-15). The Mn found in the rootcrete is probably related to biological activity (Jones, 1992a).

6.3. Breccia

6.3.1. Lithoclasts

The white dolostone lithoclasts, with their fossil-mouldic porosity, are comparable with the dolostones found in the Cayman Formation and the Pedro Castle Formation. This suggestion is further supported by (1) the stable isotopes from the dolomite that follows the same $\delta^{18}O$-$\delta^{13}C$ trend as the dolostones from these formations (Fig. 4-12), and (2) REE+Y patterns and La/Yb and Sm/Yb ratios that are akin to those in the dolostones from these formations (Figs. 4-14, 4-15). Most of these lithoclasts seem to have been derived from the Cayman Formation.

The composition and microfabrics of the Mn-rich coatings found around some of the dolostone lithoclasts is identical to the Mn-rich coatings evident in the rootcretes, suggesting that their formation was also related to root activity.

The skeletal white and black skeletal limestone lithoclasts, which contain numerous fossils (e.g., corals, foraminifera), are clearly of marine origin. The black mudstone lithoclasts are probably also of marine origin because (1) some lithoclasts are formed of intercalated mudstone and skeletal limestone (Fig. 4-9D), and (2) the REE+Y signatures of the mudstones are similar to those obtained from the skeletal limestone lithoclasts. This is contrary to opinion of Jones (1992b) who suggested that the black mudstone may have originated in fresh- to brackish-water ponds. The black and skeletal white limestone lithoclasts are intermixed with each other, indicating that they probably originated from contemporary limestone deposits. There are, however, no counterparts to these lithologies in the bedrock succession that is now exposed on Grand Cayman. The limestones layers from which these lithoclasts came were probably removed by erosion during periods of subaerial exposure.

The black color of carbonate lithoclasts has been attributed to (1) impregnation by Fe or Mn sulfides (Sugden, 1966; Maiklem, 1967; Wright, 1986), (2) forest fires (Barthel, 1974; Strasser, 1984; Shinn and Lidz, 1988), or (3) dissolved, colloidal or very finely particulate organic matter that formed under pedogenic conditions, including organic rich tidal and lacustrine environments, microbial communities, and decayed terrestrial plants (Ward et al., 1970; Folk et al., 1973; Strasser and Davaud, 1983; Strasser, 1984; Leinfelder, 1987; Lang and Tucci, 1997, Miller et al., 2013). On the Cayman Islands, discoloration due to Fe and Mn impregnation seems unlikely because no pyrite was found in the crusts and the Fe and Mn contents are similar to those of white host dolostones. Blackening of carbonates by forest fires requires temperatures between 400 and 500°C (Shinn and Lidz, 1988; Vera and de Cisneros, 1993). Although possible for the Cayman lithoclasts, there is no direct evidence to support this possibility because large forest fires are rare on Grand Cayman and any that do occur are of short duration.

The pedogenic-meteoric diagenetic model seems to be the most feasible explanation for the black limestone lithoclasts found on the Cayman Islands. The lack of black limestone lithoclasts in the sinkholes without rootcrete implies that the environment that favored rootcrete development also favored the development of black limestone lithoclasts. The development of rootcrete is associated with decaying terrestrial plants, which favors organic staining of limestones (Krumbein and Garrels, 1952; Suess, 1970; Strasser and Davaud, 1983; Strasser, 1984; Leinfelder, 1987; Lang and Tucci, 1997; Miller et al., 2013). Organic matter, however, did not blacken all of the lithoclasts in the sinkholes as many of skeletal white limestone lithoclasts remained white. Hips et al. (2011) suggested that blackening by organic matter is related to the presence of unstable minerals (e.g., aragonite and high-Mg calcite). This is because the replacement of unstable minerals would provide the opportunity for the absorption of organic matter into the crystal (Hips et al., 2011). If it is assumed that the blackening processes are linked to the diagenetic alteration of unstable minerals, then the white limestone lithoclasts must have stabilization prior to the onset of the diagenetic processes responsible for the blackening of the lithoclasts. This notion is supported by (1) the fact that some white spots are still evident inside some of the black lithoclasts, and (2) the $\delta^{13}C$ values of the black limestone lithoclasts are more negative than those from the white limestone lithoclasts.

The terrestrial oncoids in the oncoid white limestone lithoclasts and oncoid matrices are consistent with those described by Jones (1991). The subtle variations of the composition of oncoids suggest subtle changes in fine-grained detritus and the ground water (Jones, 1991).

6.3.2. Matrices

The marine fossils and REE signatures indicate that the skeletal white limestone matrices are of marine origin. The presence of aragonitic fossils suggests that these limestone matrices probably formed during or after the Pleistocene (Table 4-1). Given that these limestones have experienced meteoric diagenesis, which is similar to the limestones from the Ironshore Formation, the different $\delta^{18}O$-$\delta^{13}C$ trend for these white limestone matrices and the limestones from the Ironshore Formation indicates that they probably formed at different times (Fig. 4-12).

A terrestrial origin for the oncoid white limestone matrices is suggested by (1) the morphological and compositional similarity between these terrestrial oncoids and those described by Jones (1991), and (2) their negative $\delta^{18}O$ and $\delta^{13}C$ values, which are consistent with meteoric diagenesis in the vadose zone (Meyers and Lohmann, 1985; Lohmann, 1988). Jones (1991) suggested that terrestrial oncoids were of biogenic origin. Thus, the environment around rootcretes would be ideal for their development.

The red and orange limestone matrices do not appear to be of marine origin because they are characterized by trace amounts of chlorite, quartz and feldspar crystals, and have different isotopic compositions and REE signatures than the limestones from the Ironshore Formation. The different colors are probably related to variations in the carbonate content and the amount of detrital quartz, feldspar, and chlorite (cf., Porter, 2000; Sun et al., 2011). The quartz, feldspar, and chlorite were probably derived from airborne dust, as on other Caribbean Islands (e.g., Muhs et al., 1990, 2007; Foos, 1991; Borg and Banner, 1996; Herwitz and Muhs, 1995; Muhs, 2001; Muhs and Budahn, 2009). The variable $\delta^{18}O$ and homogenous $\delta^{13}C$ values of the red and orange limestone matrices are consistent with the $\delta^{18}O$-$\delta^{13}C$ trend that is typically associated with evaporation (Salomons et al., 1978; Rossinsky and Swart, 1993). This suggests that the red and orange limestone matrices may have been the product of in situ precipitation that was driven by evaporation.

The ∑REE+Y, the La/Yb ratios, and the Sm/Yb ratios from the red and orange limestones are different from those obtained from the Cayman Formation, the Pedro Castle Formation, and the Ironshore Formation (Figs. 4-14, 4-15), indicating that REE from authigenic minerals (e.g., Fe- and Mn-oxides) and/or terrigenous sediment (e.g., Nothdurft et al., 2004) are probably involved. For the red and orange limestone matrices, however, the poor correlation between ∑REE and Fe, between ∑REE and Mn, and between ∑REE and Al (Fig. 4-13), indicates that there is little contamination from authigenic minerals. Terrigenous contamination could, however, have come from airborne dust and/or terra rossa that is present in some areas of the Cayman Islands (Zhao and Jones, 2013).

6.4. Speleothemic calcite

Stable isotope compositions indicate that the speleothemic calcite that coats the walls of many of the voids in the sinkhole-filling deposits was formed from meteoric water. Such precipitation probably took place at the same time as speleothemic calcite was being precipitated in many of the caves on the Cayman Islands, probably as a result of high rainfall (Jones and Smith, 1988; Jones, 1992b).

7. Discussion

The sinkhole-filling deposits formed during sea-level lowstands while the subaerial unconformities were developing. On the eastern part of Grand Cayman, sinkhole development and filling have been processes since the late Pliocene (~3.6 Ma). As a result, the type of sinkhole-filling deposit varied with time as local conditions changed in accord with sea level and climate conditions.

The stable isotope signatures of the sinkhole-filling deposits are similar to those obtained from the calcrete crusts that are found on some of the unconformity surfaces in the Ironshore Formation (Fig. 4-12). The $\delta^{18}O$ and $\delta^{13}C$ values for these sinkhole fills, however, are significantly different from those that characterize the limestones from the Ironshore Formation and the dolostones and limestones of the Cayman Formation and Pedro Castle Formation (Fig. 4-12). Such comparisons support the notion that the sinkhole-filling deposits were subject to significantly different diagenetic regimes that were largely mediated by meteoric waters. Such diagenesis, which is commonly associated with erosional unconformities, is typically characterized by evaporation and/or biological activity that yields $\delta^{18}O$ values from -9 ‰ to 3 ‰ and $\delta^{13}C$ values from -12 ‰ to 4 ‰ (Talma and Netterberg, 1983; McKenzie, 1985; Salomons and Mook, 1986; Alonso-Zarza, 2003; Alonso-Zarza and Arenas, 2004). The isotopic compositions of the Cayman sinkhole-filling deposits fall within these limits, with the $\delta^{13}C$ values being near the limit of -12 to -13 ‰ known for soil carbonates (Cerling, 1984; Burns et al., 1989; Alonso-Zarza, 1999). Such comparisons also indicate that biogenic factors played an important role in the formation of sinkhole-filling deposits. The rootcrete offers clear evidence of such biogenic processes.

For terrestrial deposits, the rare earth elements La (LREE), Sm (MREE), and Yb (HREE) have commonly been used as indicators of provenance and to compare different deposits (Nakai et al., 1993; Clift et al., 2005; Muhs et al., 2007; Muhs and Budahn, 2009). The La/Yb and Sm/Yb ratios for the sinkhole-filling deposits on Grand Cayman plot along a different trend line than that derived from the Miocene dolostones, the Pliocene limestones and dolostones, and the Pleistocene limestones (Fig. 4-15). Although plotting along the same trend line as for the Jamaican terra rossa, the Cayman sinkhole-filling deposits and Jamaica terra rossa only partly overlap (Fig. 4-15). These comparisons further emphasis that the sinkhole-filling deposits evolved in a different manner than the Neogene and Pleistocene marine carbonates.

During periods of subaerial exposure, variations in local climate (e.g., rainfall, temperature, storms) would have had a major impact on the deposits that accumulated in the sinkholes. The formation and accumulation of black limestone lithoclasts, dolostone lithoclasts coated with black, Mn-rich laminae, coated grains, aeolian sediments and rootcretes, for example, probably took place during periods when semi-arid climate prevailed (Wright, 1994; D'Argenio and Mindszenty, 1995; Kosir, 2004; Miller et al., 2012a, 2013; Brlek et al., 2013). In contrast, precipitation of the speleothemic calcite required wet climates (Jones, 1992b; Miller et al., 2012a). Compared to other sinkhole-filling deposits, the red and orange limestone matrices yielded higher $\delta^{18}O$ values (Fig. 4-12), indicating that the meteoric water involved in their development had probably undergone more evaporation (cf., Li and Jones, 2014). Storm waves were also important because they commonly transported marine sediments from the shallow, offshore lagoons on land and into the sinkholes (Jones, 1992b; Ng et al., 1992).

Plant roots played an important role in the development of the deposits found in the sinkholes. As with rhizogenic calcrete horizons (Mutler and Hoffmeister, 1968; Klappa, 1980; Jones, 1988; Jones and Ng, 1988; Wright, 1994; Kosir, 2004; Alonso-Zarza and Jones, 2007), the roots (1) accelerated bedrock weathering, (2) penetrated into the substrate and thereby increased porosity and permeability, (3) created fluids supersaturated with respect to $CaCO_3$, (4) acted as centers of calcification, and (5) provided substrates and nutrients for symbiotic microorganisms, which may have enhanced the precipitation of micritic cement, formation of the terrestrial oncoids, and blackening of the limestone lithoclasts.

Roots also played a role in the development of the black limestone lithoclasts, because decayed root material and/or symbiotic microorganisms provide organic matter that acted as a coloring agent (Strasser, 1984). These roots may also have created local concentrations of calcium bicarbonate ions in the pore fluids (Miller et al., 2013), which facilitated adsorption of organic matter onto the calcite crystal surface by the alteration of unstable minerals (i.e. aragonite and high-Mg calcite) and creating alkaline and anoxic microenvironments (Krumbein and Garrels, 1952; Suess, 1970; Strasser, 1984).

Black limestone lithoclasts, like those found on the Cayman Islands, are known from many different geological settings throughout the world (e.g., Ward et al., 1970; Perkins, 1977; Beach and Ginsburg, 1980; Strasser and Davaud, 1983; Strasser, 1984; Shinn and Lidz, 1988; Lang and Tucci, 1997; Hips et al., 2011; Miller et al., 2013). Features common to all settings include (1) the angular shape of the lithoclasts, (2) the variable black coloration, (3) lithoclasts formed of mudstone (micritic) or skeletal wackestones, and (4) the lack of lithological counterparts in the surrounding bedrock succession. Although all of the black limestone lithoclasts formed under pedogenic and meteoric diagenetic conditions, commonly in association with calcrete and root cast, plants have rarely been regarded as a factor in their formation (Miller et al., 2013).

Based on the black limestone lithoclasts found in middle Miocene, late Pliocene and Pleistocene deposits across southern Australia, Miller et al. (2013) argued that these lithoclasts were calcified root cells that trapped organic matter into their cellular structures during calcification. This model, however, contrasts with the widely accepted notion that black limestone lithoclasts are reworked marine and/or lacustrine carbonate (Strasser and Davaud, 1983; Strasser, 1984; Leinfelder, 1987; Lang and Tucci, 1997; Hips et al., 2011). The black limestone lithoclasts in the Cayman examples, for example, are of marine origin and display no evidence of calcified root cells.

Some of the sinkhole-filling sediments contain trace amounts of chlorite, quartz and feldspar that could have been derived from (1) dissolution of the bedrock, (2) terra rossa, and/or (3) airborne dust. Ahmad and Jones (1969) argued that the terra rossa found on the Cayman Islands formed as the carbonate bedrock was dissolved and the insoluble residues accumulated. The dolostones and limestones of the Cayman Formation and Pedro Castle Formation, however, contain little non-carbonate material and no quartz or feldspar crystals have ever been found in them. Thus, it seems unlikely that the quartz and feldspars crystals, the immobile trace elements, (e.g., Th, Cr, Zr, Y), and that REE that are found in the sinkhole-filling deposits originated as residues generated by bedrock dissolution. Given that Grand Cayman is geographically isolated by deep oceanic water, the most probable source for these minerals and elements is from windblown material. Saharan dust has been regarded as the major contributor to the terra rossa that is found on islands throughout the Caribbean (e.g., Muhs et al., 1990, 2007; Foos, 1991; Borg and Banner, 1996; Herwitz and Muhs, 1995; Muhs, 2001; Muhs and Budahn, 2009). For the sinkhole-filling deposits on Grand Cayman, such an origin is supported by the fact that REE characteristics of the sinkhole-filling deposits are akin to those found in the terra rossa on Jamaica (Muhs and Budahn, 2009).

8. Conclusions

The sinkhole-filling deposits associated with the unconformity that caps the Cayman Formation provide insights into the processes that have been operative since the late Pliocene (~3.6 Ma). New data from these deposits have led to the following important conclusions.

- The geochemical signatures of the sinkhole-filling deposits are significantly different from those of the limestones and dolostones of Neogene and Pleistocene marine carbonates found on Grand Cayman and Cayman Brac.
- The REE signatures of the sinkhole-filling deposits are different from those of the dolostones and limestones that form the Cayman Formation, the Pedro Castle Formation, and the Ironshore Formation. Such differences may offer a means of "fingerprinting" carbonate deposits and determining if they formed in marine or non-marine settings.
- Although lithoclasts derived from the Cayman Formation are common in the sinkholes, no lithoclasts originating from the Pedro Castle Formation or Ironshore Formation have been found.
- The laminated rootcrete formed through accretionary processes that were mediated largely by plant roots.
- Many of the limestone and dolostone lithoclasts found in the sinkhole-filling deposits have no lithological counterparts in the stratigraphic succession found on the Cayman Islands today. Presumably, they came from strata that have since been stripped from the surface of the island by erosion.
- The black limestone lithoclasts are reworked carbonates that probably became blackened by

organic matter during diagenetic alteration.

- The red and orange limestone matrices found in some of the breccias are formed largely of calcite and contain trace amounts of quartz, feldspar and chlorite that probably came from airborne Saharan dust. The different colors in these matrices reflect different amount of quartz, feldspar and chlorite.

References

Ahmad, N., Jones, R.L., 1969. Occurrence of aluminous lateritic soils (bauxites) in the Bahamas and Cayman Islands. Economic Geology 64, 804-808.

Alonso-Zarza, A.M., 1999. Initial stages of laminar calcrete formation by roots: examples from the Neogene of central Spain. Sedimentary Geology 126, 177-191.

Alonso-Zarza, A.M., 2003. Palaeoenvironmental significance of palustrine carbonates and calcretes in the geological record. Earth-Science Reviews 60, 261-298.

Alonso-Zarza, A.M., Arenas, C., 2004. Cenozoic calcretes from the Teruel Graben, Spain: microstructure, stable isotope geochemistry and environmental significance. Sedimentary Geology 167, 91-108.

Alonso-Zarza, A.M., Jones, B., 2007. Root calcrete formation on Quaternary karstic surfaces of Grand Cayman. Geologica Acta 5, 77-88.

Alonso-Zarza, A.M., Wright, V.P., 2010. Calcretes. In: Alonso-Zarza, A.M., Tanner, L.H. (Eds.), Developments in Sedimentology. Elsevier, Oxford, pp. 225-267.

Arakel, A.V., 1982. Genesis of calcrete in Quaternary soil profiles, Hutt and Leeman Lagoons, Western Australia. Journal of Sedimentary Petrology 52, 109-125.

Armenteros, I., Daley, B., 1998. Pedogenic modification and structure evolution in palustrine facies as exemplified by Bembridge Limestone (late Eocene) of the Isle of Wight, southern England. Sedimentary Geology 119, 275-295.

Arts, A.E., 2000. Sedimentology and stratigraphy of the Pedro Castle Formation, southwest Grand Cayman, British West Indies. Unpublished M.Sc. Thesis, University of Alberta, Canada, 107 pp.

Barthel, K.W., 1974. Black pebbles, fossil and recent, on and near coral islands. Proceedings of 2nd International Coral Reef Symposium 2, 395-399.

Beach, D.K., Ginsburg, R.N., 1980. Facies succession of Pliocene-Pleistocene carbonates, northwestern Great Bahama Bank. American Association of Petroleum Geologists Bulletin 64, 1634-1642.

Boero, V., Premoli, A., Melis, P., Barberis, E., Arduino, E., 1992. Influence of climate on the iron oxide mineralogy of terra rossa. Clays and Clay Minerals 40, 8-13.

Borg, L.E., Banner, J.L., 1996. Neodymium and strontium isotopic constraints on soil sources in Barbados, West Indies. Geochimica et Cosmochimica Acta 60, 4193-4206.

Brlek, M., Korbar, T., Košir, A., Glumac, B., Grizelj, A., Otoničar, B., 2013. Discontinuity surfaces in Upper Cretaceous to Paleogene carbonates of central Dalmatia (Croatia): Glossifungites ichnofacies, biogenic calcretes, and stratigraphic implications. Facies 60, 467-487.

Bronger, A., Bruhn-Lobin, N., 1997. Paleopedology of terrae rossae - Rhodoxeralfs from Quaternary calcarenites in NW Morocco. Catena 28, 279-295.

Burns, S., Rossinsky, V., Humphrey, J., 1989. Late Pleistocene mixing zone dolomitization, southeastern Barbados, West Indies: discussion and reply. Sedimentology 36, 1135-1142.

Callot, G., Guyon, A., Mousain, D., 1985a. Inter-relations entre aiguilles de calcite et hyphes mycéliens. Agronomie 5, 209-216.

Callot, G., Mousain, D., Plassard, C., 1985b. Concentrations de carbonate de calcium sur les parois des hyphes mycéliens. Agronomie 5, 143-150.

Calvet, F., Juliá, R., 1983. Pisoids in the caliche profiles of Tarragona (NE Spain). In: Peryt, T.M. (Ed.), Coated Grains. Springer, Berlin, pp. 73-79.

Cerling, T.E., 1984. The stable isotope composition of modern soil carbonate and its relationships to climate. Earth and Planetary Science Letters 71, 229-240.

Clift, P.D., Chan, L.H., Blusztajn, J., Layne, G.D., Kastner, M., Kelly, R.K., 2005. Pulsed subduction accretion and tectonic erosion reconstructed since 2.5 Ma from the tephra record offshore Costa Rica. Geochemistry, Geophysics, Geosystems 6, 21pp.

Clari, P.A., Dela Pierre, F., Martire, L., 1995. Discontinuities in carbonate successions; identification, interpretation and classification of some Italian examples. Sedimentary Geology 100, 97-121.

Coyne, M.K., 2003. Transgressive-regressive cycles in the Ironshore Formation, Grand Cayman, British West Indies. Unpublished M.Sc. Thesis, University of Alberta, Canada, 98 pp.

Cramer, H., 1941. Die systematik der Karstdolinen. Neues Jahrbuch für Mineralogie, Geologie und palaontogie 85, 293-382.

D'Argenio, B., Mindszenty, A., 1995. Bauxites and related paleokarst: tectonic and climatic event markers at regional unconformities. Eclogae Geologicae Helvetiae 88, 453-499.

Daugherty, D.R., Boardman, M.R., Metzler, C.V., 1987. Characteristics and origins of joints and sedimentary dikes of the Bahama Islands. In: Curran, H.A. (Ed.), Proceedings of the Third Symposium on the Geology of the Bahamas. CCFL Bahamian Field Station, Fort Lauderdale, Florida, pp. 45-56.

DeMets, C., Wiggins-Grandison, M., 2007. Deformation of Jamaica and motion of the Gonâve microplate from GPS and seismic data. Geophysical Journal International 168, 362-378.

Der, A.J., 2012. Deposition and sea level fluctuations during Miocene times, Grand Cayman, British West Indies. Unpublished M.Sc. Thesis, University of Alberta, Canada, 101 pp.

Dietz, A., Mathews, J., 1969. Scanning electron microscopy of selected members of the Streptomyces hygroscopicus group. Applied Microbiology 18, 694-696.

Dietz, A., Mathews, J., 1971. Classification of Streptomyces spore surfaces into five groups. Applied Microbiology 21, 527-533.

Doran, E., 1954. Landforms of Grand Cayman Island, British West Indies. Texas Journal of Science VI, 360-377.

Dowsett, H.J., Cronin, T.M., 1990. High eustatic sea level during the middle Pliocene: evidence from the Southeastern U.S. Atlantic Coastal Plain. Geology 18, 435-438.

Durn, G., 2003. Terra rossa in the Mediterranean region: parent materials, composition and origin. Geologia Croatica 56, 83-100.

Durn, G., Hrenovic, J., Sekovanic, L., 2013. Terra rossa as the substrate for biological phosphate removal from wastewater. Clay Minerals 48, 725-738.

Durn, G., Ottner, F., Slovenec, D., 1999. Mineralogical and geochemical indicators of the polygenetic nature of terra rossa in Istria, Croatia. Geoderma 91, 125-150.

Durn G., Slovenec D., Čović M., 2001. Distribution of iron and manganese in terra rossa from Istria and its genetic implications. Geologia Croatica 54, 27-36.

Dwyer, G.S., Chandler, M.A., 2009. Mid-Pliocene sea level and continental ice volume based on coupled benthic Mg/Ca palaeotemperatures and oxygen isotopes. Philosophical Transactions of the Royal Society A-Mathematical Physical and Engineering Sciences 367, 157-168.

Esteban, M., Klappa, C.F., 1983. Subaerial exposure environments. In: Scholle, P.A., Bebout, D.G., Moore, C.H. (Eds.), Carbonate Depositional Environments. American Association of Petroleum Geologists Memoir 33, pp. 1-96.

Folk, R.L., 1974. The natural history of crystalline calcium carbonate: effect of magnesium content and salinity. Journal of Sedimentary Petrology 44, 40-53.

Folk, R.L., Roberts, H.H., Moore, C.H., 1973. Black phytokarst from Hell, Cayman Islands, British West Indies. Geological Society of America Bulletin 84, 2351-2360.

Foos, A.M., 1991. Aluminous lateritic soils, Eleuthera, Bahamas: A modern analog to carbonate paleosols. Journal of Sedimentary Petrology 61, 340-348.

Ford, D., 1988. Characteristics of dissolution cave systems in carbonate rocks. In: James, N.P., Choquette, P.W. (Eds.), Paleokarst. Springer-Verlag, New York, pp. 25-57.

Ford, D., Williams, P.W., 2007. Karst Hydrogeology and Geomorphology. Wiley, 562 pp.

Garcia-Gonzalez, M.T., Recio, P., 1988. Geochemistry and mineralogy of the clay fraction from some Spanish terra rossa. Agrochimica 32, 161-170.

Goudie, A.S., 1973. Duricrusts in Tropical and Subtropical Landscapes. Claredon, Oxford, 174 pp.

Goudie, A.S., 1983. Calcrete. In: Goudie, A.S., Pye, K. (Eds.), Chemical Sediments and Geomorphology: Precipitates and Residua in the Near-surface Environment. Academic Press, New York, pp. 93-131.

Harrison, R.S., 1977. Caliches profiles: indicator of near-surface subaerial diagenesis, Barbados West Indies. Bulletin of Canadian Petroleum Geology 25, 123-173.

Herwitz, S.R., Muhs, D.R., 1995. Bermuda solution pipe soils: a geochemical evaluation of eolian parent materials. In: Curran, H.A., White, B. (Eds.), Terrestrial and Shallow Marine Geology of the Bahamas and Bermuda. Geological Society of America Special Paper 300, 311-323.

Hillgärtner, H., 1998. Discontinuity surfaces on a shallow-marine carbonate platform (Berriasian, Valanginian, France and Switzerland). Journal of Sedimentary Research 68, 1093-1108.

Hips, K., Haas, J., Vidó, M., Barna, Z., Jovanović, D., Sudar, M.N., Siklósy, Z., 2011. Selective blackening of bioclasts via mixing-zone aragonite neomorphism in Late Triassic limestone, Zlatibor Mountains, Serbia. Sedimentology 58, 854-877.

James, N.P., 1972. Holocene and Pleistocene calcareous crust (caliche) profiles: criteria for subaerial exposure. Journal of Sedimentary Petrology 42, 817-836.

James, N.P., Choquette, P.W., 1990. Limestones-the meteoric diagenetic environment. In: McIlreath, I.A., Morrow, D.W. (Eds.), Diagenesis. Geological Association of Canada, Ottawa, pp. 35-74.

Jones, B., 1987. The alteration of sparry calcite crystals in a vadose setting, Grand Cayman Island. Canadian Journal of Earth Sciences 24, 2292-2304.

Jones, B., 1988. The influence of plants and micro-organisms on diagenesis in caliche: example from the Pleistocene Ironshore Formation on Cayman Brac, British West Indies. Bulletin of Canadian Petroleum Geology 36, 191-201.

Jones, B., 1991. Genesis of terrestrial oncoids, Cayman Islands, British West Indies. Canadian Journal of Earth Sciences 28, 382-397.

Jones, B., 1992a. Manganese precipitates in the karst terrain of Grand Cayman, British West Indies. Canadian Journal of Earth Sciences 29, 1125-1139.

Jones, B., 1992b. Void-filling deposits in karst terrains of isolated oceanic islands: a case study from Tertiary carbonates of the Cayman Islands. Sedimentology 39, 857-876.

Jones, B., 1992c. Construction of spar calcite crystals around spores. Journal of Sedimentary Petrology 62, 1054-1057.

Jones, B., 1994. Geology of the Cayman Islands. In: Brunt, M.A., Davies, J.E. (Eds.), The

Cayman Islands: Natural History and Biogeography. Kluwer, Dordrecht, The Netherlands, pp. 13-49.

Jones, B., 2009. Cave pearls - the integrated product of abiogenic and biogenic processes. Journal of Sedimentary Research 79, 689-710.

Jones, B., 2010a. Speleothems in a wave-cut notch, Cayman Brac, British West Indies: The integrated product of subaerial precipitation, dissolution, and microbes. Sedimentary Geology 232, 15-34.

Jones, B., 2010b. Microbes in caves: agents of calcite corrosion and precipitation. In: Pedley, H.M., Rogerson, M. (Eds.), Tufas and Speleothems: Unravelling the Microbial and Physical Controls. Geological Society of London Special Publication 336, pp. 7-30.

Jones, B., 2011. Biogenicity of terrestrial oncoids formed in soil pockets, Cayman Brac, British West Indies. Sedimentary Geology 236, 95-108.

Jones, B., Hunter, I.G., 1994. Evolution of an isolated carbonate bank during Oligocene, Miocene and Pliocene times, Cayman Brac, British West Indies. Facies 30, 25-50.

Jones, B., Kahle, C.F., 1985. Lichen and algae: agents of biodiagenesis in karst breccia from Grand Cayman Island. Bulletin of Canadian Petroleum Geology 33, 446-461.

Jones, B., Peng, X., 2014. Abiogenic growth of needle-fiber calcite in spring towers at Shiqiang, Yunnan Province, China. Journal of Sedimentary Research 84, 1021-1040.

Jones, B., Hunter, I.G., Kyser, T.K., 1994a. Revised stratigraphic nomenclature for Tertiary strata of the Cayman Islands, British West Indies. Caribbean Journal of Science 30, 53-68.

Jones, B., Hunter, I.G., Kyser, T.K., 1994b. Stratigraphy of the Bluff Formation (Miocene-Pliocene) and the newly defined Brac Formation (Oligocene), Cayman Brac, British West Indies. Caribbean Journal of Science 30, 30-51.

Jones, B., Luth, R.W., 2002. Dolostones from Grand Cayman, British West Indies. Journal of Sedimentary Research 72, 559-569.

Jones, B., Luth, R.W., 2003. Temporal evolution of Tertiary dolostones on Grand Cayman as determined by $^{87}Sr/^{86}Sr$. Journal of Sedimentary Research 73, 187-205.

Jones, B., Ng, K., 1988. The structure and diagenesis of rhizoliths from Cayman Brac, British West Indies. Journal of Sedimentary Petrology 58, 457-467.

Jones, B., Smith, D.S., 1988. Open and filled karst features on the Cayman Islands: implications for the recognition of paleokarst. Canadian Journal of Earth Sciences 25, 1277-1291.

Jones, B., Squair, C.A., 1989. Formation of peloids in plant rootlets, Grand Cayman, British West Indies. Journal of Sedimentary Petrology 59, 457-467.

Klappa, C.F., 1978. Biolithogenesis of Microcodium: elucidation. Sedimentology 25, 489-522.

Klappa, C.F., 1979. Calcified filaments in Quaternary calcretes: organo-mineral interactions in the subaerial vadose environment. Journal of Sedimentary Petrology 49, 955-968.

Klappa, C.F., 1980. Rhizoliths in terrestrial carbonates: classification, recognition, genesis and significance. Sedimentology 27, 613-629.

Kosir, A., 2004. Microcodium revisited: root calcification products of terrestrial plants on carbonate-rich substrates. Journal of Sedimentary Research 74, 845-857.

Krumbein, W.C., Garrels, R.M., 1952. Origin and classification of chemical sediments in terms of pH and oxidation-reduction potentials. Journal of Geology 60, 1-33.

Kubiëna, W.L., 1953. The soils of Europe. Thomas Murray and Company, London, 104 pp.

Lang, R.A., Tucci, P., 1997. A preliminary study of the causes of the blackening of pebbles in the Cenomanian "breccia with black pebbles" of Camporosello (Lepini Mountains, Italy). Geologica Romana 33, 89-97.

Leinfelder, R.R., 1987. Formation and significance of black pebbles from the Ota Limestone (Upper Jurassic, Portugal). Facies 17, 159-170.

Li, R., Jones, B., 2013. Heterogeneous diagenetic patterns in the Pleistocene Ironshore Formation of Grand Cayman, British West Indies. Sedimentary Geology 294, 251-265.

Li, R., Jones, B., 2014. Calcareous crusts on exposed Pleistocene limestones: a case study from Grand Cayman, British West Indies. Sedimentary Geology 299, 88-105.

Liang, T., Jones, B., 2014. Deciphering the impact of sea-level changes and tectonic movement on erosional sequence boundaries in carbonate successions: a case study from Tertiary strata on Grand Cayman and Cayman Brac, British West Indies. Sedimentary Geology 305, 17-34.

Lohmann, K.C., 1988. Geochemical patterns of meteoric diagenesis system and their application to studies of paleokarst. In: James, N.P., Choquette, P.W. (Eds.), Paleokarst. Springer-Verlag, New York, pp. 58-80.

MacDonald, K.C., Holcombe, T.L., 1978. Inversion of magnetic anomalies and sea-floor spreading in the Cayman Trough. Earth and Planetary Science Letters 40, 407-414.

Macleod, D.A., 1980. The origin of the red Mediterranean soils in Epirus, Greece. Journal of Soil Science 31, 125-136.

MacNeil, A., 2001. Sedimentology, diagenesis, and dolomitization of the Pedro Castle Formation on the Cayman Brac, British West Indies. Unpublished M.Sc. Thesis, University of Alberta, Canada, 128 pp.

MacNeil, A., Jones, B., 2003. Dolomitization of the Pedro Castle Formation (Pliocene), Cayman Brac, British West Indies. Sedimentary Geology 162, 219-238.

Maiklem, W.R., 1967. Black and brown speckled foraminiferal sand from the southern part of the Great Barrier Reef. Journal of Sedimentary Petrology 37, 1023-1030.

Matley, C.A., 1926. The geology of the Cayman Islands (British West Indies) and their relation to the Bartlett Trough. Quarterly Journal of the Geological Society of London 82, 352-387.

McCrea, J.M., 1950. On the isotopic chemistry of carbonates and a paleotemperature scale. The Journal of Chemical Physics 18, 849-857.

McKenzie, J.A., 1985. Carbon isotopes and productivity in the lacustrine and marine environment. In: Stumm, W. (Ed.), Geochemical Processes in Lakes. Wiley, New York, pp. 99-118.

McLennan, S., 1989. Rare earth elements in sedimentary rocks: influence of provenance and sedimentary processes. Reviews in Mineralogy and Geochemistry 21, 169-200.

Meyers, W.J., Lohmann, K.C., 1985. Isotope geochemistry of regionally extensive calcite cement zones and marine components in Mississippian limestones, New Mexico. In: Schneidermann, N., Harris, P.M. (Eds.), Carbonate Cements. Society of Economic Paleontologists and Mineralogists Special Publication 36, pp. 223-239.

Miller, C.R., James, N.P., 2012. Autogenic microbial genesis of middle Miocene palustrine ooids;

Nullarbor Plain, Australia. Journal of Sedimentary Research 82, 633-647.

Miller, C.R., James, N.P., Bone, Y., 2012a. Prolonged carbonate diagenesis under an evolving late Cenozoic climate: Nullarbor Plain, southern Australia. Sedimentary Geology 261-262, 33-49.

Miller, C.R., James, N.P., Kyser, T.K., 2013. Genesis of blackened limestone clasts at late Cenozoic subaerial exposure surfaces, southern Australia. Journal of Sedimentary Research 83, 339-353.

Miller, K.G., Kominz, M.A., Browning, J.V., Wright, J.D., Mountain, G.S., Katz, M.E., Sugarman, P.J., Cramer, B.S., Christie-Blick, N., Pekar, S.F., 2005. The Phanerozoic record of global sea-level change. Science 310, 1293-1298.

Miller, K.G., Mountain, G.S., Wright, J.D., Browning, J.V., 2011. A 180-million-year record of sea level and ice volume variations from continental margin and deep-sea isotopic records. Oceanography 24, 40-53.

Miller, K.G., Wright, J.D., Browning, J.V., Kulpecz, A., Kominz, M., Naish, T.R., Cramer, B.S., Rosenthal, Y., Peltier, W.R., Sosdian, S., 2012b. High tide of the warm Pliocene: implications of global sea level for Antarctic deglaciation. Geology 40, 407-410.

Miyadoh, S., Tsuchizaki, N., Ishikawa, J., Hotta, K., 1997. Digital Atlas of Actinomycetes. Society for Actinomycetes Japan, Akasura Publishing, Tokyo, Japan, 244 pp.

Moresi, M., Mongelli, G., 1988. The relation between the terra rossa and the carbonate-free residue of the underlying limestones and dolostones in Apulia, Italy. Clay Minerals 23, 439-446.

Muhs, D.R., 2001. Evolution of soils on Quaternary reef terraces of Barbados, West Indies. Quaternary Research 56, 66-78.

Muhs, D.R., Budahn, J.R., 2009. Geochemical evidence for African dust and volcanic ash inputs to terra rossa soils on carbonate reef terraces, northern Jamaica, West Indies. Quaternary International 196, 13-35.

Muhs, D.R., Budahn, J., Avila, A., Skipp, G., Freeman, J., Patterson, D., 2010. The role of

African dust in the formation of Quaternary soils on Mallorca, Spain and implications for the genesis of Red Mediterranean soils. Quaternary Science Reviews 29, 2518-2543.

Muhs, D.R., Budahn, J., Prospero, J.M., Carey, S.N., 2007. Geochemical evidence for African dust inputs to soils of western Atlantic islands: Barbados, the Bahamas and Florida. Journal of Geophysical Research 112, 1-26.

Muhs, D.R., Bush, C.A., Stewart, K.C., Rowland, T.R., 1990. Geochemical evidence of Saharan dust parent material for soils developed on Quaternary limestones of Caribbean and western Atlantic islands. Quaternary Research 33, 157-177.

Mutler, H.G., Hoffmeister, J.E., 1968. Subaerial laminated crusts of the Florida Keys. Geological Society of America Bulletin 79, 183-192.

Nakai, S, Halliday, A.N., Rea, D.K., 1993. Provenance of dust in the Pacific Ocean. Earth and Planetary Science Letters 119, 143-157.

Ng, K., Jones, B., Beswick, R., 1992. Hydrogeology of Grand Cayman, British West Indies: a karstic dolostone aquifer. Journal of Hydrology 134, 273-295.

Nothdurft, L.D., Webb, G.E., Kamber, B.S., 2004. Rare earth element geochemistry of Late Devonian reefal carbonates, Canning Basin, Western Australia: confirmation of a seawater REE proxy in ancient limestones. Geochimica et Cosmochimica Acta 68, 263-283.

Perfit, M.R., Heezen, B.C., 1978. The geology and evolution of the Cayman Trench. Geological Society of America Bulletin 89, 1155-1174.

Perkins, R.D., 1977. Depositional framework of Pleistocene rocks in south Florida. In: Enos, P., Perkins, R.D. (Eds.), Quaternary sedimentation in south Florida. Geological Society of America Memoir 147, Geological Society of America, Colorado, United States, pp. 131-198.

Phillips, S.E., Self, P.G., 1987. Morphology, crystallography and origin of needle-fibre calcite in Quaternary pedogenic calcretes of South Australia. Australian Journal of Soil Research 25, 429-444.

Pleydell, S.M., Jones, B., Longstaffe, F.J., Baadsgaard, H., 1990. Dolomitization of the Oligocene-Miocene Bluff Formation on Grand Cayman, British West Indies. Canadian Journal of Earth Sciences 27, 1098-1110.

Porter, S.C., 2000. High-resolution paleoclimatic information from Chinese eolian sediments based on grayscale intensity profiles. Quaternary Research 53, 70-77.

Reid, R.P., MacIntyre, I.G., 1998. Carbonate recrystallization in shallow marine environments: a widespread diagenetic process forming micritized grains. Journal of Sedimentary Research 68, 928-946.

Reimann, C., de Caritat, P., 1998. Chemical Elements in the Environment: Factsheets for the Geochemist and Environmental Scientist. Springer-Verlag, Berlin, 398 pp.

Riche, G., Rambaud, D., Riera, M., 1982. Etude morphologique d'un encroûtement calcaire, Région d'Irecê, Bahia, Brésil. Cahiers Orstom Série Pédologie 19, 257-270.

Rossinsky, V., Swart, P.K., 1993. Influence of climate on the formation and isotopic composition of calcretes. Geophysical Monograph 78, 67-75.

Salomons, W., Goudie, A., Mook, W.G., 1978. Isotopic composition of calcrete deposits from Europe, Africa and India. Earth Surface Processes 3, 43-57.

Salomons, W., Mook, W.G., 1986. Isotope geochemistry of carbonates in the weathering zone. In: Fritz, P., Fontes, J.Ch. (Eds.), Handbook of Environmental Isotope Geochemistry Volume 2. Elsevier, Amsterdam, pp. 239-269.

Sattler, U., Immenhauser, A., Hillgärtner, H., Esteban, M., 2005. Characterization, lateral variability and lateral extent of discontinuity surfaces on a carbonate platform (Barremian to lower Aptian, Oman). Sedimentology 52, 339-361.

Shinn, E.A., Lidz, B.H., 1988. Blackened limestone pebbles: fire at subaerial unconformities. In: James, N.P., Choquette, P.W. (Eds.), Paleokarst. Springer-Verlag, New York, pp 117-131.

Smart, P.L., Palmer, R.J., Whitaker, F., Wright, V.P., 1988. Neptunian dikes and fissure fills: an overview and account of some modern examples. In: James, N.P., Choquette, P.W. (Eds.), Paleokarst. Springer-Verlag, New York, pp. 149-163.

Smith, D.S., 1987. The genesis of speleothemic calcite deposits on Grand Cayman, British West Indies. Unpublished M.Sc. thesis, University of Alberta, Canada, 171 pp.

Sosdian, S., Rosenthal, Y., 2009. Deep-sea temperature and ice volume changes across the Pliocene–Pleistocene climate transitions. Science 325, 306-310.

Stace, H.C.T., 1956. Chemical characteristics of terra rossas and rendzinas of south Australia. Journal of Soil Science 7, 280-293.

Stephens, C.G., 1953. A Manual of Australian Soils. Commonwealth Scientific and Industrial Research Organization, Melbourne, 48 pp.

Strasser, A., 1984. Black-pebble occurrence and genesis in Holocene carbonate sediments (Florida Keys, Bahamas, and Tunisia). Journal of Sedimentary Petrology 54, 1097-1109.

Strasser, A., Davaud, E., 1983. Black pebbles of the Purbeckian (Swiss and French Jura): lithology, geochemistry and origin. Eclogae Geologicae Helvetiae 76, 551-580.

Suess, E., 1970. Interaction of organic compounds with calcium carbonate. Geochimica et Cosmochimica Acta 34, 157-168.

Sugden, W., 1966. Pyrite staining of pellety debris in carbonate sediments from the Middle East and elsewhere. Geological Magazine 103, 250-255.

Sun, Y., He, L., Liang, L., An, Z., 2011. Changing color of Chinese loess: Geochemical constraint and paleoclimatic significance. Journal of Asian Earth Sciences 40, 1131-1138.

Talma, A.S., Netterberg, F., 1983. Stable isotope abundances in calcretes. In: Wilson, R.C.L. (Ed.), Residual Deposits: Surface Related Weathering Processes and Materials. Geology Society of London Special Publication 11, Blackwell Scientific Publications, Oxford, pp. 221-233.

Torrent, J., 1995. Genesis and Properties of the Soils of the Mediterranean Regions. Dipartimento di Scienze Chimico-Agrarie, Universitá degli Studi di Napoli Federico II, 111 pp.

Tresner, H.D., Davies, M.C., Backus, E.J., 1961. Electron microscopy of Streptomycetes spore morphology and its role in species differentiation. Journal of Bacteriology 81, 70-80.

Tucker, M., 1990. Diagenetic processes, products and environments. In: Tucker, M.E., Wright, V.P., Dickson, J.A.D. (Eds.), Carbonate Sedimentology. Blackwell Scientific Publications, Oxford, pp. 314-364.

Vera, J.A., de Cisneros, J., 1993. Palaeogeographic significance of black pebbles (Lower

Cretaceous, Prebetic, southern Spain). Palaeogeography, Palaeoclimatology, Palaeoecology 102, 89-102.

Vézina J.V., 1997. Stratigraphy and sedimentology of the Pleistocene Ironshore Formation at Rogers Wreck Point, Grand Cayman: a 400 Ka Record of Sea-level Highstands. Unpublished M.Sc. Thesis, University of Alberta, Canada, 131 pp.

Vézina, J.V., Jones, B., Ford, D.C., 1999. Sea-level highstands over the last 500,000 years: evidence from the Ironshore Formation on Grand Cayman, British West Indies. Journal of Sedimentary Research 69, 317-327.

Ward, W.C., Folk, R.L., Wilson, J.L., 1970. Blackening of eolianite and caliche adjacent to saline lakes, Isla Mujeres, Quintana Roo, Mexico. Journal of Sedimentary Petrology 40, 548-555.

Wignall, B.D., 1995. Sedimentology and diagenesis of the Cayman (Miocene) and Pedro Castle (Pliocene) Formations at Safe Haven, Grand Cayman, British West Indies. Unpublished M.Sc. Thesis, University of Alberta, Canada, 110 pp.

Wright, V.P., 1986. The role of fungal biomineralization in the formation of early Carboniferous soil fabrics. Sedimentology 33, 831-838.

Wright, V.P., 1989. Terrestrial stromatolites and laminar calcretes: a review. Sedimentary Geology 65, 1-13.

Wright, V.P., 1994. Paleosols in shallow marine carbonate sequences. Earth-Science Reviews 35, 367-395.

Wright, V.P., Platt, N.H., Marriot, S.B., Beck, V.H., 1995. A classification of rhizogenic (root-formed) calcretes, with examples from the Upper Jurassic-Lower Carboniferous of Spain and Upper Cretaceous of southern France. Sedimentary Geology 100, 143-158.

Wright, V.P., Platt, N.H., Marriot, S.B., Beck, V.H., 1997. A classification of rhizogenic (root-formed) calcretes, with examples from the Upper Jurassic-Lower Cretaceous of Spain and Upper Cretaceous of southern France-reply. Sedimentary Geology 110, 305-307.

Wright, V.P., Platt, N.H., Wimbledon, W., 1988. Biogenic laminar calcretes: evidence of calcified root mat horizons in paleosols. Sedimentology 35, 603-620.

Zhao, H.W., Jones, B., 2012. Origin of "Island Dolostones": a case study from the Cayman Formation (Miocene), Cayman Brac, British West Indies. Sedimentary Geology 243-244, 191-206.

Zhao, H.W., Jones, B., 2013. Distribution and interpretation of rare earth elements and yttrium in Cenozoic dolostones and limestones on Cayman Brac, British West Indies. Sedimentary Geology 284-285, 26-38.

CHAPTER 5: CONCLUSIONS

In the terminal phase of the Miocene, the significant lowering of sea level by as much as 180 m (Berggren and Haq, 1976; Adams et al., 1977; Vail et al., 1977; Cita and Ryan, 1978; Loutit and Keigwin, 1982; Hodell and Kennett, 1986; Pigram et al., 1992; Aharon et al., 1993; Zhang and Scott, 1996), exposed many areas to subaerial weathering thereby forming surfaces that would become unconformities once buried under younger sediments. Indeed, such unconformities have been documented in the Mediterranean region (e.g., Ryan and Cita, 1978; Roveri et al., 2001; Dela Pierre et al., 2002), which is associated with the formation of evaporates (Hsü, 1973, 1987, 1988; Hsü et al., 1973, 1977; Ryan et al., 1973). Similarly, the Messinian sea-level lowstand has been also recorded in the succession found on many Pacific atolls (e.g., Lincoln and Schlanger, 1987). In the Caribbean, however, the Messinian lowstand has rarely been identified (Jones and Hunter, 1994). In Jamaica, Cuba, Great Bahama Bank and Florida, for example, although the unconformable contact produced by the drop of the Messinain sea level has been identified by biostratigraphy (Robinson, 1969; Berggren, 1993), seismic stratigraphy (Anselmetti et al., 2000), stable isotopes, and paleomagnetic anomalies (Miller et al., 1994), its topography has rarely been described and/or linked to the drop in the Messinian sea level. This is because (1) the topography of the Messinian unconformity throughout most of the Caribbean region has been disguised by the complex tectonic history (e.g., Wright, 1974; Berggren, 1993; Katz and Miller, 1993; Kindler et al., 2011), and (2) Messinian karstic surfaces were largely destroyed by the formation of fluvial systems and/or deposition and erosion of siliciclastic sediments during the post-Miocene period (e.g., Denizman and Randazzo, 2000).

To address that knowledge gap, this study focused on the Messinian unconformity, and other erosional unconformities in Cenozoic carbonate secessions found on Grand Cayman and Cayman Brac. In particular, the comparison between the successions on Grand Cayman and Cayman Brac provides important insights into the roles played by tectonic uplift as opposed to eustatic sea-level changes on the development of an erosional unconformity. Collectively, this study shows how karst surfaces developed in response to ever-changing sea levels, tectonic movements, biogenetic factors, and climatic conditions. Key conclusions in this respect are as follows.

1) Grand Cayman has been tectonically stable since the Late Oligocene. Cayman Brac, in contrast, underwent uplift of 133-173 m on the east end between the Late Pliocene (~3.6 Ma) and ~400 ka. The uplift rate on the east end of Cayman Brac was 0.04 to 0.05 mm/year.

2) Unconformities on Grand Cayman are characterized by rugged topographies, with the relief consistent with the magnitude of sea-level fall. The relief on the upper surface of the Cayman Formation indicates that the minimum estimate for the Messinian sea-level fall in Caribbean is at least 61 m.

3) Uplift of Cayman Brac tilted Tertiary strata to the west, but also enhanced the erosional processes. The Pedro Castle Formation and the upper part of the Cayman Formation, thus, were removed from most of Cayman Brac. The removal of the carbonate strata is directly related to the amount of uplift.

4) The upper surfaces of the Cayman Formation on Grand Cayman and Cayman Brac parallel Purdy's (1974) experimental results, which suggested that peripheral rims will develop if the rate of rainfall is no more than the rate of runoff. The peripheral rims present on Grand Cayman and Cayman Brac were initiated during the Messinian lowstand. Compared to those on Grand Cayman, the peripheral rims on Cayman Brac are more pronounced due to uplift.

5) Besides karst processes and uplift, coastal erosion also influenced the topography of the unconformities. Coastal erosion on Grand Cayman and Cayman Brac, which took place after the Late Pliocene (~3.6 Ma) but before ~400 ka, cut into the Cayman Formation and/or the Brac Formation and consequently modified the ancestral topography in the coastal areas.

6) The Cayman Formation is now exposed on the eastern half of Grand Cayman and much of the uplifted core on Cayman Brac. The karst landforms on these exposures, which are characterized by peripheral rims, phytokarst, sinkholes, and solution-widened joints, reflect the interplay between eustatic sea-level changes, climate, tectonic movements and phytokarst over the last 3.6 Ma.

7) Due to uplift, the peripheral rims and karst features are enhanced on the upslope margin of the uplifted core of Cayman Brac, whereas the local karst reliefs in the interior are minimized.

8) Neither Grand Cayman nor Cayman Brac exhibit typical tropical karst landforms such as cockpit, tower karst or cone karst. Sinkholes, however, are common. The fact that such landforms did not develop on these two islands suggests that uplift is not a key fact in the development of tower, cone and/or cockpit karst. Instead, the lack of those positive karst features on Grand Cayman and Cayman Brac is attributed to the poorly developed joints and faults.

9) The photolineaments on DEMs are probably the surficial expression of joints and/or faults, which were produced by the tectonic stresses along the margins of the tectonic blocks.

This study also demonstrated that a wide variety of deposits are found in the sinkholes that have developed in the Cayman Formation. These sinkhole-filling deposits provide insights into the processes that have been operative since the Late Pliocene (~3.6 Ma) and are ongoing today. A detailed study on these deposits, involving their petrographic and geochemical signatures, led to the following conclusions.

1) The geochemical signatures (i.e., isotopes and REE) of the sinkhole-filling deposits are significantly different from those of the limestones and dolostones of Tertiary and Pleistocene marine carbonates found on Grand Cayman and Cayman Brac.

2) Many of sinkhole-filling deposits cannot be correlated with any of the bedrock that is now found on Grand Cayman and Cayman Brac. Many of the limestone and dolostone lithoclasts found in the sinkhole-filling deposits, for example, have no counterparts in the stratigraphic succession found on Grand Cayman. Presumably, they came from strata that have since been stripped from the surface of the island by erosion.

3) Black limestone lithoclasts, found in many of the sinkholes, are of marine origin. They were blackened by organic matter probably after they became lithoclasts.

4) The laminar rootcrete, dominated by biogenic components, formed through accretionary processes that were mediated largely by plant roots.

5) The red and orange limestone matrices found in some of the breccias are formed largely

of calcite and contain trace amounts of quartz, feldspar and chlorite that probably came from Saharan dust. The different colors in these matrices reflect different amount of quartz, feldspar, and chlorite.

In summary, these findings obtained from this study are important, because (1) they provide a context in which the Messinian unconformities of other Caribbean islands could be viewed, (2) they have direct application to other unconformities globally that formed during the Messinian, and (3) they help to understand the development of an ancient erosional unconformities and paleokarst. Additionally, the newly proposed REE data obtained from the various sinkhole-filling deposits, herein, could serves as “fingerprint” of carbonate deposits. Such research has direct application to other cavity-filling deposits, and could increase the understanding of the depositional, erosional and diagenetic processes that occurred during an ancient erosional unconformity was developing.

References

Adams, C.G., Benson, R.H., Kidd, R.B., Ryan, W.B.P., Wright, R.C., 1977. The Messinian salinity crisis and evidence of Late Miocene eustatic changes in the world ocean. Nature 269, 383-386.

Aharon, P., Goldstein, L.S.,Wheeler, C.W., Jacobson, G., 1993. Sea-level events in the South Pacific linked with Messinian salinity crisis. Geology 21, 771-775.

Anselmetti, F.S., Eberli, G.P., Ding, Z.D., 2000. From the Great Bahama Bank into the Straits of Florida: A margin architecture controlled by sea-level fluctuations and ocean currents. Geological Society of America Bulletin 112, 829-844.

Berggren, W.A., 1993. Neogene planktonic foraminiferal biostratigraphy of eastern Jamaica. Geological Society of America Memoirs 182, 179-217.

Berggren, W.A., Haq, B.U., 1976. The Andulusian stage (Late Miocene): biostratigraphy, biochronology and paleoecology. Palaeogeography, Palaeodimatology Palaeoecology 20, 67-129.

Cita, M.B., Ryan, W.B.F., 1978. The Bou Regreg section of the Atlantic coast of Morocco: Evidence, timing and significance of a Late Miocene regressive phase. Rivista Italiana di Paleontologia e Stratigraphia 84, 1051-1082.

Dela Pierre, F., Clari, P., Cavagna, S., Bicchi, E., 2002. The Parona chaotic complex: a puzzling record of the Messinian (late Miocene) events in Monferrato (NW Italy). Sedimentary Geology 152, 289-311.

Denizman, C., Randazzo, A.F., 2000. Post-Miocene subtropical karst evolution, lower Suwannee River basin, Florida. Geological Society of America Bulletin 112, 1804-1813.

Katz, M.E., Miller, K.G., 1993. Miocene-Pliocene bathyal benthic foraminifera and the uplift of Buff Bay, Jamaica. In: Wright, R.M., Robinson, E. (Eds.), Biostratigraphy of Jamaica. Geological Society of America Memoir 182, Boulder, Colorado, pp. 219-254.

Kindler, P., Godefroid, F., Chiaradia, M., Ehlert, C., Eisenhauer, A., Frank, M., Hasler, C., Samankassou, E., 2011. Discovery of Miocene to early Pleistocene deposits on Mayaguana, Bahamas: evidence for recent active tectonism on the North American margin. Geology [Boulder] 39, 523-526.

Hodell, D.A., Kennett, J.P., 1986. Late Miocene-early Pliocene stratigraphy and paleoceanography of the South Atlantic and Southwest Pacific Ocean: a synthesis Paleoceanography 1, 285-311.

Hsü, K.J., 1973. The desiccated deep-basin model for the Messinian events. In: Drooger C.W. (Ed.), Messinian Events in the Mediterranean. North-Holland Publishing, New York, pp. 60-67.

Hsü, K.J., 1987. The desiccation of the Mediterranean Sea. Endearour 11, 67-72.

Hsü, K.J., 1988. Mediterranean model: Posterity will judge. Geotimes 5, 9.

Hsü, K.J., Montadert, L., Bernoulli, D., Cita, M.B., Erickson, A., Garrison, R.E., Kidd, R.B., Milleres, F., Müllller, C., Wright, R., 1977. History of the Mediterranean salinity crisis, Nature 267, 399-403.

Hsü, K.J., Ryan, W.B.F., Cita, M.B., 1973. Late Miocene desiccation of the Mediterranean. Nature 242, 240-244.

Jones, B., Hunter, I.G., 1994. Messinian (Late Miocene) karst on Grand Cayman, British Indies: an example of an erosional sequence boundary. Journal of Sedimentary Research 64, 531-541.

Lincoln, J.M, Schlanger, S.O., 1987. Miocene sea-level falls related to the geologic history of Midway Atoll. Geology 15, 454-457.

Loutit, T.S., Keigwin, L.D., 1982. Stable isotope evidence for latest Miocene sea-level fall in the Mediterranean region. Nature 300, 163-166.

Miller, K.G., Wright, J.D., Van Fossen, M.C., Kent, D.V., 1994. Miocene stable isotopic stratigraphy and magnetostratigraphy of Buff Bay, Jamaica. Geological Society of America Bulletin 106, 1605-1620.

Pigram, C.J., Davies, P.J., Feary, D.A., Symonds, P.A., 1992. Absolute magnitude of the second-order middle to late Miocene sea level fall, Marion Platform, Northeast Australia. Geology 20, 858-862.

Purdy, E.G., 1974. Reef configurations: cause and effect. In: Laporte, L.F. (Ed.), Reefs in Time and Space. Society of Economic Paleontologists and Mineralogists Special Publication 18, pp. 9-76.

Robinson, E., 1969. Geological field guide to Neogene sections in Jamaica, West Indies. Journal of the Geological Society of Jamaica 10, 1-24.

Roveri, M., Bassetti, M.A., Ricci Lucchi, F., 2001. The Mediterranean Messinian salinity crisis: an Apennine foredeep perspective. Sedimentary Geology 140, 201-214.

Ryan, W.B.F., Cita, M.B., 1978. The nature and distribution of Messinian erosional surfaces-Indicators of a several-kilometer-deep Mediterranean in the Miocene. Marine Geology 27, 193-230.

Ryan, W.B.F., Hsü, K.J., Cita, M.B., Dumitrica, P., Lort, J.M., Maync, W., Nesteroff, W.D., Pautot, G., Stradner, H., Wezel, F.C., Kaneps, A.G., 1973. Initial reports of the Deep Sea Drilling Project, covering Leg 13 of the cruises of the drilling vessel Glomar Challenger Lisbon, Portugal to Lisbon, Portugal, August-October 1970. Initial Reports of the Deep Sea Drilling Project 13, Part 1 and 2, U.S. Government Print Office, Washington, D.C., 516 pp.

Vail, P.R., Mitchum, R.M., Thompson, S., 1977. Seismic stratigraphy-applications to hydrocarbon exploration. American Association of Petroleum Geologists Memoir 26, 99-116.

Wright, R.M., 1974. Field guide to selected Jamaican geological localities. Mines and Geology Division Special Publication 1, Kingston, Jamaica, 57 pp.

Zhang, J., Scott, D.B., 1996. Messinian deep-water turbidites and glacioeustatic sea-level changes in the North Atlantic: linkage to the Mediterranean salinity crisis. Paleoceanography 11, 277-297.

Appendix 1. Summary of geochemical data obtained from sinkhole-filling deposits in the exposed Cayman Formation on Grand Cayman and Cayman Brac[a]

Locality	Sample No.	Lithology [b]	Type	Calcite		Dolomite		Al (ppm)	Fe (ppm)	Mn (ppm)
				$\delta^{13}C$ (‰ PDB)	$\delta^{18}O$ (‰ PDB)	$\delta^{13}C$ (‰ PDB)	$\delta^{18}O$ (‰ PDB)			
EEP	#1-1	Limestone	White, skeletal limestone lithoclast	-4.37	-4.76			16.1	85.5	13.1
EEP	#1-2	Limestone	Black limestone lithoclast	-9.81	-4.81			1708.4	955.4	50.5
EEP	#1-3	Limestone	Orange limestone matrix	-10.43	-5.11			2586.6	985.9	61.6
EEP	#1-4	Limestone	Speleothemic calcite	-11.31	-5.76			600.4	531.2	142.8
EEP	#1-5	Limestone	Rootcrete	-10.22	-3.35			331.1	289.0	110.0
EEP	#1-6	Limestone	Rootcrete	-10.61	-4.39			340.1	279.4	36.3
EEP	#1-7	Limestone	White, skeletal limestone matrix	-8.54	-4.16			950.6	532.1	17
EEP	#1-8	Limestone	White, oncoid limestone lithoclast	-11.05	-5.02			1341.4	564.3	41.3
EEP	#1-9	Limestone	White, skeletal limestone lithoclast	-6.24	-4.63					
EEP	#1-10	Limestone	Black limestone lithoclast	-8.77	-5.60					
EEP	#1-11	Limestone	Black limestone lithoclast	-7.94	-4.58					
EEP	#3-1	Limestone	Red limestone matrix	-8.36	-4.24			2767.1	778.8	25.2
EEP	#3-2	Limestone	Rootcrete	-10.31	-5.46			4678.6	3415.1	1257.6
EEP	#3-3	Limestone	White, oncoid limestone matix	-8.024	-4.37			1401.6	647.0	80.5
EEP	#3-4	Calcite cement	Bedrock	-10.48	-4.83			619.6	405.6	57.6
EEP	#6-1	Limestone	Red limestone matrix	-10.02	-5.17			2533.2	768.8	56.7
EEP	#6-2	Limestone	Rootcrete	-10.28	-4.31			1224.1	738.8	907.6
EEP	#6-3	Calcite cement	Bedrock	-6.55	-4.46			108.3	191.5	32.7
EEP	#6-4	Calcite cement	Bedrock	-8.34	-4.53			265.7	232.9	38.0
EEP	#11-1	Calcite cement	Uncoated dolostone lithoclast	-7.98	-5.06			94.3	172.3	13.1
EEP	#11-2	Limestone	Rootcrete	-9.81	-3.91			1348.3	1205.3	49.7
EEP	#11-3	Limestone	White, skeletal limestone matrix	-6.88	-3.76			1396.4	908.8	10.2
EEP	#11-4	Limestone	White, skeletal limestone matrix	-7.33	-3.81			1954.9	1143.7	26.3
EEP	#11-5	Limestone	Rootcrete	-9.69	-4.65			1929.4	1215.7	55.3
EEP	#11-6	Limestone	Rootcrete	-11.45	-5.18			395.2	381.6	40.5
EEP	#11-7	Limestone	Rootcrete	-10.86	-5.03			774.6	714.1	27.3
EEP	#11-8	Limestone	Rootcrete	-9.88	-4.93			1078.4	960.9	43.9
EEP	#11-9	Calcite cement	Uncoated dolostone lithoclast	-8.73	-5.36					
EEP	#13-1	Limestone	Orange limestone matrix	-8.99	-3.73			25972.8	12585.6	79.5
EEP	#13-2	Limestone	Rootcrete	-9.54	-3.93			4350.0	10.8	2634.4
EEP	#13-3	Limestone	White, skeletal limestone lithoclast	-8.50	-3.63			8327.4	7.8	1087.3
EEP	#13-4	Calcite cement	Uncoated dolostone lithoclast	-7.24	-4.59			11972.9	2.9	284.3
EEP	#13-5	Calcite cement	Bedrock	-6.18	-4.08			55.5	166.3	18.9
EEP	#13-6	Calcite cement	Bedrock	-7.77	-4.40			134	350.3	26.3

Appendix 1. Summary of geochemical data obtained from sinkhole-filling deposits in the exposed Cayman Formation on Grand Cayman and Cayman Brac[a] (continued)

Locality	Sample No.	Lithology [b]	Type	Calcite		Dolomite		Al (ppm)	Fe (ppm)	Mn (ppm)
				$\delta^{13}C$ (‰ PDB)	$\delta^{18}O$ (‰ PDB)	$\delta^{13}C$ (‰ PDB)	$\delta^{18}O$ (‰ PDB)			
EEP	#13-7	Calcite cement	Bedrock	-9.24	-4.23			2229.3	1269.9	141.0
EEP	#15-1	Calcite cement	Uncoated dolostone lithoclast	-6.16	-5.01			87.5	118.7	13.7
EEP	#15-2	Limestone	Rootcrete	-6.81	-5.11					
EEP	#15-3	Limestone	Rootcrete	-11.044	-4.35			2791.1	972.5	110.9
EEP	#15-4	Calcite cement	Uncoated dolostone lithoclast	-6.60	-4.66					
EEP	#15-5	Limestone	Rootcrete	-10.78	-4.59			1255.8	382.9	88.8
EEP	#15-6	Limestone	Rootcrete	-10.64	-3.88			1073.1	527.8	73.9
EEP	#15-7	Limestone	Rootcrete	-11.61	-5.13			1432.9	841.5	266.8
EEP	#15-8	Limestone	Rootcrete	-11.40	-5.61			1099.2	1262.9	129.9
EEP	#15-9	Calcite cement	Uncoated dolostone lithoclast	-6.29	-4.81			133.3	147.8	17.0
EEP	#15-10	Limestone	Rootcrete	-10.91	-5.59			826.7	593.9	71.1
EEP	#15-11	Limestone	Rootcrete	-11.29	-5.23			955.5	482.1	21.7
EEP	#15-12	Limestone	Rootcrete	-10.93	-4.41					
EEP	#18-1	Limestone	Red limestone matrix	-10.32	-5.37			4162.2	871.2	68
EEP	#18-2	Limestone	Rootcrete	-11.49	-3.49			3951.3	2020.2	299.7
EEP	#18-3	Limestone	White, oncoid limestone matrix	-10.64	-5.49			692.4	396.9	28.3
EEP	#19-1	Limestone	Black limestone lithoclast	-7.96	-4.91					
EEP	#26-1	Limestone	White, skeletal limestone matrix	-7.02	-4.24			1138.9	472.2	57.9
EEP	#26-2	Calcite cement	Uncoated dolostone lithoclast	-4.93	-4.51			41.3	104.9	17.2
EEP	#26-3	Limestone	Black limestone lithoclast	-10.65	-4.48			285.7	183.8	39.2
EEP	#26-4	Limestone	Rootcrete	-10.36	-4.84			1995.2	1043.1	504.7
EEP	#26-5	Limestone	Rootcrete	-10.38	-4.44			1667.3	923.6	417.0
EEP	#26-6	Limestone	Rootcrete	-10.01	-4.17			537.4	599.0	181.4
EEP	#26-7	Limestone	White, skeletal limestone matrix	-7.42	-3.60			713.9	386.9	53.3
EEP	#26-8	Limestone	White, oncoid limestone matrix	-11.35	-4.67			814.3	561.0	36.9
EEP	#29-1	Limestone	White, skeletal limestone lithoclast	-6.14	-4.08			1305.4	812.0	45.3
EEP	#29-2	Limestone	Orange limestone matrix	-9.84	-2.97					
EEP	#29-3	Limestone	Orange limestone matrix	-8.42	-0.76					
EEP	#29-4	Limestone	Rootcrete	-11.09	-4.37			1058	1762.9	958.4
EEP	#29-5	Limestone	Rootcrete	-11.28	-4.54					
EEP	#29-6	Limestone	Rootcrete	-10.25	-4.59			1061	2341.8	423.8
EEP	#29-7	Limestone	Rootcrete	-10.05	-4.42			989	2553.4	262.1
EEP	#341-1	Limestone	Black limestone lithoclast	-11.09	-5.72			53.2	128.8	33.3

Appendix 1. Summary of geochemical data obtained from sinkhole-filling deposits in the exposed Cayman Formation on Grand Cayman and Cayman Brac[a] (continued)

Locality	Sample No.	Lithology[b]	Type	Calcite		Dolomite		Al (ppm)	Fe (ppm)	Mn (ppm)
				$\delta^{13}C$ (‰ PDB)	$\delta^{18}O$ (‰ PDB)	$\delta^{13}C$ (‰ PDB)	$\delta^{18}O$ (‰ PDB)			
EEP	#341-2	Limestone	White, skeletal limestone lithoclast	-8.223	-3.99			94.8	197.0	20.6
EEP	#341-3	Limestone	Speleothemic calcite	-10.52	-6.16			62.7	127.0	112.1
EEP	#341-4	Limestone	Black limestone lithoclast	-6.49	-4.72			44.9	111.8	38.5
EEP	#341-5	Limestone	White, skeletal limestone lithoclast	-7.60	-4.66			26.3	128.7	16.8
EEP	#341-6	Limestone	White, skeletal limestone matrix	-11.15	-5.52			84.0	127.3	29.3
HRQ	#2-2-1	Limestone	Red limestone matrix	-9.52	-2.17			2802.5	437.1	192.3
HRQ	#2-2-2	Dolostone	Mn-coated dolostone lithoclast			2.47	4.31	329.8	604.5	42.2
HRQ	#2-2-3	Limestone	Red limestone matrix	-9.47	-2.25			3625.8	745.8	1064.3
HRQ	#2-2-4	Dolostone	Mn-coated dolostone lithoclast			1.46	3.85	1116.6	532.2	180.9
HRQ	#2-2-5	Dolostone	Mn-coated dolostone lithoclast			1.55	4.15			
HRQ	#2-5-1	Dolostone	Unconated dolostone lithoclast			2.21	3.86			
HRQ	#2-5-2	Dolostone	Unconated dolostone lithoclast			1.89	4.22			
HRQ	#3-1	Limestone	Rootcrete	-6.44	-3.22			5625.9	1987.4	515.0
HRQ	#3-2	Limestone	Rootcrete	-9.73	-4.88			5246.7	1387.3	1547.6
HRQ	#3-3	Limestone	Rootcrete	-10.20	-4.06					
HRQ	#3-4	Dolostone	Bedrock			1.93	3.77	194	210.8	28.7
HRQ	#3-2-1	Limestone	Rootcrete	-7.61	-3.26			4201.9	965.0	550.3
HRQ	#3-2-2	Limestone	Rootcrete	-5.55	-2.89					
HRQ	#3-2-3	Limestone	Rootcrete	-9.04	-2.65			4014.4	627.3	223.5
HRQ	#3-2-4	Dolostone	Bedrock			1.36	2.99	150.9	151.0	29.6
HRQ	#3-2-5	Dolostone	Bedrock			1.74	2.98			
HRQ	#3-2-6	Dolostone	Bedrock			0.7	3.16			
HRQ	#3-3-1	Limestone	Red limestone matrix	-11.40	-5.46					
HRQ	#3-3-2	Limestone	Orange limestone matrix	-9.61	-3.72					
HRQ	#3-3-3	Limestone	Unconated dolostone lithoclast			1.87	3.98			
SQW	#2-1	Limestone	Rootcrete	-10.67	-4.02			335.1	281.6	68.6
SQW	#2-2	Limestone	Rootcrete	-8.94	-5.59			273.8	203.0	31.0
SQW	#2-3	Limestone	Rootcrete	-9.60	-4.39			4076.6	735.6	268.0
SQW	#2-4	Limestone	Rootcrete	-9.76	-5.47			997.1	622.2	69.5
SQW	#2-5	Dolostone	Bedrock			0.37	3.64	1535.4	631.7	53.5
SQW	#2-6	Limestone	Speleothemic calcite	-7.59	-4.94			497.6	329.0	10.6
SQW	#3-1	Limestone	Rootcrete	-8.99	-6.36			175.0	212.6	77.5
SQW	#3-2	Limestone	Rootcrete	-8.68	-5.82			197.5	118.5	24.2

Appendix 1. Summary of geochemical data obtained from sinkhole-filling deposits in the exposed Cayman Formation on Grand Cayman and Cayman Brac[a] (continued)

Locality	Sample No.	Lithology[b]	Type	Calcite		Dolomite		Al (ppm)	Fe (ppm)	Mn (ppm)
				$\delta^{13}C$ (‰ PDB)	$\delta^{18}O$ (‰ PDB)	$\delta^{13}C$ (‰ PDB)	$\delta^{18}O$ (‰ PDB)			
SQW	#3-3	Limestone	Rootcrete	-7.75	-6.02			841.3	634.1	84.9
SQW	#3-4	Dolostone	Bedrock			2.50	4.14	85.0	156.8	23.6
SQW	#3-5	Dolostone	Bedrock			2.34	3.69	124.6	138.4	23.3
SQW	#12-1	Limestone	Orange limestone matrix	-10.23	-5.11			1942.3	604.8	257.9
SQW	#12-2	Limestone	Red limestone matrix	-9.99	-5.64			2642.1	753.2	50.5
SQW	#12-3	Limestone	Orange limestone matrix	-9.64	-5.78			2410.4	729.0	190.0

[a] Except for SQW that is located on Cayman Brac, the rest localities are from Grand Cayman. See Methods section for explanations of derivation of each parameter.
[b] Lithology is based on the X-ray diffraction analysis. Dolostone contains dolomite > 50%, whereas limestone contains dolomite < 50%.
Detection limits (ppm): Al (0.2), Fe (3.7), Mn (0.03).

Appendix 2. Summary of rare earth elements and yttrium data obtained from sinkhole-filling deposits in the exposed Cayman Formation on Grand Cayman and Cayman Brac[a]

Locality	Sample No.	Y (ppm)	La (ppm)	Ce (ppm)	Pr (ppm)	Nd (ppm)	Sm (ppm)	Eu (ppm)	Gd (ppm)	Tb (ppm)	Dy (ppm)	Ho (ppm)	Er (ppm)	Tm (ppm)	Yb (ppm)	Lu (ppm)	La_N/Yb_N[b]	Sm_N/Yb_N[b]
EEP	#1-1	2.13	0.34	0.25	-	0.26	-	-	0.15	-	0.17	-	0.13	-	0.11	-	0.23	-
EEP	#1-2	3.36	1.96	3.58	0.47	1.97	0.40	0.10	0.48	-	0.42	-	0.25	-	0.21	-	0.70	1.00
EEP	#1-3	5.05	3.08	6.26	0.77	3.12	0.67	0.17	0.80	0.11	0.65	0.14	0.40	-	0.33	-	0.69	1.03
EEP	#1-4	1.51	0.84	1.44	0.21	0.85	0.18	-	0.23	-	0.19	-	0.11	-	-	-	-	-
EEP	#1-5	1.71	0.49	0.86	0.12	0.54	0.12	-	0.18	-	0.16	-	0.11	-	-	-	-	-
EEP	#1-6	1.01	0.38	0.63	0.11	0.39	-	-	0.12	-	0.10	-	-	-	-	-	-	-
EEP	#1-7	3.37	1.37	2.15	0.30	1.27	0.33	-	0.39	-	0.37	-	0.24	-	0.20	-	0.50	0.83
EEP	#1-8	3.18	1.40	2.31	0.32	1.32	0.29	-	0.37	-	0.33	-	0.23	-	0.20	-	0.52	0.74
EEP	#3-1	16.3	1.75	5.30	0.76	4.36	1.60	0.45	2.18	0.34	2.15	0.46	1.34	0.21	1.13	0.17	0.11	0.72
EEP	#3-2	17.7	4.07	10.6	1.47	7.15	1.81	0.47	2.26	0.32	2.07	0.45	1.29	0.20	1.12	0.16	0.27	0.82
EEP	#3-3	4.04	1.25	2.49	0.33	1.48	0.34	-	0.46	-	0.42	0.10	0.28	-	0.25	-	0.37	0.71
EEP	#3-4	2.50	0.82	1.43	0.23	0.93	0.23	-	0.30	-	0.26	-	0.18	-	0.15	-	0.42	0.79
EEP	#6-1	13.3	2.84	7.74	0.99	4.89	1.36	0.36	1.72	0.24	1.60	0.33	0.98	0.15	0.82	0.12	0.25	0.84
EEP	#6-2	10.6	4.38	7.37	1.21	5.37	1.18	0.28	1.35	0.17	1.12	0.23	0.65	0.10	0.51	-	0.63	1.17
EEP	#6-3	1.57	0.30	0.33	-	0.30	-	-	0.12	-	0.11	-	-	-	-	-	-	-
EEP	#6-4	2.10	0.43	0.64	0.10	0.47	0.12	-	0.18	-	0.17	-	0.13	-	-	-	-	-
EEP	#11-1	0.83	0.23	0.25	-	0.23	-	-	0.09	-	0.08	-	-	-	-	-	-	-
EEP	#11-2	5.70	2.55	4.47	0.68	2.93	0.65	0.17	0.78	0.11	0.69	0.15	0.45	-	0.35	-	0.54	0.96
EEP	#11-3	3.64	1.65	3.09	0.46	1.92	0.42	0.11	0.53	0.07	0.47	0.10	0.30	-	0.24	-	0.51	0.89
EEP	#11-4	4.16	1.95	3.95	0.56	2.32	0.50	0.13	0.62	0.09	0.56	0.12	0.34	-	0.28	-	0.51	0.89
EEP	#11-5	5.40	3.01	5.58	0.76	3.29	0.69	0.17	0.83	0.11	0.70	0.15	0.43	-	0.34	-	0.64	1.01
EEP	#11-6	0.90	0.43	0.85	0.11	0.49	0.11	-	0.14	-	0.11	-	0.08	-	0.06	-	0.49	0.86
EEP	#11-7	2.46	1.10	1.94	0.29	1.29	0.27	-	0.37	0.05	0.31	0.07	0.21	-	0.16	-	0.49	0.85
EEP	#11-8	3.11	1.79	3.46	0.45	1.92	0.40	0.10	0.53	0.07	0.41	0.09	0.26	-	0.22	-	0.60	0.94
EEP	#13-2	7.19	2.70	5.53	0.72	3.27	0.81	0.21	1.07	0.15	0.97	0.22	0.60	0.09	0.49	-	0.40	0.83
EEP	#13-3	6.61	1.74	3.57	0.50	2.17	0.59	0.17	0.86	0.12	0.84	0.18	0.52	0.08	0.43	-	0.30	0.70
EEP	#13-4	1.12	0.35	0.54	-	0.37	-	-	0.14	-	0.13	-	0.08	-	-	-	-	-
EEP	#13-5	1.03	0.21	0.21	-	0.22	-	-	0.10	-	0.11	-	0.08	-	-	-	-	-
EEP	#13-6	0.90	0.26	0.34	-	0.27	-	-	0.11	-	0.11	-	0.08	-	-	-	-	-
EEP	#13-7	11.6	2.76	6.07	0.84	3.98	1.05	0.31	1.64	0.24	1.61	0.36	1.01	0.15	0.78	0.12	0.26	0.68
EEP	#15-1	1.12	0.25	0.27	-	0.24	-	-	0.09	-	-	-	-	-	-	-	-	-
EEP	#15-3	12.2	2.28	4.56	0.75	3.71	1.00	0.26	1.32	0.18	1.19	0.25	0.74	0.11	0.59	-	0.29	0.87
EEP	#15-5	6.68	0.93	2.38	0.36	1.88	0.56	0.14	0.75	0.11	0.70	0.15	0.44	-	0.36	-	0.19	0.68
EEP	#15-6	3.12	1.04	1.70	0.26	1.15	0.26	-	0.33	-	0.29	-	0.20	-	0.16	-	0.47	0.82
EEP	#15-7	6.10	2.08	2.90	0.56	2.49	0.57	0.14	0.70	-	0.60	0.13	0.37	-	0.30	-	0.51	0.97

Appendix 2. Summary of rare earth elements and yttrium data obtained from sinkhole-filling deposits in the exposed Cayman Formation on Grand Cayman and Cayman Brac[a] (continued)

Locality	Sample No.	Y (ppm)	La (ppm)	Ce (ppm)	Pr (ppm)	Nd (ppm)	Sm (ppm)	Eu (ppm)	Gd (ppm)	Tb (ppm)	Dy (ppm)	Ho (ppm)	Er (ppm)	Tm (ppm)	Yb (ppm)	Lu (ppm)	La_N/Yb_N[b]	Sm_N/Yb_N[b]
EEP	#15-8	3.13	1.20	1.67	0.34	1.41	0.32	-	0.41	-	0.34	-	0.20	-	0.16	-	0.55	1.01
EEP	#15-9	1.75	0.42	0.47	-	0.43	0.10	-	0.16	-	0.16	-	0.11	-	-	-	-	-
EEP	#15-10	3.07	1.01	1.59	0.28	1.22	0.29	-	0.35	-	0.32	-	0.21	-	0.18	-	0.42	0.82
EEP	#15-11	3.08	0.91	1.67	0.26	1.12	0.28	-	0.34	-	0.32	-	0.21	-	0.18	-	0.38	0.79
EEP	#18-1	20.0	1.94	6.76	0.97	5.51	1.80	0.48	2.37	0.35	2.28	0.49	1.45	0.22	1.19	0.18	0.12	0.77
EEP	#18-2	26.8	3.90	17.1	2.00	10.2	2.64	0.66	3.17	0.45	2.89	0.62	1.80	0.27	1.45	0.21	0.20	0.93
EEP	#18-3	2.12	0.62	1.06	0.15	0.70	0.16	-	0.20	-	0.19	-	0.14	-	0.12	-	0.39	0.68
EEP	#26-1	6.11	1.24	4.49	0.48	2.43	0.65	0.17	0.84	0.12	0.77	0.17	0.49	-	0.42	-	0.22	0.79
EEP	#26-2	1.01	0.24	0.24	0.05	0.23	-	-	0.09	-	-	-	-	-	-	-	-	-
EEP	#26-3	1.88	0.38	0.57	0.13	0.59	0.14	-	0.21	-	0.19	-	0.13	-	0.11	-	0.26	0.68
EEP	#26-4	8.19	2.95	4.75	0.84	3.86	0.86	0.23	1.07	0.15	0.92	0.20	0.59	-	0.48	-	0.45	0.92
EEP	#26-5	3.46	1.89	3.57	0.45	1.86	0.40	0.11	0.48	-	0.41	-	0.26	-	0.22	-	0.63	0.92
EEP	#26-6	2.15	0.72	1.47	0.19	0.82	0.19	-	0.26	-	0.23	-	0.17	-	0.12	-	0.42	0.77
EEP	#26-7	4.35	1.66	2.88	0.41	1.79	0.40	0.10	0.51	-	0.50	0.11	0.33	-	0.25	-	0.48	0.80
EEP	#26-8	6.52	2.76	3.99	0.63	2.84	0.57	0.15	0.76	0.11	0.69	0.15	0.45	-	0.39	-	0.52	0.73
EEP	#29-1	3.78	1.11	2.93	0.33	1.52	0.41	0.11	0.57	0.08	0.53	0.12	0.33	-	0.30	-	0.28	0.70
EEP	#29-4	13.9	1.69	6.08	0.69	3.66	1.14	0.33	1.72	0.25	1.73	0.39	1.14	0.17	0.94	0.14	0.13	0.61
EEP	#29-6	6.12	0.98	2.63	0.32	1.68	0.51	0.15	0.78	0.11	0.78	0.18	0.51	0.08	0.44	-	0.16	0.58
EEP	#29-7	5.13	1.84	4.08	0.52	2.07	0.49	0.14	0.67	0.09	0.66	0.14	0.42	-	0.38	-	0.36	0.67
EEP	#341-1	0.91	0.18	0.26	-	0.20	-	-	0.08	-	-	-	-	-	-	-	-	-
EEP	#341-2	1.03	0.25	0.22	-	0.26	-	-	0.09	-	0.10	-	-	-	-	-	-	-
EEP	#341-3	0.14	0.04	0.11	-	0.05	-	-	-	-	-	-	-	-	-	-	-	-
EEP	#341-4	0.56	0.11	0.14	-	0.12	-	-	-	-	-	-	-	-	-	-	-	-
EEP	#341-5	1.22	0.23	0.22	-	0.22	-	-	0.11	-	0.10	-	-	-	-	-	-	-
EEP	#341-6	0.23	0.08	0.13	-	0.08	-	-	0.03	-	-	-	-	-	-	-	-	-
HRQ	#2-2-1	12.8	6.41	9.40	1.56	6.61	1.42	0.34	1.69	0.23	1.47	0.32	0.90	0.13	0.70	0.10	0.68	1.04
HRQ	#2-2-2	2.31	0.87	0.69	0.19	0.77	0.16	-	0.23	-	0.21	-	0.14	-	0.11	-	0.61	0.77
HRQ	#2-2-3	25.3	12.1	13.5	2.75	11.4	2.32	0.58	2.88	0.39	2.56	0.56	1.61	0.23	1.23	0.17	0.72	0.96
HRQ	#2-2-4	6.40	2.97	2.65	0.67	2.72	0.56	0.14	0.71	-	0.63	0.14	0.40	-	0.29	-	0.74	0.96
HRQ	#3-1	29.1	14.1	11.6	3.29	13.9	2.93	0.76	3.71	0.51	3.34	0.72	2.04	0.29	1.42	0.19	0.73	1.05
HRQ	#3-2	42.6	22.9	19.2	5.32	22.5	4.66	1.19	5.77	0.78	5.11	1.09	3.05	0.43	2.14	0.30	0.79	1.10
HRQ	#3-4	3.48	1.26	0.67	0.28	1.28	0.27	0.08	0.39	-	0.37	0.08	0.25	-	0.18	-	0.52	0.75
HRQ	#3-2-1	47.7	28.6	13.8	6.27	25.6	4.96	1.20	5.83	0.77	5.03	1.05	2.96	0.42	2.08	0.28	1.02	1.21
HRQ	#3-2-3	103.0	62.1	20.3	13.7	55.4	10.6	2.53	12.3	1.64	10.7	2.31	6.46	0.92	4.59	0.62	1.00	1.17

Appendix 2. Summary of rare earth elements and yttrium data obtained from sinkhole-filling deposits in the exposed Cayman Formation on Grand Cayman and Cayman Brac[a] (continued)

Locality	Sample No.	Y (ppm)	La (ppm)	Ce (ppm)	Pr (ppm)	Nd (ppm)	Sm (ppm)	Eu (ppm)	Gd (ppm)	Tb (ppm)	Dy (ppm)	Ho (ppm)	Er (ppm)	Tm (ppm)	Yb (ppm)	Lu (ppm)	La_N/Yb_N[b]	Sm_N/Yb_N[b]
HRQ	#3-2-4	3.64	1.32	1.18	0.30	1.27	0.26	-	0.36	-	0.35	-	0.23	-	0.17	-	0.58	0.78
SQW	#2-1	1.74	0.62	0.88	0.17	0.74	0.15	-	0.20	-	0.18	-	0.11	-	-	-	-	-
SQW	#2-2	0.77	0.31	0.44	-	0.32	-	-	0.09	-	-	-	-	-	-	-	-	-
SQW	#2-3	19.3	6.13	12.7	1.85	8.07	1.87	0.48	2.4	0.34	2.18	0.47	1.38	0.21	1.10	0.16	0.41	0.86
SQW	#2-4	3.33	1.50	2.36	0.38	1.60	0.33	0.08	0.42	-	0.36	-	0.23	-	0.20	-	0.56	0.85
SQW	#2-5	6.75	2.86	3.11	0.58	2.46	0.52	0.13	0.73	0.10	0.71	0.16	0.48	-	0.38	-	0.55	0.69
SQW	#2-6	1.38	0.60	1.02	0.14	0.58	0.12	-	0.17	-	0.18	-	0.10	-	-	-	-	-
SQW	#3-1	0.69	0.23	0.34	-	0.25	-	-	0.08	-	0.07	-	0.05	-	-	-	-	-
SQW	#3-2	0.45	0.28	0.27	-	0.16	-	-	0.06	-	-	-	-	-	-	-	-	-
SQW	#3-3	2.37	1.14	1.74	0.31	1.09	0.24	0.06	0.32	-	0.29	0.06	0.19	-	0.15	-	0.56	0.82
SQW	#3-4	0.83	0.33	0.30	-	0.29	-	-	0.10	-	0.08	-	0.06	-	-	-	-	-
SQW	#3-5	1.13	0.42	0.43	-	0.38	-	-	0.14	-	0.13	-	0.08	-	-	-	-	-
SQW	#12-1	13.9	4.51	10.3	1.36	6.00	1.38	0.35	1.77	0.24	1.57	0.34	0.99	0.15	0.81	0.12	0.41	0.86
SQW	#12-2	13.5	6.06	15.4	1.76	7.47	1.75	0.44	2.16	0.30	1.90	0.40	1.13	0.16	0.91	0.13	0.49	0.98
SQW	#12-3	11.2	5.49	19.5	1.58	6.63	1.53	0.37	1.84	0.25	1.60	0.34	0.95	0.14	0.78	0.11	0.52	0.99

[a] Except for SQW that is located on Cayman Brac, the rest localities are from Grand Cayman. See Methods section for explanations of derivation of each parameter.
[b] N-shale normalized.
Detection limits (ppm): Y (0.02), La (0.03), Ce (0.03), Pr (0.04), Nd (0.03), Sm (0.04), Eu (0.03), Gd (0.03), Tb (0.03), Dy (0.04), Ho (0.02), Er (0.04), Tm (0.06), Yb (0.05), Lu (0.04).
-below the detection limit.